Late Quaternary glacial history and paleoceanographic reconstructions along the East Greenland continental margin: Evidence from high-resolution records of stable isotopes and ice-rafted debris

Spätquartäre Vereisungsgeschichte und paläozeanographische Rekonstruktionen am ostgrönländischen Kontinentalrand

Seung-Il Nam

Seung-Il Nam

Alfred-Wegener-Institut für Polar- und
Meeresforschung
Postfach 120161
Columbusstraße
D-27568 Bremerhaven

CONTENTS

Contents

APPENDICES

The data of this publication are available through:

Alfred Wegener Institute for Polar and Marine Research

Department of Marine Geology

Columbusstrasse

27568 Bremerhaven, Germany

Phone: +49 471 4831 220

Fax: +49 471 4831 149
E-mail: sepan@awi-bremerhaven.de

ABSTRACT

High-resolution stable oxygen and carbon isotope analyses and detailed sedimentological and geochemical investigations were performed in order to i) reconstruct the paleoclimate and paleoceanography of the Greenland Sea associated with late Quaternary glacial-interglacial cycles, and ii) to link the terrestrial and deep-sea climatic records. The reconstruction of the paleoenvironmental history of the East Greenland margin and the correlation between the terrestrial and deep sea records are major objectives of the ESF-PONAM-Programme (European Science Foundation - Polar North Atlantic Margins). For this study 16 gravity and 2 box cores were recovered along the East Greenland continental margin between 69°N and 72°N on three W-E transects running from the shelf to the deep sea.

The glaciomarine sediments recovered from the heavily ice-covered East Greenland continental margin reflect changes associated with the glacial-interglacial climatic cycles of the last 240 ka. The glaciomarine sediments are characterised by a dominance of terrestrially derived components and a lower content of biogenic components. Glaciomarine sedimentation processes, terrigenous sediment input, and biogenic productivity in the study area are strongly influenced by fluctuations in the extent of the Greenland Ice Sheet, extent of the sea-ice cover, rate of iceberg drifting, meltwater input, and changes in the East Greenland Current (EGC).

The relatively low carbonate content (<10 %) and the dominant occurrence of *N. pachyderma* sin. (>95 %) throughout the sediment sequences indicate a low biological productivity in the surface water resulting from the extensive sea-ice cover and the strong influence of cold and low-saline polar waters of the EGC. An increase in the surface-water productivity, on the other hand, occurred during certain periods within interglacial and glacial stages. This indicates that the sea ice along the western margin of the Greenland Sea was at least seasonally reduced during these time intervals.

Based on the accumulation rates of the coarse terrigenous matter (>63 µm) and amounts of IRD, the advance and retreat of East Greenland glaciers over the past 200 ka can be correlated with those postulated from the terrestrial records. At least five repeated advances and retreats of glaciers beyond the coastline are proposed between the late Early to Middle Weichselian (65-61, 59-51, 48-42, 35-31, and 28-25 ka). Maximum fluxes of IRD recorded along the continental margin between 21 and 16 ka, reflect the maximum extent of East Greenland glaciers probably reaching the shelf break at that time.

The stable oxygen isotope records measured on the planktonic foraminifer *N. pachyderma* sin. reveal some excursions from the global climate record due to a local and/or regional overprint through meltwater supply and/or cold water masses of the EGC. Distinct meltwater events are documented during Terminations II and I and at the beginning of stage 3 resulting from the collapse of the Greenland Ice Sheet. The early period of all glacial stages (i.e. 7/6, 5/4, and 3/2) was subjected to an abrupt and rapid build-up of a sea-ice cover. Hence, a distinct decrease in the carbonate content, the low number of planktonic foraminifers, and light $\delta^{13}C$ values reflect the strong reduction in

the CO_2 exchange between the atmosphere and ocean, and the surface-water productivity, resulting from a meltwater cap and/or an extensive sea-ice cover.

The onset of Termination I is characterised by a distinct shift towards light $\delta^{18}O$ values, a dramatic decrease in the IRD-flux, and a marked increase in organic matter, indicating the rapid retreat of East Greenland glaciers and a reduced sea-ice cover. According to distinct shifts toward light $\delta^{18}O$ and heavy $\delta^{13}C$ values of *N. pachyderma* sin. and *O. umbonatus*, the present-day circulation patterns of surface- and deep-water masses were probably established between 7.4 and 6.1 ka. This is very similar to the timing estimated from studies on microfossil assemblages of the Greenland Sea.

In particular, the distinct IRD peaks correlate with the fluctuations of the Greenland Ice Sheet during the last two glacial-interglacial cycles. Most of the major IRD peaks correspond to periods of cooling of air temperatures over Greenland. During the interval between 225 and 60 ka, the IRD peaks are in phase (at the 23-kyr orbital processional cycle) with maximum summer insolation at 70°N. This suggests that the Greenland Ice Sheet may have experienced a predominantly 23-kyr cycle of growth and decay, and therefore, collapsed and discharged large volumes of icebergs to the Greenland Sea when summer insolation reached its maxima.

During the last glacial period, there is a strong correlation between major pulses in the supply of IRD, and the Bond Cycles and the Heinrich Events recorded in the GRIP ice core and North Atlantic deep-sea sediments. Furthermore, the higher frequency of IRD events on millennial scales matches the cooling phase of the abrupt Dansgaard-Oeschger Cycles recorded in the GRIP ice core. Consequently, the apparent evidence of millennial scale IRD events in the North Atlantic and the GIN Sea suggests coherent fluctuations of the large northern hemisphere ice sheets (i.e. the Fennoscandian/Barents Sea and Laurentide/Greenland ice sheets) during the last glacial period.

1. INTRODUCTION AND OBJECTIVES

1.1 Introduction

During the late Quaternary, the high-latitude oceans have been strongly influenced by repeated expansion and retreat of the great continental ice sheets caused by abrupt glacial-interglacial climatic oscillations (Hughes et al. 1977; CLIMAP 1981). In the northern hemisphere, the Laurentide, Fennoscandian, Barents Sea, and Greenland ice sheets have exerted a major influence on changes in paleoclimate and paleoceanography during the late Quaternary. Global climatic changes are detected through $\delta^{18}O$ records from several of the Greenland ice cores (e.g. Dansgaard et al. 1982, 1993; Johnsen et al. 1992; Oeschger 1992; Grootes et al. 1993). Recent studies from both Greenland ice cores, GRIP (Greenland Ice-core Project; Dansgaard et al. 1993) and GISP2 (Greenland Ice Sheet Project 2; Grootes et al. 1993), show abrupt climatic oscillations on millennial time scales that are contemporaneously reflected within marine (e.g. Bond et al. 1993; Fronval et al. 1995; Thunell & Mortyn 1995) and terrestrial sediments (e.g. Grimm et al. 1993; Porter & Zhisheng 1995). In general, the Quaternary glacial-interglacial climatic oscillations are controlled by the astronomical cycles of precession, tilt of the earth's axis, and eccentricity of the orbit with periodicities of about 23, 41 and 100 kyr, respectively (Broecker & van Donk 1970; Hays et al. 1976; Imbrie et al. 1984, 1992, 1993). The primary evidence that climate responds to orbital changes has been obtained from oxygen isotope records of foraminifers from deep-sea sediments (Hays et al. 1976; Imbrie et al. 1984).

Throughout the late Quaternary, the Greenland-Iceland-Norwegian (GIN) Sea has played a key role in the global climate system through the permanent and/or seasonal sea-ice cover, migration of the oceanographic front system, transfer of latent heat to the atmosphere, deep-water formation, and global deep-water ventilation. In particular, the GIN Sea is a region of major deep-water renewal in the northern polar ocean (Gordon 1986). Dense water in this region is formed by air-sea-ice interactions which act to cool the water and increase its salinity through evaporation and salt rejection during sea-ice formation. Therefore, the GIN Sea, as one of the most important regions of the world's ocean, is a critical contributor to the global thermohaline circulation controlling global heat and gas transfer, and world climate (e.g. Broecker & Denton 1989).

In general, marine sediments within the GIN Sea reflect the properties of surface water masses, ocean circulation patterns, variations in sea-ice cover, and the waxing and waning of the adjacent continental ice sheets. Extensive research has been carried out on marine sediments from the central and eastern GIN Sea (e.g. Kellogg 1976, 1977, 1980; Kellogg et al. 1978; Henrich et al. 1989, 1995; Bleil & Gard 1989; Gard & Backman 1990; Vogelsang 1990; Henrich 1992; Baumann et al. 1993, 1994, 1995; Goldschmidt 1994; Koç & Jansen 1994; Wagner & Henrich 1994) and has significantly contributed to our understanding of changes in the paleoclimate and paleoceanography associated with Quaternary glacial-interglacial cycles.

The Greenland Sea has been consistently influenced by the cold and low-saline polar water of the East Greenland Current (EGC), the growth and decay of the Greenland Ice Sheet, permanent and/or seasonal sea-ice cover, calving

3

of icebergs, meltwater input, and discharge of terrigenous sediments from the adjacent large fjord systems (e.g. Scoresby Sund) (Marienfeld 1991, 1992a-b; Mienert et al. 1992; Stein et al. 1993; Dowdeswell et al. 1994a-b.; Nam et al. 1995a). The wide and irregular continental margin of East Greenland is a major conduit of cold polar surface water that outflows from the Arctic Ocean via the Fram Strait. Glacial records from the East Greenland continental margin are complicated by differing local factors, and by the vertical movements of sediments resulting from local ice-loading processes. Clear traces of glacial activity are highlighted within glaciomarine sediments in the form of ice-rafted debris (IRD) that originates mainly from the adjacent Greenland continent via icebergs calved from the glaciers draining the Greenland Ice Sheet (e.g. Nam et al. 1995a). Accordingly, the western part of the Greenland Sea is an ideal region in which to study glaciomarine processes and paleoenvironments in relation to late Quaternary glacial-interglacial cycles. The glacial history of East Greenland has also been investigated on terrestrial sediments (e.g. Hjort 1981; Funder 1984, 1989; Möller et al. 1991; Funder et al. 1994 & further references therein). In particular, periglacial lake sediments combined with the ice core records (e.g. Dansgaard et al. 1993) and marine records, provide new data on both the late Quaternary glacial-interglacial history of East Greenland, and a correlation between the land and ocean records (e.g. Hubberten et al. 1995). Several sedimentological and micropaleontological investigations have been carried out on glaciomarine sediments along the East Greenland continental margin. However, these studies are mainly confined to time scales not older than the last deglaciation (Koç Karpuz & Schrader 1990; Marienfeld 1991, 1992a-b; Baumann & Matthiessen 1992; Mienert et al. 1992; Dowdeswell et al. 1993, 1994a-b; Stein et al. 1993; Williams 1993; Matthiessen 1995). Therefore, there is little information on the glacial history of the East Greenland continental margin and in the adjacent deep sea with regard to last glacial-interglacial cycles (cf. Nam et al. 1995a; Stein et al. 1996).

1.2. Objectives

During the last five years (1990-1994), the main objective of the ESF-PONAM programme (European Science Foundation - Polar North Atlantic Margins) (Elverhøi & Dowdeswell 1991) was to study the major climatic variations over the past 5 million years, driving mechanisms of climate change, and their influence on the environment around the Polar North Atlantic. During this period the cyclical waxing and waning of glaciers has dramatically changed the landscape and depositional environments along the Polar North Atlantic margins (PONAM Final report 1995). The basic approach was to investigate, 1) the glacial history and climatic development between the East Greenland and Svalbard continental margins, and 2) the correlation between terrestrial signals and the adjacent marginal area and deep-sea marine records for the latest interglacial-glacial cycle (approximately 130 - 10 ka). For time scales younger than 30 ka an absolute chronology can established by means of AMS ^{14}C datings which are used to correlate various short-events and the reconstruction of the paleoclimate and paleoceanography (Elverhøi & Dowdeswell 1991).

The present study attempts, 1) to establish a stable oxygen isotope stratigraphy from the western part of the Greenland Sea for the last two glacial-interglacial cycles using the planktonic foraminifer *N. pachyderma* sin.; 2) to reconstruct sedimentary processes and paleoenvironments, and paleoclimatic and paleoceanographic changes along the East Greenland continental margin throughout the glacial-interglacial cycles of the late Quaternary; 3) to correlate the terrestrial signals with those in the marine records along the East Greenland continental margin over the past 200 ka; 4) to correlate the millennial-scale climate events documented in Greenland deep-sea sediments with the Dansgaard-Oeschger cycles recorded in the GRIP ice core during the last glacial period. Furthermore, this study will focus on the correlation between the ice-rafted debris (IRD) events of the Greenland Sea and the North Atlantic Heinrich events in order to address the question of whether or not the Greenland Ice Sheet fluctuated coherently with the Laurentide Ice Sheet during the last glaciation.

2. PHYSIOLOGICAL SETTING

2.1 Bathymetry

The Greenland-Iceland-Norwegian (GIN) Sea is connected in the north to the Arctic Ocean via the Fram Strait, and linked in the south to the North Atlantic Ocean through the Denmark Strait and the Iceland-Færoe Island-Shetland Channel. The complex bathymetry and sea floor of the GIN Sea is a result of the Cenozoic plate tectonic development in relation to the opening of the Greenland-Norwegian Sea (Talwani & Eldholm 1977). In the GIN Sea, the three major basins, (Greenland/Boreas, Norwegian, and Lofoten basins) are separated by the mid-oceanic ridge system and several fracture zones (e.g. Vogt 1986). The Norwegian Sea comprises two abyssal plains associated with the Norwegian and Lofoten Basins, and the Vøring Plateau. The Greenland Fracture Zone separates the Greenland Basin into the northern Boreas and southern Greenland basins. The Iceland Sea, subdivided into the western and eastern plateaus by the Kolbeinsey Ridge, is the region between Greenland, Iceland, and Jan Mayen. The study area covers the western part of the Greenland Sea and Iceland Sea (72-68°N; 22-17°W) (Figs. 1-2). The bathymetry of the GIN Sea is described in more detail elsewhere (Johnson & Eckhoff 1966; Perry et al. 1980; Johannessen 1986; Perry 1986; Hopkins 1991).

2.2 Hydrographic structure and circulation in the GIN Sea

Figure 3 shows a schematic view of the surface water and deep water circulation, and processes within the Arctic Ocean and the GIN Sea.

2.2.1 Surface currents and water masses

In the GIN Sea, the circulation dynamics and the distribution of water masses are strongly influenced by the seafloor topography (Johannessen 1986; Hopkins 1991). The surface water circulation is mainly controlled by the two major current systems: the North Atlantic Current (NAC) and the East Greenland Current (EGC).

The NAC transports relatively warm (>3°C) and high-saline (>34.9‰) water masses into the GIN Sea through the Færoe-Shetland Channel (Bourke et al. 1987). The NAC flows northward through the Fram Strait into the Arctic Ocean. A westward branch of the NAC diverges before entering the Arctic Ocean, returning via the East Greenland Current (EGC) system, and contributing substantially to the Return Atlantic Intermediate Water (RIMW). The eastward flowing branch of the NAC enters the Barents and Kara seas. In addition, a branch of warm Atlantic Water enters the GIN Sea through the eastern Denmark Strait contributing to the North Irminger Current (NIC).

The EGC transports cold (<0°C) and low-saline (<34.4‰) polar water southward from the Arctic Ocean through the Fram Strait and finally through the Denmark Strait. The polar water occupies the upper layer of the EGC and in places extends down to depths of ~200 m (Aagaard & Coachman 1968a;

Bourke et al. 1987). The depth to which the polar water extends significantly decreases eastward (e.g. Fig. 4). The temperatures of the upper layers of the polar water seasonally deviate from freezing point (Coachman & Aagaard 1974). A branch of the EGC flows eastward north of Jan Mayen, and forms the Jan Mayen Polar Current (JMPC) (Aagaard 1968). Another branch of the EGC
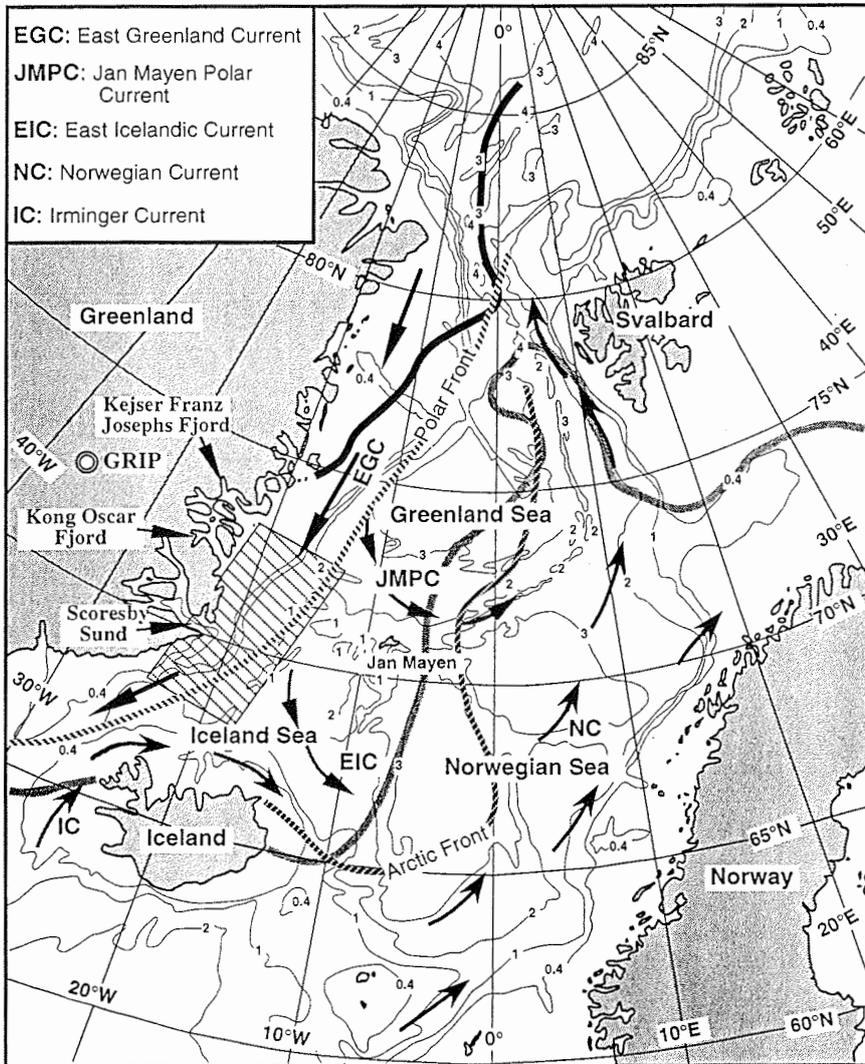
Fig. 1. Bathymetry and major surface current patterns of the Greenland-Iceland-Norwegian Sea (after Perry et al. 1980). Depth contours are in thousand meters. The study area is hatched (*see* Fig. 2). The heavy black line marks typical limit of the ice edge in a mild summer while the heavy gray line marks typical limit of the ice edge in a severe winter (modified after Hurdle 1986). Polar and Arctic oceanic fronts are shown (modified after Quadfasel & Meincke 1987). The abbreviation of GRIP is the Greenland Ice-core Project (Dansgaard et al. 1993).
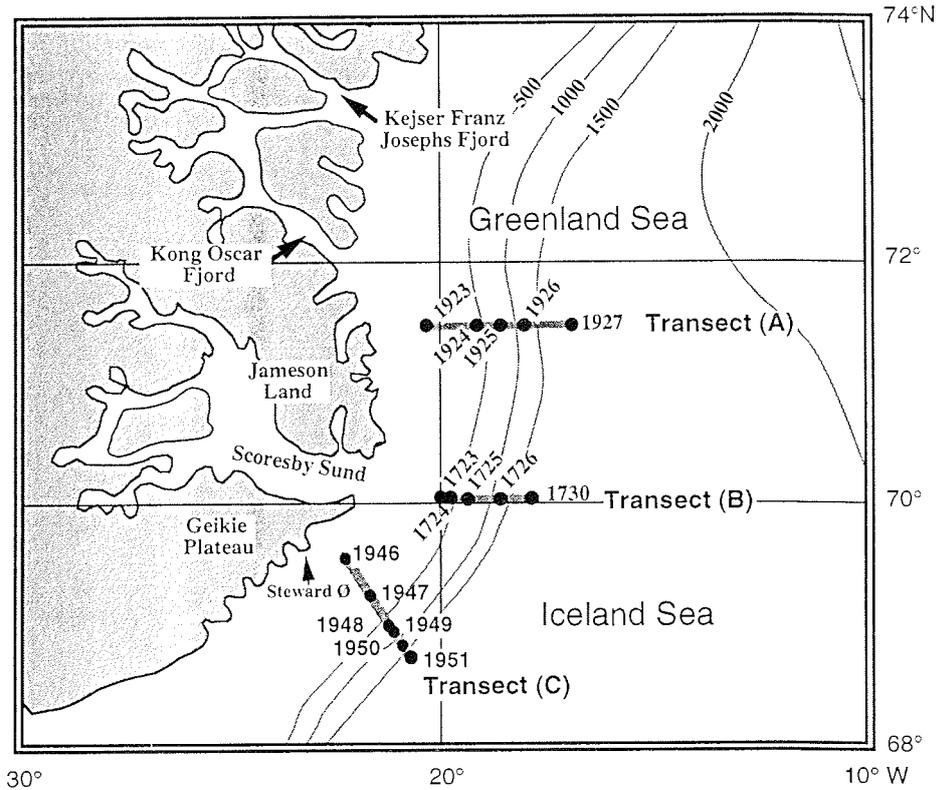
Fig. 2. Study area and core locations along three W-E transects perpendicular to the East Greenland continental margin between 68° and 72°N. Depth contours are in meters.

flows southeast along the continental slope northeast of Iceland forimg the East Icelandic Current (EIC) (Swift & Aagaard 1981; Swift 1986).

In general, there are two pronounced hydrographic regions in the GIN Sea resulting from the influence of Polar and Atlantic water masses (Swift & Aagaard 1981). The region influenced by the Polar water mass is termed the Polar Domain, and the region dominated by the Atlantic water mass is referred to as the Atlantic Domain. A transition zone between the two domains is formed from a mixture of both water masses, and is defined as the Arctic Domain in which the water mass is warmer (0 to 4°C) and more saline (34.4 to 34.9‰) than Polar waters and colder and less saline than Atlantic waters. Furthermore, the different properties of the cold and warm surface water masses create two distinct oceanographic front systems (Hansen & Meincke 1979; Swift & Aagaard 1981; Hopkins 1991): The Polar Front is the boundary between the low saline Polar waters and the high saline Arctic waters; and the Arctic Front is the boundary between the cold Arctic waters and the warm Atlantic waters (Fig. 1). The modern oceanographic conditions of the Polar Front influence the present surface current system in the study area which lies between the eastern continental margin of Greenland and the western Greenland Sea.

8

A

B
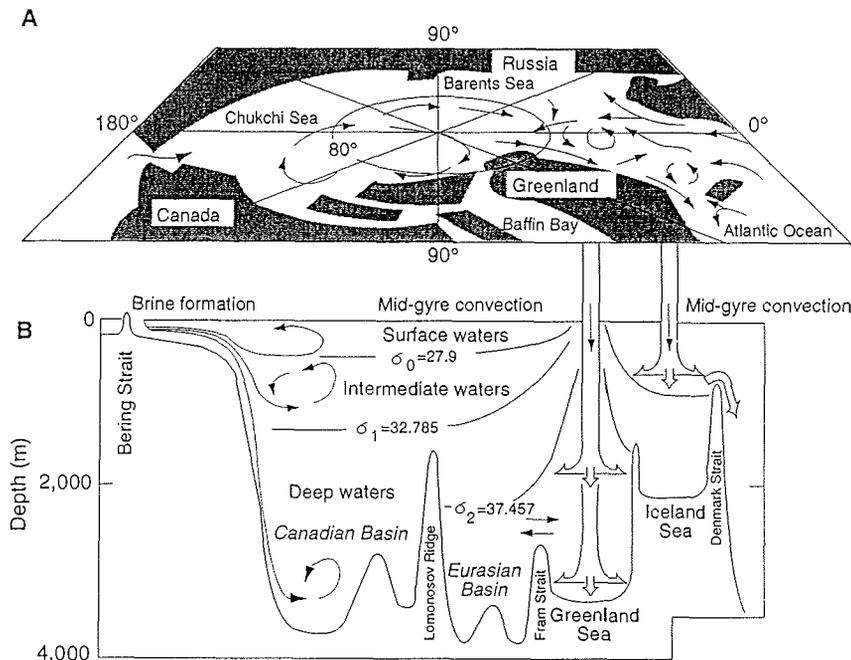
Fig. 3. Schematic drawing of the circulation and water mass structure in the Arctic Ocean and the GIN Sea (after Aagaard et al. 1985). (A) The upper map shows the major elements of the Arctic Ocean and the GIN Sea. (B) The lower panel describes the water budget of northern polar deep-sea basin intermediate and deep water movements. The selected isopycnals (σ_0, σ_1, σ_2) separate surface, intermediate and deep waters. (From Myhre et al. 1995).

2.2.2 Intermediate and deep water masses

The Return Atlantic Intermediate Water (RAIW) mass underlies the Polar Water mass and flows at depths of 150-800 m (Aagaard 1968) along the eastern continental margin of Greenland. The temperature of the RAIW varies between 0 and 2°C, and the salinity between 34.9 and 35.0‰ (Aagaard 1968; Aagaard & Coachman 1968a; Hopkins 1991) (e.g. Fig. 4). The remaining intermediate waters found in the GIN Sea are described in detail in Aagaard and Coachman (1968b) and Hopkins (1991). The temperature of the deep water below the RAIW is less than 0°C and the salinity ranges between 34.87 and 34.95‰ (Aagaard & Coachman 1968a; Hopkins 1991). In the GIN Sea, the deep waters of both the Greenland Sea Deep Water (GSDW) and the Norwegian Sea Deep Water (NSDW), are volumetrically the most dominant water masses (Swift 1986) and play a very important role in the world ocean system. The GSDW is colder (<-1.3°C) and fresher (34.89‰) than the NSDW (~1.05°C, ~34.91‰) (Swift & Koltermann 1988; Hopkins 1991). The characteristics of both the GSDW and NSDW are well summarized in Swift and Aagaard (1981), Swift and Koltermann (1988), and Hopkins (1991).
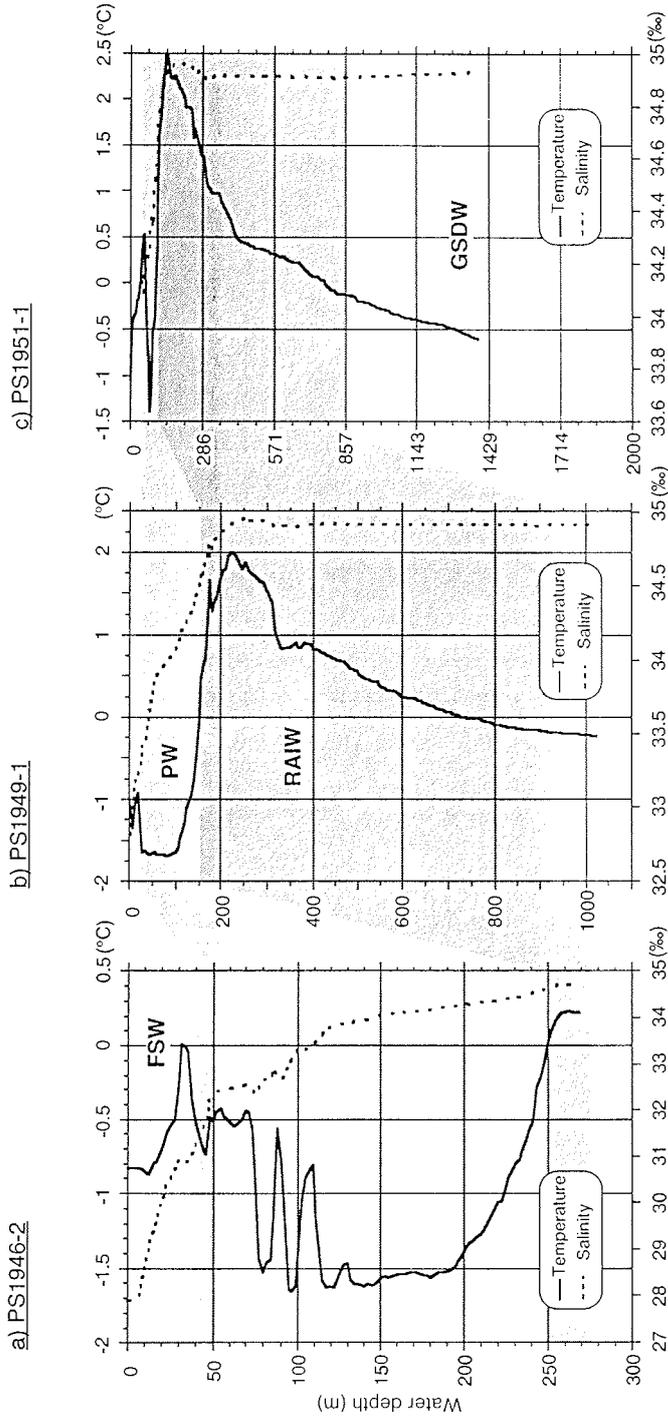
Fig. 4. Temperature and salinity measurements along a W-E transect (Transect C; 68.5°N) from south of Scoresby Sund (see Fig. 2). Temperature and salinity measured with a memory-CTD during the ARK VII/3 (September 27th, 1990). Water mass boundaries are tentatively indicated according to Aagaard & Coachman (1968a), Swift & Aagaard (1981) and Swift (1986), and Hopkins (1991). FSW = Fjord Surface Water; PW = Polar Water; RAIW = Return Atlantic Intermediate Water; GSDW = Greenland Sea Deep Water.
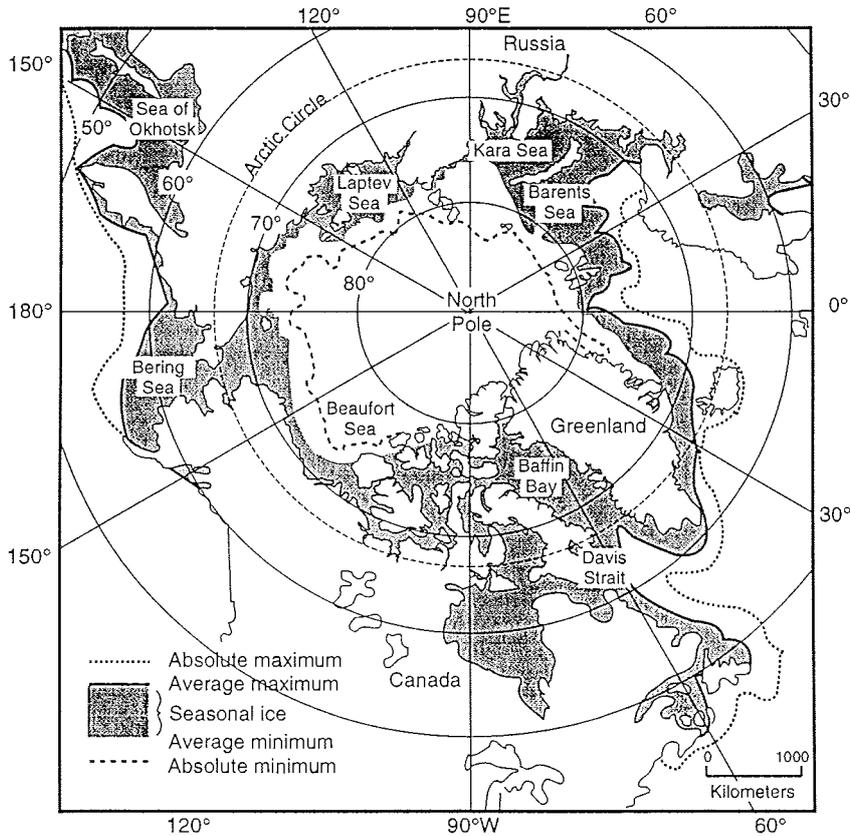
Fig. 5. The mean and extreme sea-ice limits (>1/8-ice) in the northern subpolar and polar oceans after CIA (1978) and Barry (1989). Adapted from Myhre et al. (1995).

2.3 Sea ice, pack ice, and icebergs

In the Greenland Sea, three characteristic types of ice are observed in the form of sea ice, icebergs, and pack ice. The ice cover on the Greenland Sea exhibits a seasonal, annual, and interannual variability (Vinje 1977). The properties of surface currents control the ice formation and ice cover: the advection of warm and saline water masses inhibits ice formation, while the advection of cold and low saline water masses accelerates the formation (Hopkins 1991). The mean ice edge corresponds approximately to the surface manifestation of the Polar Front (PF) (Paquette et al. 1985). Normally, the East Greenland continental margin is covered with sea ice from October to late June. In addition, the area of maximum ice extent within the Greenland Sea occurs during March, whereas the minimal extent of the ice cover occurs during September (e.g. Vinje 1977). In other words, the summer sea-ice margin lies to the west of the Polar Front, whereas the maximum winter sea-ice margin extends to the west of the Arctic Front (Figs. 1 & 5).

11

A large volume of icebergs are derived from fast-flowing outlet glaciers of the Greenland Ice Sheet (Dowdeswell et al. 1993). Along the East Greenland continental margin, the supply and drift of icebergs into the EGC is controlled by the prevailing conditions of the adjacent large fjord systems (e.g. Scoresby Sund and Kong Oscar Fjord) and ice dynamics of Greenland Ice Sheet. The icebergs discharged along the East Greenland continental shelf are often grounded and/or trapped (Dowdeswell et al. 1991, 1993; Hopkins 1991; Mienert et al. 1992). In contrast, most East Greenland icebergs drift through the major fjord systems and reach the Greenland continental margin in significant numbers (Robe 1980; Reeh 1989; Dowdeswell et al. 1992).
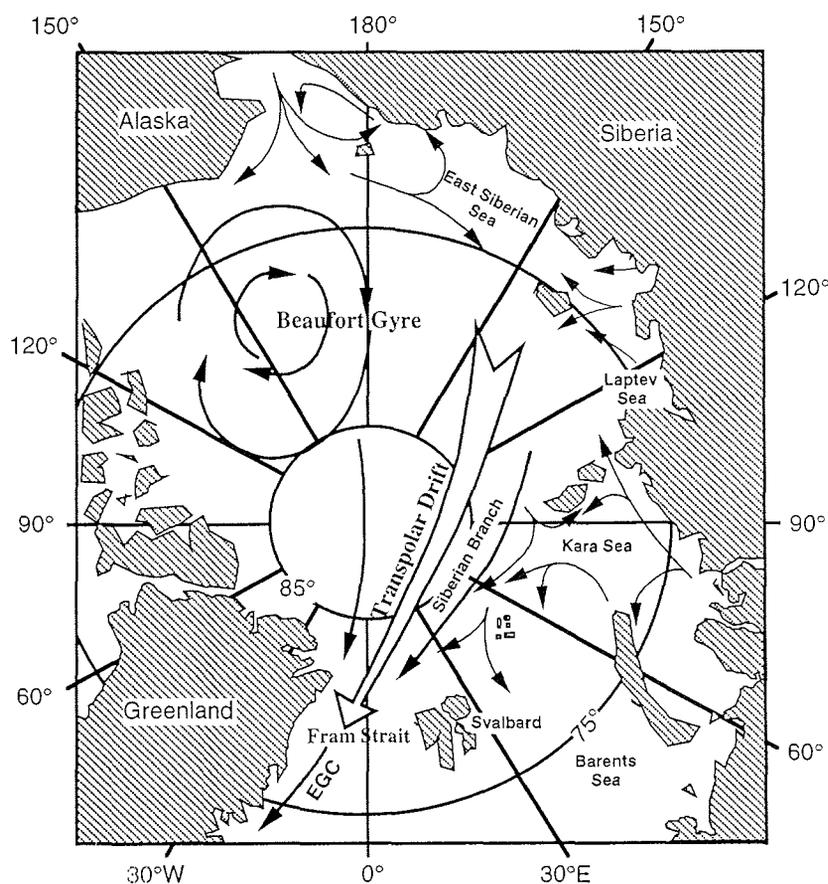
Fig. 6. Mean sea-ice drift within the Arctic Ocean and its transport through the Fram Strait into the Greenland Sea via the EGC (East Greenland Current) (after Gordienko & Laktionov 1969).

About 95 % of all the pack ice that originates from the Arctic Ocean is transported through the Fram Strait into the western Greenland Sea via the EGC (Kvambekk & Vinje 1993) (Fig. 6). Changes in the input of pack ice into the Greenland Sea is related primarily to the variability in current transport. The thickness of multi-year pack ice varies from 3 to 10 m (Hastings 1960;

the Greenland Sea is related primarily to the variability in current transport. The thickness of multi-year pack ice varies from 3 to 10 m (Hastings 1960; Wadhams 1986; Weeks 1986), and from 0.2 to rarely more than 2 m for first-year ice (Weeks 1986). First-year ice usually melts entirely during ice break up. The amount of first-year pack ice changes seasonally (Weeks 1986). The boundary between the pack ice and open waters is referred to as the marginal ice zone (MIZ) which may be on the order of 100 km wide (Hopkins 1991). Furthermore, the leads or open waters, termed polynyas (Wadhams 1986), are commonly found within the pack-ice covering the East Greenland continental margin, and are produced by various mechanisms that include surface water transport divergence. In particular, the polynya adjacent to the Scoresby Sund system resulted from both powerful tidal currents and an outflow of fresh water from fjords (Wadhams 1986).

3. MATERIAL AND METHODS

3.1 CORE MATERIAL

During the expeditions, ARK V/3 (1988) and ARK VII/3 (1990) of R.V. *Polarstern*, sediment cores were recovered by the giant box core (GKG) and gravity core (SL) methods along three west-east transects running from the East Greenland continental margin to the deep sea (Fig. 2 & Table 1). On board Polarstern, each gravity core was cut into 1 m sections and kept horizontal in cold storage (4°C) until the core was split. The selection of the geological sampling locations was based on high-resolution 3.5 kHz sediment ecosoundings during ARK V/3, and Parasound and Hydrosweep profiling during ARK VII/3. A total of 16 gravity cores and 2 box cores were investigated in this study.

Table 1. Core numbers, coring method, geographical positions, water depth of cores, and core length investigated. GKG is Großkarstengreifer. SL is Schwerelot.

Cruise	Core no.	Coring method	Latitude (°N)	Longitude (°W)	Water depth (m)	Core length (cm)
ARK-V/3	PS1723-1	SL	70°07.1′	19°59.9′	283	85
ARK-V/3	PS1724-2	SL	70°07.2′	19°13.3′	363	129
ARK-V/3	PS1725-2	SL	70°06.9′	18°49.9′	879	516
ARK-V/3	PS1726-1	SL	70°07.0′	18°38.9′	1174	600
ARK-V/3	PS1730-2	SL	70°07.2′	17°42.1′	1617	779
ARK-V/3	PS1726-2	GKG	70°06.6′	18°38.1′	1182	41
ARK-V/3	PS1730-1	GKG	70°07.0′	17°41.7′	1622	37
ARK-VII/3	PS1923-2	SL	71°29.7′	20°31.0′	260	98
ARK-VII/3	PS1924-1	SL	71°30.0′	19°10.9′	288	105
ARK-VII/3	PS1925-2	SL	71°30.0′	18°43.5′	811	215
ARK-VII/3	PS1926-1	SL	71°29.6′	18°16.5′	1493	319
ARK-VII/3	PS1927-2	SL	71°29.7′	17°07.1′	1734	491
ARK-VII/3	PS1946-2	SL	69°36.3′	22°22.6′	320	50
ARK-VII/3	PS1947-1	SL	69°16.5′	21°45.6′	379	50
ARK-VII/3	PS1948-2	SL	69°04.4′	21°17.3′	624	255
ARK-VII/3	PS1949-1	SL	68°59.1′	21°09.0′	1106	411
ARK-VII/3	PS1950-2	SL	68°53.4′	20°55.7′	1480	421
ARK-VII/3	PS1951-1	SL	68°50.5′	20°49.2′	1481	789

3.2 METHODS

3.2.1 MAGNETIC SUSCEPTIBILITY

The magnetic susceptibility is proportional to the concentration of magnetic minerals per unit sediment mass. The principle and measurement of magnetic susceptibility are described in detail elsewhere, e.g. Cordes (1990) and Norwaczyk (1991). The magnetic susceptibility (10^{-5} SI) was measured on

gravity cores prior to opening. Measurements were made using a Bartington M.S.2.C Magnetic Susceptibility Meter with a core scanning sensor with an internal diameter of 135 mm. The measurement was performed continuously at 1-2 cm intervals on board Polarstern during ARK VII/3 (1990), and at the AWI for three cores (PS1725-2, PS1726-1, and PS1730-2) recovered during ARK V/3 (1988).

3.2.2 CORE DESCRIPTION AND SAMPLING

Each core section was longitudinally split with a double-edged vibration saw: One half of the split core was chosen as the working part and the other as the archive part. Both halves of the split cores were photographed. The archive half of each core section was visually described to include all sedimentary features such as colour, lithological change, laminations, bioturbation, dropstones, etc. The sediment colours were described according to the Munsell Soil Colour Charts (1954).

The working half sediments of each core section were routinely sampled at 10 cm intervals, or where there were changes in lithology and/or colour, additional samples were taken. At each sample interval a number of subsamples were taken for detailed sedimentological, organic-geochemical, and stable oxygen and carbon isotope analyses, and to determine AMS ^{14}C-dates. In addition, samples from giant box cores (GKG) were taken at 3 to 5 cm intervals.

3.2.3 X-RADIOGRAPHS AND ICE-RAFTED DETRITUS (IRD)

Prior to sampling, X-radiographs were made in order to investigate sedimentary structures and to determine the coarse-grained detritus (>2 mm) (IRD) content. The working half was divided into ca. 10 * 27.5 cm sections with 1 cm thick plastic slabs and then sealed within non-colour vinyl plastics. All sediment slabs were X-rayed with 30-35 kV and 3 mA for 10-13 minutes using a 'Hewlett Packard' X-ray machine (Model 43855 A). The exposure time and kilovoltage (kV) were mainly dependent on the lithological nature of the sediments.

Using the X-radiographs, the ice-rafted detritus (IRD) content was evaluated by counting the coarse-grained detritus (>2 mm) for every 1 cm intervals (Grobe 1987). The IRD values were smoothed by a 5-point moving average filter in order to eliminate high-frequency perturbations.

3.2.4 PHYSICAL SEDIMENT PROPERTIES

In order to investigate physical properties such as water content, porosity, and grain density the sediments were sampled with a 5 ml plastic syringe. The wet sediment samples were weighed and then freezed for 24 hours. These samples were further freeze-dried for another 24 hours using a freeze-dryer (Lyoval GT2, Leybold-Heraeus) and then weighed again. The water content was calculated using equation 3·1:

$$\text{water content (\%)} = \frac{(\text{wet weight - dry weight})}{\text{wet weight}} * 100 \qquad [3 \cdot 1]$$

The freeze-dried 5 cm^3 samples were homogeneously powdered using a ball-bearing mill. Grain density (Gd) was measured on the powdered sediments using a Beckmann Air Comparison Pycnometer (Model 930). The wet density (W$_d$) and porosity (PO) were calculated using equations 3·2 and 3·3 respectively (Gealy 1971; Hamilton 1971):

$$\text{wet density (g/cm}^3\text{)} = 100 / ((100 - H_2O) / G_d - H_2O * 3.5 / (96.5 \bullet 2.1) + H_2O * 100 / (96.5 * 1.024)) \qquad [3 \cdot 2]$$

$$\text{porosity (\%)} = 100 * (H_2O * 100 / (96.5 * 1.024)) / ((100 - H_2O) / G_d - H_2O * 3.5 / (96.5 * 2.1) + H_2O * 100 / (96.5 \bullet 1.024)) \qquad [3 \cdot 3]$$

where

H_2O = water content (%), G_d = grain density (g/cm^3),
1.024 = density (g/cm^3) of sea water at 23°C,
3.5 = salinity (%),
and 2.1 = salt density (g/cm^3).

3.2.5 DETERMINATION OF ORGANIC CARBON, CARBONATE, NITROGEN, AND SULPHUR CONTENTS

Organic carbon and carbonate contents were determined on all samples collected from nine cores (*see* Appendix B) using a Heraeus CHN-Analyser. In order to control the accuracy of the measured values, acetanilid and a homogeneously powdered Lias-black shale (ST 001) were used as the standard reference material. Approximately 30 mg of the powdered bulk sediments were analysed to determine the total carbon content (TC %). Prior to determining the total organic carbon content (TOC %), the bulk sediments were first treated with 10 %-HCl for 24 hours to remove the carbonate. The residues were washed three to five times with deionized water and dried in an oven at 50°C. The carbonate-free sediments were again homogenized using an agate mortar, and approximately 30 mg of the carbonate-free sediment (TOC′ %) were analyzed using the Heraeus CHN-Analyser. The total organic carbon content of the bulk sediment (TOC %) was calculated using equation 3·4:

$$\text{TOC (\%)} = \frac{[100 - (8.333 * TC)]}{[(100 / TOC') - 8.333]} \qquad [3 \cdot 4]$$

The carbonate content (%) was calculated using equation 3·5:

$$CaCO_3 \text{ (\%)} = (TC - TOC) * 8.333 \qquad [3 \cdot 5]$$

16

assuming that the carbonate is predominantly composed of calcite.

In addition, the total carbon (TC) and total sulphur (TS) content of all six shelf cores (PS1923-2, PS1924-1, PS1723-1, PS1724-2, PS1946-2, and PS1947-1) and three slope cores (PS1925-2, PS1948-2, and PS1949-1) were determined using a LECO CS-125 Analyser (Carbon-Sulphur Determinator) (*see* Appendix B). The total organic carbon (TOC) was determined with the LECO CS-125 analyser following the treatment of the powdered sediments with 35 %-HCl to remove the inorganic (carbonate) carbon. The inorganic carbon (IC %) was calculated using equation 3·6:

$$IC\ (\%) = TC\ (\%) - TOC\ (\%)\qquad\qquad [3·6]$$

and the carbonate content was calculated using equation 3·7:

$$CaCO_3\ (\%) = IC\ (\%) * 8.333\qquad\qquad [3·7]$$
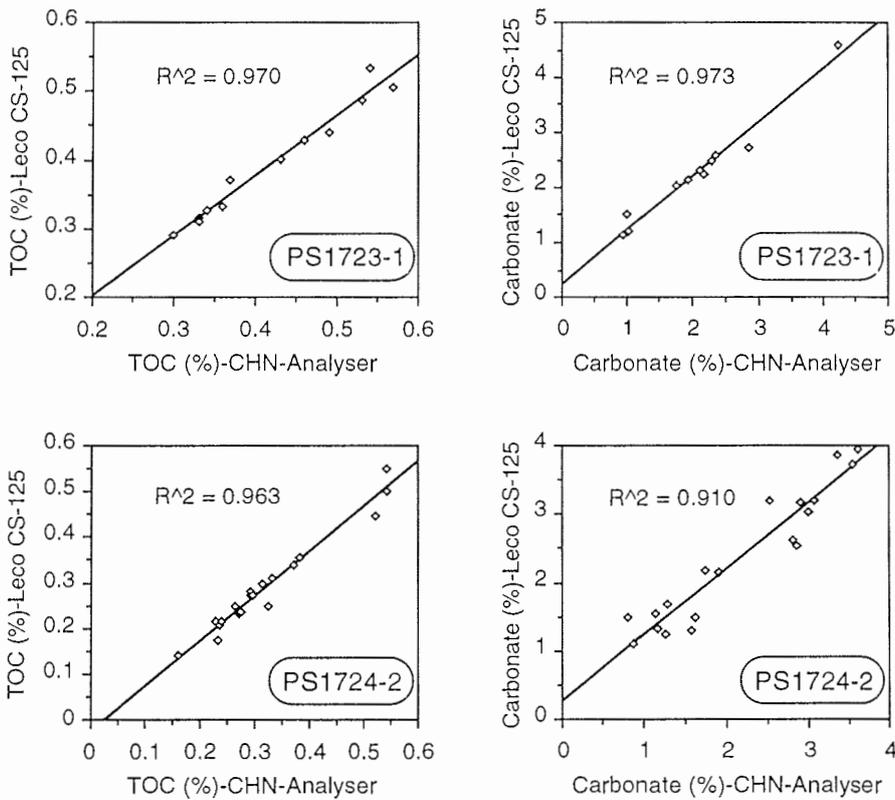
Fig. 7. Correlation between TOC (%) and carbonate (%) measured on the sediments from the shelf (cores PS1723-1 and PS1724-2) using the CHN-Analyser and LECO CS-125.

17

In order to test the extent to which the organic carbon and carbonate data from the CHN and LECO CS-125 analysers can be correlated, measurements were additionally performed on all samples from two shelf cores (PS1723-1 and PS1724-2) using the same laboratory techniques. Both data sets correlate well (Fig. 7).

Total organic carbon to total nitrogen (C/N) ratios were calculated in order to characterise the organic matter composition of Quaternary marine sediments (cf. Stein 1991 & further references therein). In general, organic matter in marine sediments are either of a marine or terrestrial origin (Emerson & Hedges 1988). The mean C/N ratios of organic matter produced by marine plankton are approximately 6-7, whereas mean C/N ratios of more than 15 correspond to terrigenous organic matter (Redfield et al. 1963; Bordowskiy 1965; Emerson & Hedges 1988; Stein et al. 1989). However, C/N ratios must be cautiously interpreted in organic-carbon-poor sediments (cf. Stein et al. 1989). In these sediments, the amount of inorganic nitrogen (fixed as ammonium ions in the interlayers of clay minerals such as illite) may form a major proportion of the total nitrogen causing a lowering in C/N ratios (e.g. Müller 1977).

In addition, the total organic carbon to total sulphur (C/S) ratios were calculated and are listed in Appendix D.

3.2.6 ROCK-EVAL PYROLYSIS

Rock-Eval pyrolysis was carried out on bulk sediment samples in order to determine the type of organic matter. The classification of the type of organic matter is based on the hydrogen and oxygen richness, and temperature of maximum pyrolysis yield (T_{max} values). The procedure and operating technique of this method are described in detail in Espiltalié et al. (1977), Tissot & Welte (1984), and Dean et al. (1994). The powdered sample (ca. 100 mg) was progressively heated to 550°C under an inert atmosphere using a special temperature programme. Pyrolysis took place in three stages (S_1, S_2 and S_3 peaks) (Fig. 8). The S_2 and S_3 peaks, as calibrated and normalized to organic carbon (C-org %), yield a hydrogen index and an oxygen index displayed as HI (mgHC/gC) and OI (mgCO$_2$/gC), respectively. In immature sediments, the indices are mainly dependent on the elemental composition of the organic matter (Tissot & Welte 1984). Furthermore, the temperature (T_{max}) corresponding to the maximum hydrocarbon generation during pyrolysis is used to evaluate the thermal maturity of the organic matter.

3.2.7 GRAIN-SIZE DISTRIBUTION

To analyse the grain-size distribution, 5 cm^3 of sediment was oxidized with 3 %-H$_2$O$_2$ for 24 hours. Concomitantly the mixture was agitated using a shaking table in order to disperse the sediments. The samples were wet-sieved through a 63 μm mesh to separate the coarse fraction (>63 μm). The coarse fraction was dried at 50°C, and sieved into gravel and sand fractions.

The clay and silt fractions was separated using the Atterberg method (settling time based on Stoke's Law). The sediment particles (<63 μm) were dispersed

18

by the addition of deionized water mixed with ca. 0.001 %-ammonia solution (NH$_3$) and compressed using an air pump. The sediments were allowed to settle for 20-24 hours under corresponding temperatures of 24-19°C, respectively. The suspended particles (<2 µm) were removed and collected into 5 l plastic buckets. Approximately 20 ml of a 50 %-MgCl$_2$ solution were added to the content of each plastic bucket in order to induce agglomeration and settling of the suspended particles. The entire process was repeated 9 to 12 times until the amount of clay remaining in the samples was negligible. In order to remove the 50 %-MgCl$_2$ solution, the clay fraction was centrifuged twice for 10 and 20 minutes at 5500 R.P.M. and the clear supernatant water decanted. The clay fraction was dried at 50°C and weighed. The silt fraction residue remaining in the cylinders was dried at 50°C and weighed. Each fraction was calculated as weight-% of the total sediment.
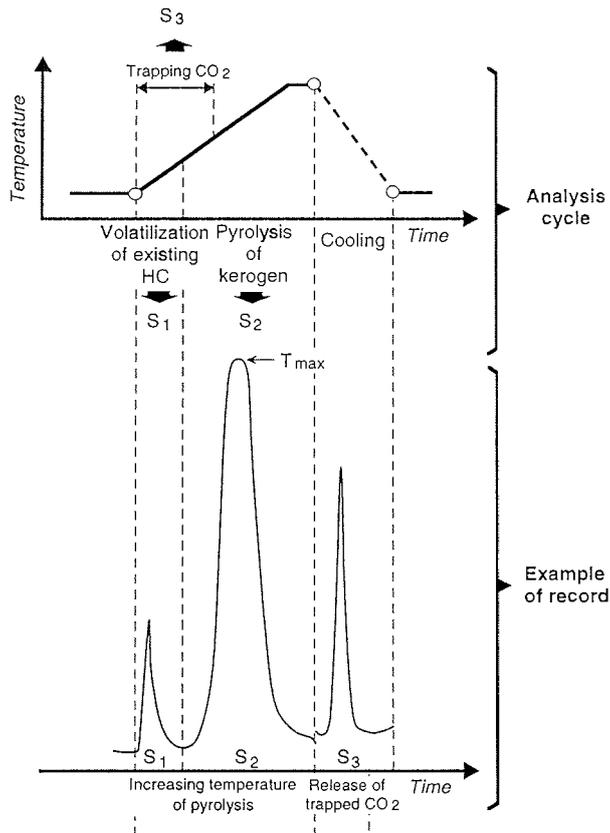
Fig. 8. Cycle of analysis and example of record obtained by the pyrolysis method of Espitalié et al. (1977). Adapted from Tissot & Welte (1984).

19

3.2.8 COMPONENT ANALYSIS

Approximately 30 cm^3 of sediment was sampled and wet-sieved through a 63 μm sieve. The >63 μm fraction was dried at 50°C and further sieved for 10 minutes using a dry-screening sieve machine (AMT Sonic Sifter, Model L3P) with five different size-meshes. The coarse fraction was separated into six different size-subfractions of 63-125, 125-250, 250-500, 500-1000, 1000-2000 μm. The gravel content within the fraction between 4 and 2 mm was counted and weighed. Each sand subfraction was weighed and expressed as a percentage relative to the total sand fraction. In cores PS1726-1 and PS1730-2, the 125-250 μm subfraction was used for the component analysis as it contains both siliciclastic and biogenic components. Approximately 500 grains were counted from the 125-250 μm subfraction using a binocular microscope. Components were classified into siliciclastic components (quartz+feldspar, rock fragments, mica, basalt) and biogenic components (calcareous planktonic foraminifers, calcareous benthic foraminifers, agglutinated benthic foraminifers, biogenic opal such as radiolarians, diatoms, and sponge spicules), and volcanic ash. The amount of each component was expressed in grain-% of the coarse fraction.

3.2.9 STABLE OXYGEN AND CARBON ISOTOPE MEASUREMENTS

Using a Finnigan MAT 251 mass spectrometer, stable oxygen and carbon isotope measurements were performed on 6-8 specimens per sample of the planktonic foraminifer *Neogloboquadrina pachyderma* (Ehrenberg) sin.. For this study, isotope analyses were carried out on 10-13 specimens of the benthic foraminiferal species *Oridorsalis umbonatus* (Reuss) from deep-sea core PS1730-2. Both species were picked from the 125-250 μm subfraction.

Stable isotope measurements were further performed on 2-3 specimens of the benthic foraminifer *Cibicidoides wuellerstorfi* (Schwager) as this species is indicative of interglacial stages (e.g. 5, 3, and the Holocene) (e.g. Streeter et al. 1982; Vogelsang 1990). *C. wuellerstorfi* appeared exclusively within interglacial stage 5 and the Holocene of the three deep-sea cores (PS1927-2, PS1730-2, and PS1951-1). This species was picked from the 250-500 μm subfraction.

The oxygen and carbon isotope ratios were calculated as relative deviations (per mil) from the mean ratios of a standard value (Shackleton & Opdyke 1973) as shown in equations 3·8 and 3·9:

$$\delta^{18}O = \frac{\{(^{18}O/^{16}O)\ sample - \{(^{18}O/^{16}O)\ standard\}}{\{(^{18}O/^{16}O)\ standard\}} * 1000 \quad [3\text{·}8]$$

$$\delta^{13}C = \frac{\{(^{13}C/^{12}C)\ sample - \{(^{13}C/^{12}C)\ standard\}}{\{(^{13}C/^{12}C)\ standard\}} * 1000 \quad [3\text{·}9]$$

The isotope composition was measured against a laboratory standard_which is calibrated to the PDB (Pee Dee Belemnite) scale using the National Bureau of Standard (NBS-20). The standard deviation of the measurements are 0.06‰ for $\delta^{18}O$ and 0.04‰ for $\delta^{13}C$ (Hubberten & Meyer 1989). The $^{18}O/^{16}O$ and $^{13}C/^{12}C$ isotopic ratios are expressed as $\delta^{18}O$ and $\delta^{13}C$ versus the PDB standard.

The $\delta^{18}O$ record of *C. wuellerstorfi* was adjusted to seawater equilibrium by adding of +0.64‰ versus the reference species *Uvigerina peregrina* (Cushman) (Duplessy et al. 1984) while $\delta^{13}C$ values are unadjusted. In contrast, the $\delta^{18}O$ record of *O. umbonatus* can be calibrated by comparing the $\delta^{18}O$ values of *O. umbonatus* and *C. wuellerstorfi*. Therefore, the $\delta^{18}O$ of *O. umbonatus* was adjusted by the addition of +0.36‰ to the measured values (Duplessy et al. 1988b; Vogelsang 1990).

3.2.10 AMS ^{14}C-AGE DATING

In contrast to the conventional method of $^{14/12}C$ measurement, the accelerator mass spectrometry (AMS) ion counting technique allows the determination of radiocarbon ages from small-sized samples (e.g. about 40-50 mg of *N. pachyderma* sin.). The AMS ^{14}C dating method provides the basis for establishing a high-resolution stratigraphy for the last 50 ka in deep-sea sediment cores (Bard 1988). AMS ^{14}C-age dating was carried out on twenty-six samples from seven selected sediment cores. About 2,000 specimens of the planktonic foraminifer *N. pachyderma* sin. from the 125-250 μm size-fraction per sample were hand-picked for absolute age determination. The measurement was performed at the AMS ^{14}C dating laboratory of the Institute of Physics and Astronomy, Åarhus University, Denmark. For a comparison of marine AMS ^{14}C records with terrestrial climatic events, AMS ^{14}C dated ages were subtracted by 550 years to account for the radiocarbon difference between the atmosphere and the surface waters of the ocean (Stuiver et al. 1986).

3.2.11 LINEAR SEDIMENTATION RATE AND MASS ACCUMULATION RATE

The linear sedimentation rates (LSR; cm/kyr) were calculated using the oxygen isotope stratigraphy and AMS ^{14}C-age datings. Mass accumulation rates (MAR; g cm^{-2} kyr^{-1}) were calculated from LSR, wet bulk densitiy, and porosity following van Andel et al. (1975):

$$MAR = LSR * \{WBD - 1.026 * (PO/100)\} \qquad [3\cdot10]$$

where

LSR = linear sedimentation rate (cm/kyr),
WBD = wet bulk density (g/cm^3), and
PO = porosity (%).

The accumulation rates of individual sediment components (organic carbon, carbonate, and terrigenous matter; MAR_{cpx}) were calculated from bulk sediment accumulation rates using equation 3·11:

$$MAR_{cpx} = (CP/100) * MAR \qquad [3·11]$$

where
CP_x = sediment component (%).

The accuracy of the accumulation rate is strongly dependent on the stratigraphic resolution of the AMS ^{14}C dated fix points used for calculation of the LSR (e.g. Bohrmann et al. 1990).

4. STRATIGRAPHY AND CHRONOLOGY

Precise stratigraphic correlation and age control of sediment cores are necessary for the reconstruction of the paleoclimatic and paleoceanographic history in relation to late Quaternary glacial-interglacial cycles. The age control and stratigraphic correlation of all investigated sediment cores are based primarily on stable oxygen and carbon isotope records obtained from the planktonic foraminifer species *N. pachyderma* sin. (Figs. 9-10). In addition, the benthic foraminifer *O. umbonatus* from the deep-sea core PS1730-2, is further used for stratigraphic correlation (Fig. 12). Reference ages were derived from the $\delta^{18}O$ record by detailed correlation with the SPECMAP stacked $\delta^{18}O$ signal (Martinson et al. 1987). The determination of ages younger than approximately 30 ka are based on twenty six AMS ^{14}C dates (Table 2 & Fig. 11). AMS ^{14}C ages measured from the planktonic foraminifer *N. pachyderma* sin. are corrected by 550 years for ocean reservoir effects. Furthermore, specific volcanic ash layers are used for detailed stratigraphic age control and correlation. In addition, other terrigenous and biogenic parameters showing significant single peaks were used to define the stratigraphic framework of the sediment cores. The five long sediment cores PS1725-2, PS1726-1, PS1730-2, PS1927-2, and PS1951-1 were chosen to obtain a detailed stratigraphic framework because of their high-resolution stratigraphy.

4.1 STRATIGRAPHY OF THE LAST GLACIAL STAGE 2 TO THE HOLOCENE

The last glacial stage 2 is characterised by markedly heavy $\delta^{18}O$ values of 4 to 4.66‰. The coldest phase of isotope stage 2 lasted about 5 kyr (~20-15 ka). The boundary between oxygen isotope stages 3 and 2 within the five long cores investigated is dated at 24.9 ka (Table 3 & Figs. 9-11). A distinct shift in $\delta^{18}O$ values of 1.14 to 2.24‰ is recorded in the three deep-sea cores (PS1730-2, PS1927-2, and PS1951-1) and is indicative of Termination Ia. Termination Ia represents the lower part of the transition between isotope stages 2 and 1. The shift of $\delta^{18}O$ values at Termination Ia is to some extent higher than compared to the global ice effect of about 1.3‰ (Duplessy et al. 1984; Shackleton et al. 1984; Chappell & Shackleton 1986; Labeyrie et al. 1987).

The onset of Termination Ia is dated in deep-sea core PS1730-2 at approximately 15.8 ka, which is about 1.8 ka earlier than that at the two slope cores PS1725-2 and PS1726-1 from the same profile adjacent to Scoresby Sund (Fig. 11). Termination Ia began at approximately 15 ka in two cores PS1926-1 and PS1927-2 from the northern profile adjacent to Carlsberg Fjord (Fig. 11). A similar date for the transition from the LGM to the last deglaciation event is recorded within cores PS1950-2 and PS1951-1 from the northwestern Iceland Plateau (Fig. 11). During the Holocene, no isotope data are available from cores PS1725-2 and PS1726-1 as both slope cores are barren of calcareous foraminiferal tests.

In deep-sea core PS1730-2, a shift to heavy $\delta^{18}O$ values prior to a shift to light $\delta^{18}O$ values of Termination Ib represent the Younger Dryas Event (Broecker et al. 1988b; Fairbanks 1989; Duplessy et al. 1993). This event was further

23

identified by means of the Vedde ash (10.6 ka; Mangerud et al. 1984) in many deep-sea cores from the GIN Sea and the northern North Atlantic together with in the ice cores on Greenland. The occurrence of the Vedde ash layer is recorded within two slope cores PS1725-2 and PS1726-1 and the deep-sea core PS1730-2 at depths of 20 cm, 40 cm, and 35 cm, respectively. This ash layer is also recorded at a depth of 7 cm in core PS1951-1, from the deep sea of the NW Iceland Plateau. Following the Younger Dryas, a distinct $\delta^{18}O$ shift towards light values is inferred to represent Termination Ib (Duplessy et al. 1981), and AMS dated at 7.9 ka within core PS1730-2. The two shelf cores adjacent to the Carlsberg Fjord may represent the entire Holocene, further supported by the AMS ^{14}C date of 10.4 ka within core PS1923-2. The four other shelf cores on the other hand only represent the upper part of the Holocene (cf. Stein et al. 1993).

Table 2. AMS ^{14}C-age datings of seven sediment cores (measured on the planktonic foraminifer N. pachyderma sin.). Lab no.[*] indicates the sample numbers of the AMS Laboratory at the Institute of Physics and Astronomy, Åarhus University, Denmark. The age of the Vedde ash[†] is after Mangerud et al. (1984). Depth of core PS1730-2 is the corrected core depth.

Core	Lab no.[*]	Core depth (cm)	Age (years)	Reservoir corr. age (years)
PS1923-2	AAR-1300	50	10980±210	10430±210
PS1926-1	AAR-1301	1	540±110	-10±110
	AAR-1302	32	15490±210	14940±210
	AAR-1303	8	6630±90	6080±90
	AAR-1304	52	13760±170	13210±170
PS1927-2	AAR-1305	72	16620±160	16070±160
	AAR-1704	100	18910±210	18360±210
	AAR-1705	140	21240±250	20690±250
	AAR-1306	170	23230±240	22680±240
		40	Vedde ash[†]	10600
	AAR-1149	60	15590±130	15040±130
PS1726-1	AAR-1150	80	18900±170	18350±170
	AAR-1701	90	19950±270	19400±270
	AAR-1151	120	27500±330	26950±330
	AAR-1152	43	8460±110	7910±110
		58	Vedde ash[†]	10600
	ARR-1153	93	14870±140	14320±140
PS1730-2	AAR-1154	103	16820±150	16270±150
	AAR-1155	113	19150±190	18600±190
	AAR-1156	163	23550±360	23000±360
	AAR-1157	183	25450±310	24900±310
	AAR-1158	223	28500±650	27950±650
PS1950-2	AAR-1307	58	14710±140	14160±140
		7	Vedde ash[†]	10600
	ARR-1308	60	15050±130	14500±130
PS1951-1	AAR-1309	72	15840±140	15290±140
	ARR-1702	83	17380±190	16830±190
	AAR-1703	123	19760±240	19210±240
	AAR-1310	156	22060±240	21510±240

The Vedde ash layer is absent from both of the box cores PS1726-2 and PS1730-1 and therefore, they are interpreted to represent a time interval younger than the Younger Dryas. According to oxygen isotope values within box core PS1730-1 (obtained from the same location as the gravity core PS1730-2), the uppermost 23 cm are lost. Therefore, all depths within the gravity core PS1730-2 are corrected by 23 cm. A loss of surface sediments from all investigated cores can not be excluded, but the surface sediments of core PS1926-1 have been dated as recent.

A prominent organic carbon peak dated at approximately 19.9 to 19.2 ka, is also used to correlate between cores. This discrete signal is associated with high C/N ratios, and correlates with an abrupt decrease in the carbonate content (Figs. 20e, 21c,e & 22f). These signals reflect an increased input of terrigenous matter, and relate to a contemporaneous event recorded throughout the GIN Sea as it is clearly identified in many other sediment cores, e.g. from the northern Iceland Plateau and Vøring Plateau (Wagner 1993; Wagner & Henrich 1994), Fram Strait southwest of Spitsbergen (Hebbeln 1991; Hebbeln et al. 1994), and the continental slope of NW Spitsbergen (Knies 1994).

4.1.2 STRATIGRAPHY OF THE LAST 245 ka

The two slope cores PS1725-2 and PS1726-1, and the deep sea core PS1730-2, represent a geological history dating from oxygen isotope stages 7 to 1 (Fig. 9). The bottom of deep sea core PS1927-2 extends back to isotope substage 5.3 whereas deep sea core PS1951-1 is not older than isotope substage 6.5 (Fig. 10).

In the three long cores located on the slope and in the deep sea adjacent to Scoresby Sund, interglacial stage 7 is characterised by relatively light $\delta^{18}O$ and $\delta^{13}C$ values in comparison to other interglacial periods (mostly in the lower part of the sediment sequence), reflecting major meltwater discharge within this interval (Jünger 1994). The occurrence of a specific ash layer at depths of 369 cm (core PS1725-2), 460 cm (core PS1726-1), and 730 cm (core PS1730-2) is also used to identify oxygen isotope stage 7 (Fig. 9). This ash zone, based on the distribution of major elements measured in the volcanic glass particles (cf. Lackschewitz 1991; Lackschewitz & Wallrabe-Adams 1991; Wallrabe-Adams pers. commun. 1993), can be correlated to other deep-sea cores within the GIN Sea (Sejrup et al. 1989; Birgisdórttir 1991; Lackschewitz 1991; Baumann et al. 1993).

During glacial substage 6.2, heavy $\delta^{18}O$ values of 4.60 to 4.68‰ corresponding to light $\delta^{13}C$ values (-0.01 to 0.03 ‰) are clearly recorded in the two slope cores PS1725-2 and PS1726-1, and the two deep-sea cores PS1730-2 and PS1951-1 (Figs. 9 & 10). Distinctly lighter $d^{18}O$ and $d^{13}C$ values occur during substages 6.5 and 6.3, and correspond to regional meltwater events recorded within the GIN Sea (Vogelsang 1990; Jünger 1994). These signals are especially recorded within the three long cores located adjacent to Scoresby Sund (Fig. 9). The timing and pattern of substages 6.2 through to 6.6 are identified in the $\delta^{18}O$ and $\delta^{13}C$ values of both *N. pachyderma* sin. and *O. umbonatus* (cf. Jünger 1994) (Fig. 12).

25
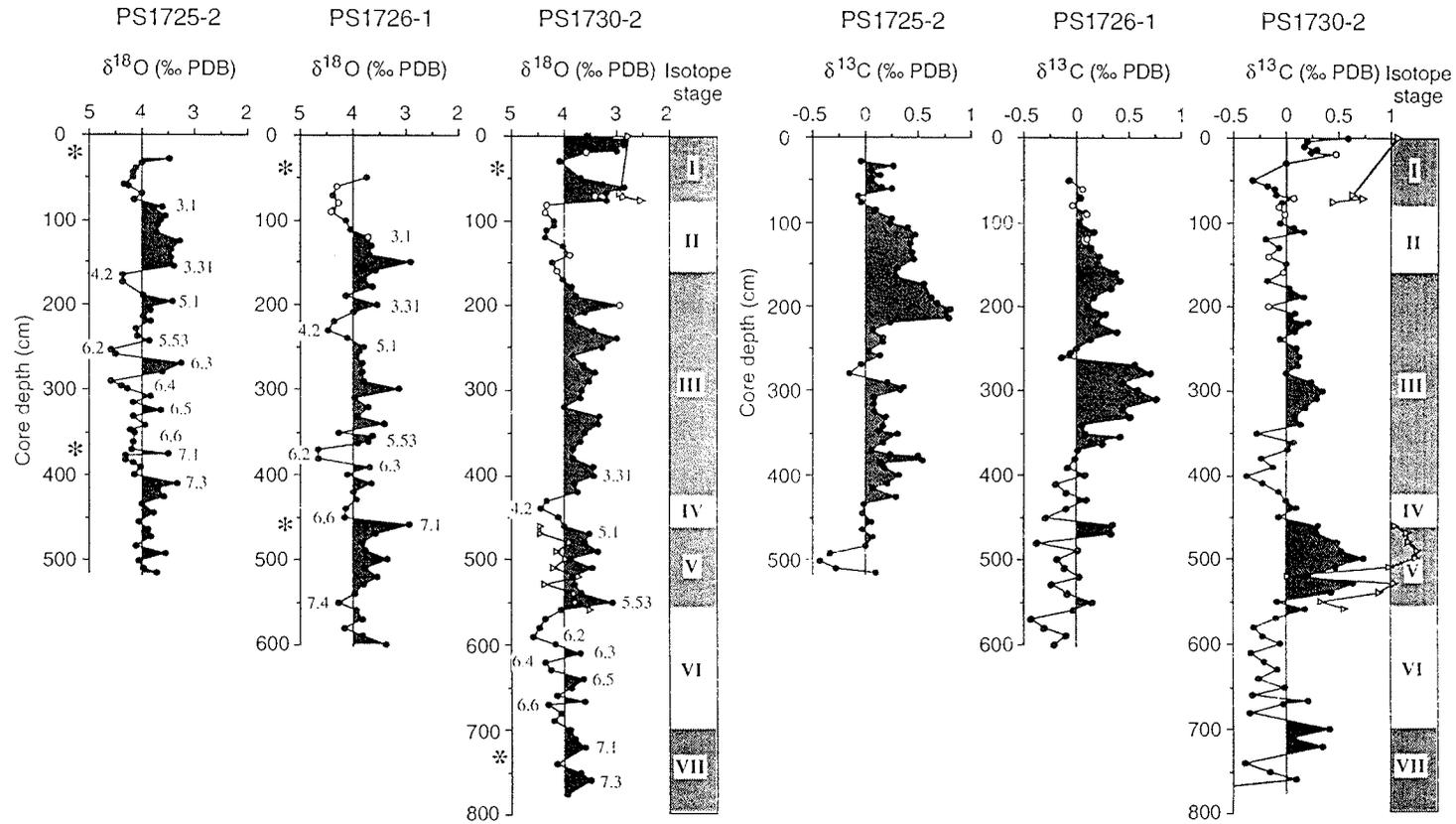
Fig. 9. Isotope stratigraphy of the planktonic foraminifer *N. pachyderma* sin. of slope cores PS1725-2, PS1726-1, and deep-sea core PS1730-2 off Scoresby Sund. Numbers in oxygen isotope records are substages (Martinson et al. 1987). Open circles in the oxygen and carbon isotope records indicate AMS-dated samples (*see* Table 2 & Fig. 11). Open triangles in stages 5 and 1 of core PS1730-2 indicate the oxygen and carbon isotope records of the benthic foraminifer *C. wuellerstorfi*. The benthic $\delta^{18}O$ records have not been corrected (cf. Section 3.2.9). Asterisks within stages 7 and 1 mark volcanic ash layers
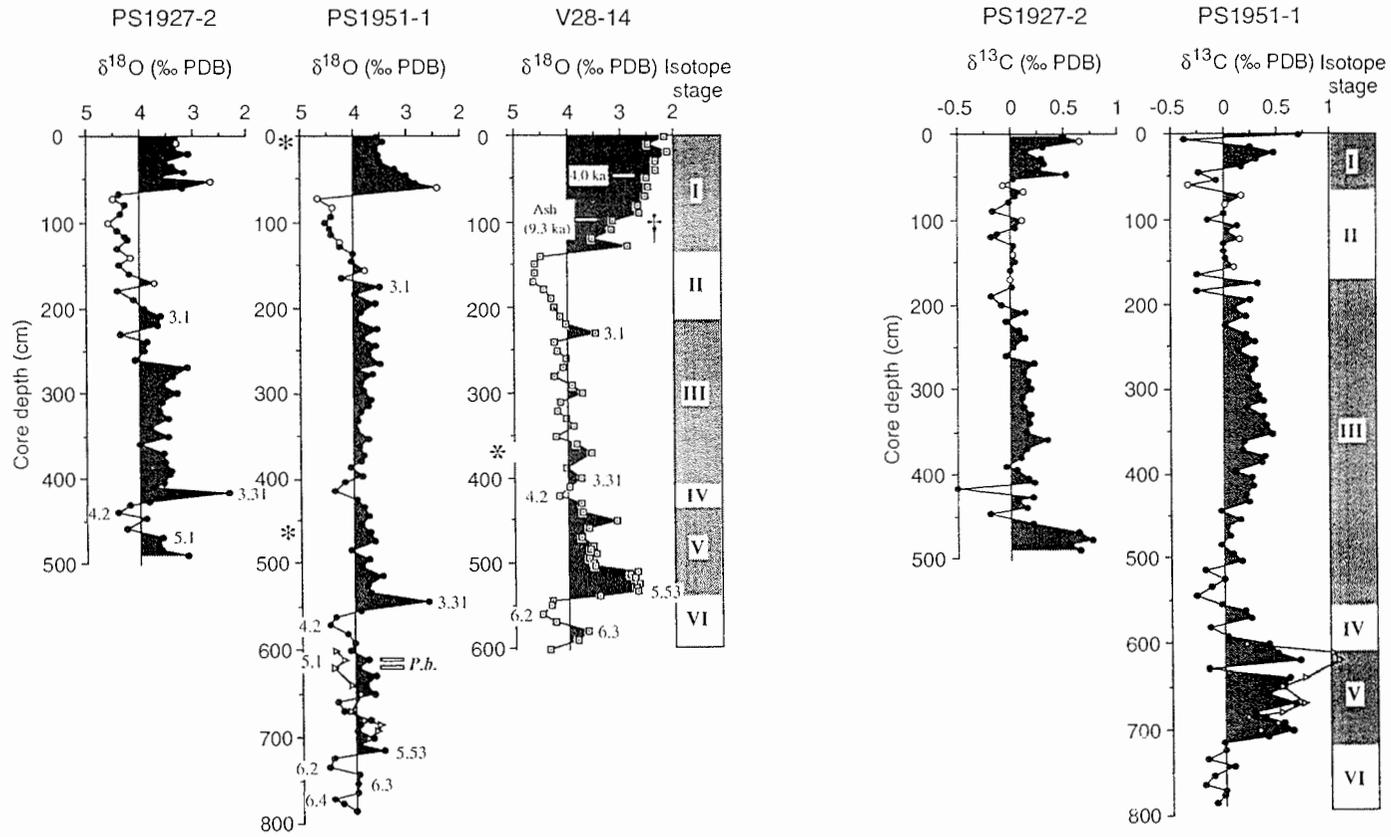
Fig. 10. Isotope stratigraphy of the planktonic foraminifer *N. pachyderma* sin. of cores PS1927-2 and PS1951-1 from the Greenland deep sea, and V28-14 from the Denmark Strait (Kellogg et al. 1978). Numbers in oxygen isotope records are substages (Martinson et al. 1987). Open triangles in stage 5 of core PS1951-1 indicate the oxygen and carbon isotope records of the benthic foraminifer *C. wuellerstorfi*. The benthic δ^{18}O records have not been corrected (cf. Section 3.2.9). Open circles in the oxygen and carbon isotope records indicate AMS-dated samples (*see* Table 2 & Fig. 11). Asterisks within stages 3 and 1 mark volcanic ash layers. Note the ash layer of core V28-14 occurs at a depth of 105 cm, which is dated at 9.3 ka (Ruddiman & Glover 1972). The abbreviation *P.b.* of core PS1951-1 indicates the appearance of the benthic foraminifer *P. bulloides* within substage 5.1.
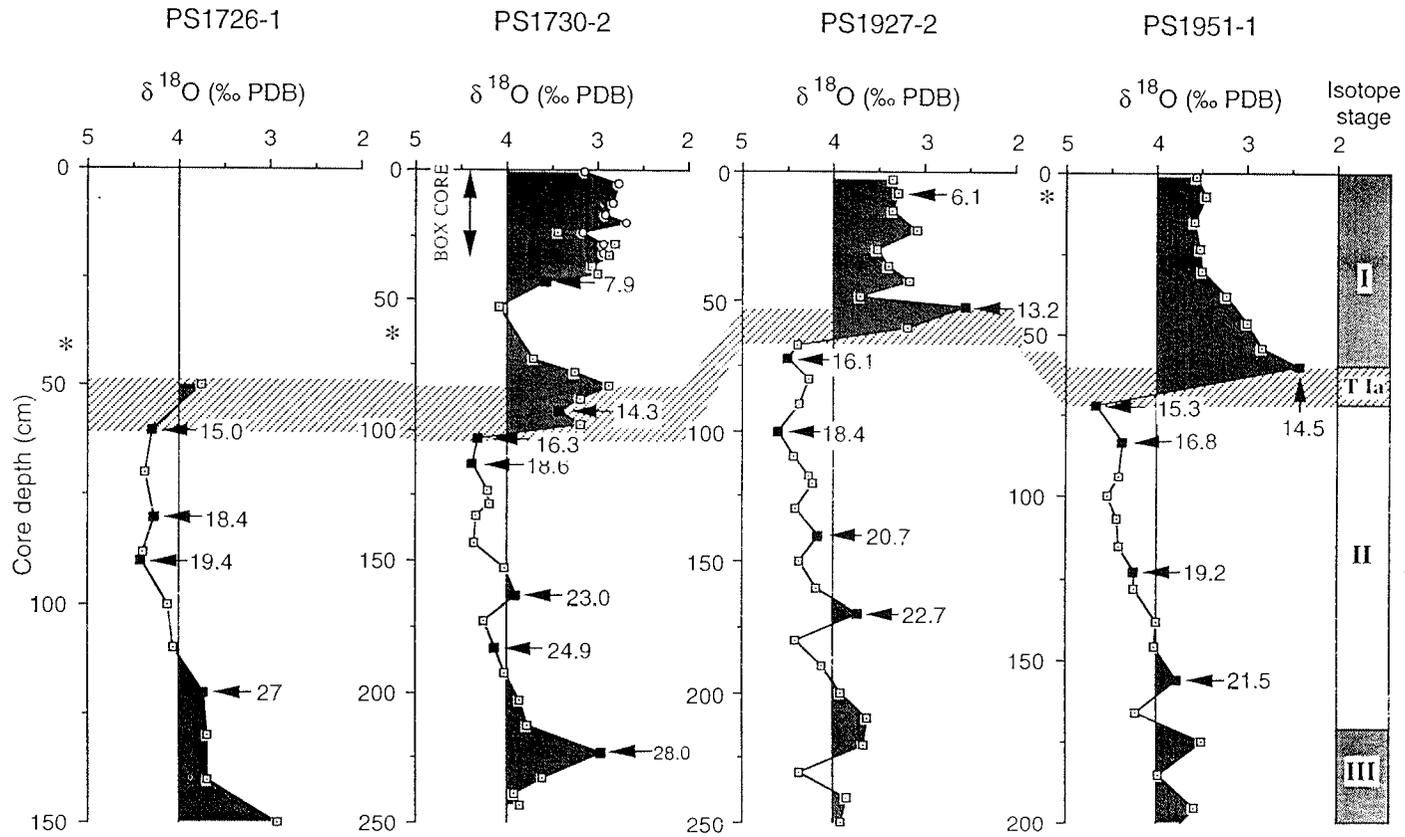
Fig. 11. Oxygen isotope stratigraphy and AMS[14]C-age dating measured on the planktonic foraminifer *N. pachyderma* sin. during the last 30 ka (*see* Table 2). Core depth of PS1730-2 is corrected by addition of 23 cm from box core PS1730-1 (open circles). Asterisks mark the Vedde ash layer, which is dated at 10.6 ka (Mangerud et al. 1984). The abbreviation of TIa is Termination Ia which is hatched.
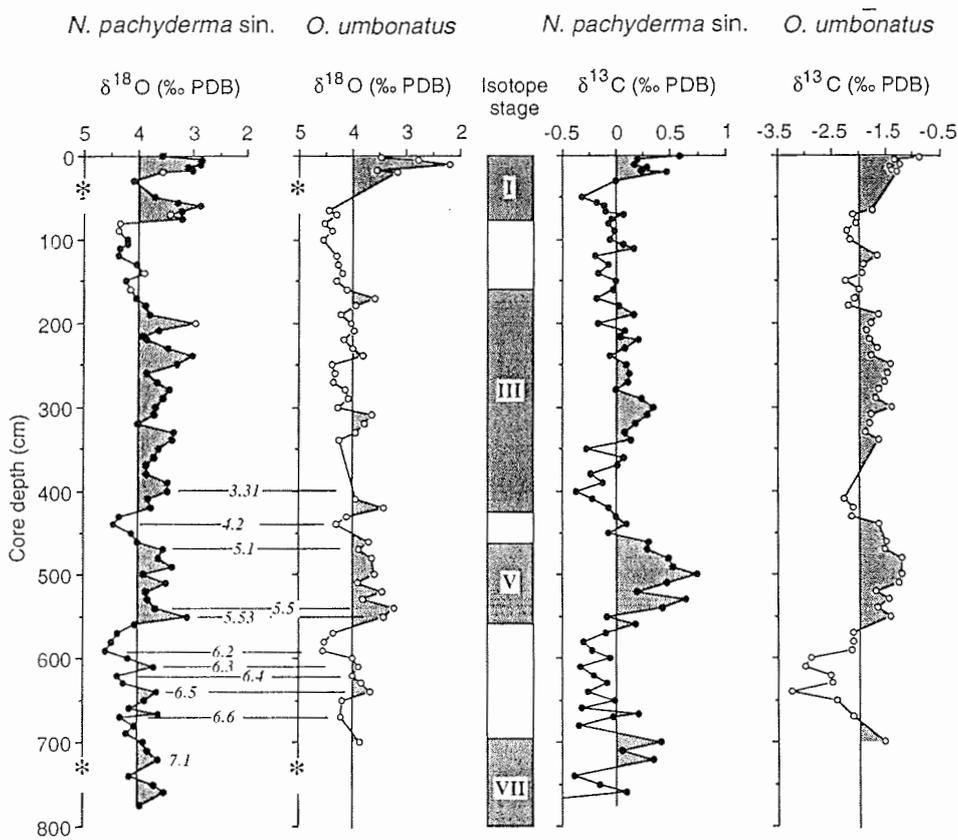
Fig. 12. Isotope stratigraphy based on the planktonic foraminifer *N. pachyderma* sin. and the benthic foraminifer *O. umbonatus* of core PS1730-2 from the deep-sea. The benthic $\delta^{18}O$ records have not been corrected (cf. Section 3.2.9 & Fig. 34a). Substages are indicated by the italics in oxygen isotope records. Open circles in oxygen isotope records of *N. pachyderma* sin. indicate AMS dated samples (see Table 3 & Fig. 11). Asterisks mark volcanic ash layers.

The identification of isotope stage 5 is based on the relatively light $\delta^{18}O$ values and the heavy $\delta^{13}C$ values of up to 0.77‰. In particular, stage 5 is also recognized by the occurrence of the benthic foraminifer species *C. wuellerstorfi* together with the marked shifts in the $\delta^{18}O$ and $\delta^{13}C$ records of the planktonic foraminifer *N. pachyderma* sin., and benthic foraminifers *C. wuellerstorfi* and *O. umbonatus* (Figs. 9, 10, 11 & 12) (e.g. Streeter et al. 1982; Belanger et al. 1981; Vogelsang 1990; Jünger 1994). The benthic foraminifer *Pullenia bulloides* (D´Orbigny) occurs at depths of 612 to 620 cm within deep-sea core PS1951-1 (Fig. 10). This species is indicative of substage 5.1 within the GIN Sea (e.g. Haake & Pflaumann 1989; Hebbeln 1992).

29

Glacial stage 4 is mainly identified by the relatively heavy $\delta^{18}O$ values (substage 4.2) of both *N. pachyderma* sin. and *O. umbonatus*. The $\delta^{18}O$ values are slightly lighter than compared to those recorded from glacial stage 6. A distinct shift towards light $\delta^{13}C$ values at the stage 5/4 boundary is indicated in deep-sea cores PS1927-2, PS1730-2, and PS1951-1 (Figs. 9-10).

Table 3. Correlation of age versus depth in sediment cores PS1725-2, PS1726-1, PS1730-2, PS1927-2, and PS1951-1. Ages are based on the oxygen isotope events dated by Martinson et al. (1987) and AMS ^{14}C age datings (*). Core depth in parenthesis of core PS1730-2 is the corrected core depth by addition of 23 cm from box core PS1730-1 (*see* above in Text).

$\delta^{18}O$-Event	Termination	Age (ka)	PS1725-2 Depth (cm)	PS1726-1 Depth (cm)	PS1730-2 Depth (cm)
	End **T Ib**	7.4*			17 (40)
	Beginning **T Ib**	9.7*			30 (53)
	End **T Ia**	13.2*			60 (83)
2/1		14.5*	38	58	71 (94)
	Beginning **T Ia**	15* -	41	60	
		16.3*			80 (103)
3/2		24.9*	81	112	160 (183)
3.1		25.4	84		
3.31		55.5	155	200	400 (423)
4/3		59.0	160	210	425 (448)
4.22		65.2	175	230	440 (463)
5/4		73.9	190	244	460 (483)
5.1		79.3	197	250	470 (493)
5.3		96.2		300	
5.33		103.3	220	340	510 (533)
5.5		123.8			
5.53		125.2	242	360	550 (573)
6/5	**T II**	129.8	250	363	560 (583)
6.2		135.1	253	370	590 (613)
6.3		142.3	270	390	610 (633)
6.4		152.6	290	400	620 (643)
6.5		175.1	323	430	640 (663)
6.6		183.3			670 (693)
7/6		189.6	360	450	698 (721)
7.1		193.1	377	460	720 (743)
7.2		200.6		480	740 (763)
7.3		215.5	410	500	760 (783)
7.4		224.9	483	550	776 (793)
7.5		240.2	516	600	

Table 3. Continued.

δ¹⁸O- Event	Termination	Age (ka)	PS1927-2 Depth (cm)	PS1951-1 Depth (cm)
	End TIa	13.2 *	52	
2/1		14.5 *	61	60
	Beginning T Ia	15 * - 16.3 *	65	72
3/2		24.9 *	160	172
3.1		25.4		175
3.31		55.5	418	545
4/3		59.0	432	555
4.22		65.2	440	572
5/4		73.9	463	592
5.1		79.3	470	612
5.3		91.3	491	
5.4		110.8		660
5.5		123.8		
5.53		125.2		715
6/5	T II	129.8		720
6.2		135.1		735
6.3		142.3		754
6.4		152.6		772
6.5		175.1		786

In general, isotope stage 3 shows relatively light δ¹⁸O records and heavy δ¹³C values. In particular, the markedly light δ¹⁸O values of isotope substage 3.31 are recorded in deep-sea cores PS1927-2, PS1730-2, and PS1951-1. The light δ¹⁸O values coincide with very light δ¹³C values, and indicate strong meltwater discharge during this interval (cf. Vogelsang 1990; Köhler 1992). During early isotope stage 3, a prominent ash layer is recorded at a depth of 465 cm in deep-sea core PS1951-1 from the northwestern Iceland Plateau (Fig. 10). This ash zone seems to correlate with that recorded in core V28-14 (Fig. 10; Kellogg et al. 1978) and core 0017-2 (Lackschewitz 1991), located in the deep sea south of the Denmark Strait and west of the Iceland Plateau, respectively. The age of the ash layer based on linear interpolation is suggested to be approximately 49 ka. In sediment cores from the North Atlantic, this ash layer is well known as Ash Layer II and is dated by linear extrapolation at approximately 65 ka (Ruddiman & Glober 1972; Kellogg 1976). However, the age of the Ash Layer II was later corrected based on the oxygen isotope records of *N. pachyderma* sin., and thus corresponds to early interglacial stage 3 (cf. Kellogg et al. 1978).

5. LINEAR SEDIMENTATION RATE AND MASS ACCUMULATION RATE

5.1 LINEAR SEDIMENTATION RATE (LSR)

Linear sedimentation rates are calculated for five cores based on the isotope stage boundaries of Martinson et al. (1987) and twenty-six AMS ^{14}C age datings. Table 4 and Figure 13 illustrate the mean sedimentation rates obtained from the five long sediment cores.

Table 4. Linear sedimentation rates calculated for five cores based on the oxygen isotope stratigraphy and AMS ^{14}C age datings. The stage 3/2 and 2/1 boundaries are dated at 24.9 and 14.5 ka, respectively (see Fig. 12).

Isotope stage	PS1725-2 (cm/kyr)	PS1726-1 (cm/kyr)	PS1730-2 (cm/kyr)	PS1927-2 (cm/kyr)	PS1951-1 (cm/kyr)
1	>2.3	>3.9	6.5	>4.3	>4.5
2	4.1	5.2	8.6	12.6	10.6
3	2.3	2.9	7.8	7.1	11.2
4	2.0	2.3	2.3	2.1	2.5
5	1.1	2.1	1.8	-	3.0
6	1.8	1.5	2.3	-	-

The mean sedimentation rates of the six shelf cores and the relatively short five slope cores were also calculated and are listed in Tables 4 and 5. The mean sedimentation rates of the Holocene calculated from the six shelf cores range from 5.0 to 12.9 cm/kyr. In particular, the mean Holocene sedimentation rates of the four shelf cores are calculated on the assumption that the basal age of the cores is approximately 10 ka (cf. Marienfeld 1991; Stein et al. 1993). In the five short slope cores, the mean Holocene sedimentation rates range between 3.3 and 8.0 cm/kyr. In order to calculate the sedimentation rates for the five slope cores, the basal ages are assumed to date back at maximum to glacial stage 2 (Table 6). During stage 2, mean sedimentation rates range between >9.5 (core PS1925-2) and >33.0 cm/kyr (core PS1949-1).

Table 5. Sedimentation rates calculated from six shelf cores. Holocene ages are the assumed basal age of each core.

Holocene (ka)	PS1723-1 (cm/kyr)	PS1724-2 (cm/kyr)	PS1923-2 (cm/kyr)	PS1924-1 (cm/kyr)	PS1946-2 (cm/kyr)	PS1947-1 (cm/kyr)
10	8.5	12.9			5.0	5.0
14.5			6.8	7.2		

According to five high-resolution sediment cores, sedimentation rates are distinctly higher in the deep sea than on the slope. Relatively high sedimentation rates occur during stages 3 and 2, whereas lower

sedimentation rates occur during interglacial stage 5. In the two slope-cores PS1725-2 and PS1726-1, mean sedimentation rates vary between 1.1 and 2.3 cm/kyr during oxygen isotope stages 6 to 4, and increase to values between 2.4 to 5.2 cm/kyr during stages 3 and 2. During the Holocene, the sedimentation rates of both slope cores vary between 2.4 and 3.9 cm/kyr.

Table 6. Sedimentation rates calculated from five slope cores. The basal ages of each core are assumed to date back at maximum to 24.9 ka.

Isotope satge	Age (ka)	PS1925-2 (cm/kyr)	PS1926-1 (cm/kyr)	PS1948-2 (cm/kyr)	PS1949-1 (cm/kyr)	PS1950-2 (cm/kyr)
1	14.5	>8.0	3.7	>3.3	>4.7	>5.7
2	24.9	>9.5	>25.5	>19.9	>33.0	>32.5
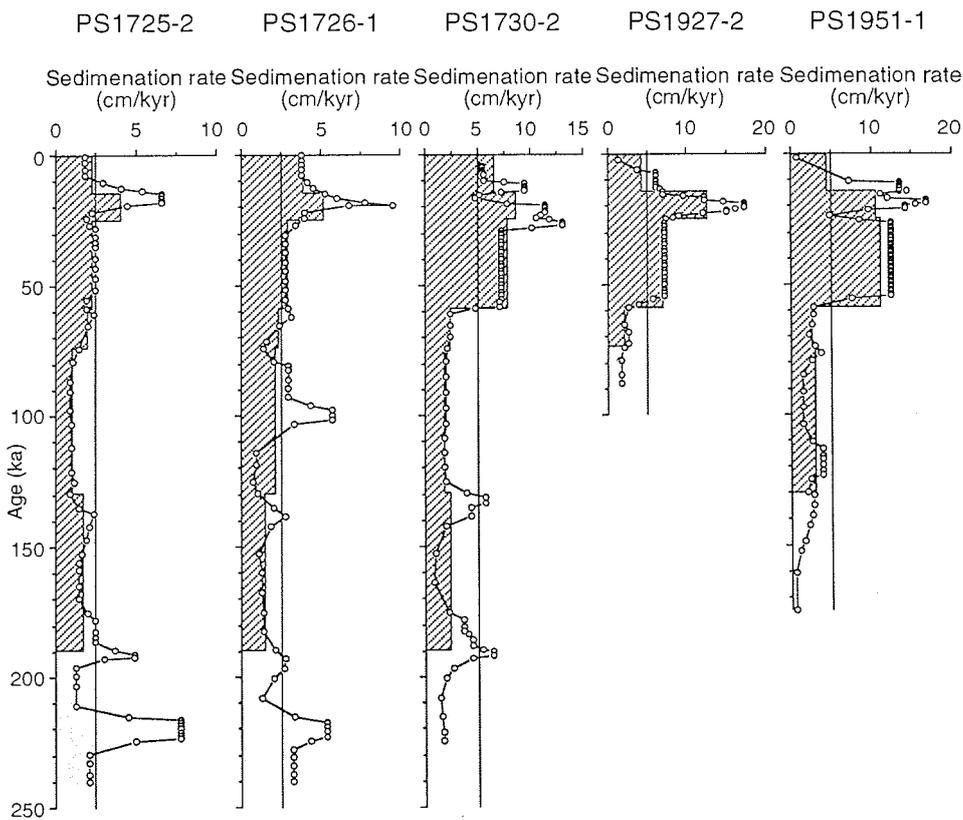
Fig. 13. Linear sedimentation rates (LSR) of slope cores PS1725-2 and PS1726-1 and deep-sea cores PS1730-2, PS1927-2, and PS1951-1 during the last 240 ka. The LSR are calculated according to the oxygen isotope events of Martinson et al. (1987) and AMS ^{14}C age datings (cf. Table 3). The hatched mean sedimentation rates are based on the isotope stage boundaries (cf. Table 4).

In the three deep-sea cores PS1927-2, PS1730-2, and PS1951-1, the mean sedimentation rates of isotope stages 6 to 4 are generally low with values of 1.8 to 3.0 cm/kyr. In contrast, the mean sedimentation rates reach higher values of 7.1 to 12.6 cm/kyr during isotope stages 3 and 2. The Holocene mean sedimentation rates range from 4.3 to 6.5 cm/kyr. According to the more detailed AMS[14]C age datings, the sedimentation rates reach the highest values of up to 17.2 cm/kyr during the interval of 21 to 18 ka (e.g. PS1927-2 & Table 7).

Table 7. Sedimentation rates during the last 28 ka based on AMS[14]C age datings. Age of Vedde ash is after Mangerud et al. (1984). Core depth in parenthesis of core PS1730-2 is the corrected depth by addition of 23 cm from box core PS1730-1 (see Section 4).

Core	Depth (cm)	[14]C Age (ka) (reservoir corr. 550 years)	Sedimentation rate (cm/kyr)
PS1726-1	40	10.6 (Vedde ash)	>3.8
	60	15.0	4.6
	80	18.4	5.9
	90	19.4	10.0
	120	27.0	4.0
PS1927-2	8	6.1	>1.3
	52	13.2	6.2
	72	16.1	7.0
	100	18.4	12.1
	140	20.7	17.2
	170	22.7	15.2
PS1730-2	20 (43)	7.9	5.4
	35 (58)	10.6 (Vedde ash)	5.6
	70 (93)	14.3	9.5
	80 (103)	16.3	5.0
	90 (113)	18.6	4.4
	140 (163)	23.0	11.4
	160 (183)	24.9	10.5
	180 (223)	28.0	12.9
PS1951-1	7	10.6 (Vedde ash)	>0.7
	60	14.5	13.6
	72	15.3	15.0
	94	16.9	13.8
	123	19.2	12.6
	156	21.5	14.4

5.2 MASS ACCUMULATION RATE (MAR)

The mass accumulation rates are calculated from the five long cores (PS1725-2 and PS1726-1, PS1927-2, PS1730-2, and PS1951-1), and are illustrated in Figure 14. The accumulation rate pattern is generally very similar to that in the mean sedimentation rates. The mass accumulation rates generally increase from the upper slope towards the deep sea. A marked increase in the

accumulation rates occurs at the stage 4/3 boundary. During stages 3 and 2, the three deep-sea cores display relatively higher accumulation rates (5 to 20 g cm^{-2} kyr^{-1}) than compared to those of the continental slope (2.5 to 12 g cm^{-2} kyr^{-1}). During the interval from isotope stages 6 to 4, the accumulation rates reveal relatively lower values and range between 0.7 and 6.4 g cm^{-2} kyr^{-1}. During stage 3, the accumulation rates fluctuate with high-amplitude and range between 2.6 and 12.1 g cm^{-2} kyr^{-1}. The highest accumulation rates are documented within glacial stage 2 and reach a maximum value of 19.8 g cm^{-2} kyr^{-1} at 17.5 ka. A similar maximum in the flux is recorded within slope core PS1726-1 during the interval 19.4 to 18.4 ka. The bulk accumulation rates decrease during the Holocene. In particular, the bulk accumulation rates within the deep-sea core PS1951-1 markedly decrease to 5.1 g cm^{-2} kyr^{-1} at 10.1 ka, and drop to a minimum value of <0.6 g cm^{-2} kyr^{-1} after this time span. However, it has to be noted that the extremely low accumulation rates during the interval after 10.1 ka may be incorrect due to a loss of the uppermost surface sediments.
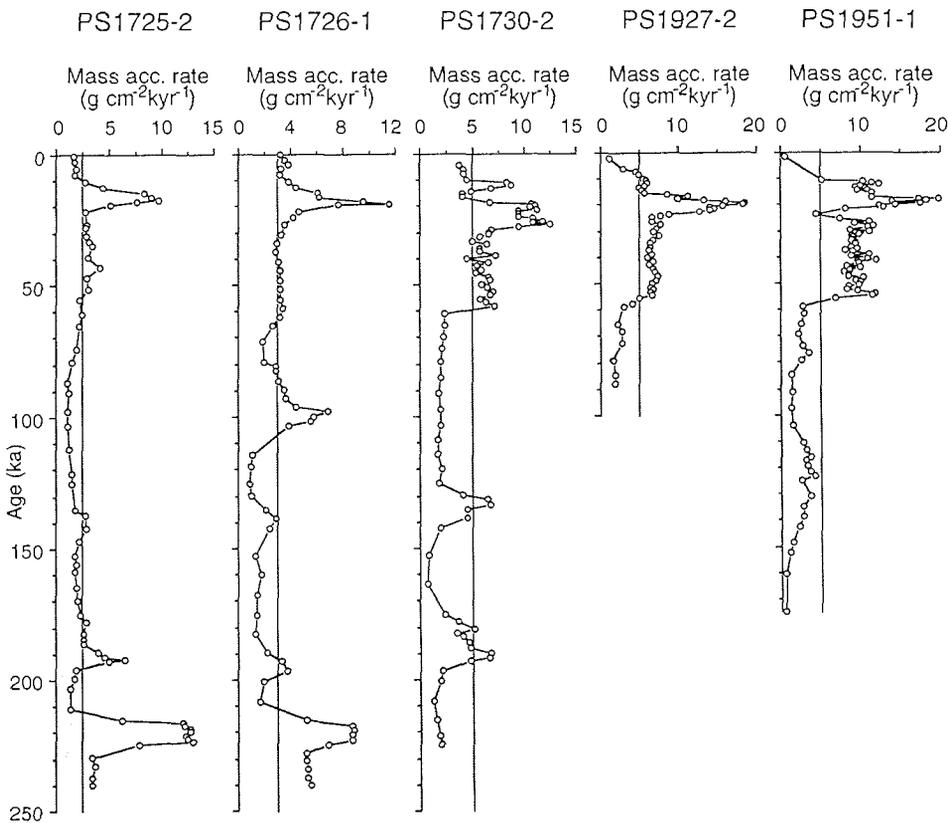

Fig. 14. Mass accumulation rates (MAR) of two slope cores (PS1725-2 and PS1726-1) and three deep-sea cores (PS1730-2, PS1927-2, and PS1951-1) during the last 240 ka.

6. RESULTS

6.1 BOX CORE SURFACE SEDIMENTS

Two box cores, PS1726-2 and PS1730-1, are used in this study to compensate for surface sediments lost from the gravity cores. Box cores PS1726-2 and PS1730-1 are recovered from the lower slope and deep sea (adjacent to Scoresby Sund) in water depths of 1182 and 1622 m respectively. Both cores are located close to the respective gravity cores PS1726-1 and PS1730-2. The surface sediments in both cores are mostly composed of dark grayish brown mud with an absence of ice-rafted dropstones (IRD), and displaying strong *Chondrite*-type bioturbation. The Vedde ash layer (Mangerud et al. 1984) is not documented within the surface sediment sequences, and therefore, both cores are likely to represent time interval younger than the Younger Dryas cooling event (10.6 ka).

The very low carbonate content (<2 %) within box core PS1726-2 are similar to those recorded within the Holocene sediment sequence of the gravitiy core PS1726-1 (Fig. 21d-e). Stable isotope records were not measured due to the absence of calcareous foraminifers, that probably results from carbonate dissolution. The relative increase in the organic carbon content (0.4-0.7 %) is analogous to that recorded within the uppermost interval of gravity core PS1726-1. The C/N ratios (>5) are slightly higher than those from the same period in gravity core PS1726-1. In contrast, the hydrogen index values of 70-125 mgHC/gC are relatively lower.

The box core PS1730-1 is characterised by relatively light $\delta^{18}O$ (<3‰) and $\delta^{13}C$ (<0.5‰) values measured from the planktonic foraminifer *N. pachyderma* sin. (Fig. 21f) The $\delta^{18}O$ and $\delta^{13}C$ values of the benthic foraminifer *O. umbonatus* display relatively higher-amplitude fluctuations than compared to those of *N. pachyderma* sin..

The box core PS1730-1 is characterised by a relatively low carbonate content (<4 %), increased organic carbon contents (0.5-0.8 %), low C/N ratios (<10), and very low HI values (<50 mgHC/gC) (Fig. 21f). According to the Tmax values between 350 and 390°C, the surface sediments in both cores are very immature (cf. Peters 1986).

6.2 GRAVITY CORE SEDIMENTS

6.2.1 MAGNETIC SUSCEPTIBILITY

Figure 15 shows the magnetic susceptibility (MS) values measured on sediment cores from three W-E transects along the East Greenland continental margin. In general, the MS values reveal a fluctuating pattern through time, but do not reflect changes with respect to glacial-interglacial cycles. However, the MS values reveal a marked decrease near the stage 2/1 boundary. During interglacial stage 3, an increase in the MS values occurs in three deep-sea cores PS1927-2, PS1730-2, and PS1951-1. With the exception of two slope cores PS1725-2 and PS1726-1, another five cores recovered from the
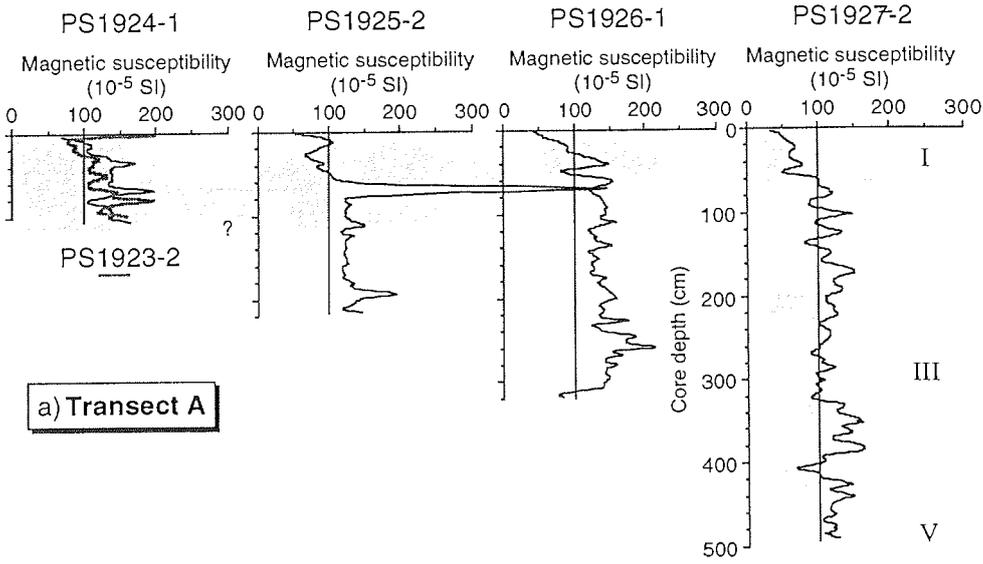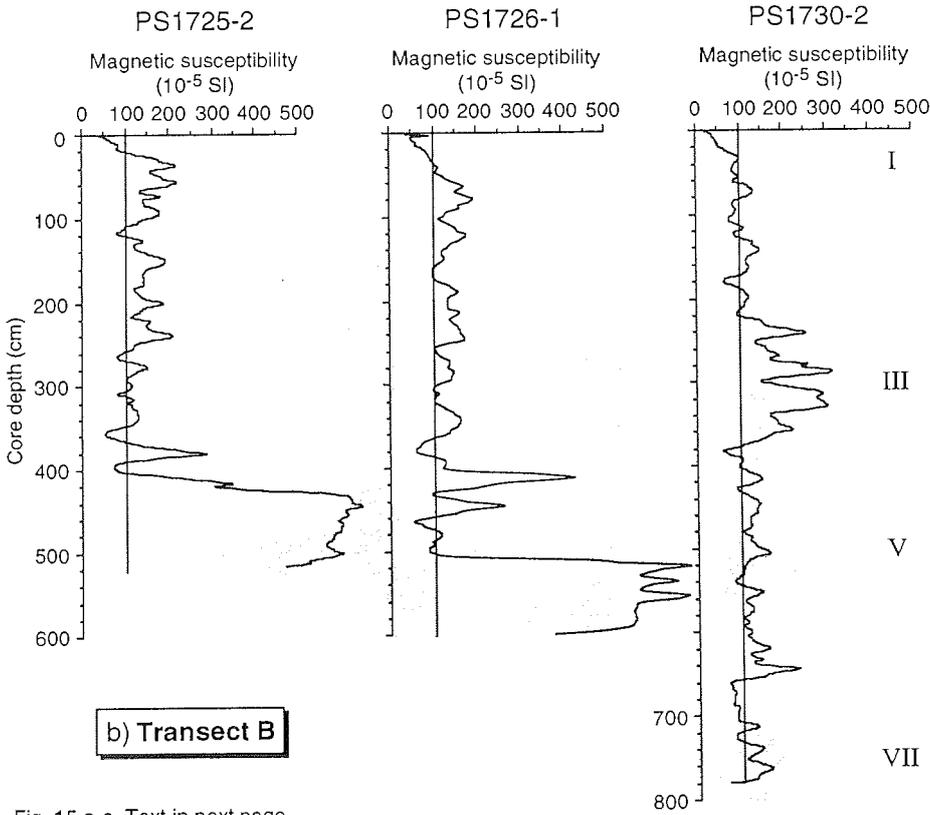
Fig. 15 a-c. Text in next page.
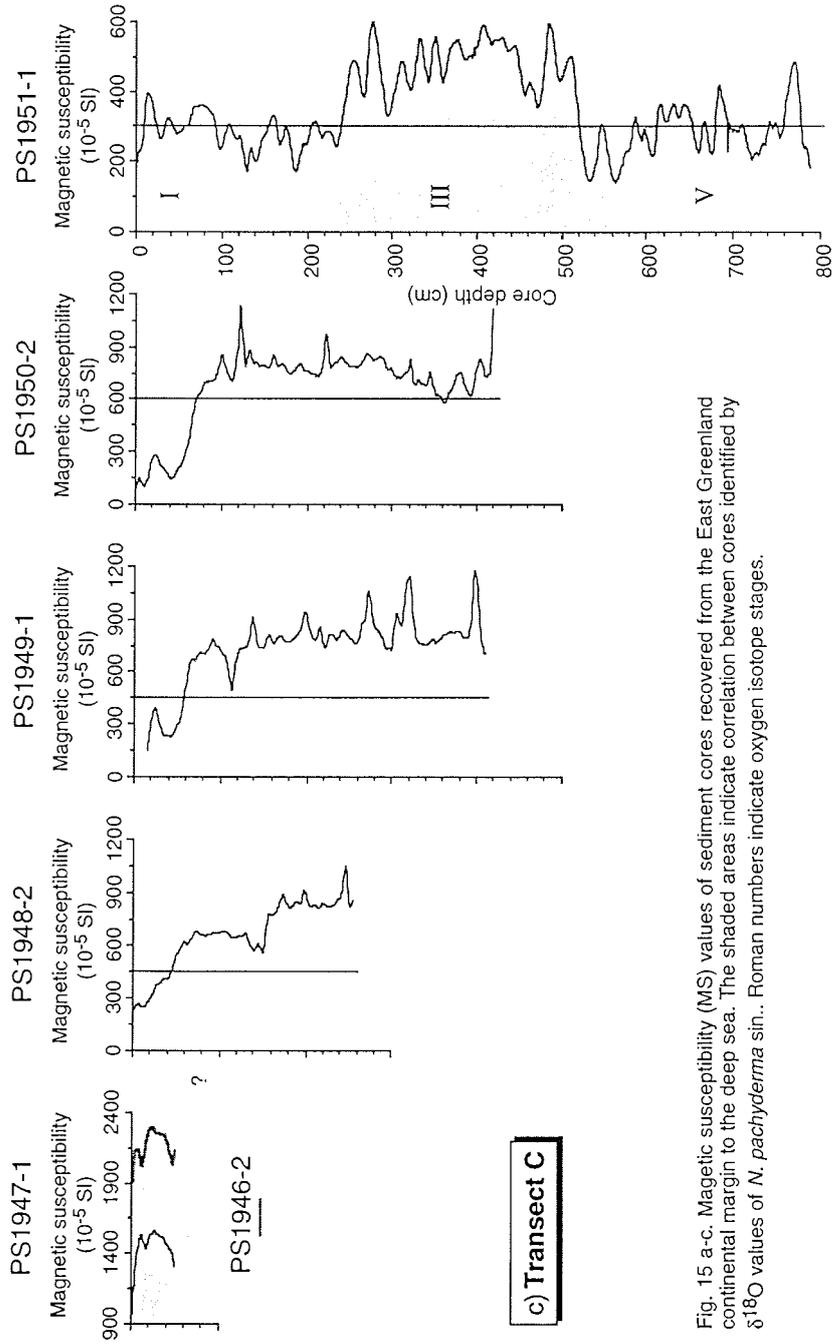
Fig. 15 a-c. Magetic susceptibility (MS) values of sediment cores recovered from the East Greenland continental margin to the deep sea. The shaded areas indicate correlation between cores identified by $\delta^{18}O$ values of *N. pachyderma* sin.. Roman numbers indicate oxygen isotope stages.

c) Transect C

continental slope north and south of the margin adjacent to Scoresby–Sund, display relatively constant MS values.

The MS values from the transect (Transect A) north of Scoresby Sund range from <50 to 200 10^{-5} SI except for a peak of approximately 500 10^{-5} SI in core PS1925-2 from the upper slope (Fig. 15a). Similarly, the MS values of the three cores from the continental margin adjacent to Scoresby Sund have values of <200 10^{-5} SI (Fig. 15b). However, higher MS values of up to 650 10^{-5} SI are recorded within the two slope cores PS1725-2 and PS1726-1 during interglacial stage 7. The slope core PS1726-1 reveals two peaks in the MS record during glacial stage 6. In contrast, all sediment cores from south of Scoresby Sund are characterised by distinctly higher MS values (Fig. 15c). In particular, the inner shelf core PS1946-2 reveals the highest MS values that reach up to 2300 10^{-5} SI. These values decrease markedly towards the deep-sea (core PS1951-1).

6.2.2 SEDIMENT DESCRIPTION

The lithology of all cores were classified based on visual descriptions and grain size determinations. In this section, the results of the sediment description will be briefly summarised. The more detailed descriptions of all the investigated sediment cores are found in Appendix A.

The Holocene sediments of six cores (PS1923-2, PS1924-1, PS1723-1, PS1724-2, PS1946-2, and PS1947-1) taken from the inner and outer shelf region adjacent to East Greenland, are mainly composed of very dark gray to dark grayish brown sandy mud to sandy silt. In general, only the upper part of the sediments are bioturbated with the exception of two cores PS1946-2 and PS1947-1. The sediment sequences of all shelf cores contain moderate to high amount of dropstones with varying grain sizes.

The Holocene sediments of cores PS1925-2 and PS1926-1 recovered from the upper to lower slope adjacent to Carlsberg Fjord, are characterised by olive brown, dark grayish brown mud to sandy mud. In contrast, the glacial sediments are mainly composed of dark gray sandy mud. The strongly bioturbated sequence is only observed in the uppermost part of the Holocene. The Holocene sequences recorded in cores PS1948-2, PS1949-1, and PS1950-2, recovered from the upper to lower slope adjacent to the Geikie Plateau, consist of dark grayish brown to brown bioturbated mud to sandy mud. In contrast, the glacial (isotope stage 2) sediments are characterised by very dark gray nonbioturbated sandy mud. In general, the Holocene sequences of five slope cores contain relatively lower amounts of dropstones than the glacial sediment sequence that is characterised by moderate to high amounts of coarse grained ice-rafted detritus (IRD). Slope cores PS1725-2 and PS1726-1, recovered from the margin adjacent to Scoresby Sund, reveal an alternating sequence of mud and sandy mud with high-amplitude variation in the dropstone content. In general, sediments show a brownish colour throughout the interval from stage 5 through to the Holocene, and a grayish to dark gray colour from the interval from stage 7 to stage 6.

In general, the sediments of the three deep-sea cores PS1927-2, PS1730-2, and PS1951-1 are represented by dark grayish brown to dark gray mud, that

is independent of glacial-interglacial fluctuations. With the exception of glacial stages 6 and 4, the sedimentary sequences of the deep-sea cores are strongly bioturbated throughout.

6.2.3 GRAIN SIZE DISTRIBUTION

The grain size distribution analysed from 2 box cores (GKG) and 16 gravity cores (SL) is plotted in ternary diagrams using the sand plus gravel, silt, and clay fractions (Figs. 16-18). In general, the grain size distribution appears to be closely related to the water depth. The general change in grain size in relation to the water depth is well recorded within sediments from the shelf to the deep sea adjacent to Scoresby Sund (Fig. 17). In all the investigated cores along the continental margin, coarse ice-rafted sediments are dominant, and the
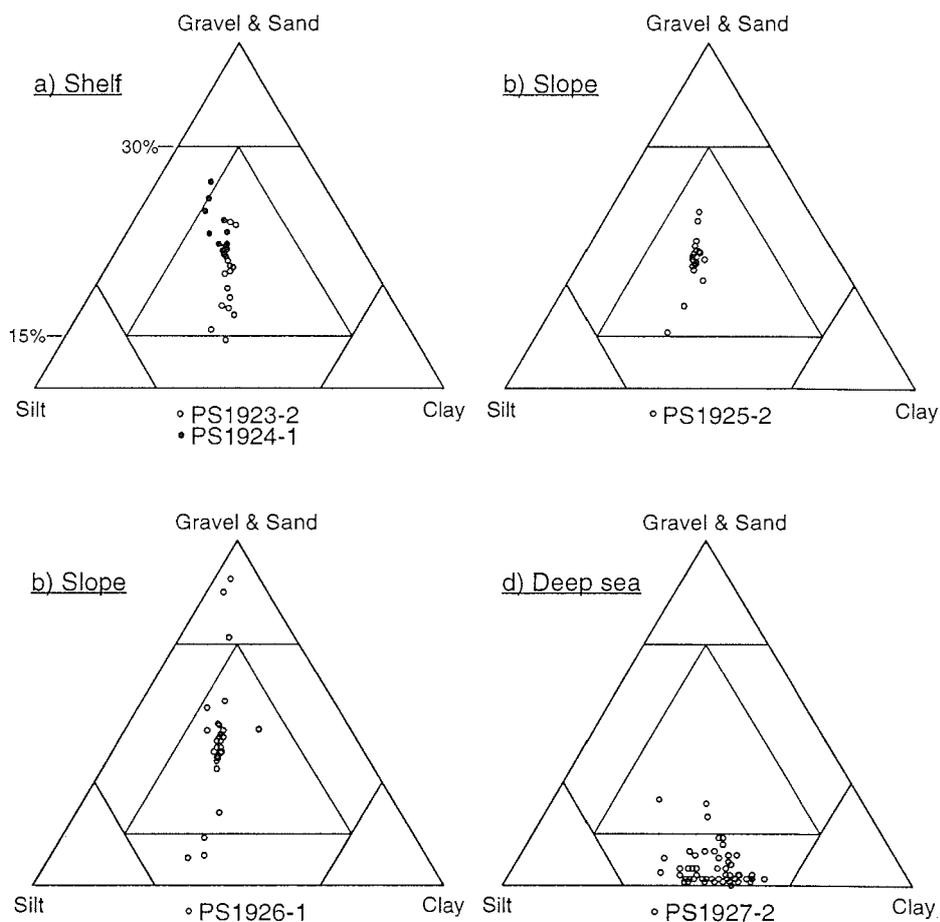
Fig. 16. The grain size distributions of five cores collected from the shelf to the deep sea adjacent to Carlsberg Fjord (at about 71.30°N) are plotted in the ternary diagram (modified after Shepard 1954). The gravel and sand fraction are represented together.

a) Shelf

Gravel & Sand

Silt

° PS1723-1
• PS1724-2

Clay

b) Slope

Gravel & Sand

Silt

° PS1725-2

Clay

c) Slope

Gravel & Sand

Silt

° PS1726-1

Clay

d) Deep sea

Gravel & Sand

Silt

° PS1730-2

Clay

e) Box core

Gravel & Sand

Silt

° PS1726-2GKG
• PS1730-1GKG

Clay
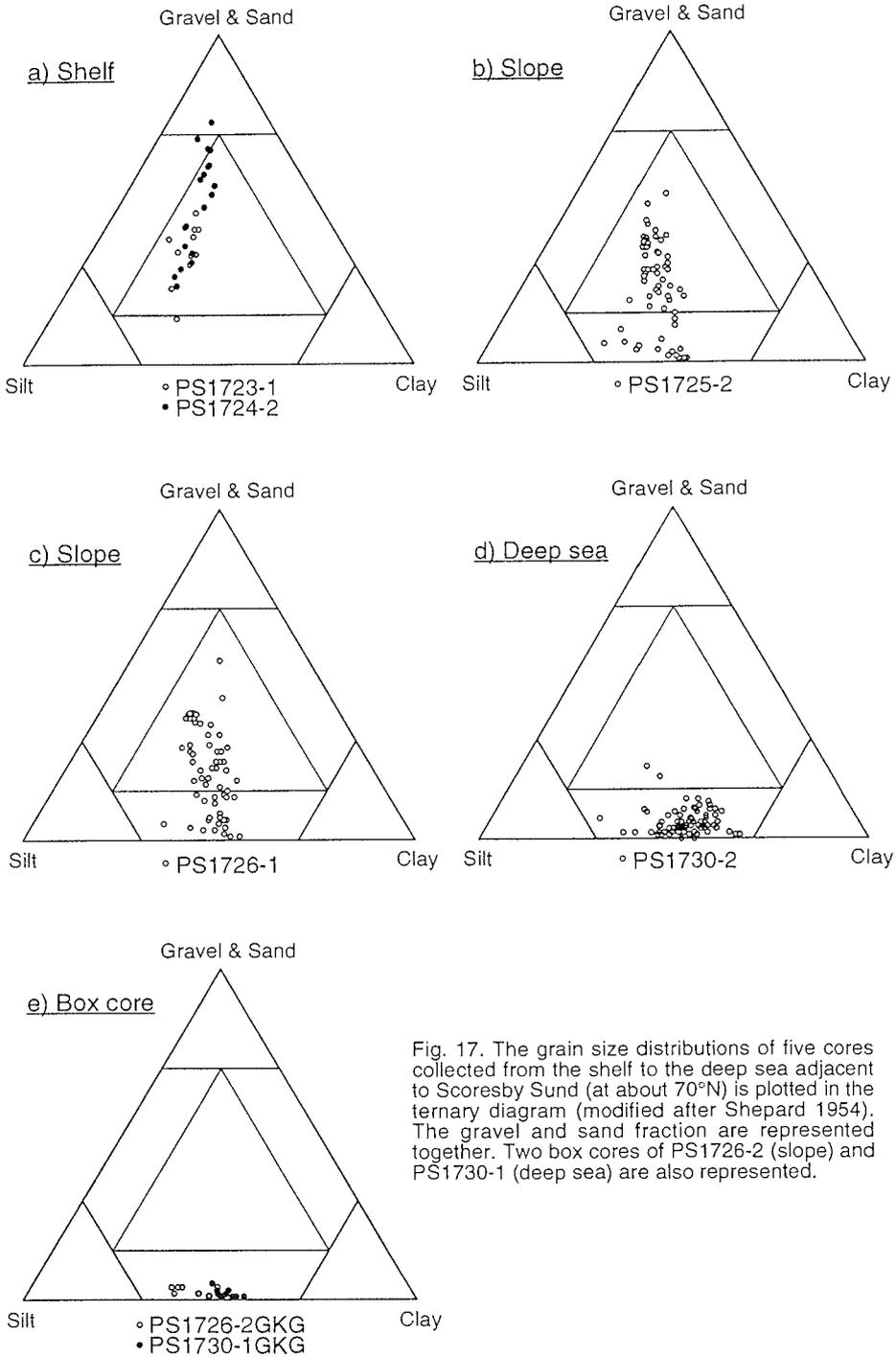
Fig. 17. The grain size distributions of five cores collected from the shelf to the deep sea adjacent to Scoresby Sund (at about 70°N) is plotted in the ternary diagram (modified after Shepard 1954). The gravel and sand fraction are represented together. Two box cores of PS1726-2 (slope) and PS1730-1 (deep sea) are also represented.

41

Gravel & Sand

a) Shelf

Silt

° PS1946-2
• PS1947-1

Clay

Gravel & Sand

b) Slope

Silt

° PS1948-2

Clay

Gravel & Sand

c) Slope

Silt

° PS1949-1

Clay

Gravel & Sand

d) Slope

Silt

° PS1950-2

Clay

Gravel & Sand

e) Deep sea

Silt

° PS1951-1

Clay
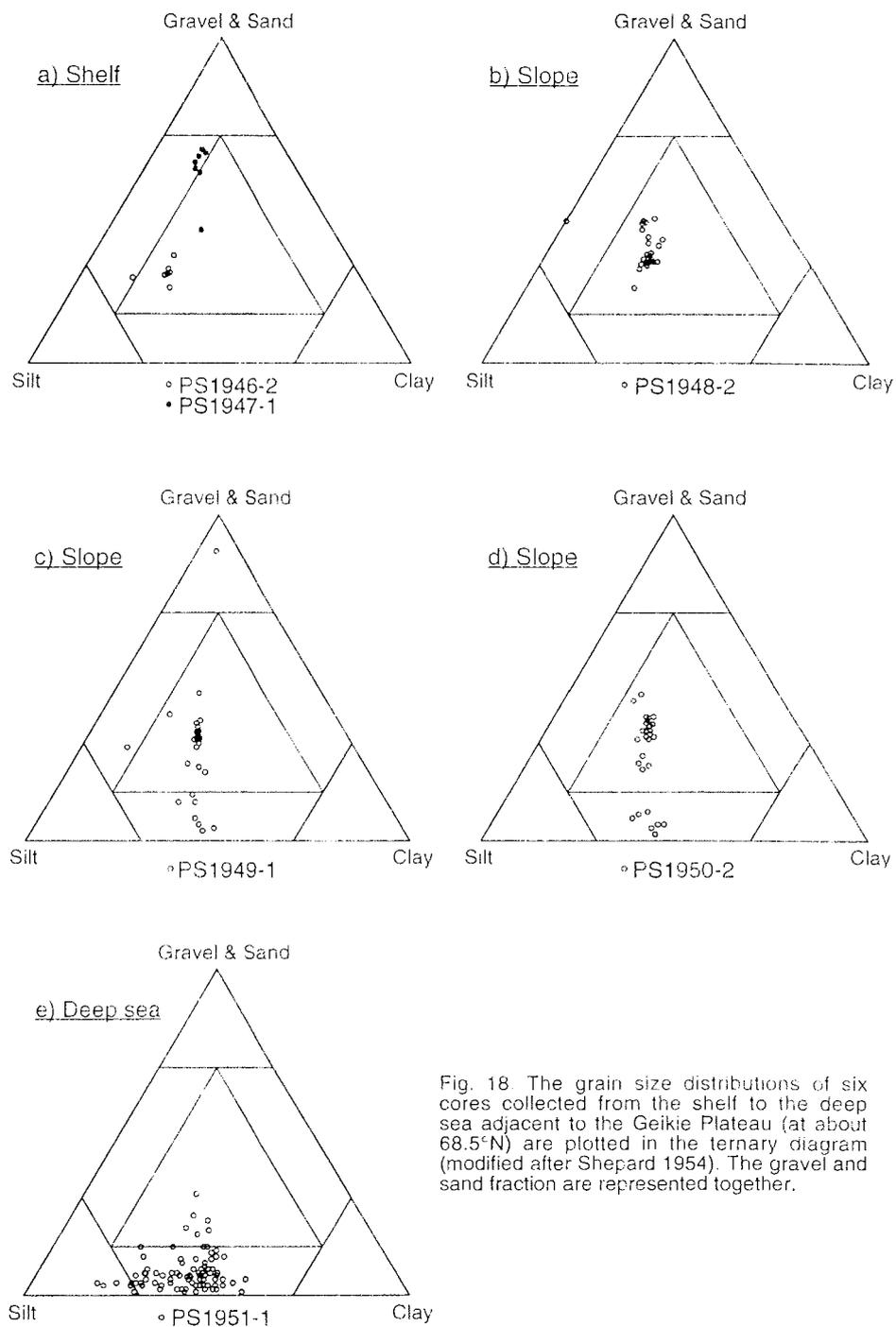
Fig. 18. The grain size distributions of six cores collected from the shelf to the deep sea adjacent to the Geikie Plateau (at about 68.5°N) are plotted in the ternary diagram (modified after Shepard 1954). The gravel and sand fraction are represented together.

dropstone content abruptly decreases towards the deep sea. The gravel (wt.-%) content calculated from the grain-size analysis correlates well with the IRD-records estimated from the X-radiographs (Figs. 20-22)

The general sediment distribution is finer on the inner shelf than on the outer shelf (Figs. 16-18). Subsequently, the sediments from the inner shelf are mostly composed of sandy mud, whereas the sediments from the outer shelf are mainly composed of sandy mud to silty sand. The sediment distribution on the slope shows a general increase in the fine fraction concentration towards the lower slope. The grain size distribution on the slope is mostly dominated by sandy mud with varying amounts of coarse sand and gravely dropstones. In contrast, the Holocene sediments consist mostly of mud. The sediments of the three deep-sea cores PS1927-2, PS1730-2, and PS1951-1 consist predominantly of mud with a low IRD content. The silt content in the three deep-sea cores slightly increases from the north (PS1927-2) to the south (PS1951-1).

6.2.4 DISTRIBUTION OF COARSE TERRIGENOUS SEDIMENT

The terrigenous derived coarse sand of 0.5-2 mm and gravel of 2-4 mm are calculated for two slope cores (PS1725-2 and PS1726-1) and three deep-sea cores (PS1927-2, PS1730-2, and PS1951-1), and are illustrated in Figure 19. The coarse terrigenous sediment record (0.5-4 mm) includes a small amount of the benthic foraminiferal species *Pyrgo rotalaria* (Loeblich & Tappan), and varying amounts of agglutinated benthic foraminifers. *P. rotalaria* is neglected because of its sporadic and limited occurrence at specific core depths. In general, the coarse terrigenous sediment record determined from the grain-size distribution seem to correlate with the IRD record estimated from X-radiographs (*see* Figs. 20e, 21c,e,g & 22f).

There are a number of general trends observed in the fluctuating coarse terrigenous sediment record (Fig. 19). In general, there seems to be a periodical increase in the content of terrigenous ice-rafted matter. The amount of terrigenous coarse ice-rafted sediment decreases from the upper slope to the deep sea. In the deep-sea cores, the IRD content increases from the north to the south. The prominent peaks representing an increase in the IRD content are larger on the slope than in the deep sea.

In general, the two slope cores PS1725-2 and PS1726-1 seem to be very similar in their terrigenous coarse IRD content. An increase in the IRD content occurs at the stage boundaries. Several major pulses of increased terrigenous coarse-grained material occur within cold glacial stages as well as within warm interglacial stages. In particular, the terrigenous coarse sediment content of glacial stage 6 is relatively lower than that recorded during the last glacial stage 2. This is further substantiated by the IRD record estimated from X-radiographs (cf. Figs. 20e, 21c,e,g & 22f). A high amount of terrigenous coarse sediment are deposited throughout interglacial stage 7. The Holocene, on the other hand, is characterised by a predominantly reduced IRD content.

In the three deep-sea cores PS1927-2, PS1730-2, and PS1951-1, the amplitude of the terrigenous coarse ice-rafted sediment content is distinctly smaller than compared to that observed within the slope cores. In particular,

43

three major pulses of increased terrigenous IRD are recorded within the last glacial stage 2.
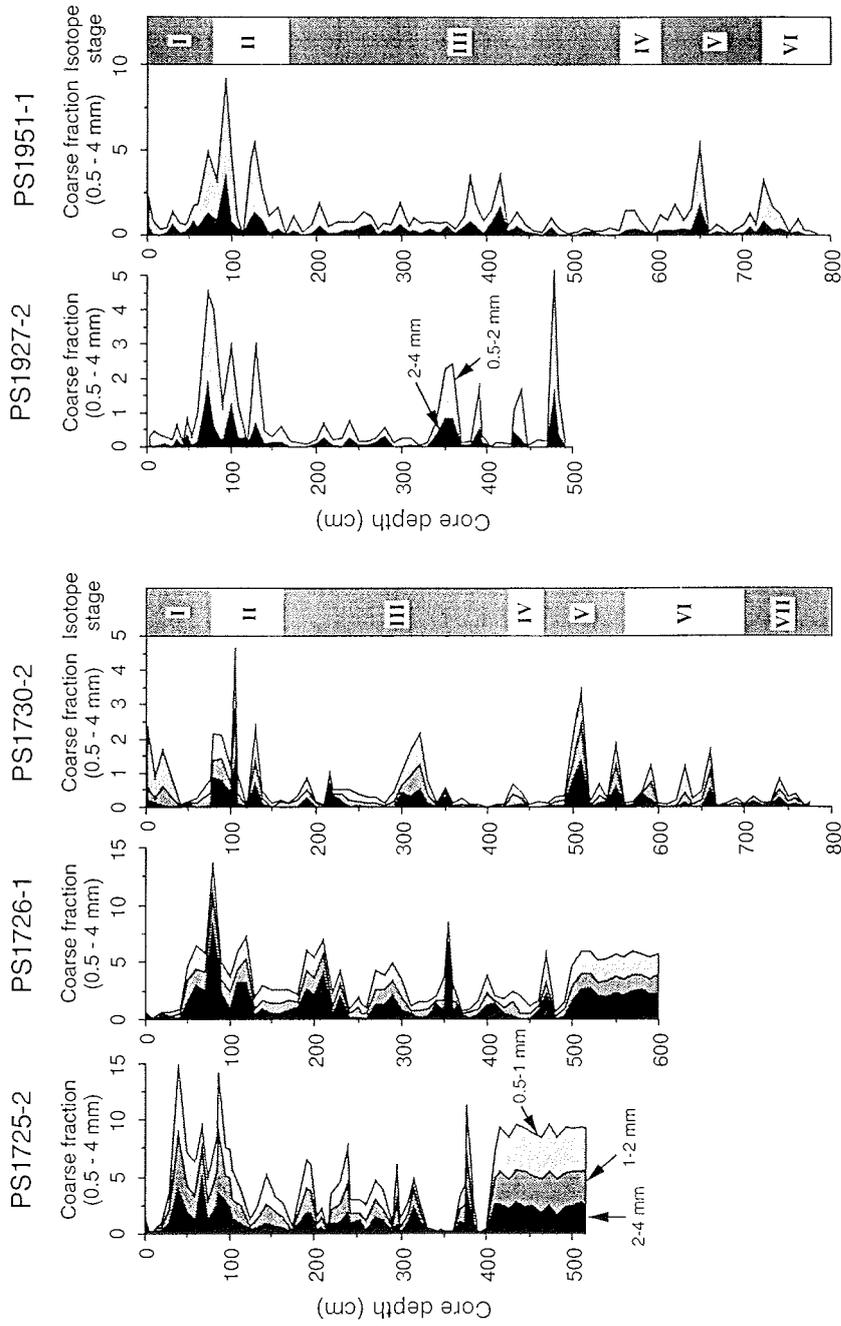
Fig. 19. Distribution (wt. %) of coarse terrigenous sediment fraction (0.5-4 mm) of five sediment cores PS1725-2, PS1726-1, PS1730-2, PS1927-2, and PS1951-1.
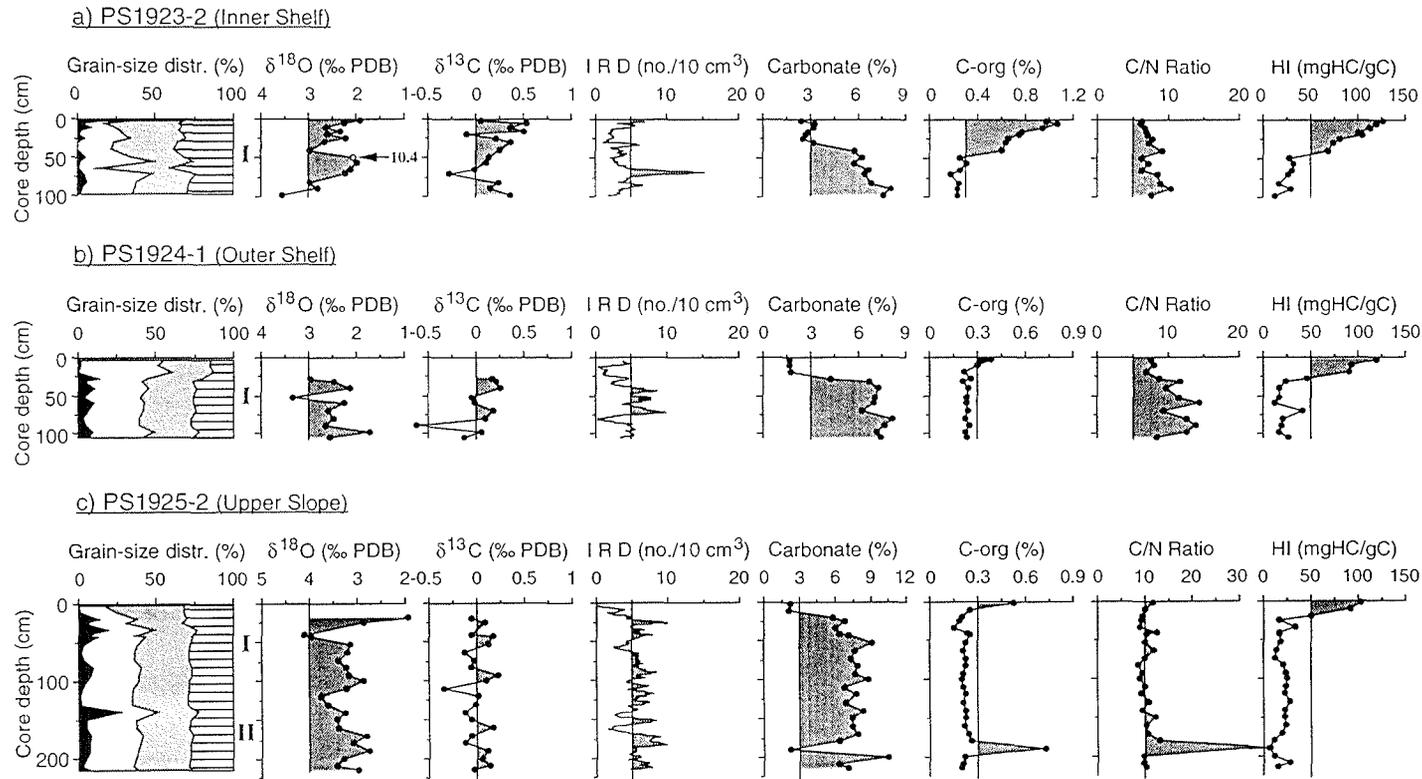
Fig. 20 a-e. Records of sediment cores from Transect A (*see* Fig. 2) (a) PS1923-2 and (b) PS1924-1 (shelf), (c) PS1925-2 and (d) PS1926-1 (slope), and (e) PS1927-2 (deep sea). For all cores, grain-size distributions, stable oxygen and carbon isotope values (measured on the planktonic foraminifer *N. pachyderma* sin.), amount of ice-rafted debris (IRD, i.e. gravel fraction >2 mm, counted in X-radiographs, smoothed by the 5-point moving average methods and expressed as numbers per 10 cm[3]), contents of carbonate and organic carbon, organic carbon/nitrogen (C/N) ratios, and hydrogen index (HI) values (HI expressed as mg hydrocarbons per gram organic carbon) are shown. Roman numbers indicate oxygen isotope stages. Arrows in the oxygen isotope record of cores PS1923-2, PS1926-1 and PS1927-2 mark AMS[14] C-age dated samples (for detailed data *see* Fig. 11 and Table 2). Thick black bars in the carbon isotope record for core PS1927-2 mark samples in which the benthic foraminifer *C. wuellerstorfi* is present.

d) PS1926-1 (Lower Slope)

e) PS1927-2 (Deep Sea)

Fig. 20 a-e. continued.

a) PS1723-1 (Inner Shelf)

b) PS1724-2 (Outer Shelf)

c) PS1725-2 (Upper Slope)
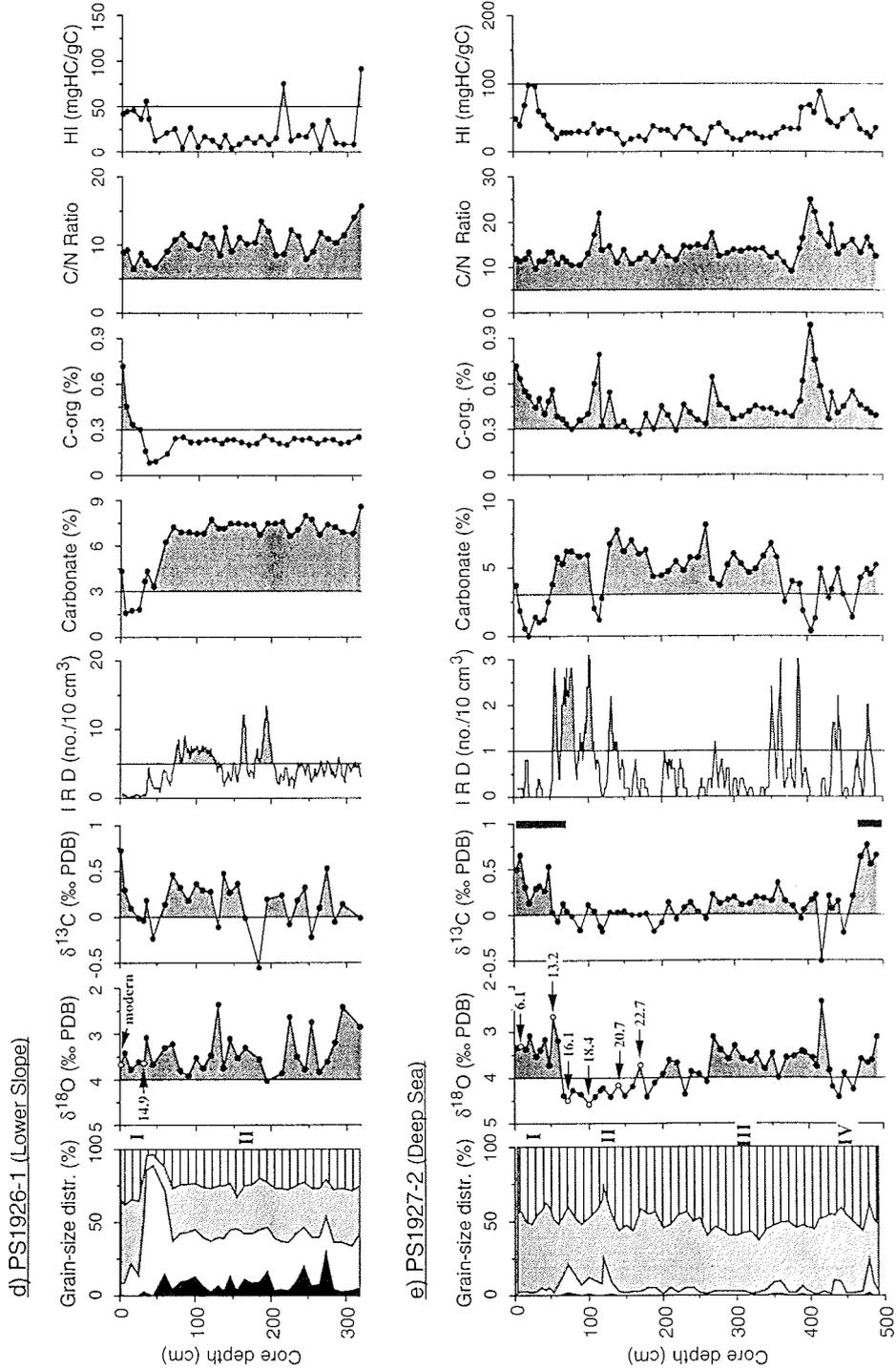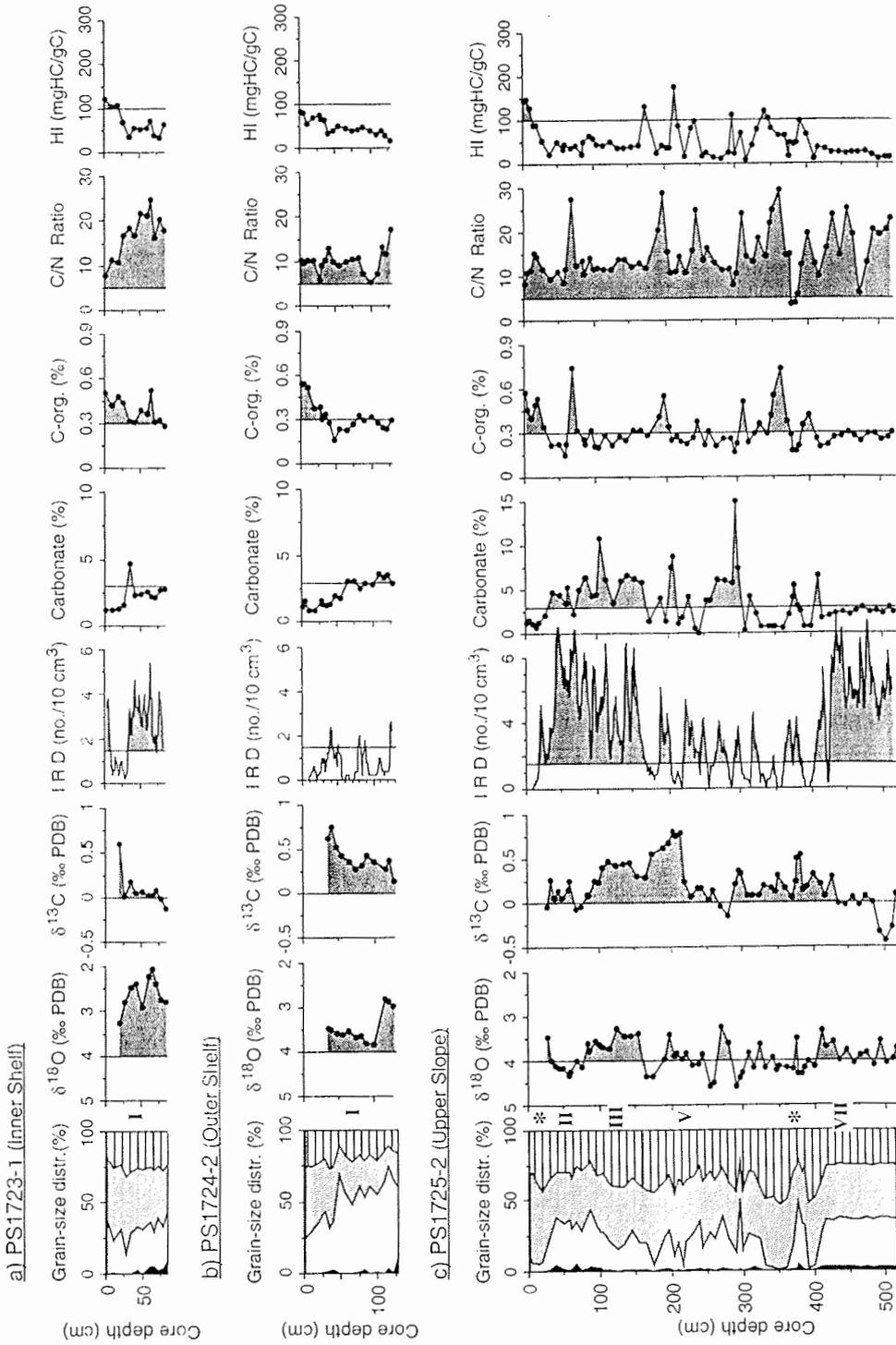
Fig. 21 a-g. Text in next page.

47

d) PS1726-2 GKG

e) PS1726-1 (Lower Slope)
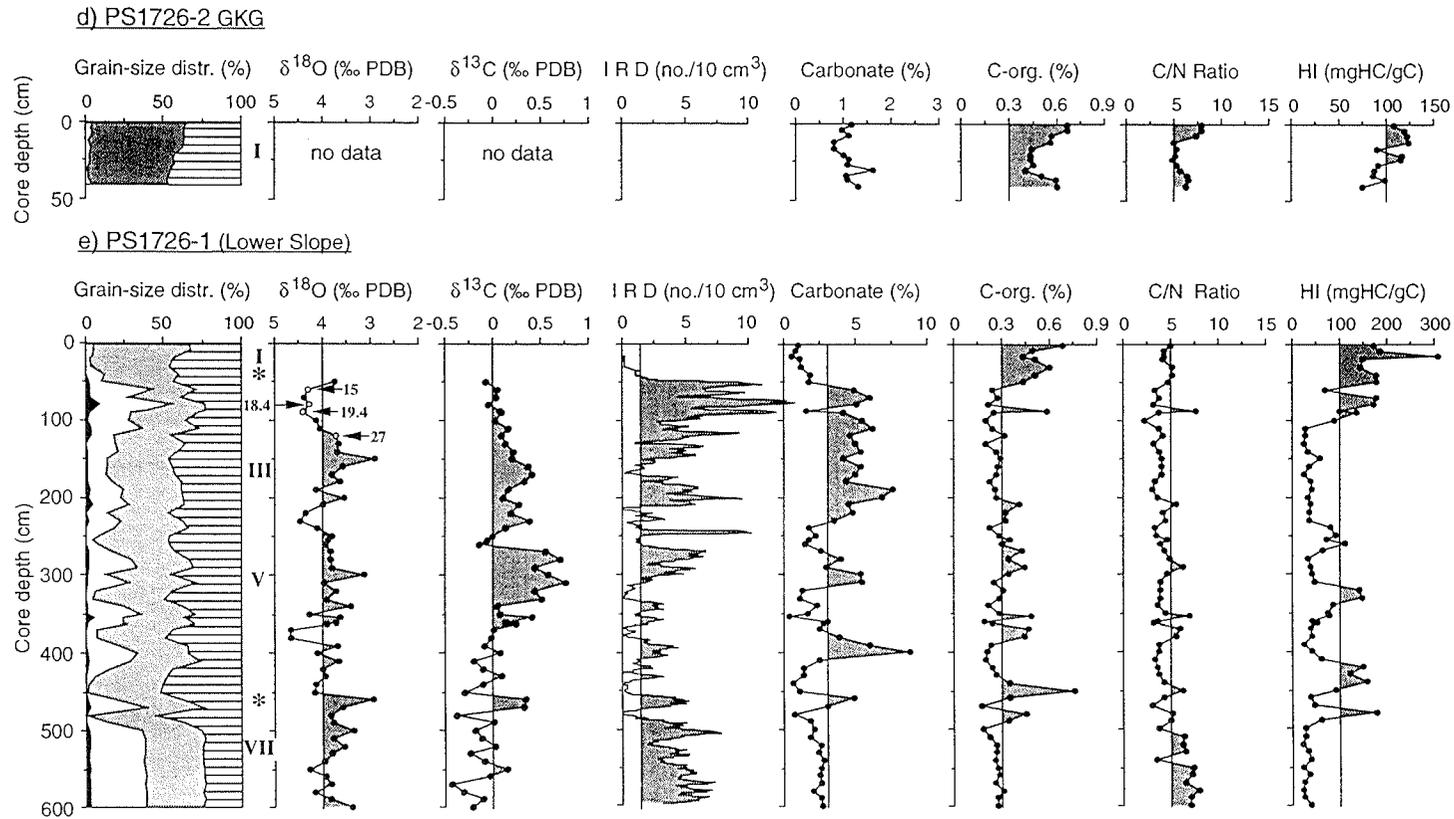
Fig. 21 a-g. Records of sediment cores from Transect B (*see* Fig. 2) (a) PS1723-1 and (b) PS1724-2 (shelf), (c) PS1725-2 and (e) PS1726-1 (slope), and (g) PS1730-2 (deep sea). Records of two box cores (d) PS1726-2 (slope) and (f) PS1730-1 (deep sea) are also shown. For all cores, grain-size distributions, stable oxygen and carbon isotope values (measured on the planktonic foraminifer *N. pachyderma* sin.), amount of ice-rafted debris (IRD, i.e. gravel fraction >2 mm, counted in X-radiographs, smoothed by the 5-point moving average methods and expressed as numbers per 10 cm^3), contents of carbonate and organic carbon, organic carbon/nitrogen (C/N) ratios, and hydrogen index (HI) values (HI expressed as mg hydrocarbons per gram organic carbon) are shown. Roman numbers indicate oxygen isotope stages. Arrows in the oxygen isotope record of cores PS1726-1 and PS1730-2 mark AMS[14]C-age dated samples (for detailed data *see* Fig. 11 and Table 2). Thick black bars in the carbon isotope record for core PS1730-2 mark samples in which the benthic foraminifer *C. wuellerstorfi* is present. Asterisks indicate ash layers. Stable oxygen and carbon values from the bentic foraminifer *O. umbonatus* are additionally present in box core PS1730-1.

f) PS1730-1 GKG

g) PS1730-2 (Deep Sea)

Fig. 21 a-g. continued.

a) PS1946-2 (Inner Shelf)

Grain-size distr. (%) $\delta^{18}O$ (‰ PDB) $\delta^{13}C$ (‰ PDB)   I R D (no./10 cm^3)   Carbonate (%)   C-org (%)   C/N Ratio   HI (mgHC/gC)

b) PS1947-1 (Outer Shelf)

Grain-size distr. (%) $\delta^{18}O$ (‰ PDB) $\delta^{13}C$ (‰ PDB)   I R D (no./10 cm^3)   Carbonate (%)   C-org (%)   C/N Ratio   HI (mgHC/gC)

c) PS1948-2 (Upper Slope)

Grain-size distr. (%) $\delta^{18}O$ (‰ PDB) $\delta^{13}C$ (‰ PDB)   I R D (no./10 cm^3)   Carbonate (%)   C-org (%)   C/N Ratio   HI (mgHC/gC)
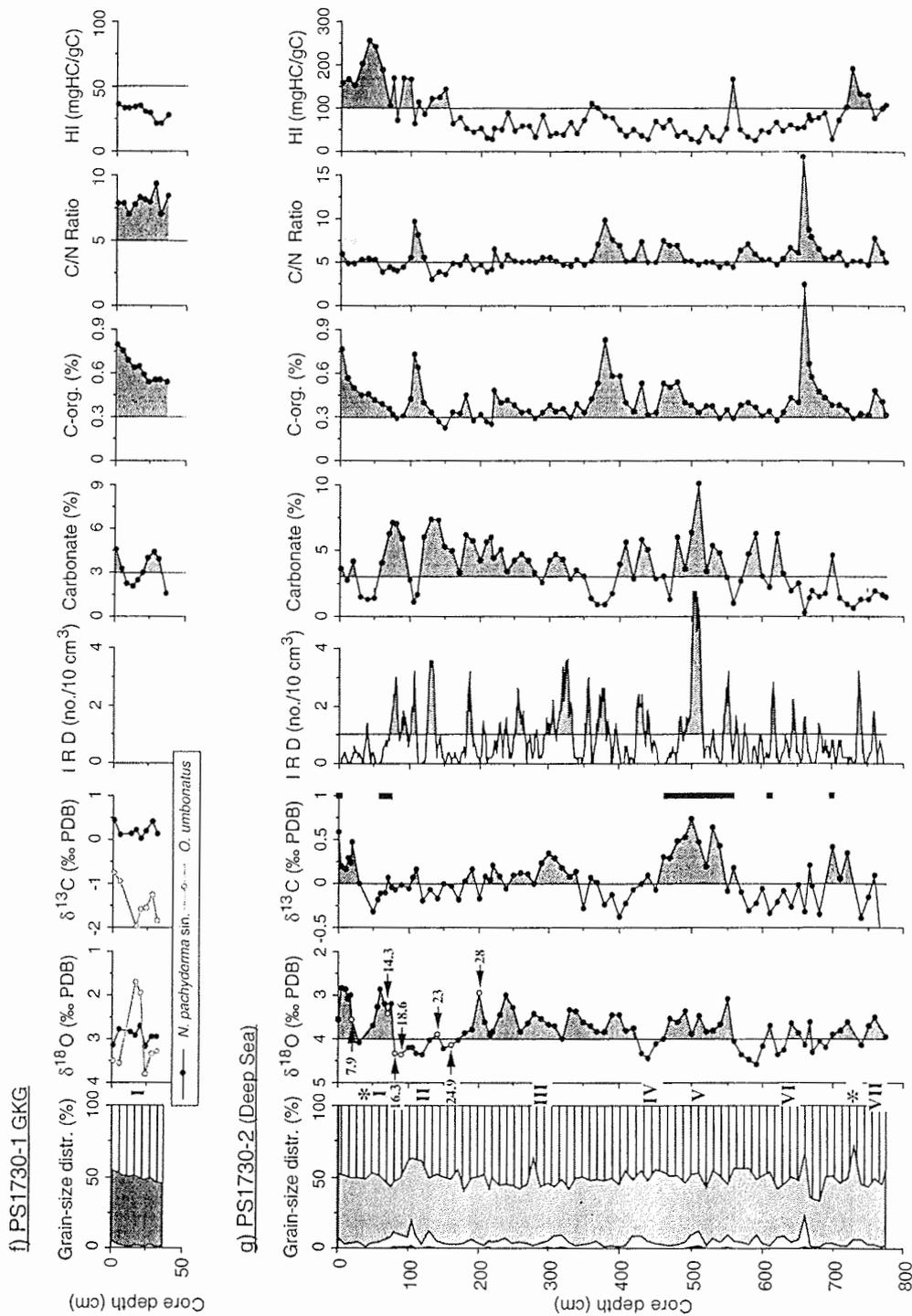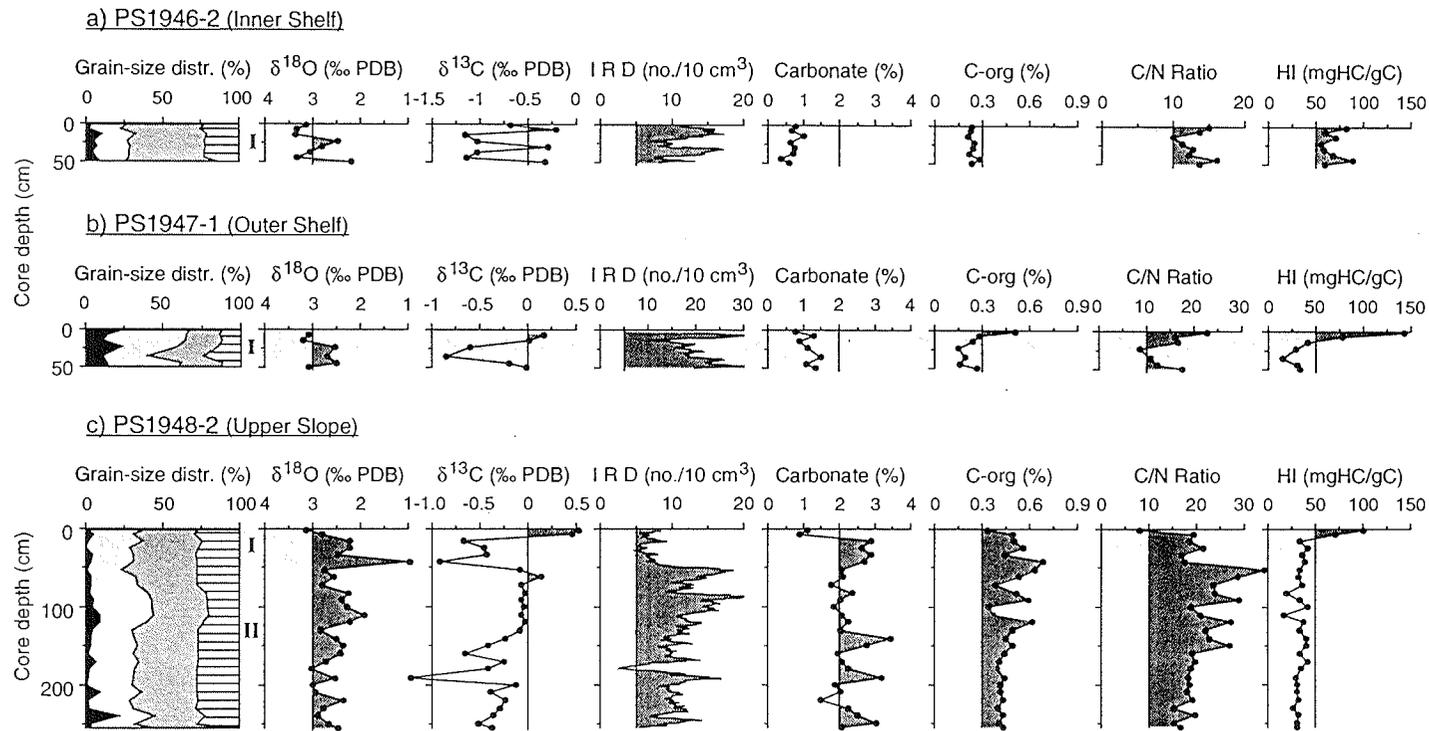
Fig. 22 a-f. Records of sediment cores from Transect C (*see* Fig. 2). (a) PS1946-2 (shelf) and (b) PS1947-1 (shelf), (c) PS1948-2 (slope), (d) PS1949-1 (slope) and (e) PS1950-2 (slope), and (f) PS1951-1 (deep sea). For all cores, grain-size distributions, stable oxygen and carbon isotope values (measured on the planktonic foraminifer *N. pachyderma* sin.), amount of ice-rafted debris (IRD, i.e. gravel fraction >2 mm, counted in X-radiographs, smoothed by the 5-point moving average methods and expressed as numbers per 10 cm^3), contents of carbonate and organic carbon, organic carbon/nitrogen (C/N) ratios, and hydrogen index (HI) values (HI expressed as mg hydrocarbons per gram organic carbon) are shown. Roman numbers indicate oxygen isotope stages. Arrows in the oxygen isotope record and numbers of cores PS1950-2 and PS1951-1 mark AMS[14]C-age dated samples (for detailed data see Fig. 11 and Table 2). Thick black bars in the carbon isotope record of core PS1951-1 mark samples in which the benthic foraminifer *C. wuellerstorfi* is present. Asterisks indicate ash layers. The abbreviation *P.b.* of core PS1951-1 indicates the appearance of the benthic foraminifer *P. bulloides* within substage 5.1.

d) PS1949-1 (Middle Slope)

e) PS1950-2 (Lower Slope)

Fig. 22a-f. continued

f) PS1951-1 (Deep Sea)
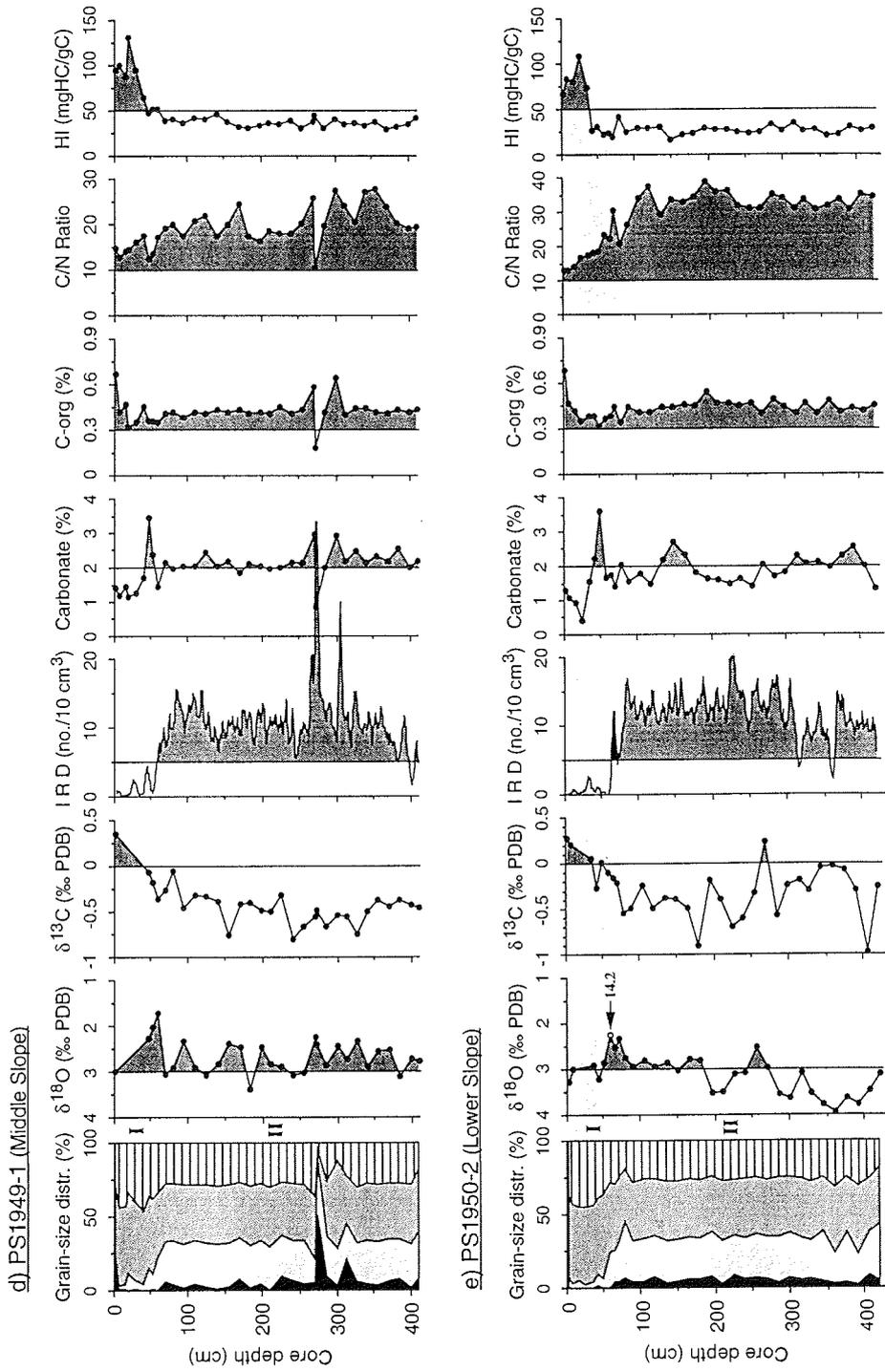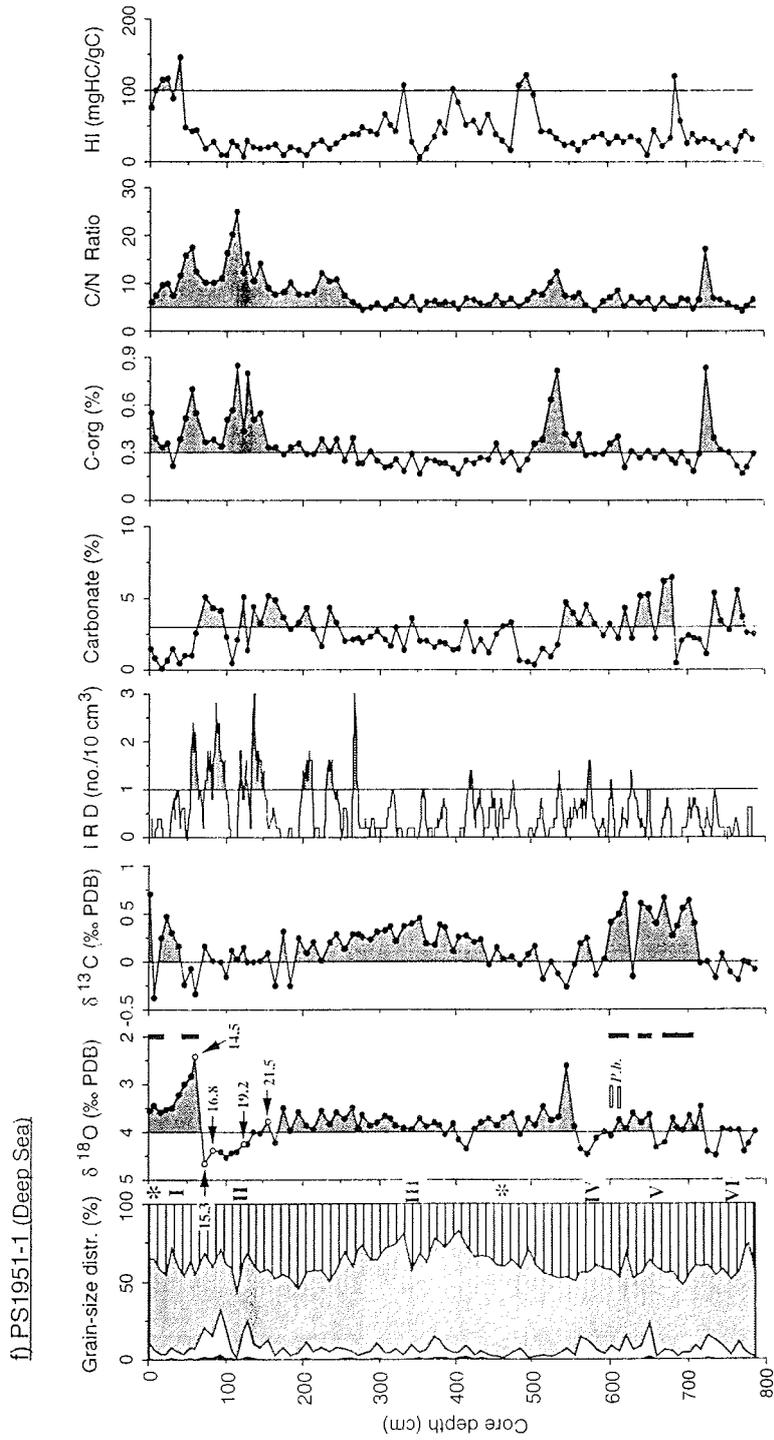
Fig. 22 a-f. continued.

6.2.5 INPUT OF ICE-RAFTED DETRITUS (IRD >2 mm)

In high-latitude oceans, an important component of glaciomarine sediments is terrigenous ice-rafted material transported by icebergs and sea-ice. The ice-rafted debris (IRD >2 mm) estimated from X-radiographs of all investigated sediment cores are presented in Figures 20, 21, and 22.

Moderate to high amounts of IRD are observed during the Holocene in the two shelf cores PS1923-2 and PS1924-2. A distinct decrease in the supply of ice-rafted terrigenous material during the Holocene is recorded in two slope cores PS1925-2 and PS1926-1. The last glacial stage 2, on the other hand, is characterised by an increased IRD content with high-amplitude variations. Deep-sea core PS1927-2 shows a reduced input of coarse ice-rafted detritus throughout (Fig. 20e). There are also indications of increased IRD content within glacial stage 2. Three major peaks representing an increase in the IRD content recorded during the last glacial stage 2 are also identified in the two other deep-sea cores (PS1730-2 and PS1951-1). The intervals characterised by a distinct increase in the IRD content is further substantiated by a major increase in the total terrigenous coarse fraction (0.5 to 4 mm) estimated from the grain-size analysis (cf. Fig. 19).

The two cores PS1723-1 and PS1724-2, collected from the shelf adjacent to Scoresby Sund, contain low to moderate amounts of IRD within the Holocene sequence (Fig. 21a.b). The high amount of the coarse-sand fraction, and IRD in response to glacial-interglacial climatic cycles over the last 240 ka are very well documented in the two slope cores PS1725-2 and PS1726-1 (Fig. 21c,e). In both slope cores, an increase in the IRD content correlates to a similar trend recorded in the total terrigenous coarse fraction (Fig. 19). The variations in the amount of IRD in the upper slope core PS1725-2 are identical to those recorded in the lower slope core PS1726-1. In addition, a moderate to high amount of IRD occurs throughout interglacial stage 7, but decreases during glacial stage 6. The IRD content of stage 6 is relatively low compared to that recorded for the last glacial stage 2. However, there is a periodic increase in the supply of coarse terrigenous material during this interval. Moderate amounts of IRD-input are documented during interglacial stage 5, but decrease in glacial stage 4. A predominant increase in IRD content occurs at the stage 4/3 boundary, and continues from stages 3 through to the stage 2/1 boundary, i.e. Termination Ia (Fig. 21c,e). The same pattern is also reflected in the total coarse terrigenous sediment fraction (Fig. 19). The Holocene sequence is mostly characterised by a decrease in the IRD content. However, one peak corresponding to an increase in the IRD is observed within core PS1725-2. This peak appears to be related to the Younger Dryas cooling event.

In deep-sea core PS1730-2, the IRD content is very similar to the trend recorded in other deep-sea cores. Core PS1730-2 exhibits a relatively decreased input of IRD with some high-amplitude variations. The cyclic input of distinctly increased coarse IRD (Fig. 21g) is observed throughout the entire sequence. A drastic increase in IRD-input is documented within interglacial stage 5.

Cores PS1946-2 and PS1947-1, recovered from the shelf south of Scoresby Sund, reveal a high amount of IRD during the Holocene (Fig. 22a-b).

Furthermore, cores PS1948-2, PS1949-1, and PS1950-2, recovered from the upper to the lower slope, display a drastica decrease in the IRD content during the Holocene. Large amounts of IRD are documented within the three slope cores throughout stage 2. In general, the distinct increase in the IRD content correlates with very light $\delta^{18}O$ and $\delta^{13}C$ values (Fig. 22c,e). The deep-sea core PS1951-1 reveals a decreased IRD content throughout the whole sequence.However, the interval between glacial stage 2 and Termination Ia displays an increased IRD content. Additionally, a periodic increase in the terrigenous coarse ice-rafted sediment fraction (Fig. 22f) is to some extent observed throughout the entire sediment sequence.
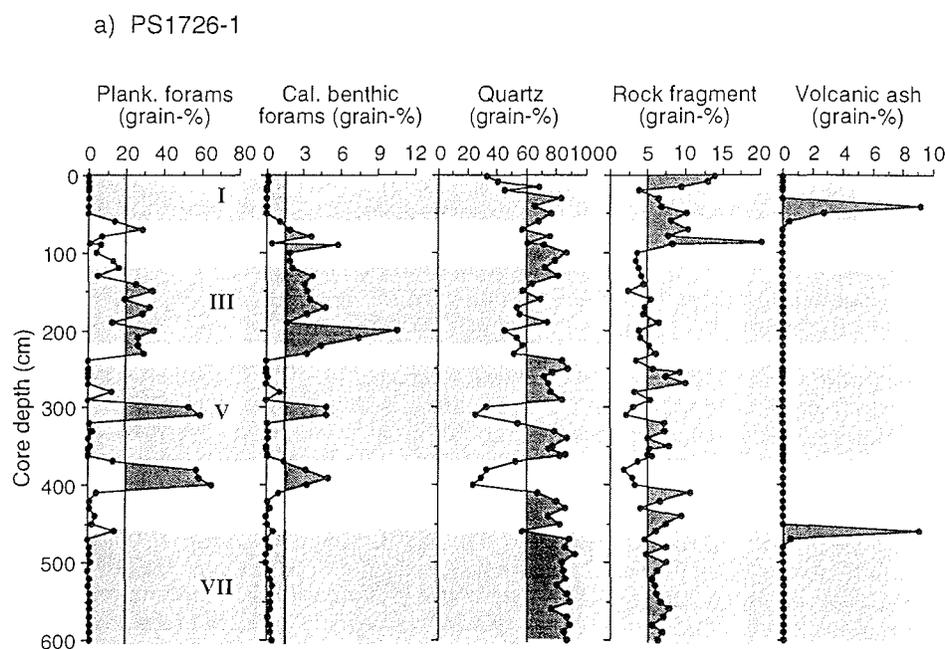
a) PS1726-1

Fig. 23 a-b. Variations in the major biogenic and siliciclastic sediment components and volcanic ash from the 125-250 μm sand fraction (represented as grain-%). For cores a) PS1726-1 and b) PS1730-2. Roman numbers indicate oxygen isotope stages 7 to 1.

6.2.6 DISTRIBUTION OF BIOGENIC AND TERRIGENOUS COMPONENTS

The downcore variations in the biogenic and terrigenous sediment composition of cores PS1726-1 and PS1730-2 are illustrated in Figure 23a-b. According to the component analysis of the 125-250 μm sand fraction, biogenic components are dominated by the monospecific planktonic foraminifer *N. pachyderma* sin., and minor amounts of benthic foraminifers (mainly *C. teretis, C. lobatulus* and *O. umbonatus*). In addition, the uppermost sediment sequences comprise high amounts of agglutinated benthic

foraminiferal assemblages that reach 38.3 grain-% in core PS1726-1 and 53.2 grain-% in core PS1730-2 (Appendix F). In deep-sea core PS1730-2, a minor amount of ostracod shells (<0.6 grain-%) are recorded throughout the sediment sequence. Sponge spicules are the most dominant component of the biogenic opal fraction with minor amounts of radiolarians and diatoms (*see* Appendix F). The terrigenous sediment components are mainly composed of quartz (+ feldspars), rock fragments (crystalline and sedimentary rocks), basalt, and mica. The amount of volcanic glass within ash layer of interglacial stage 7 and the Holocene are around 9 grain-% in core PS1726-1 and between 20 and 75 grain-% in core PS1730-2.

b) PS1730-2
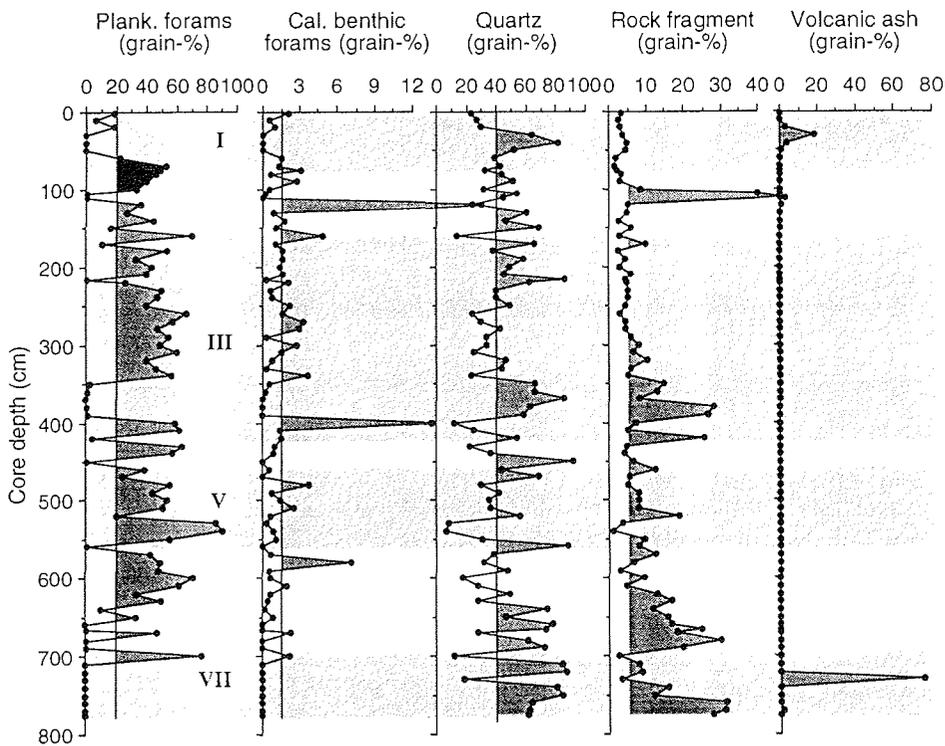
Fig. 23 a-b. continued.

There are no obvious variations in the distribution of biogenic and terrigenous sediment components in response to distinct glacial-interglacial climate cycles. Moreover, it should be noted that the results of the component analysis of the 125-250 µm sand fraction can not be representative of the bulk sediment compositions. Nevertheless, there is a general negative correlation between the biogenic and terrigenous compositions. A dramatic decrease in

the number of foraminiferal specimens, and a distinct increase in the terrigenous components occurs mostly at stage boundaries. The pattern of planktonic foraminiferal occurrences is very similar to that of benthic foraminiferal assemblages. Three distinct benthic foraminiferal peaks, identified in both cores, correspond to the light $\delta^{18}O$ and light $\delta^{13}C$ values (cf. Fig. 21 e,g).

Slope core PS1726-1, is mostly characterised by a lower amount of biogenic components, and a higher content of siliciclastic components in comparison to those recorded in the deep-sea core PS1730-2. In general, fluctuations in biogenic and terrigenous components are relatively lower in core PS1726-1 than in deep-sea core PS1730-2. The sediment sequences of stage 7 and the Holocene are characteristically barren of biogenic components.

In deep-sea core PS1730-2, the planktonic and benthic foraminifers display high-amplitude fluctuations between 0 and 90.5 grain-% and 0 and 21.3 grain-%, respectively. The distribution of terrigenous components also reveals high-amplitude fluctuations. During the interval between early stage 7.4 and early stage 3.3, the rock fragment content fluctuates with high-amplitude between 2 and 35 grain-%.

6.2.7 STABLE OXYGEN AND CARBON ISOTOPE RECORDS

6.2.7.1 Stable oxygen and carbon isotope records of the planktonic foraminifer N. pachyderma sin.

Transect A (shelf to the deep sea adjacent to Carlsberg Fjord) (Fig. 2)

The two shelf cores, PS1923-2 and PS1924-1, are characterised by light $\delta^{18}O$ values that range between 1.72 and 3.56‰. $\delta^{18}O$ values within core PS1923-2, located on the shelf adjacent to Carlsberg Fjord, are generally lighter than those on the outer shelf (core PS1924-1) (Fig. 20a-b). In contrast, $\delta^{13}C$ values are about 0.25‰ lighter on the outer shelf than on the inner shelf, with the lightest value of reaching as low as -0.63‰.

Relatively light $\delta^{18}O$ values ranging between 4.12 and 1.98‰ are also recorded throughout the sequences of cores PS1925-2 and PS1926-1 from the slope (Fig. 20c-d). In contrast to light $\delta^{18}O$ values, $\delta^{13}C$ values ranging between -0.53 and 0.73‰, are heavier than those recorded from the other slope cores (e.g. PS1725-2, PS1726-1, PS1948-2, PS1949-1, and PS1950-2) for the same time interval. In addition, $\delta^{13}C$ values recorded in core PS1926-1 from the lower slope are heavier than those from the upper slope. Without AMS ^{14}C dating, the light $\delta^{18}O$ values of the two slope cores PS1925-2 and PS1926-1 could be interpreted to represent the Holocene. However, the stage 2/1 boundary is dated at 14.9 ka at a depth of 32 cm within the lower slope core PS1926-1. During glacial stage 2, $\delta^{18}O$ values are much lighter than those of the adjacent deep-sea core PS1927-2.

The $\delta^{18}O$ and $\delta^{13}C$ records of core PS1927-2 from the deep sea exhibit the global isotope pattern as reflected within other studies from the GIN Sea (e.g. Vogelsang 1990; Köhler 1992; Jünger 1994). Generally, the light $\delta^{18}O$ values correspond well to the heavy $\delta^{13}C$ values during interglacial stages. On the other hand, glacial stages 4 and 2 are characterised by heavy $\delta^{18}O$ and light $\delta^{13}C$ values. The lightest $\delta^{18}O$ value of 2.32‰ from early stage 3.3, which is about 1‰ lighter than that recorded in other regions of the GIN Sea (cf. Vogelsang 1990; Jünger 1994), corresponds to the lightest $\delta^{13}C$ value of -0.52‰. The heavier $\delta^{18}O$ values recorded between 20 and 16 ka correlate well with light $\delta^{13}C$ values and an increase in the terrigenous IRD content. A silmilar trend is also recorded within the $\delta^{18}O$ and $\delta^{13}C$ records of the other two deep-sea cores (Figs. 21g & 22f). A distinct shift in $\delta^{18}O$ values of 1.67‰ is recorded during Termination Ia, and is dated between 16.1 and 13.2 ka (Fig. 11).

Transect B (shelf to the deep sea adjacent to Scoresby Sund) (Fig. 2)

In core PS1723-1 recovered from the inner shelf, the light $\delta^{18}O$ and $\delta^{13}C$ records throughout the sediment sequence range between 2.05 to 3.28‰ and -0.12 to 0.6‰ respectively (Fig. 21a). The $\delta^{18}O$ and $\delta^{13}C$ values are distinctly lower than those recorded within core PS1724-2 on the outer shelf (Fig. 21b).

In cores PS1725-2 and PS1726-1 recovered from the slope adjacent to Scoresby Sund, the heaviest oxygen isotope values are recorded during glacial stage 6 (4.65-4.7‰) (Fig. 21c,e). In addition, light $\delta^{18}O$ and $\delta^{13}C$ values are also recorded within both slope cores during glacial stage 6 as well as interglacial stage 7. Interglacial stage 5 within core PS1725-2 from the upper slope is not clearly indicated in the $\delta^{18}O$ record, but more so in the heavier $\delta^{13}C$ record. In general, heavy $\delta^{13}C$ values are characteristic of interglacial stages. In particular, the heavy $\delta^{13}C$ values of up to 0.79‰ are characteristic of interglacial stage 5. A shift in $\delta^{18}O$ values of 0.53 to 0.64‰ recorded during Termination Ia is much smaller than compared to the glacial-interglacial ice volume effect of 1.3‰ (e.g. Duplessy et al. 1984; Shackleton et al. 1984; Chappell & Shackleton 1986). These values are also much lower than those recorded within the deep-sea cores (e.g. core PS1927-2).

The $\delta^{18}O$ and $\delta^{13}C$ records of core PS1730-2 from the deep sea show a typical global isotope pattern similar to that recorded in other deep-sea cores (cf. Imbrie et al. 1984; Martinson et al. 1987). The records in core PS1730-2 reflect general glacial-interglacial oscillations that extend back to oxygen isotope substage 7.4 (Fig. 21g). The interglacial stages are generally marked by light $\delta^{18}O$ and heavy $\delta^{13}C$ values, whereas the values at the transition from glacial to interglacial stages are characterised by light $\delta^{13}C$ values. As recorded within both slope cores, the heaviest $\delta^{18}O$ values and lightest $\delta^{13}C$ values, are recorded during glacial stage 6. In general, heavy $\delta^{13}C$ values are recorded within interglacial stages (with the exception of the early periods of

stage 3) and light $\delta^{13}C$ values during glacial stages. Distinctly heavier $\delta^{13}C$ values are recorded within interglacial stage 5. The $\delta^{18}O$ record during stage 3 displays five cyclic light-heavy $\delta^{18}O$ values, which are interpreted as the Dansgaard-Oeschger events (e.g. Broecker & Denton 1989). Termination Ia within core PS1730-2 is characterised by a distinct shift in the oxygen isotope record by 1.14‰. The Younger Dryas cooling event is characterised by relatively heavy $\delta^{18}O$ and light $\delta^{13}C$ values.

Transect C (shelf to the deep sea south of Scoresby Sund) (Fig. 2)

The two cores PS1946-2 and PS1947-1 recovered from the shelf are characterised by light $\delta^{18}O$ values of 3.36 to 2.19‰ and the lightest $\delta^{13}C$ values of up to -1.2‰, that exhibit high-amplitude variations (Fig. 22a-b). Along this transect, the inner shelf exhibits relatively lighter $\delta^{18}O$ and $\delta^{13}C$ values than compared to the outer shelf.

Light $\delta^{18}O$ and $\delta^{13}C$ values are recorded within the whole sequence from three cores PS1948-2, PS1949-1, and PS1950-2 on the slope (Fig. 22c-e). The lightest $\delta^{18}O$ values accompanied by extremely light $\delta^{13}C$ values, are recorded during glacial stage 2 and the Holocene within the three slope cores. A change towards slightly heavier $\delta^{18}O$ values is recorded from the upper slope to the lower slope south of Scoresby Sund. The $\delta^{13}C$ values throughout the three cores are generally lighter than 0‰, and display high-amplitude oscillations. In core PS1948-2 from the upper slope, the lightest $\delta^{18}O$ value of 0.92‰ corresponds to a lightest $\delta^{13}C$ value of -0.91‰. This is interpreted as Termination Ia and is dated in core PS1950-2 at approximately 14.2 ka (Fig. 22e). The light $\delta^{18}O$ and $\delta^{13}C$ values recorded throughout glacial stage 2, are in good accordance with an increase in the IRD content, further indicated by an increase in the accumulation of sand and gravel during this interval (Fig. 22c-e).

The $\delta^{18}O$ and $\delta^{13}C$ values of core PS1951-1 from the deep sea correlate well with the global isotope record and its typical glacial-interglacial oscillations. The $\delta^{18}O$ and $\delta^{13}C$ records are very similar to that shown in the other two deep-sea cores. Distinct shifts in the $\delta^{18}O$ records occur at the boundaries between glacial and interglacial periods, i.e. 6/5, 4/3, and Termination Ia. This remarkable shift to lighter $\delta^{18}O$ values is usually accompanied by a similar trend in the $\delta^{13}C$ record. A distinct shift in the oxygen isotope value of 2.24‰ is recorded at Termination Ia and is dated at 15.3 to14.5 ka (Fig. 11). As shown in the other four long cores PS1725-2, PS1726-1, PS1730-2, and PS1927-2, heavy $\delta^{13}C$ values are representative of interglacial stages. Interglacial stage 5 is characterised by the heaviest $\delta^{13}C$ values of up to 0.71‰.

6.2.7.2 Stable oxygen and carbon isotope records of benthic foraminifers *C. wuellerstorfi* and *O. umbonatus*

The $\delta^{18}O$ and $\delta^{13}C$ records of *C. wuellerstorfi* are characteristic of interglacial stage 5 and the Holocene within core PS1730-2, and stage 5 within core PS1951-1 from the deep sea (Figs. 9-10). The $\delta^{18}O$ values of *C. wuellerstorfi* during the Holocene are about 1‰ heavier than those of stage 5, whereas the $\delta^{13}C$ values show a similar range between 0 and 1.25‰ in both stages. In contrast, the oxygen and carbon isotope records of *O. umbonatus* extend back to the stage 7/6 boundary within core PS1730-2 (Fig. 9). There is no isotope data for stage 7 as *O. umbonatus.* is absent during this interval. In general, the $\delta^{18}O$ and $\delta^{13}C$ records of *O. umbonatus* show a similar correlation with record of *N. pachyderma* sin. (Fig. 12). The interglacial stages, with the exception of stage 3, exhibit light $\delta^{18}O$ values. The $\delta^{18}O$ values of stage 3 fluctuate in response to both interstadial and stadial periods within this interval. The $\delta^{18}O$ compositions of glacial stages exhibit relatively heavy values compared to the interglacial stages, and are in general close to the record of *N. pachyderma* sin.. Termination Ia according to *O. umbonatus* occurs at approximately 12.2 ka, but lags behind that of *N. pachyderma* sin. by approximately 3.6 ka probably as a result of bioturbation (A. Mackensen pers. commun. 1994). However, the timing of the onset of Termination Ia according to *C. wuellerstorfi* is close to that of *N. pachyderma* sin. (Fig. 12).

In general, *O. umbonatus* shows distinctly lighter $\delta^{13}C$ values than compared to those of *N. pachyderma* sin.. The difference in the amplitude of the glacial-interglacial $\delta^{13}C$ record between *N. pachyderma* sin. and *O. umbonatus* is generally >1.0‰. A similar pattern is recorded within sediments from the Greenland Sea (Jünger 1994) and the continental margin of the Weddell Sea (cf. Mackensen et al. 1994). In particular, the lightest $\delta^{13}C$ values of <-3‰ are present during glacial substages 6.5 and 6.3, suggesting a change in bottom water masses. However, the general pattern of the $\delta^{13}C$ record of *O. umbonatus* is very similar to that observed in *N. pachyderma* sin., and reflects the characteristic glacial-interglacial cycles with low $\delta^{13}C$ values during glacials (cf. Mackensen et al. 1994).

6.2.8 CALCIUM CARBONATE DISTRIBUTION

Transect A (shelf to the deep sea adjacent to Carlsberg Fjord) (Fig. 2)

The cores, PS1923-2 and PS1924-1, are characterised by relatively low carbonate content that reach a maximum value of 8 % (Fig. 20a-b). In general, a distinct change occurs within surface sediments where the carbonate content decreases to less than 3 %. Some benthic foraminifers were present within the interval between 56 and 65 cm within core PS1923-1 on the inner shelf.

The carbonate distribution within cores PS1925-2 and PS1926-1 from the slope is similar to that observed within the shelf cores (Fig. 20c-d). Glacial

stage 2 displays a higher carbonate content than that within the Holocene. The carbonate content ranges between 5.7 and 10.5 % with the exception of one point at a depth of 190 cm within core PS1925-2 from the upper slope where a minimum value of 2.2 % is recorded. This interval corresponds to higher organic carbon values, and high C/N ratios (*see* below). The markedly lower carbonate values are also identified within core PS1927-2 recoverd from the deep sea along the same transect. An abrupt decrease in the carbonate content occurs at the stage 2/1 boundary (Termination Ia). The Holocene sedimentary sequence is characterised by lower carbonate values that range between 1.5 and 4.5 %.

In core PS1927-2, the carbonate composition differs from that recorded from the cores on the continental margin. The carbonate in the deep sea mainly originates from the planktonic foraminifer *N. pachyderma* sin., and from minor amounts of benthic foraminifers. Nevertheless, carbonate values are relatively low and range between 0 and 8 % throughout the sedimentary sequence (Fig. 20e). In addition, the fluctuation in the carbonate content does not seem to reflect glacial-interglacial changes. This is clearly different from the pattern recorded within the central and eastern GIN deep sea, where the carbonate values generally reflect glacial-interglacial cycles (e.g. Kellogg 1976, 1977; Kellogg et al. 1978). From early stage 3 to Termination Ia, the carbonate content reveals an increase in values relative to other intervals. A distinct reduction in carbonate values of down to 0 % is recorded at the stage 5/4 boundary, within early stage 3, and during the interval between 20 and 19 ka and between 13 and 6 ka. Within early stage 3, the lower carbonate values correspond to a distinct increase in organic carbon values, higher C/N ratios, and the lightest $\delta^{18}O$ and $\delta^{13}C$ values.

Transect B (shelf to the deep sea adjacent to Scoresby Sund) (Fig. 2)

The cores PS1723-1 and PS1724-2 are characterised by a relatively low carbonate content <5 % (Fig. 21a-b). In the upper part of the Holocene sequence, the carbonate content decreases to a minimum of <2 %.

The carbonate content of two cores PS1725-2 and PS1726-1 from the slope is mainly <10 %, with the exception of two discrete peaks with values ranging up to 15 % (PS1725-2; Fig. 21c,e). These correlate to a maximum within the calcareous foraminiferal content (Fig. 23a). In contrast, the carbonate within stage 7 seems to be of a terrigenous origin as there is an absence of biogenic components within the sediments (*see* Fig. 23a). Distinct carbonate peaks occur within both slope cores during glacial stage 6. The period between stage 7 and middle stage 6 is marked by a relatively lower carbonate content that varies at low-amplitude. This is followed by increased values that fluctuate at high-amplitude upto the stage 2/1 boundary, i.e. Termination Ia. Following this interval, lower carbonate values of <2 % (which show a negative correlation with the organic carbon values) are observed within the Holocene. It is obvious that the minimum carbonate values are mostly recorded at the stage boundaries, e.g. 7/6, 6/5, 5/4, and Termination Ia (Fig. 21c,e). A marked decrease in the carbonate content is recorded during the interval between 19.4 and 19.2 ka within the LGM.

The carbonate content of core PS1730-2 from the deep sea is characterised by relatively low values typically <7.5 % with the exception of one distinct peak within interglacial stage 5. In general, the carbonate fluctuations within this core do not correlate to glacial-interglacial oscillations (cf. Kellogg 1976, 1977). As recorded in the other long cores (PS1725-2, PS1726-1, PS1927-2, and PS1951-1), a decrease in the carbonate content occurs at the stage boundaries (Fig. 21g). In general, a distinct decrease in the carbonate content correlates with a distinct maxima in the organic carbon content, high C/N ratios (e.g. stages 6, 3 and 2), and relatively light $\delta^{18}O$ and $\delta^{13}C$ values (e.g. stages 6, 3, and the Holocene). During the LGM, the carbonate content is relatively higher than that of the Holocene. However, an abrupt decrease in the carbonate content occurs during the interval between 20 and 19 ka.

Transect C (shelf to the deep sea south of Scoresby Sund) (Fig. 2)

The carbonate content of cores PS1946-2 and PS1947-1 are characterised by extremely low values of <1 % (Fig. 22a-b). A decrease in the carbonate content from 8 % to 1.5 % occurs along the shelf regions from Carlsberg Fjord via Scoresby Sund to Steward Ø. The minimum carbonate values seem to coincide with light $\delta^{13}C$ values and an increased IRD content.

In cores PS1948-2, PS1949-1, and PS1950-2 from the slope, the carbonate values are also lower (<3.6 %) than those recorded in the other slope regions (Fig. 22c-e). The general trend towards lower carbonate values is observed along the transect from the upper slope towards the lower slope. The minimum carbonate values occur within the uppermost section of the Holocene sequence. During Termination Ia, there is a slight increase in the carbonate content. During the last glacial stage 2, the carbonate content fluctuates with low-amplitude. An abrupt increase in the supply of gravel-sized ice-rafted detritus at this time seems to be responsible for the dilution of the carbonate content within sediments.

In core PS1951-1 from the deep sea, the carbonate content exhibits values of <6.5 % (Fig. 22f). As recorded in the other four long cores (PS1725-2, PS1726-1, PS1730-2, and PS1927-2), the change towards lower carbonate values is mostly recorded at the stage boundaries, e.g. 6/5, 5/4, and Termination Ia. These intervals are characterised by the lowest carbonate content, and conspicuously light $\delta^{18}O$ and $\delta^{13}C$ values. The carbonate distribution of stage 3 reveals consistently low values that vary at low-amplitude. A distinct increase in the carbonate content is recorded during Termination Ia. Following this period, considerably lower carbonate values are recorded during the Holocene. Two distinct events, displayed by an abrupt decrease in the carbonate content, occur during the last glacial stage 2 at approximately 19.6 and 18.3 ka, respectively.

6.2.9 DISTRIBUTION AND COMPOSITION OF ORGANIC CARBON

Transect A (shelf to the deep sea adjacent to Carlsberg Fjord) (Fig. 2)

Four sediment cores along the continental margin adjacent to Carlsberg Fjord are characterised by a very low organic carbon content of <0.3 %. An exception to this are the near-surface sediments that are characterised by a distinct increase in the organic carbon content of up to 1.1 % (Fig. 20a-d). In addition, the lower organic carbon content coinciding with the C/N ratios of >10 for the LGM and the early Holocene. However, an the exception to this is the single peak within core PS1925-2 from the upper slope. In core PS1927-2 from the deep-sea, the organic carbon content reveals a relative increase from 0.3 to 1 % (Fig. 20e). During stages 3 and 2, several peaks representing an increase in the organic carbon content correlate well with peaks of increased C/N ratios.

The C/N ratios of the four cores along the continental margin range between 6 and 15 (Fig. 20a-d). The C/N ratios of the deep-sea core PS1927-2 vary around 13, with the highest values of up to 25 (Fig. 20e). In general, low hydrogen index (HI) values of <100 mgHC/gC are recorded within all the five cores adjacent to Carlsberg Fjord, reflecting the dominance of terrigenous organic carbon throughout the sequence. HI values (100 mgHC/gC) are only exhibited within the uppermost surface sediments.

Based on a van Krevelen-type diagram, most of the organic matter in these five sediment cores falls consistently into the type III field (i.e. low hydrogen and high oxygen index values) (Fig. 24a-c), indicating a predominance of immature terrigenous organic matter. Tmax values of <435°C are characteristic of all the sediment cores adjacent to Carlsberg Fjord, and support the immature nature of the organic matter. Only a few higher Tmax values of >435°C are recorded from the Holocene sequence (Appendix D).

Transect B (shelf to the deep sea adjacent to Scoresby Sund) (Fig. 2)

The five sediment cores along a transect from the shelf to the deep sea perpendicular to Scoresby Sund are characterised by relatively low organic carbon values that range between 0.1 and 0.8 % (Fig. 21a-g), except for one single peak of 1.5 % at a depth of 660 cm within core PS1730-2. During the transition from the LGM to the Holocene, drastic changes in the organic carbon content are not observed throughout the entire sediment sequences. Distinct peaks of high organic carbon values during stages 6, 3, and 2 correlate well with high C/N ratios and low HI values, indicating events of increased input of terrigenous organic matter. In addition, the high organic carbon content mostly correspond to dark greyish lithological facies (see core description in Appendix A). The brownish Holocene sediment sequence is also enriched in organic carbon with contents ranging between 0.3 and 0.7 % in accordance with relatively low C/N ratios, and markedly increased HI values between 100 and 300 mgHC/gC.

Generally, higher C/N ratios between 10 and 30 are recorded within sediment cores from the inner shelf to the upper slope. In contrast, the two cores from the lower slope and the deep sea display lower C/N ratios of approximately 5,

with a maximum value of 18 at a depth of 660 cm within core PS1730-2. With the exception of stage 7, core PS1726-1 from the lower slope shows relatively lower C/N ratios of <5 throughout the sediment sequence. However, the interval from stage 7 to early stage 2 is characterised by lower HI values (Fig. 21e).

With some exceptions, all five cores show low HI values between 50 and 100 mgHC/gC, reflecting higher amounts of terrigenous material. This sequence is generally accompanied with higher C/N ratios and an increased input of sand-sized rock fragments. During the interval from the Last Glacial Maximum to the Holocene, both cores PS1726-1 and PS1730-2 display relatively high HI values of >100 to 300 mgHC/gC and low C/N ratios <10 (Fig. 21e,g).

In a van Krevelen-type diagram, most of the organic matter of all five cores have low HI and high OI values indicating a terrigenous source (kerogen type III) (Fig. 24d-f). There is some evidence of a slightly increased amount of material of a marine origin within stages 7, 5, 2, and during the Holocene. According to Tmax values of <435°C, the organic matter within cores PS1723-1 and PS1724-2 from the shelf appears to be very immature (cf. Stein 1991). In general, Tmax values of >435°C are recorded within the three long cores (PS1725-2, PS1726-1, and PS1730-2) during interglacial stages (Appendix D).

Transect C (shelf to the deep sea south of Scoresby Sund) (Fig. 2)

The organic carbon contents within the two sediment cores from the shelf adjacent to Steward Ø show very low values of <0.3 %, that coincide with high C/N ratios of >10 and low HI values of <100 mgHC/gC (Fig. 22a-b). Tmax values are generally lower than 435°C (Appendix D).

In the three cores from the upper to the lower slope, the organic carbon content varies between 0.3 and 0.7 % (Fig. 22c-e). An increase in the organic carbon content within core PS1948-2 occurs during the interval from late stage 2 to the stage 2/1 boundary, and correlates well with an increased IRD content, a decreased carbonate content, and higher C/N ratios (Fig. 22c). C/N ratios from the three slope cores are consistently higher (15-40) than compared to those from the other slope cores (e.g. PS1725-2 and PS1726-1). Although C/N ratios are still somewhat high in value, an apparent decrease in the C/N ratios occurs within cores PS1949-1 and PS1950-2 at the stage 2/1 boundary. Tmax values are homogenous within the three slope cores at around 435°C during stage 2 and >435°C during the Holocene. (Appendix D).

In core PS1951-1 from the deep-sea, the organic carbon values fluctuate with high-amplitude and range between 0.17 and 0.85 % (Fig. 22f). The minimum organic carbon values are characteristic of interglacial stages 5 and 3. Five distinct, single peaks of high organic carbon values are documented at the stage 6/5 boundary and within stages 3, 2, and 1. The peaks correlate well with increased C/N ratios. One single peak of organic carbon recorded at approximately 18.7 ka corresponds to a finely laminated layer in which IRD is absent, whereas the other four discrete peaks correlate well with an increased IRD content. The interval below a depth of 255 cm, with the exception of two discrete peaks, exhibits low C/N ratios. In contrast, the interval from early stage

63
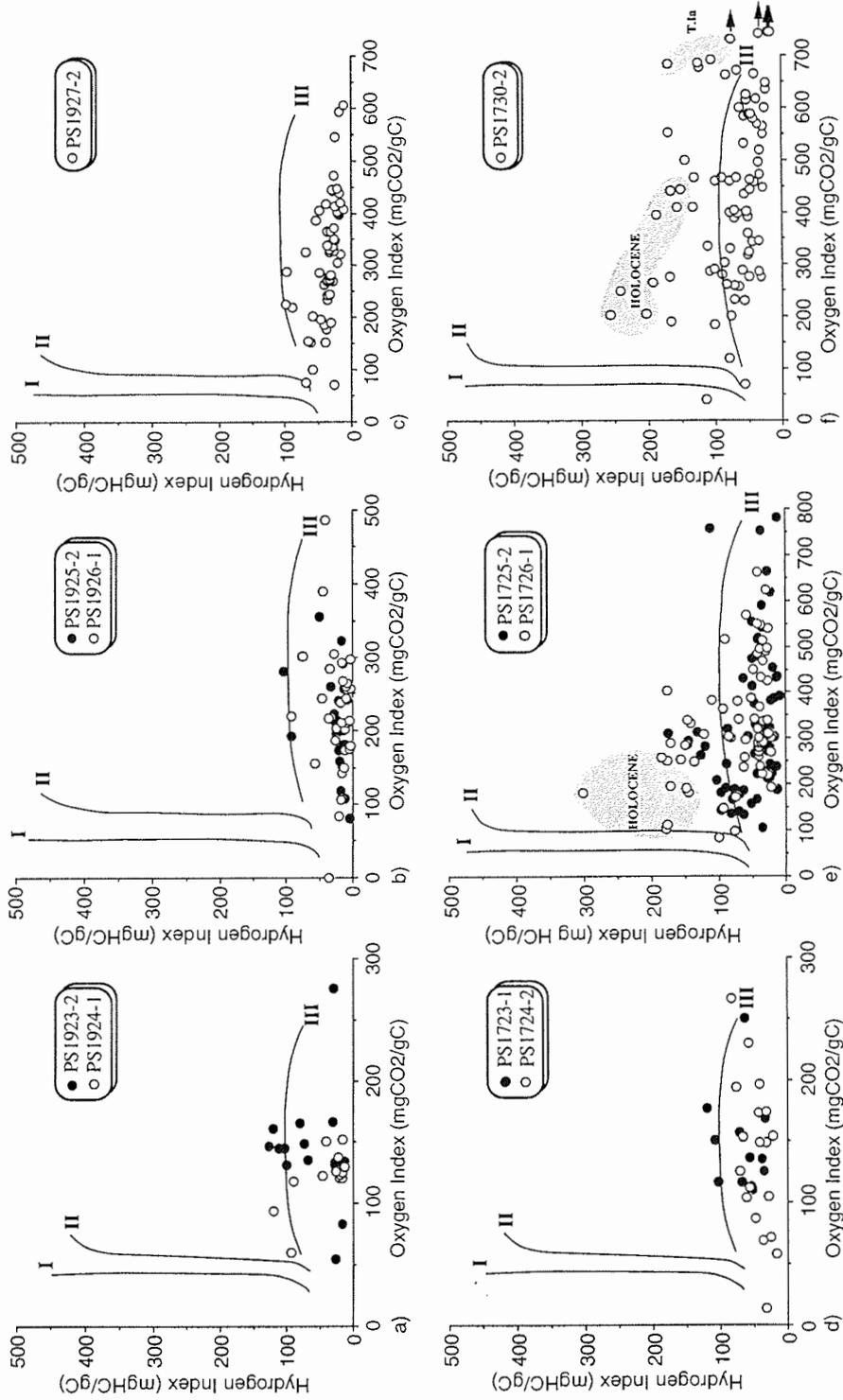
Fig. 24 a-i. Text in next page.

3 to the Holocene, is characterised by C/N ratios that vary with a high-amplitude from 6 to 25. This interval also corresponds to an increased organic carbon content. The whole sediment sequence, except for the Holocene, is characterised by low HI values of <50 mgHC/gC. Tmax values fluctuate with high-amplitude between 300 and 533°C (Appendix D).

The low HI and OI values of the two shelf cores fall close to the origin within a van Krevelen-type diagram and, therefore seem to reflect higher amounts of reworked and probably more mature organic matter (Stein et al. 1993) (Fig. 24g). In contrast, the Holocene sequence within the three slope cores, as indicated by the low HI and high OI values, may be composed of highly oxidized organic matter (cf. Stein et al. 1989). In particular, it is interesting to note that within the LGM diamicton sequence of these three cores, the composition of the organic matter as indicated by the low HI and OI values, is very similar to those shown within the Holocene of both shelf cores (Fig. 23a-b). Most of the organic matter in the sediments of core PS1951-1 from from the deep-sea is of type III, i.e. of terrigenous origin (Fig. 24i). Therefore, only the Holocene organic matter is likely to be a mixture of terrestrial and marine origin.
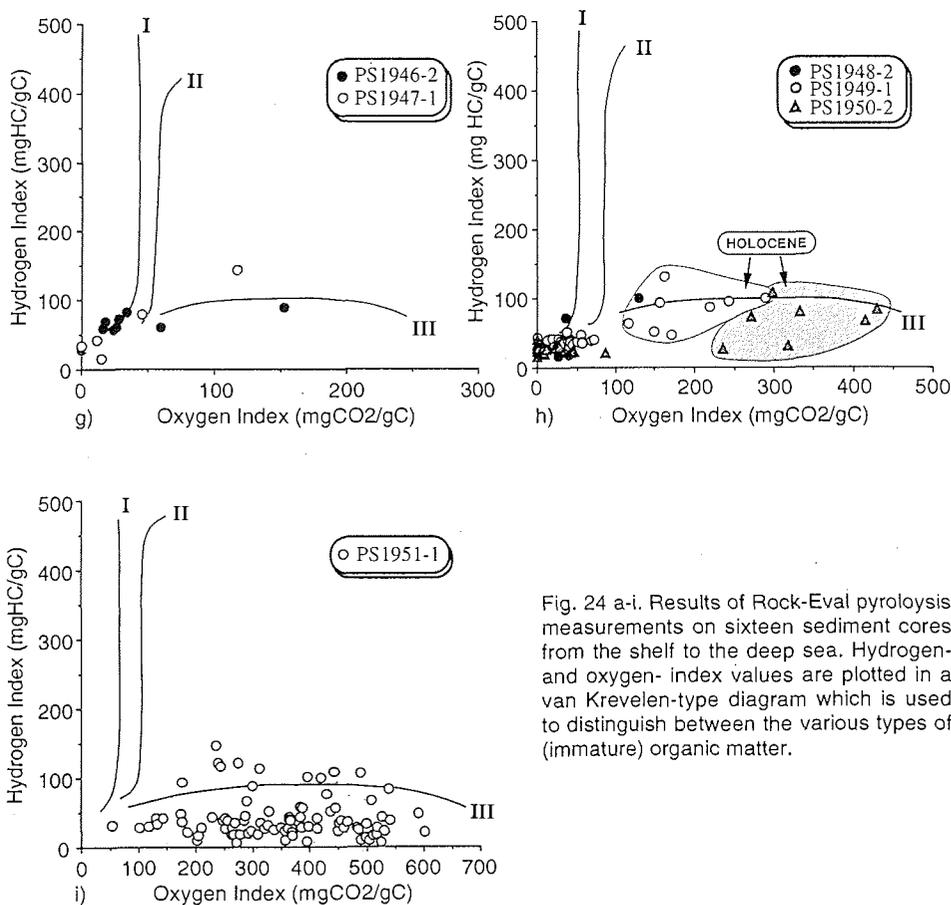
Fig. 24 a-i. Results of Rock-Eval pyroloysis measurements on sixteen sediment cores from the shelf to the deep sea. Hydrogen- and oxygen- index values are plotted in a van Krevelen-type diagram which is used to distinguish between the various types of (immature) organic matter.

6.2.10 ACCUMULATION RATES OF BIOGENIC AND TERRIGENOUS MATTER

6.2.10.1 Carbonate accumulation rate

In general, the carbonate fluxes calculated from the five long cores do not reflect glacial-interglacial cycles. The carbonate accumulation rates from the slope exhibit distinctly lower values and range between 0 and 0.5 g cm^{-2} kyr^{-1} (Fig. 25). The carbonate flux rates from the deep-sea cores vary with a relatively high-amplitude, and range between <0.1 and 1.1 g cm^{-2} kyr^{-1} (Fig. 25). In general, a distinct increase in the carbonate flux rate occurs at the stage 4/3 boundary.
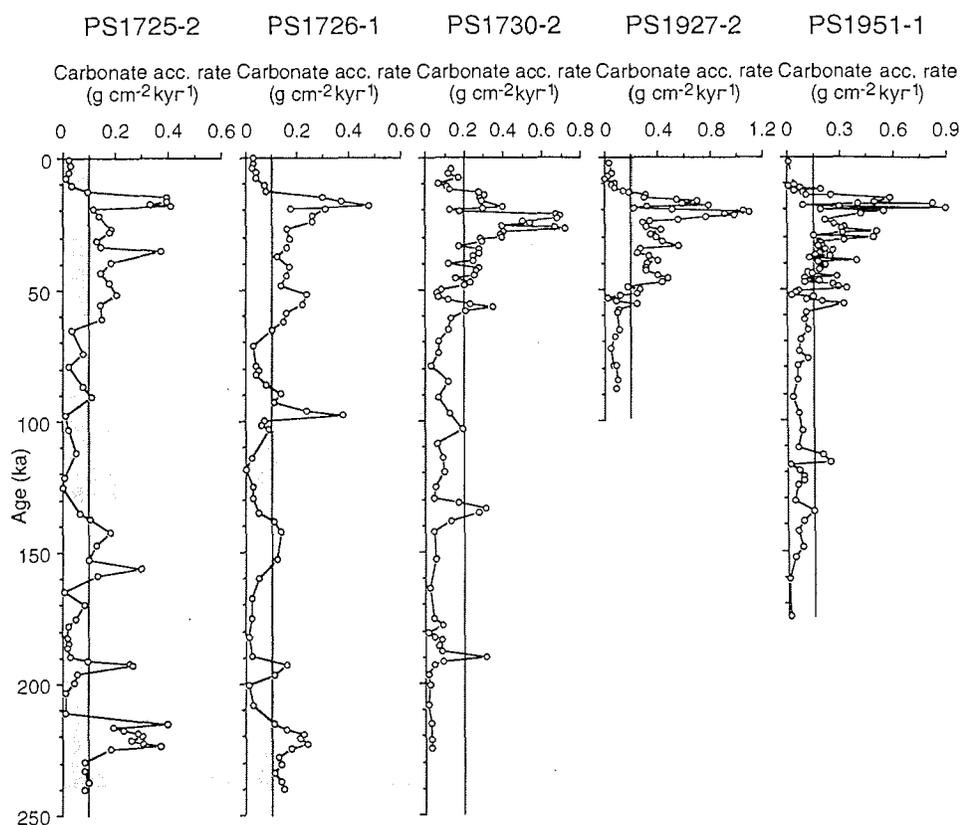
Fig. 25. Carbonate accumulation rates of two cores PS1725-2 and PS1726-1 from the slope, and three cores PS1730-2, PS1927-2, and PS1951-1 from the deep sea during the last 240 ka.

In cores PS1725-2 and PS1726-1 from the slope adjacent to Scoresby Sund, low carbonate accumulation rates of <0.1 g cm^{-2} kyr^{-1} are recorded for the

interval between stages 6 and 4. A slight increase in the carbonate accumulation rate of $\geq$0.1 g cm^{-2} kyr^{-1} is recorded during stages 7 and 6, and at the stage 7/6 boundary. A distinct increase in the carbonate flux occurs during stages 3 to 2. A maximum value of 0.5 g cm^{-2} kyr^{-1} is recorded during the interval between 20 and 15 ka. Within the Holocene, the carbonate flux decreases to a minimum value of 0.01 g cm^{-2} kyr^{-1}. The pattern of carbonate accumulation rate within the deep-sea cores is also very similar to that recorded in the slope cores. The lower values of <0.2 g cm^{-2} kyr^{-1} occur during stage 7 to stage 4. In general, increased values of >0.2 g cm^{-2} kyr^{-1} occur during stages 3 and 2. Within stage 3, cores PS1730-2 and PS1951-1 frequently reveal lower values of <0.2 g cm^{-2} kyr^{-1}. The high-amplitude variations in the carbonate flux are displayed within the three deep-sea cores during stages 3 and 2. In particular, distinct higher values of $\geq$ 0.4 g cm^{-2} kyr^{-1} are recorded in cores PS1730-2 and PS1927-1 during the interval between 28.0 and 21.2 ka, and 23.8 to 19.5 ka, respectively. The higher carbonate accumulation rates are also recorded in core PS1951-1 during the interval between 21.5 and 15.3 ka. The carbonate flux rates decrease drastically at Termination Ia, and reach a minimum value of $\leq$0.01 g cm^{-2} kyr^{-1} during the Holocene.
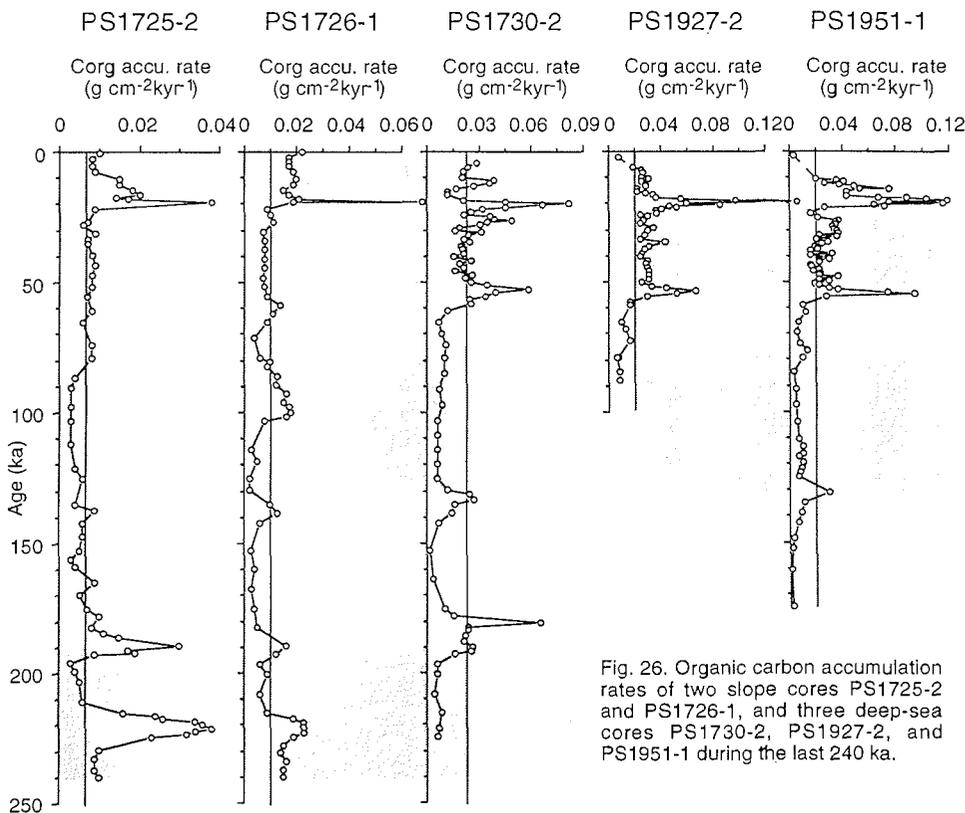
Fig. 26. Organic carbon accumulation rates of two slope cores PS1725-2 and PS1726-1, and three deep-sea cores PS1730-2, PS1927-2, and PS1951-1 during the last 240 ka.

6.2.10.2 Organic carbon accumulation rate

In general, the accumulation rate of total organic carbon is characterised by much lower values on the slope than in the deep sea. The entire sequence of the slope cores PS1725-2 and PS1726-1, with the exception of the distinct peaks within stages 7 and 2 and at the stage 7/6 boundary, reveals lower values of <0.02 g cm^{-2} kyr^{-1} (Fig. 26). In general, the interval from stage 6 to stage 3 displays the lowest values of ≤0.01 g cm^{-2} kyr^{-1}. In the deep-sea cores PS1730-2, PS1927-2, and PS1951-1, a trend towards lower organic carbon flux occurs between stage 7 and stage 4. Compared to the two slope cores, the organic carbon flux of the three deep-sea cores increases to >0.02 g cm^{-2} kyr^{-1} at the stage 4/3 boundary. In the three deep-sea cores, the highest organic carbon accumulation rate ranges between 0.08 and 0.15 g cm^{-2} kyr^{-1}, and occurs during the interval between 20.1 and 17.8 ka (Fig. 26). During the Holocene, the organic carbon flux of the two slope cores increases from <0.01 g cm^{-2} kyr^{-1} on the upper slope to about 0.02 g cm^{-2} kyr^{-1} on the lower slope. In the three deep-sea cores, the organic carbon flux decreases towards values typical of the late Holocene.
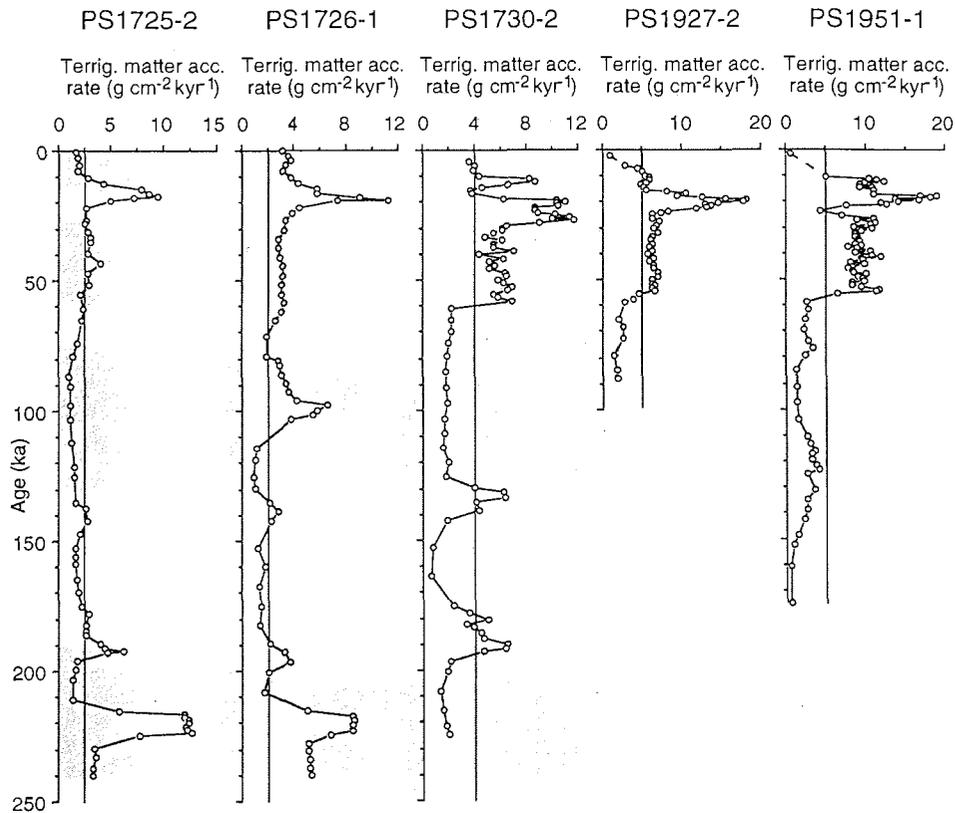
Fig. 27. Terrigenous matter accumulation rates of two slope cores PS1725-2 and PS1726-1 and three deep-sea cores PS1730-2, PS1927-2, and PS1951-1 during the last 240 ka.

6.2.10.3 Accumulation rate of terrigenous matter

The accumulation rate of terrigenous matter (Fig. 27) calculated from the five long cores shows very similar trends to that within the bulk mass accumulation rate (Fig. 14) as the sediments are mostly composed of terrigenous material. The accumulation rate within cores PS1725-2 and PS1726-1 from the slope, with the exception of stages 7 and 2, are represented by low values of <4 g cm^{-2} kyr^{-1}. At the stage 7/6 and 4/3 boundaries, a trend towards increased accumulation rates is characteristic of the two slope cores. Compared to the slope cores, a general trend of increasing terrigenous flux is recorded in the three deep-sea cores. However, a more distinct increase in the terrigenous flux occurs at the stage 4/3 boundary. The rates increase distinctly in the five long cores during stage 2, and rise to maximum values of 18.9 g cm^{-2} kyr^{-1} during the interval between 21.2 and 17.5 ka. During the Holocene, the terrigenous matter accumulation rates decrease to a low value of ≤0.99 g cm^{-2} kyr^{-1}.

7. LATE QUATERNARY GLACIAL-INTERGLACIAL SEDIMENT COMPOSITION ALONG THE EAST GREENLAND CONTINENTAL MARGIN AND PALEOCEANOGRAPHIC IMPLICATIONS

7.1. Sediment composition and paleoceanographic implications during the last two glacial-interglacial cycles

Marine sediments within the GIN Sea reflect variations in the surface water properties, oceanic circulation patterns, sea-ice cover, and the waxing and waning of the surrounding continental ice sheets during late Quaternary climatic cycles (Kellogg 1976, 1977, 1980; Kellogg et al. 1978; Ramm 1988; Henrich et al. 1989, 1995; Jansen et al. 1990; Baumann et al. 1993, 1995; Hebbeln et al. 1994; Johannessen et al. 1994; Wagner & Henrich 1994; Nam et al. 1995a; Stein et al. 1996). The EGC transports very cold and low-saline polar water masses, and a high volume of icebergs southward along the western part of the GIN Sea from the Arctic Ocean. In contrast, the northward inflow of relatively warm and high-saline North Atlantic water contributes to the transport of heat and moisture towards the high-latitude continents and is sensitive to late Quaternary climatic changes. The strong gradients that exist between the ice covered Polar waters and the relatively warm Atlantic waters enable the GIN Sea to be a key region for understanding the changes in paleoclimate and paleoceanography during late Quaternary glacial-interglacial cycles.

In the high-latitude northern oceans, variations in the sediment composition are closely related to surface-water productivity, supply of terrigenous ice-rafted debris, and resuspended material transported by icebergs, sea-ice, and currents. Due to a relatively low sea-level stand, an increase in the sea-ice cover and discharge of icebergs, and extended continental ice sheets during glacial periods, the sediment supplied to the deep-sea floor is dominated by non-biogenic material (e.g. Ruddiman & McIntyre 1976; Ruddiman 1977). In contrast, during interglacial periods, open-water conditions coupled with a high sea-level stand have contributed not only to the reduced supply of terrigenous sediment, but also to an increase in surface-water productivity resulting in enhanced flux-rates of biogenic material to the sea floor (Kellogg 1976, 1980; Gard & Backman 1990).

In general, a number of extensive investigations within the GIN Sea have gained an insight into the properties of sediment composition and their response to changes in the paleoclimate and paleoceanography (e.g. Ramm 1988; Henrich et al. 1989; Baumann et al. 1993). The most common features of deep-sea sediments are the colour changes (varying between dark and light layers) reflecting glacial-interglacial climatic cycles (e.g. Henrich et al. 1989, 1995; Hebbeln 1991; Bond et al. 1992a). The results from the GIN Sea indicate characteristic variations in the sediment composition that reflect differential development and prevailing conditions of surface water, and the subsequent sedimentary processes and environments through glacial-interglacial periods (Kellogg 1976, 1977, 1980; Kellogg et al. 1978; Damuth 1978; Jansen & Erlenkeuser 1985; Ramm 1988; Henrich et al. 1989, 1995; Baumann et al. 1993, 1994, 1995; Nam et al. 1995a).

70

Until now, little information concerning sedimentary processes and environments, and the paleoclimatic and paleoceanographic history is ascertained from the heavily ice-covered western margin of the Greenland Sea (Stein et al. 1993, 1996; Jünger 1994; Antonow 1995; Nam et al. 1995a). In fact, most of the sedimentological, micropaleontological, organic-geochemical, and stable isotopic data for the region are based on studies from the central and eastern part of the GIN Sea, and are used in the interpretation of paleoclimatological and paleoceanographical changes during late Quaternary glacial-interglacial cycles (e.g. Kellogg 1976, 1977; Henrich et al. 1989, 1995; Vogelsang 1990; Sarnthein et al. 1992, 1995; Baumann et al. 1993, 1994; Wagner & Henrich 1994; Goldschmidt 1995). Therefore, the investigated glaciomarine sediments along the East Greenland continental margin provide an important new data set for the reconstruction of the paleoclimate and paleoceanography of the GIN Sea associated with late Quaternary climatic change.

7.1.1 Biogenic carbonate records and their response to glacial-interglacial climate change along the East Greenland continental margin

The biogenic carbonate content (e.g. coccoliths and calcareous foraminifers) of marine sediments are generally related to water-mass properties and biological productivity (Kellogg 1976; Gard 1988; Samtleben & Schröder 1992; Samtleben et al. 1995). Other factors such as water depth, sedimentation, preservation, and dissolution are also of major importance (e.g. Anderson 1975; Biscaye et al. 1976; Kellogg 1980; Broecker & Peng 1982; Henrich 1986; Gard 1987; Carstens 1988; de Vernal et al. 1992; Steinsund & Hald 1994). Within the GIN Sea, the distribution of biogenic carbonate reveals a significant decrease towards the west due to a distinct gradient within surface-water masses (Kellogg 1976, 1977, 1980; Gard 1988; Henrich et al. 1989; Paetsch et al. 1992; Samtleben & Schröder 1992; Baumann et al. 1993, 1994). The carbonate content reveals a marked decrease landward due to dilution by an increased input of terrestrial derived non-carbonate sediment (e.g. Baumann et al. 1994; Nam et al. 1995a). Changes in surface-water masses are well reflected in the distribution of planktonic floral and faunal assemblages (e.g. Kellogg 1976; Gard 1988; Eide 1990; Gard & Backman 1990; Schrader & Koç Karpuz 1990; Johannessen et al. 1994; Matthiessen 1995; Samtleben et al. 1995). Currently, the biogenic carbonate records are used as an indicator for understanding the dynamics of climatic and paleoceanographic change during late Quaternary glacial-interglacial cycles. In the central and eastern GIN Sea, the carbonate content is generally higher during interglacials than during glacial periods resulting from the inflow of warm Atlantic water and reduced sea-ice cover (Kellogg 1976, 1980; Gard 1988; Paetsch et al. 1992; Baumann et al. 1993, 1994).

Compared to the central and eastern region, the western margin of the GIN Sea displays a different carbonate distribution pattern that results from the strong influence from cold and low-saline Polar water and the severe sea-ice cover (Fig. 28a-e; e.g. Kellogg 1976). The carbonate fluctuations do not seem to reflect the general glacial-interglacial climatic changes (cf. Kellogg 1976, 1977, 1980; Baumann et al. 1994). Carbonate contents are typically <10 % except for a peak of approximately 15 % in substage 6.4 for core PS1725-2 from the upper slope. These values are distinctly lower than compared to

those from the central and eastern GIN Sea. This suggests that there has been little incursion of North Atlantic water along the western margin of the GIN Sea throughout the last 245 ka. A relative increase in the carbonate content is not consistently recorded during interglacial stages, i.e. stages 5 and 1, as is observed in the central and eastern regions of the GIN Sea (cf. Kellogg 1976, 1980). In contrast, there is evidence of relatively enhanced carbonate flux during glacial stages 6, 4, and 2. The most conspicuous event involving higher foraminiferal abundances is documented between 153 and 135 ka (substages 6.4, 6.3, and 6.2) in the slope and deep-sea cores corresponding to the Saalian glaciation (Fig. 28a-c, e). A significantly increased carbonate content is also displayed during this interval. During substages 6.4 and 6.2, the coarse terrigenous IRD content reveals a distinct decrease probably resulting from an extensive sea-ice cover (Nam et al. 1995a; *see* Section 7.2). In contrast, during substage 6.3, the higher abundance of foraminifers coincides with an increased IRD content reflecting an increase in iceberg calving and melting (e.g. core PS1726-1), which may in turn contribute to the high nutrient supply necessary to sustain the productivity blooms along the continental slope (e.g. Lloyd et al. 1996b). The increased carbonate content during interglacials and glacials correlates well to a high abundance in planktonic foraminifers indicating a major proportion of the carbonate originating from biogenic material (Fig. 28b-c).

An increased abundance of foraminifers indicates that there was a strong, seasonally reduced sea-ice coverage, and/or open-ocean conditions during interglacial and glacial stages (Kellogg 1980). According to the investigation into the phytoplankton biomass and productivity of the Fram Strait (Smith et al. 1987; Hebbeln & Wefer 1991), higher biogenic productivity took place at the ice-margin during summer months. Similarly, a high concentration of zooplankton (mostly planktonic foraminifers) is recorded in the water masses near the ice margin from the southern part of the Greenland Sea (Thiede & Hempel 1991). The productivity and abundance rapidly decrease under the ice but are less rapid towards the open water environment (Hebbeln & Wefer 1991; Carstens & Wefer 1992). The high biological productivity probably relates to an increased nutrient supply that results from ice-edge upwelling, which commonly occurs at the sea-ice margins (Jacobs et al. 1979; Smith et al. 1987). During substages 6.4 and 6.2, heavier $\delta^{18}O$ values than those of the last glacial stage 2 suggest very low SST at the extensive sea-ice margin. During severe glacial conditions such as substages 6.4 and 6.2, the ice-margin is considered to have extended to the continental shelf break along the eastern margin of Greenland (*see* Section 7.2). However, some ice-free conditions along the fluctuating ice margin may have been induced by summer melting during peak glacial periods. Nutrients are often concentrated in sea ice by the aeolian transport of terrestrial particles (Smith et al. 1987), whereas calving icebergs commonly have a higher nutrient concentration than that of the ambient sea water (Jacobs et al. 1979). Due to an increased influx of nutrients from the melting marginal ice zone, there was higher foraminiferal productivity during peak glacial periods. Heavy $\delta^{13}C$ values in the upper slope core PS1725-2 may support some ice-free conditions along the fluctuating ice margin during this interval.

Along the western margin of the GIN Sea, cold and low saline polar waters of the EGC, sea-ice coverage, and increased calving and melting of icebergs coupled with the corresponding high supply of IRD have crucially controlled

the surface productivity and the preservation of biogenic carbonate during the last two glacial-interglacial intervals. The very high abundance (>95 %) of *N. pachyderma* sin. along the East Greenland continental margin (*see* Appendix F) reflects very low SST and a permanent winter sea-ice cover (Kellogg 1976, 1980; Johannessen et al. 1994). The predominance of terrigenous IRD within glaciomarine sediments indicates an increase in the discharge of icebergs and meltwater (*see* Section 7.2). The northern Greenland Sea, and the
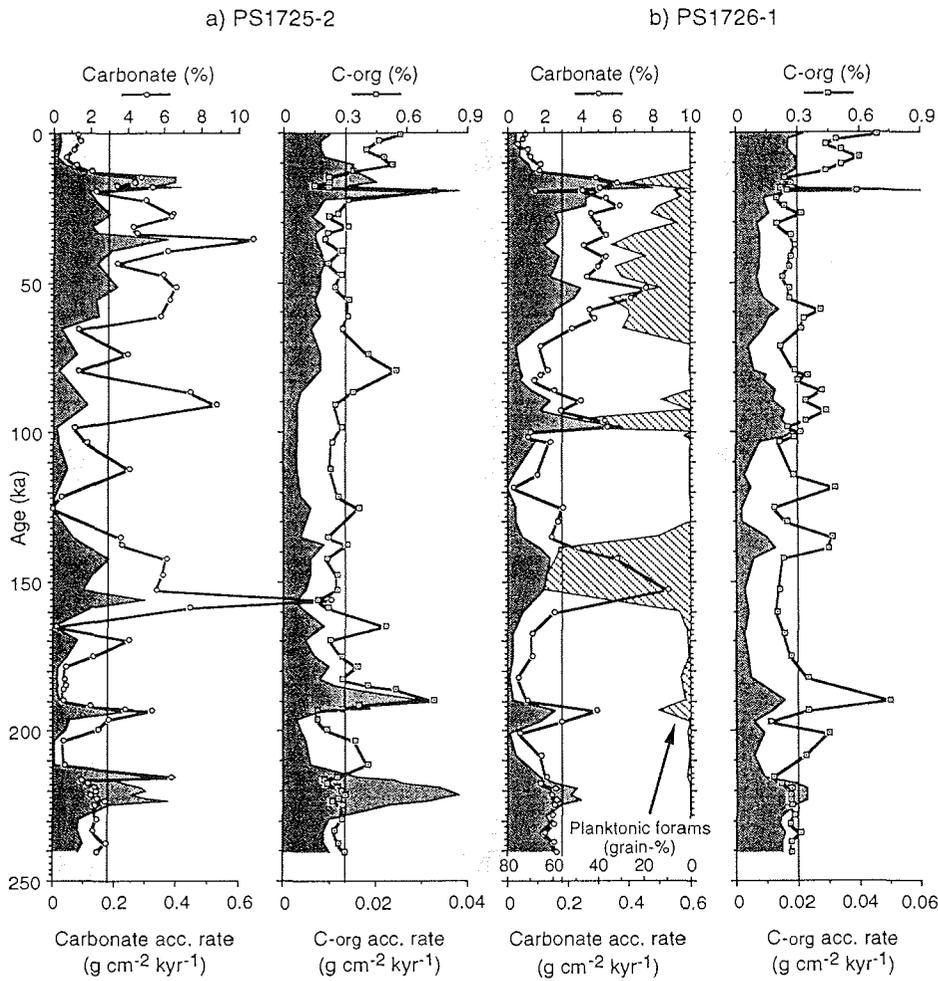
a) PS1725-2   b) PS1726-1

Fig. 28 a-e. Carbonate and organic carbon contents, and accumulation rates of carbonate and organic carbon of five cores a) PS1725-2, (b) PS1726-1, (c) PS1730-2, (d) PS1927-2, and (e) PS1951-1 are plotted against age (ka). The relative abundance of planktonic foraminifer from the sand fraction (125-250 μm) is represented as grain-% (cores PS1726-1 and PS1730-2). Interglacial stages are shaded.
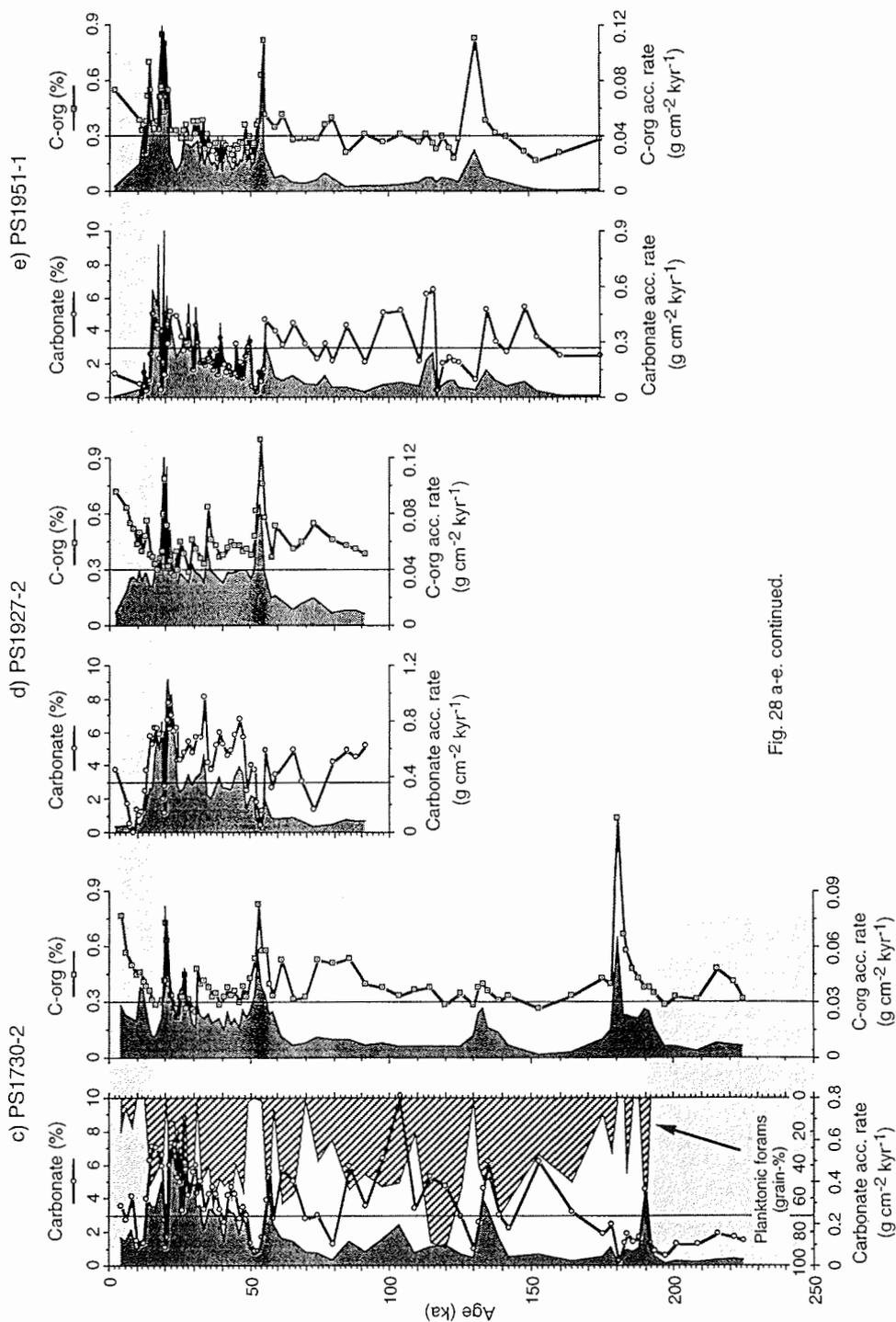
Fig. 28 a-e. continued.

74

Iceland Plateau are similarly characterised by a significantly reduced influx of carbonate during the past 200 ka (Baumann et al. 1994; Grobe et al. unpub. data). This region is also characterised by an increased coarse IRD content (Baumann et al. 1994; Stein et al. 1996). The Jan Mayen Polar Current (JMPC) and the East Icelandic Current (EIC) may not have only been responsible for a restriction in the planktonic productivity, but also the transportation of large amounts of icebergs along the western margin of the GIN Sea from eastern Greenland and the Arctic Ocean. A high input of coarse IRD may have caused an increased dilution, and therefore, dissolution of the biogenic carbonate. Along the slope adjacent to Scoresby Sund (cores PS1725-2 and PS1726-1), the increased coarse IRD content within interglacial stage 5 has most likely induced the dilution of biogenic carbonate, further reflected in the absence of the planktonic foraminifers in core PS1726-1. On the other hand, low carbonate values on the slope area may have resulted from low carbonate productivity due to a persistently strong influence of cold and low saline polar waters and an enhanced sea-ice coverage.

With the onset of glacial periods (i.e. 7/6, 5/4, and 3/2), the carbonate content decreases considerably implying reduced surface-water productivity. During the transitional interval from interglacials to glacials, all sediment cores exhibit a distinct reduction in the terrigenous sediment content representing a reduction in the supply to the western margin of the Greenland Sea. The reduced input of biogenic carbonate and a strong decrease in the coarse terrigenous sediment content may be interpreted as a response to the abrupt and very fast extension of sea-ice cover over the surface water during the early part of glacial periods. As suggested previously, the rapid drop in SST during the interglacial-glacial transition may have not only contributed to reduced iceberg melting, but also accelerated the extensive growth of the sea-ice cover. Consequently, the heavily ice-covered East Greenland continental margin suppressed foraminiferal productivity in the surface water, and reduced or even prevented iceberg drifting towards the deep sea resulting in the remarkably decreased supply of carbonate and coarse IRD onto the sea floor.

The early part of the interglacial stages is similarly marked by a minimal carbonate content and a limited occurrence of planktonic foraminifers. This is attributed not only to the increased dilution from terrigenous matter, but also to decreased production of biogenic carbonate in the stratified surface waters resulting from major meltwater discharge (Nam et al. 1995a). For instance, Termination II and Ia and substage 3.31 are indicated by large meltwater events in the GIN Sea (see Section 8.2). Due to the deglaciation of the adjacent continental ice sheets, an extensive inflow of isotopically light meltwater contributed to the drastic reduction in deep-water ventilation (e.g. Broecker et al. 1988b). This led to less oxygenated and nutrient-enriched bottom water masses causing strong carbonate dissolution (Henrich 1986). During the same time slices, the input of terrigenous organic matter increased, and a subsequent rise in the pCO_2 of bottom waters resulted from the decomposition of organic carbon. This process can contribute to additional $CaCO_3$ dissolution at the sea floor (de Vernal et al. 1992; Steinsund & Hald 1994). A similar effect on carbonate dissolution is suggested for the Holocene due to increased flux of marine-origin organic matter (see Section 8.2.8).

7.2 Fluctuations in the input of terrigenous sediment and response to the advance and retreat of East Greenland glaciers

Numerous investigations on marine sediments from the eastern GIN Sea (Hebbeln 1992; Svendsen et al. 1992; Baumann et al. 1994, 1995; Hebbeln et al. 1994; Elverhøi et al. 1995; Goldschmidt 1995; Lloyd et al. 1996a) coupled with those on terrestrial deposits (Miller et al. 1987, 1989; Mangerud & Svendsen 1992) were performed in order to reconstruct the growth and decay of the Scandinavian Ice Sheet and the Barents Sea Ice Sheet during the last two glacial-interglacial cycles. In particular, a good correlation between the IRD signal from marine sediments and the glacial record from the surrounding continents can be used to reconstruct the glacial activities and fluctuations of continental glaciers (Baumann et al. 1995; Elverhøi et al. 1995; Goldschmidt 1995; Lloyd et al. 1996a).

In East Greenland, the reconstruction of the glacial history based on terrestrial sediments is much more difficult than that derived from Scandinavia and Svalbard because of the recurrence of hiatuses on land records (e.g. Funder et al. 1994; Möller et al. 1994). For instance, the mountain and upland sediments were transported mainly by ice and meltwater reflecting major glaciations whereas deposits of the ice-free intervals are rarely identified due to hiatuses (Möller et al. 1994). On the other hand, the ice-free warm periods are predominantly documented in fluvial and marine sediments distributed along the coastal region (Hansen et al. 1994; Landvik et al. 1994; Lyså & Landvik 1994). Based on several sedimentary successions in the uplands and along the coastal region adjacent to the Jameson Land area a composite chronostratigraphical scheme has been devised by Funder et al. (1994).

In comparison to the knowledge of the late Quaternary glacial history of the Scandinavian Ice Sheet and the marine-based Barents Sea Ice Sheet, the history of the advance and retreat of the Greenland Ice Sheet is relatively unknown due to the limited investigations of glaciomarine sediments along the East Greenland continental margin (cf. Mienert et al. 1992; Nam et al. 1995a; Stein et al. 1996). Therefore, it is currently difficult to reconstruct the advance and retreat of East Greenland glaciers, and to correlate their terrestrial signals with those in the marine records of the Greenland Sea. For this reason, use is made of the accumulation rates of coarse terrigenous matter (>63 μm; cAR), the estimated terrigenous coarse IRD content between 0.5 and 4 mm (wt-%), and the IRD (>2 mm) content counted on X-radiographs from five high-resolution sediment cores in order to gain an insight into the understanding of the glacial history related to the advance and retreat of East Greenland glaciers during the last two glacial-interglacial cycles (Fig. 29a-e). Furthermore, the glacial advance and retreat of the Greenland Ice Sheet will be correlated with those of the Scandinavian Ice Sheet and the Barents Shelf Ice Sheet over the last 200 ka.

Although the component analysis of the 125-250 μm sand fraction was performed on only two cores PS1726-1 and PS1730-2, the result seems to provide limited information concerning the provenance of the terrigenous sediment components. This is probably the result of two reasons: 1) the sand subfraction is dominated by specific siliciclastic components such as quartz as well as by a biogenic component (Fig. 23a-b); and 2) the deposition of the
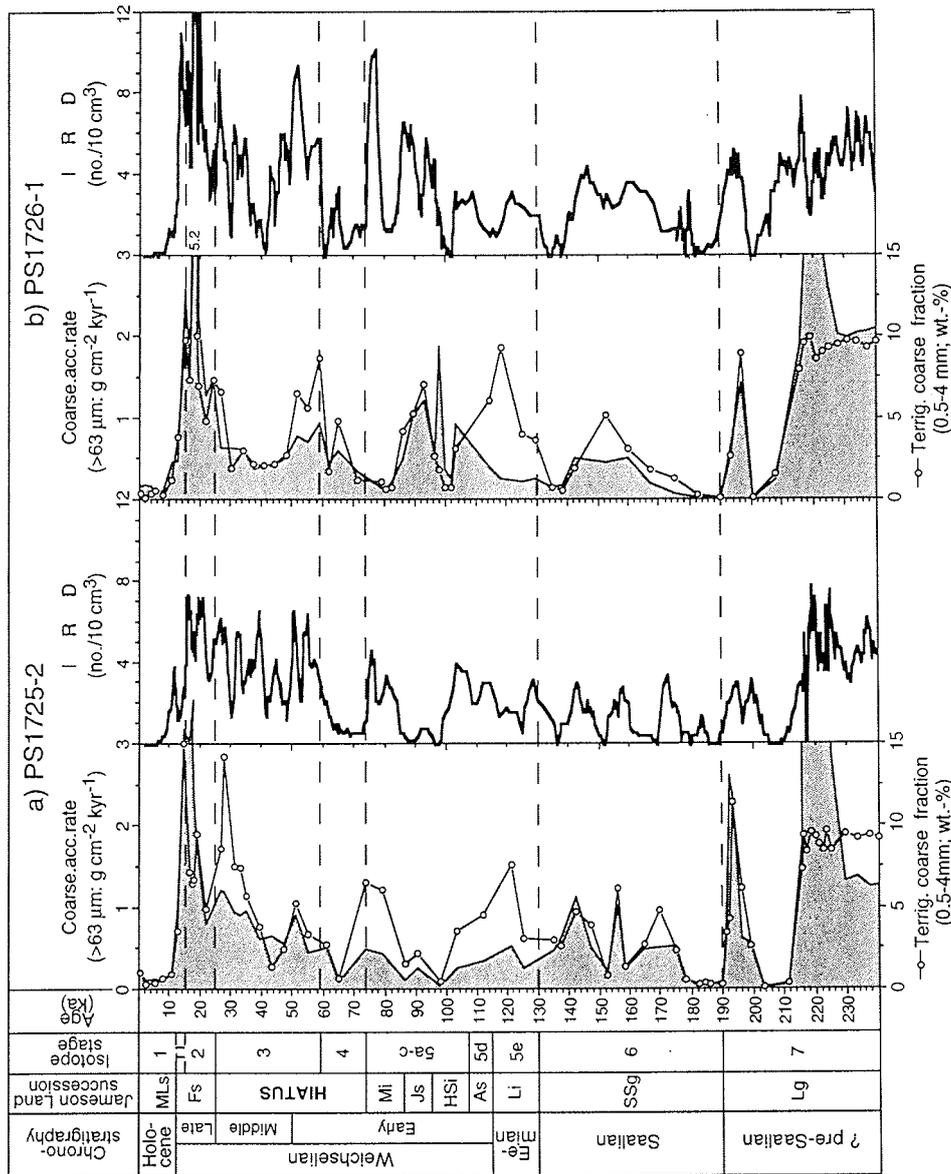
Fig. 29 a-e. Comparison of the accumulation rate of coarse terrigenous matter (>63 µm; cAR), the estimated terrigenous coarse IRD content (0.5-4 mm; wt-%), and the IRD (>2 mm) content counted on X-radiographs from five high-resolution sediment cores with the Quaternary succession on Jameson Land, East Greenland (devised by Funder et al. 1994), and its proposed correlation with North European chronostratigraphy and marine oxygen isotope stratigraphy. MLs, Milne Land stade; Fs, Flakkerhuk stade; Mi, Mønselv interstate; Js, Jyllandselv stade; HSi, Hugin Sø interstade; As, Aucellaelv stade; Li, Langelandselv interglaciation; SSg Scoresby Sund glaciation; Lg, Lollandselv glaciation. The abbreviation of TI is Termination I.
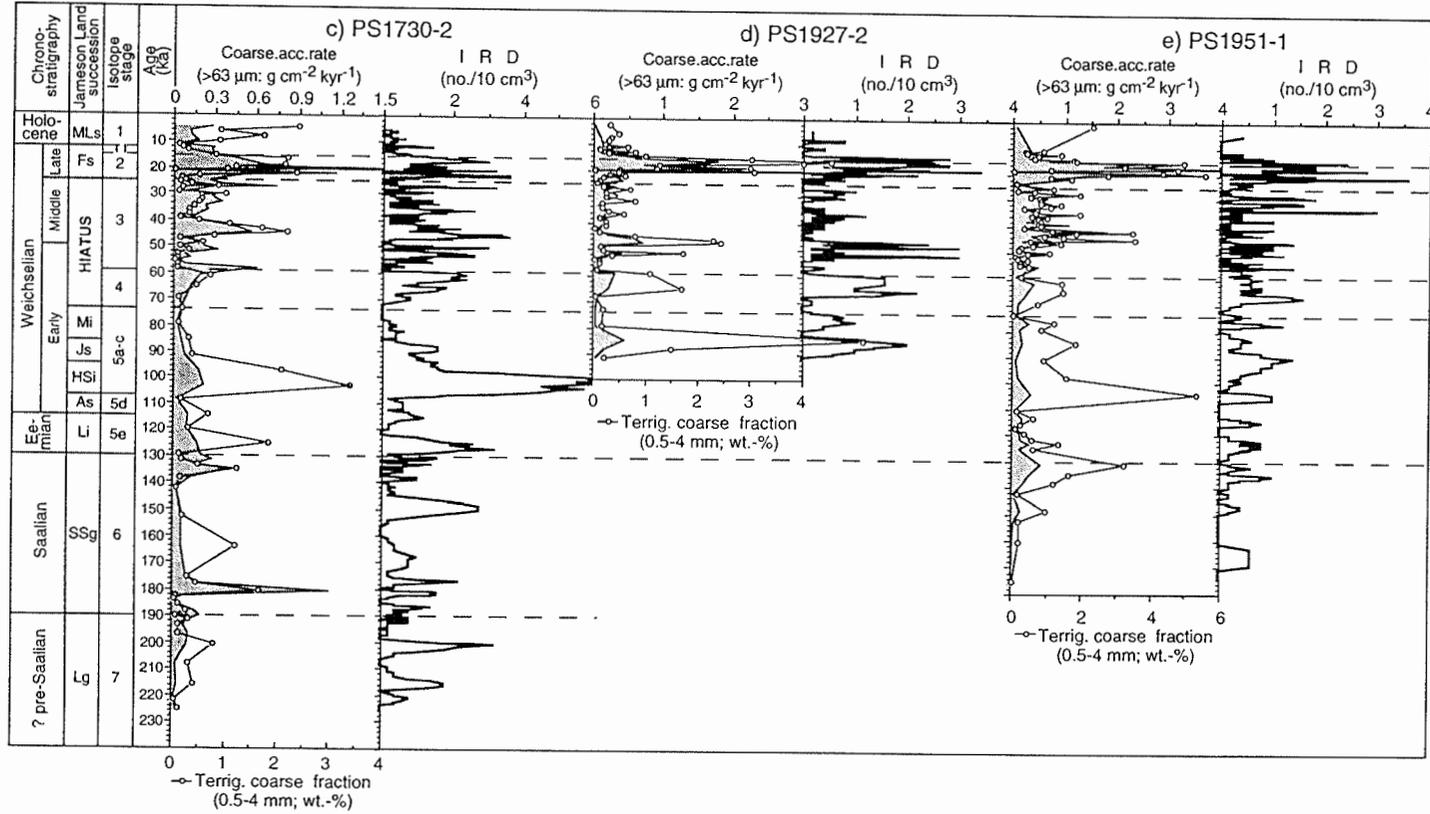
78

Fig. 29 a-e. continued.

terrigenous components within this subfraction can be additionally controlled by other transport mechanisms (e.g. sea-ice) (e.g. Pfirman et al. 1989; Nürnberg et al. 1994). In general, sediment particles >500 µm are assumed to be derived from iceberg processes (Grobe 1986; Elverhøi et al. 1995). In the high-latitude oceans terrigenous particles >500 µm within marine sediments have been preferentially used for provenance studies in order to reconstruct past iceberg drift paths and the sediment source regions associated with the waxing and waning of the continental ice sheets (Bischof et al. 1990; Bischof 1991, 1994; Spielhagen 1991; Elverhøi et al. 1995; Goldschmidt 1995).

Provenance investigations were not performed on the terrigenous IRD component (i.e. 0.5-4 mm) in this study. Due to the proximity of the investigated cores to the major outlet glaciers draining the eastern margin of the Greenland Ice Sheet, it is possible to assert that the majority of IRD deposited along the East Greenland continental margin have been transported via icebergs from eastern Greenland. This is corroborated by the identification and correlation between the cyclic number, duration, and timing of IRD-events recorded along the East Greenland continental margin, and from the GRIP ice core (for detailed discussion *see* Section 9). In addition, it can not be ruled out that the terrigenous particles found in these cores, to a certain but limited extent, originated from the more northern regions of the Arctic (e.g. the Arctic Ocean, the Svalbard area, and the Barents Sea) via the EGC (e.g. Bischof et al. 1990; Bischof 1994; Goldschmidt 1995).

Approximately fifteen major IRD pulses along the western margin of the Greenland Sea strongly indicate fluctuations in the stability of glaciers along the eastern margin of the Greenland Ice Sheet through the last 200 ka. This is best documented in cores PS1725-2 and PS1726-1 recovered from the slope adjacent to Scoresby Sund (Fig. 29a-b). A similar pattern is also documented in the deep-sea cores and reflects a reduced supply of icebergs and associated melting and therefore, IRD-supply onto the deep-sea floor (Fig. 29c-e). In general, major pulses of terrigenous IRD occur close to the stage boundaries reflecting the advance and/or collapse of East Greenland glaciers. Furthermore and with the exception of the Holocene, these pulses also occur within certain intervals of glacial and interglacial stages. Stein et al. (1996) presented a similar pattern of distinct, high-amplitude variations in the supply of the sand fraction and IRD in the northern part of the continental slope adjacent to Hochstetterbugten. This implies that the glaciers advanced and retreated along the East Greenland continental margin during glacial and interglacial stages. Therefore, large volumes of icebergs discharged from outlet glaciers may have supplied terrigenous sediments into the EGC system.

A very dark, overconsolidated massive diamicton sequence is recorded within stage 7 of two slope cores adjacent to Scoresby Sund. This diamicton sequence contains a maximum IRD content and a high sand fraction content. This sequence may correlate with the pre-Saalian "Lolleandshelv glaciation" recorded on Jameson Land (Funder et al. 1994; Stein et al. 1996) (Fig. 29a-b). The magnetic susceptibility (MS) of this interval reveals remarkably higher values (>600 10^{-5} SI) than compared to those of the last glaciation. Furthermore, the MS values are very similar to those recorded for the LGM on the slope south of Scoresby Sund (Fig. 15c). Therefore, it is assumed that the source region for the older IRD material and corresponding high MS values is most probably the basalts derived from the Geikie Plateau, and the inner fjords

of the Scoresby Sund system (e.g. Marienfeld 1992a). The diamicton sequence is interpreted to have been deposited by subaqueous mass movement processes (i.e. debris flows). According to Parasound and 3.5 kHz records (e.g. Damuth 1978; Niessen & Whittington 1995; Vanneste et al. 1995), the occurrence of slumps and debris flows is a common feature along the East Greenland continental margin. Debris flow deposits (up to 10 m in thickness) underlying a relatively uniform drape of approximately 10 m of well stratified sediments are recognized over a relative large distance along the slope adjacent to Scoresby Sund (Fig. 30; Niessen & Whittington 1995).
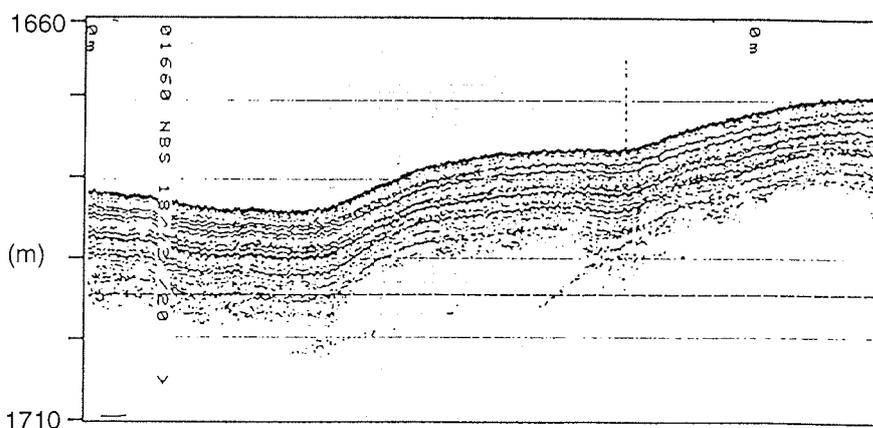
Fig. 30. Parasound record at the slope off Scoresby Sund (70°30.8'N, 18°18.0'W and 70°28.9'N, 18°18.5'W (from Niessen & Whittington 1995).

An increased accumulation rate of coarse-grained material (cAR) and a high IRD content in both slope cores adjacent to Scoresby Sund occur between substage 7.2 (201 ka) and the end of substage 7.1 (193 ka) and probably reflect an increased rate of iceberg calving. An increased cAR is recorded in the deep-sea core PS1730-2 at the stage 7/6 boundary (193 to 183 ka) reflecting a rapid waxing of East Greenland glaciers. The glacial interval between the stage 7/6 boundary (189.6 ka) and the onset of substage 6.5 (175.6 ka) is characterised by very low cARs coupled with a lowered IRD supply to the continental margin. Similarly, a distinctly reduced supply of IRD to the western Greenland Sea is recorded during this interval (Goldschmidt 1995; Henrich et al. 1995). This suggests that only little icebergs reached the western margin of the Greenland Sea due to a rapid and expanded build-up of sea ice at this time. However, a large peak in the accumulation rate of IRD is recorded during this interval in the eastern part of the GIN Sea and reflects that the Scandinavian Ice Sheet may have been in the phase of rapid waxing and a relatively slow waning (Goldschmidt 1995).

In general, the cAR and coarse IRD content greatly decrease within the slope cores during stadial periods, i.e. 6.6, 6.4, and 6.2. During the same interval, a relative increase in the cAR and coarse IRD is recorded in core PS1730-2

from the deep sea. In contrast, during interstadials 6.5 and 6.3, the cAR and coarse IRD display a significant increase in the slope cores PS1725-2 and PS1726-1 and a distinct decrease in the deep-sea core PS1730-2 (Fig. 29a-c). The terrestrial records near Scoresby Sund indicate that the Saalian glaciation (stage 6) was the most extensive glaciation in East Greenland (Hjort 1981; Funder 1984, 1989; Funder et al. 1994; Möller et al. 1994). A similarly extensive glaciation is recorded on the west coast of Spitsbergen (Miller et al. 1987) and on Iceland (Norddahl 1981, 1983). Compared to the highest peak in the cAR and the high coarse IRD content associated with the last glacial stage 2, the western margin of the Greenland Sea is characterised by lower cAR and reduced coarse terrigenous IRD supply during the Saalian glaciation. This is probably attributed to the extensive sea-ice cover which could have prevented the drift of icebergs towards the deep sea during extreme cold glacial periods (Nam et al. 1995a). Alternatively, as suggested by the GRIP ice core records (cf. Dansgaard et al. 1993), the Greenland Ice Sheet may have been relatively stable during the Saalian glaciation in comparison to the middle and early Weischelian glaciation. This suggests that ice stagnation resulting from the reduced moisture supply to Greenland led to a reduction in the calving rates at the ice ablation zone. Therefore, a relatively small amount of icebergs were calved from glaciers with a subsequent reduction in the drift towards the deep sea. On the other hand, cold SST as suggested by heavier $\delta^{18}O$ values (*see* Section 8.2.2), would reduce the melting rate of icebergs causing a decrease in the deposition of coarse IRD.

During interstadials 6.5 and 6.3, the SST is thought to have been, to some extent, warmer than during stadials (e.g. 6.6 and 6.2) due to an incursion of warm Atlantic water into the GIN Sea (e.g. Hebbeln 1991; Henrich 1992; Bauch 1993; Henrich et al. 1995). A reduced sea-ice coverage on the shelf, and an increase in the SST could have contributed to the relatively increased iceberg drift and melting over the continental slope. This may account for the increased cAR and coarse IRD content in the slope cores. The advance and retreat of the continental ice sheets have recently been reconstructed by a good correlation of peaks within the IRD accumulation rate, and the land glaciation record (Hebbeln 1992; Baumann et al. 1995; Goldschmidt 1995; Lloyd et al. 1996a). The repeated fluctuation of the Saalian Scandinavian Ice Sheet is interpreted from a correlation between land and marine-based data (Mangerud 1991; Baumann et al. 1995; Goldschmidt 1995). As a result, repeated pulses of cAR and coarse IRD supply suggest that during the Saalian glaciation rapid advance and retreat of East Greenland glaciers appear to have taken place coherently with those of the Scandinavian Ice Sheet.

At the 6/5 transition, an increased cAR and enhanced IRD supply to the western margin of the Greenland Sea indicate the repeated collapse of the East Greenland Ice Sheet built-up during the Saalian glaciation. The increased rate of iceberg calving from the outlet glaciers draining into the Scoresby Sund fjord system can be monitored through the peaks of cAR and IRD in the deep-sea core PS1951-1, and an increased supply of coarse IRD within the slope cores PS1725-2 and PS1726-1. During the early period of the Eemian, the East Greenland continental margin was still affected by cold polar waters of the EGC and a strong sea-ice coverage (*see* Section 8.2.3). Therefore, this interval was characterised by a very low carbonate content, absence of planktonic foraminifers, and a relatively low amount of IRD. The

cAR and IRD content reach higher peaks in both slope cores during the interval 125 to 118 ka. Before this interval, the deep sea cores reflect a strong meltwater event during the penultimate deglacial interval that probably results from the influence of warm Atlantic water (*see* Section 8.2.3). With the advent of the Eemian interglaciation, the sediments near the Langelandselv coastal area adjacent to Jameson Land have yielded subarctic marine molluscan faunas that suggest a stronger advection of warm Atlantic water into the Scoresby Sund fjord system than during the Holocene (Landvik et al. 1994; Vosgerau et al. 1994).

According to the luminescence dates of shallow and fluvial sediments, Mejdahl and Funder (1994) suggested that the timing of the incursion of warm Atlantic water may have took place at about 120±19 ka. This timing is very similar to the peak of cAR and coarse IRD content in both slope cores adjacent to Scoresby Sund suggesting the beginning of a major deglaciation event associated with East Greenland glaciers. This interval is further indicated by a very low carbonate content and an absence of planktonic foraminifers within both slope cores. A large discharge of icebergs, and a subsequent increase in the input of coarse terrigenous matter would have restricted biogenic carbonate production in surface water, and increased the dilution of biogenic carbonate supplied to the sea floor. In the deep-sea cores, a distinct rise in the carbonate content coupled with a peak in the planktonic foraminiferal content occurs between 120 and 115 ka. This implies the occurrence of enhanced open-water conditions resulting from an inflow of warm Atlantic water. However, the presence of more than 95 % *N. pachyderma* sin. indicates that an input of Atlantic water may not have propagated fully into the western margin of the Greenland Sea in order to change the surface water oceanography during this peak interglacial period, but instead contributed to the strongly reduced ice covered water conditions. This further indicates that this core position (70°07.2′N, 17°42.1′W) was situated under the Polar front during the Eemian-period similar to that within the Holocene.

Between the end of stadial 5d and interstadial 5c, the slope cores PS1725-2 and PS1726-1 and the deep-sea cores PS1730-2 and PS1951-1 show a marked increase in the cARs, and coarse IRD content. Stein et al. (1996) suggested that the most prominent IRD peak found within the western Greenland Sea for mid stage 5 may coincide with the "Aucellaelv stade" described in the Scoresby Sund area by Funder et al. (1994), Israelson et al. (1994), and Lyså and Landvik (1994). During this period, glaciers advanced out to the mouth of Scoresby Sund and retreated thereafter to somewhere north of Lollandselv (Funder et al. 1994). Therefore, the increased cAR and the increased coarse IRD content are most likely related to the collapse and/or retreat of east Greenland glaciers developed during substage 5d.

A distinct increase in the cARs and the coarse IRD content is recorded within cores PS1726-1 and PS1927-2, between substages 5.2 and 5.1. This may similarly be attributed to the decay of glaciers built-up during substage 5.2 ("Jyllandselv stade") when the glaciers reached the outer fjord of the Scoresby Sund system (Tveranger et al. 1994). During a similar interval (i.e. 90 ka), the Scandinavian Ice Sheet may have reached the coast or somewhat beyond this depositing high amounts of IRD (Baumann et al. 1995; Goldschmidt 1995). An increase in the cAR and coarse IRD is recorded on the upper slope adjacent to Scoresby Sund between mid substage 5a and the stage 5/4

boundary. This may signal an advance or retreat of the local outlet glaciers entering the Scoresby Sund fjord system. As a consequence and further supported by an elevated increase in the cARs and coarse IRD content along the East Greenland continental margin, at least two major advances and retreats of East Greenland glaciers are probable during interglacial stage 5 (cf. Stein et al. 1996).

Before the last major glacial advance associated with the Late Weichselian or "Flakkerhuk stade", there is no terrestrial record on eastern Greenland. A hiatus of ca. 50 ka probably resulted for two reasons; 1) lowering sea level to levels below that of the Holocene, where fluvial and marine sediments were deposited below the present sea level, and thereafter were eroded by glaciers; 2) from over-simplified and/or undated stratigraphy (Funder et al. 1994). In general, glacial stage 4 is characterised by low cARs and a distinct decrease in the coarse IRD supply onto the upper slope adjacent to Scoresby Sund. An extended sea-ice cover over the shelf area may have prevented the seaward drift of icebergs causing a decrease in the sedimentation rate (Nam et al. 1995a). Low SSTs may have prohibited significant melting of discharged icebergs along the continental slope which is further supported by heavier $\delta^{18}O$ values than compared to those in the LGM. The time span between 65 and 61 ka is displayed by a higher abundance of planktonic foraminifers, and relatively heavier $\delta^{13}C$ values than during the last glacial stage 2 indicating reduced sea-ice cover resulting from summer melting. From the lower slope to the deep sea, there is evidence for both increased cARs and coarse IRD supply during the same time interval. Therefore, it is considered that this pulse of coarse terrigenous material may be a signal of a small advance/retreat of the glaciers. During the same time period, a small advance and/or retreat of the Barents Sea Ice Sheet is suggested by Hebbeln (1992), Mangerud and Svendsen (1992), and Lloyd et al. (1996a).

The interval between 59 and 25 ka (i.e. glacial stage 3) is indicated by three major pulses in the cARs and coarse IRD to the continental margin. The rapid increase in the cARs and coarse IRD occurs between 59 and 51 ka. The first peak of maximum IRD coincides with a large meltwater event within the GIN Sea (for detailed discussion see Section 8.2.5). The maximum IRD supply corresponding to the large meltwater event indicates a major collapse of East Greenland glaciers. A good correlation between the two events is found in the eastern and northern GIN Sea reflecting the large surging of the Scandinavian and the Barents Sea ice sheets (Hebbeln 1992; Baumann et al. 1995; Goldschmidt 1995; Lloyd et al. 1996a). The coherent collapse of the high-latitude northern continental ice sheets during early stage 3 is considered to have been triggered by a climatically driven mechanism such as the Milankovitch solar radiation changes. This suggestion is derived from the major melting of the three high-latitude Northern Hemisphere ice sheets occurring as the summer insolation reaches its maximum.

A second small advance and retreat of glaciers is reflected on the slope adjacent to Scoresby Sund by an increase in the cARs coupled with a distinct increase in the supply of coarse IRD between 35 and 31 ka (Fig. 29a-b). Prior to this IRD-event, a small advance/retreat of East Greenland glaciers is recorded between 48 and 42 ka. These two intervals reflect the fluctuating extent of East Greenland glaciers, and appear to correlate with the growth and decay of the Scandinavian and Barents Sea ice sheets (Baumann et al. 1995;

Goldschmidt 1995; Lloyd et al. 1996a). East Greenland glaciers are considered to have started a renewed advance between 28 and 25 ka before the last glacial maximum advance onto the continental margin (Fig. 32). The IRD records indicate that the onset of this glaciation occurred widely in the GIN Sea prior to the beginning of the LGM. Therefore, the advance/retreat of the glaciers is recorded in the northern Greenland Sea (e.g. Jünger 1994; Stein et al. 1996), the Fram Strait (e.g. Hebbeln 1992), and in the Norwegian Sea (e.g. Baumann et al. 1995; Fronval et al. 1995; Goldschmidt 1995). Furthermore, there is evidence for massive discharge of icebergs into the North Atlantic from the Laurentide Ice Sheet (Bond et al. 1992b, 1993) suggesting a considerable surging phase associated with the waxing and/or waning of the Northern Hemisphere continental ice sheets. This time span coincides with the cooling air temperatures recorded from the GRIP ice core (cf. Dansgaard et al. 1993). As formerly suggested by increased cARs and coarse IRD content, the advance and retreat of East Greenland glaciers most likely correlate with the cold phase of "Dansgaard-Oeschger cycles" recorded in the GRIP ice core (for detailed discussion *see* Section 9).

7.3 Advance and retreat of East Greenland glaciers during the Late Weichselian

During the last glacial stage 2, the continental margins of the GIN Sea were subjected to the repeated advance and retreat of terrestrial-based glaciers (e.g. Hughes et al. 1977). Based on terrestrial (e.g. Hjort 1981; Funder 1984, 1989) and glaciomarine records (e.g. Mienert et al. 1992; Stein et al. 1993; Hubberten et al. 1995), outlet glaciers draining the eastern margin of the Greenland Ice Sheet during the LGM, may have grounded on the sea floor and advanced onto the East Greenland continental shelf. Stein et al. (1993) suggested that the overconsolidated, stiff diamictons underlying a Holocene glaciomarine sequence may have been more widespread over the East Greenland continental margin during this interval. Only part of the stiff diamictons have been recovered from the East Greenland shelf, but it is possible to suggest that outlet glaciers reached the shelf region during the LGM (e.g. Mienert et al. 1992; Hubberten et al. 1995). Without a success in the recovery of complete LGM sediment sequences to date, the extent of the Greenland Ice Sheet and the associated advance and retreat of marine-based outlet glaciers on the East Greenland continental margin still remains unsolved (cf. Möller et al. 1991 & further references therein).

Based on oxygen isotope records and AMS ^{14}C datings, only cores PS1725-2 and PS1726-1 recovered from the slope adjacent to Scoresby Sund, penetrated a complete last glacial sediment sequence, whereas the remaining five slope cores recovered from north and south of Scoresby Sund, seem to have only penetrated a part of the last glacial stage 2. In particular, the latter LGM sequence comprises a homogeneously overconsolidated massive diamicton facies formed by debris flow mass movement. According to the massive diamictons deposited on the slope areas north and south of Scoresby Sund, the maximum seaward extent of a grounded ice sheet may have been at the continental shelf break during the LGM (about 21-16 ka). During this period, there was a massive IRD supply to the western margin of the Greenland Sea and a distinct increase in the accumulation rate of terrigenous matter, probably supporting the advance of East Greenland glaciers onto the shelf (Figs. 32-33). During the maximum glacial conditions on the shelf break, it is probable that iceberg calving rates increased near the fluctuating ice-sheet margin as calving near the waterline is generally considered the dominant mode of glacier ablation (Anderson & Molnia 1989). Therefore, it is thought that there was a massive and rapid sediment input onto the shelf break and/or the steep upper slope north and south of Scoresby Sund. This situation led to oversteepened slopes and/or excess pore fluid pressures in accumulated glacial sediments, which subsequently triggered instability and subaqueous mass movement (Vorren et al. 1989). It is generally known that mass movement on high-latitude slope is closely associated with rain-out of glacial debris when the grounding-line of an ice mass reaches the shelf break (Hambrey 1994). On the other hand, sediment supply directly from ice-sheet margins to the shelf break north and south of Scoresby Sund was greater than compared to that discharged to the slope areas adjacent to Scoresby Sund, which was fed for the most part by icebergs calved from outlet glaciers.

During the LGM, diamicton sequences were deposited north and south of Scoresby Sund and comprise large amounts of coarse IRD (>2 mm) particularly on the slope areas. These sequences are associated with light

$\delta^{18}O$ (3 to 2‰) and $\delta^{13}C$ (0 to -1‰) values similar to those of the Holocene (*see* Section 8.2.6), reflecting strong melting processes near the ice-shelf margin probably during the peak glacial summer. In particular, very light $\delta^{18}O$ and $\delta^{13}C$ values from the slope cores (e.g. PS1948-2, PS1949-1, and PS1950-2) south of Scoresby Sund imply an enhanced discharge of icebergs and meltwater plume activity. High magnetic susceptibility (MS) values of 600 to 1200 (10^{-5} SI) are characteristic of these LGM diamictons (Fig. 15c). These values are similar to those documented in the Holocene glaciomarine sediments from the shelf (Fig. 15c). Additionally, the high magnetic susceptibility values correspond well to the dominance of basaltic minerals within the diamicton sequence (Evans in prep.), indicating the supply of terrigenous material from the basalt terrains of Scoresby Sund and the Geikie Plateau. On the other hand, LGM diamicton sediments from the slope cores of the same profile fall within the origin (i.e. low HI of ≤100 mgHC/gC and OI of ≤ 100 mgCO$_2$/gC) of a van Krevelen-type diagram (*see* Fig. 24h), pointing to the predominance of reworked and overmature organic matter (e.g. Stein et al. 1993). Such organic matter is also identified within Holocene glaciomarine sediments from the shelf south of Scoresby Sund (Fig. 24g). Based on the identical composition of terrigenous organic material, the dominance of basaltic minerals, and higher MS values of the glacial diamicton sequences of the slope and the Holocene glaciomarine sequence of the shelf, the terrestrial sediment supply to the East Greenland continental margin is directly related to the advance and/or retreat of glaciers during the LGM and the Holocene, respectively (e.g. Fig. 31).

During intervals when the outlet glaciers draining the Greenland Ice Sheet extended onto the continental shelf south of Scoresby Sund (Geikie Plateau), the ice shelf was fed directly by valley- and/or outlet-glaciers from the Geikie Plateau. The till at Kikiakajik south of Scoresby Sund was most likely deposited by the outlet glaciers from the Geikie Plateau (Mangerud & Funder 1994). Dowdeswell et al. (1994b) have documented a moraine extending across the mouth of Scoresby Sund adjacent to Kap Brewster (*see* Figs. 5 & 8 in Dowdeswell et al. 1994b), probably indicating the most easterly position of the glacier front at the culmination of the "Flakkerhuk glaciation" (see Fig. 31B; Funder et al. 1994). Due to the close proximity of the glacier front (Mangerud & Funder 1994), an increase in sediment flux onto the slope adjacent to Scoresby Sund is recorded during the LGM (Nam et al. 1995a). During the same interval, very high mean sedimentation rates are recorded on the slope areas north and south of Scoresby Sund (*see* Section 5). This event may coincide in its age and duration with the culmination of the "Flakkerhuk stade" and the formation of the Kap Brewster moraine (Funder et al. 1994; Mangerud & Funder 1994). During this interval, valley glaciers may also have extended from the Carlsberg and/or Kong Oscar fjords onto the adjacent shelf, and discharged high volumes of icebergs. In support of this, moraines are found close to the mouth of both fjords (Niessen & Whittington 1995). The terrestrial carbonate deposited on the slope southeast of Kong Oscar Fjord were transported by meltwater plumes and icebergs originating from Canning Land and Scoresby Land (*see* Section 7.4.2). Glaciers that reached the shelf adjacent to both Carlsberg and Kong Oscar fjords are considered to have been smaller than those that extended onto the shelf south of Scoresby Sund. This is supported by the relatively lower IRD content and higher $\delta^{18}O$ and
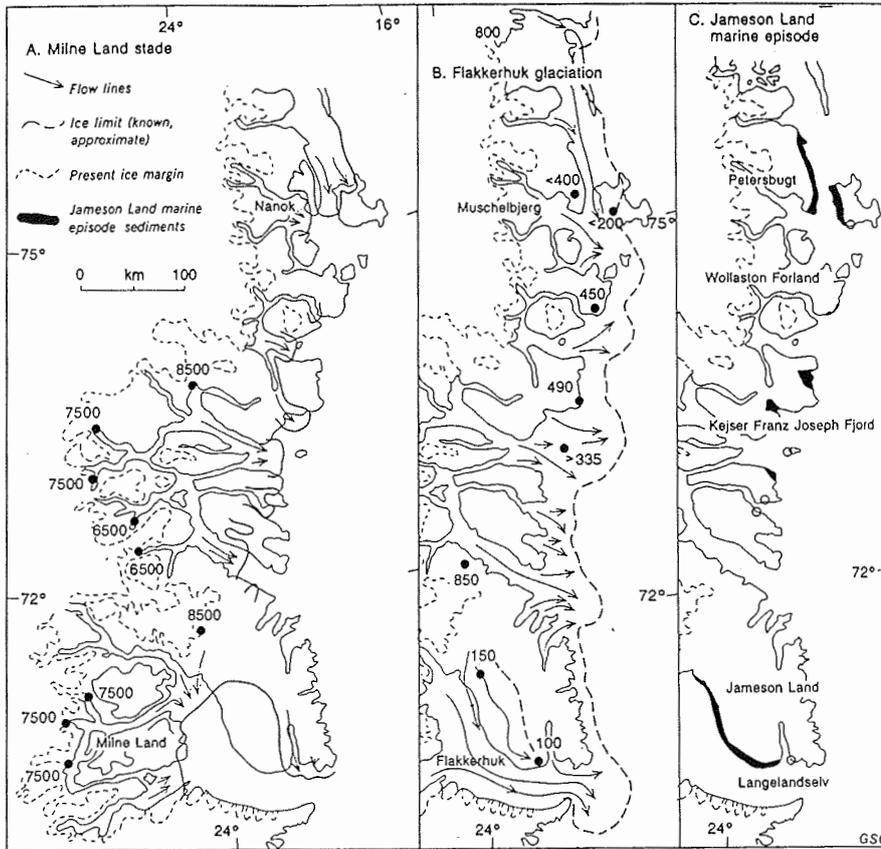
Fig. 31. Past and present glaciation in the East Greenland fjord zone. A) Known ice limit during Milne Land stade (10 ka), flow lines, and minimum dates for deglaciation of sites at the present ice margin (^{14}C years BP). Sources: Funder and Hjort (1978), Hjort (1979), and Funder (unpublished). B) Conceptual model of Flakkerhuk glaciation (ca. 14 ka), ice distribution, major flow lines, and ice thickness (metres above present sea level), based entirely on land evidence. Sources: Hjort (1981) and Funder (1984). Surface elevations based on weathering limits quoted from the regional studies. C) Distribution of sediments from the Jameson Land marine episode (Early and Middle Weichselian). Circles show location of shells from sample episode, reworked in younger till. Source: Funder (1984). From Funder (1989).

87

88
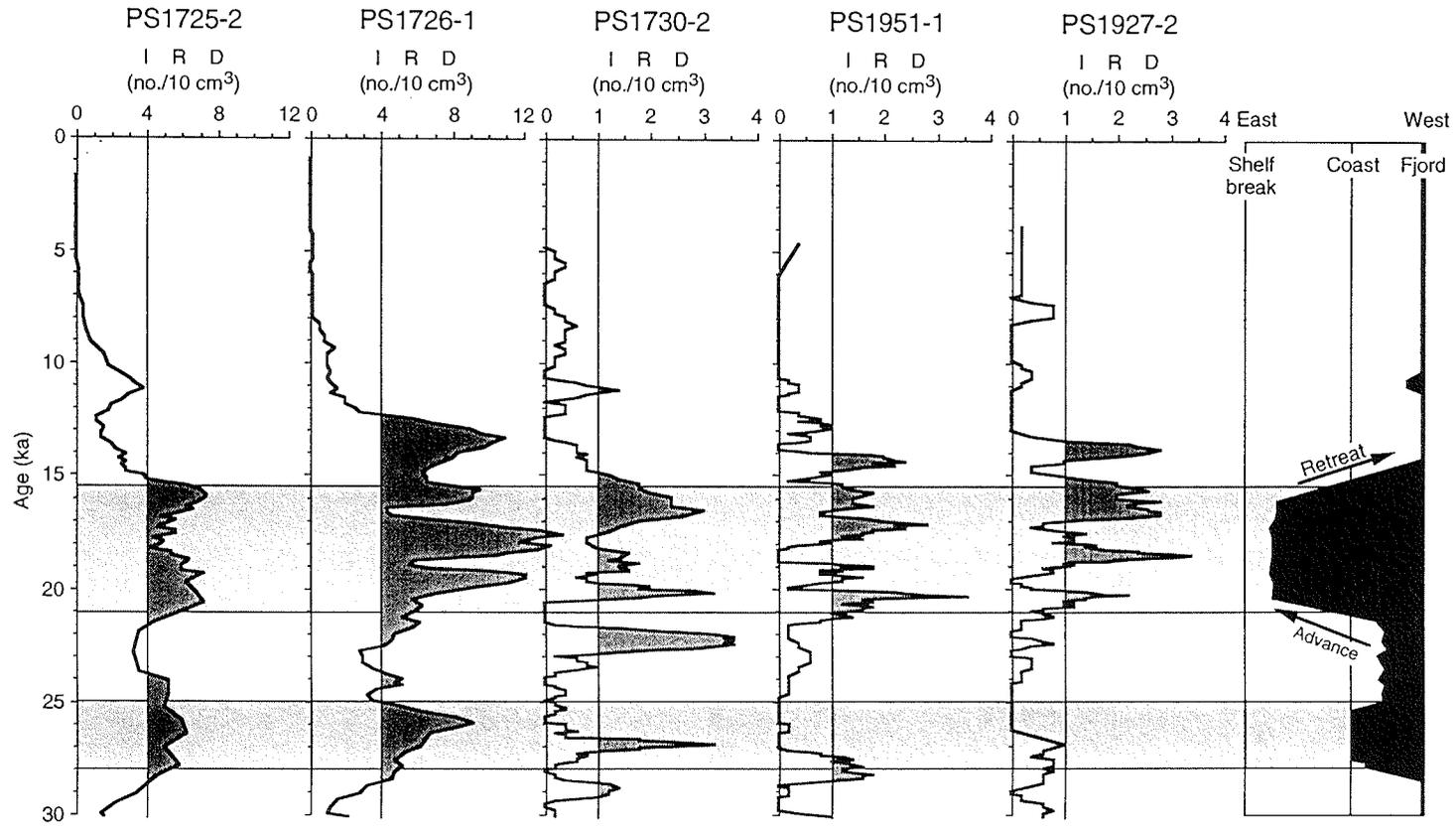
Fig. 32. Postulated advance and retreat of East Greenland glaciers based on the IRD supply onto the East Greenland continental margin and the adjcent deep sea during the last 30 ka.
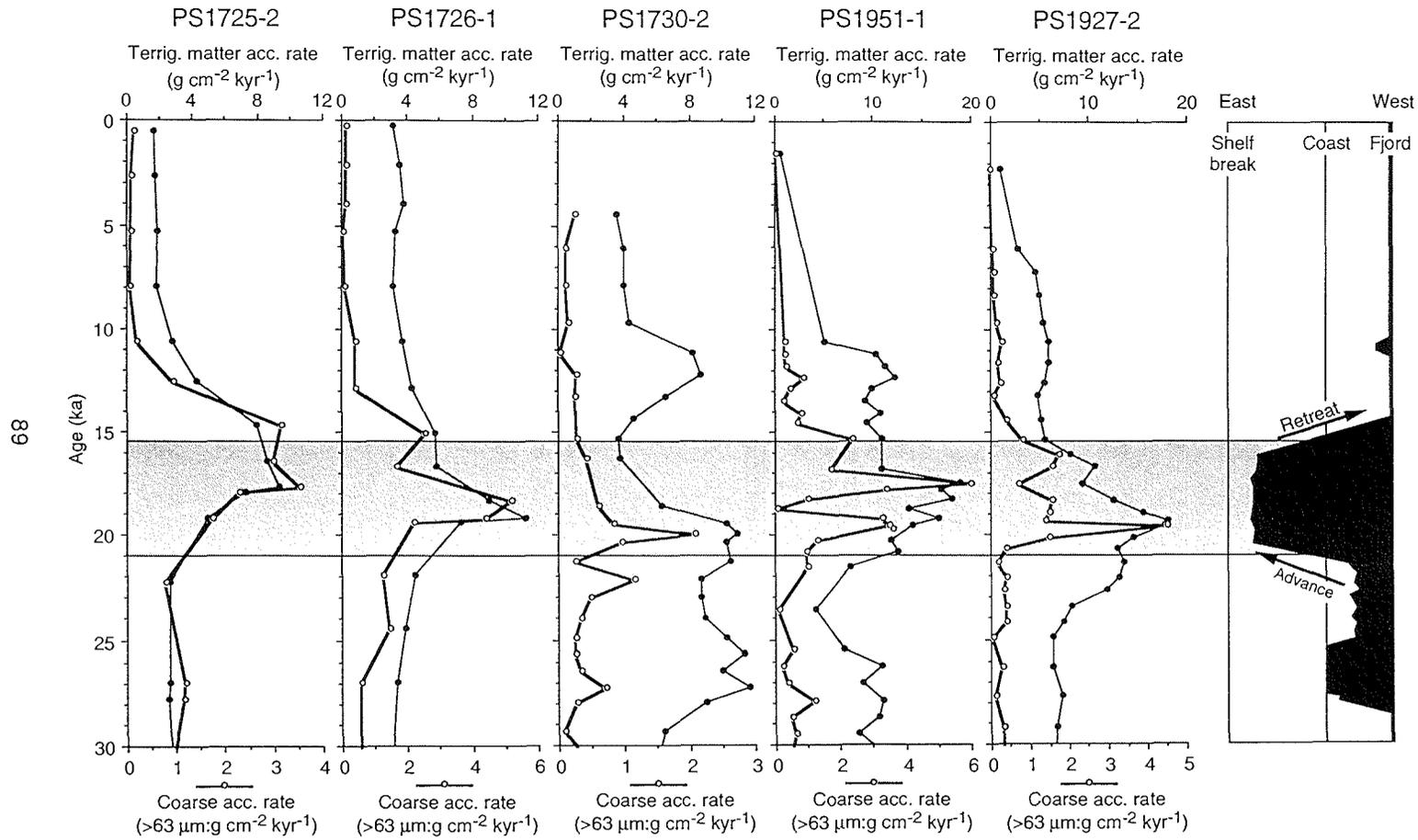
Fig. 33. Comparison of terrigenous matter accumulation rate, and accumulation rate of coarse accumulation rate (>63 µm; cAR) and postulated glacial advance and retreat of the Greenland Ice Sheet during the last 30 ka.

$\delta^{13}C$ values of *N. pachyderma* sin. compared to those recorded from the slope cores south of Scoresby Sund. Funder (1984, 1989) and Funder et al. (1994) suggested that the grounded glaciers filled the outer Scoresby Sund fjord system, and extended onto the inner shelf during the Late Weichselian Glaciation (the "Flakkerhuk stade") (Fig. 31B). Therefore, large amounts of terrigenous material might have been derived from the inner region of the Scoresby Sund system where it is inferred that soft sediments were eroded by outlet glaciers during the LGM (Dowdeswell et al. 1991; Marienfeld 1991; Uenzelmann-Neben et al. 1991; Stein et al. 1993). Outlet glaciers are the dominant source of debris-enriched icebergs as they exhibit rapid calving processes, and possess thick basal diamict layers (e.g. Drewry 1986). Large volumes of icebergs drifted onto the slope adjacent to Scoresby Sund further indicated by the large amount of coarse terrigenous sediment deposited on the continental slope from the extended glaciers. Glaciomarine sediments on the slope adjacent to Scoresby Sund indicate that the glacial influence was less intense than that on the continental margin north and south of Scoresby Sund. The early part of stage 2 (i.e. 25 to 21 ka) was probably covered by intense sea-ice as indicated by a relatively reduced IRD and carbonate content (relating to a decrease in the foraminiferal abundance) compared to the following interval of the last glacial maximum (21 to 16 ka). Despite the processes associated with the glacial maximum around eastern Greenland, the surface water between 21 and 16 ka is unlikely to have been covered by perennial sea ice adjacent to Scoresby Sund. Therefore, compared to the Saalian glaciation, icebergs could drift into the offshore regions and release much more IRD onto the slope. On the other hand, the increased foraminiferal abundance and high HI values (>100 mgHC/gC) can also be ascribed to at least a seasonally fluctuating sea-ice coverage (Nam et al. 1995a).

7.4 Holocene glaciomarine sediments on the East Greenland continental margin

7.4.1 Holocene sedimentary processes and environments along the East Greenland continental margin

Holocene sediments from the GIN Sea and the Arctic Ocean are characterised by a reduced coarse terrigenous ice-rafted debris content, and an increase in the biogenic productivity (e.g. Gard 1988; Gard & Backman 1990; Henrich 1992; Baumann et al. 1993, 1994, 1995; Stein et al. 1994d; Cronin et al. 1995). In contrast, Holocene glaciomarine sediments on the East Greenland continental shelf are marked by an increase in the IRD content, and a decrease in the biogenic content (e.g. Marienfeld 1991, 1992a-b; Stein et al. 1993; Nam et al. 1994, 1995a), reflecting the strong influence of glacial associated processes. The sediments consist of sandy to pebbly mud with a predominance of ice-rafted dropstones (e.g. Marienfeld 1991; Stein et al. 1993; Dowdeswell et al. 1994a-b; Nam et al. 1995a). Among others, the extent of the adjacent fjord complex systems, meltwater plumes, and iceberg rafting of debris are the major factors controlling sedimentary processes on the East Greenland continental margin. However, this pattern changes markedly beyond the shelf break. The supply of coarse terrigenous sediments through icebergs and sea ice to the mid to lower slope significantly decreases and reflects the gradual transition from glacial dominated processes of the LGM to Holocene glaciomarine processes. This pattern is well reflected in sediment cores recovered from the continental margin adjacent to Scoresby Sund (Fig. 21a-g).

Iceberg rafting of debris is the dominant factor controlling the input of coarse terrigenous sediments to the fjords and shelf of East Greenland associated with the large volume of icebergs calved from glaciers at the head of the large fjord complexes (Marienfeld 1991; Dowdeswell et al. 1992, 1994a-b). In contrast to the Arctic continental margin (e.g. Pfirmen et al. 1989; Wollenburg 1993; Nürnberg et al. 1994), sediment transport along the East Greenland continental margin by sea ice seems to be of relatively limited importance (e.g. Dowdeswell et al. 1994b), as water depths within the fjords and on the shelf are often too deep for the sea ice to contact the sea floor. Subsequently, a distinct decrease in the coarse IRD content on the slope is most likely attributed to the decrease in the supply of icebergs across the shelf associated with the retreat of glaciers following the last deglaciation (e.g. Stein et al. 1993; Nam et al. 1995a). This change to more open-ocean conditions with a seasonal fluctuation in sea-ice cover resulted in an increase in biogenic components delivered to the slope.

As indicated by light $\delta^{18}O$ and $\delta^{13}C$ values, water on the inner shelf is subjected to a more intensive supply of meltwater derived from iceberg melting and glacier meltwater discharge than on the outer shelf (see Section 8.2.8). A similar pattern is also recorded within the Holocene sequences of the Kejser Franz Josephs Fjord and the adjacent shelf region of East Greenland (Evans in prep.). However, the coarse sand fraction contains a higher IRD content and is distributed more on the outer shelf than on the inner shelf. This suggests that on the outer shelf, the southward flowing bottom current of the EGC system may have winnowed out the fine sediment and organic matter fraction. This process will have contributed to the deposition of sandy mud with

91

a higher concentration of coarse IRD on the outer shelf (e.g. Mienert et al. 1992; Nam et al. 1995a). This correlates well with the common occurrence of the benthic foraminifer *Cibicides lobatulus* (Walker & Jacob) on the outer shelf. In general, *C. lobatulus* is the dominant benthic foraminiferal species within these coarse-grained sediments reflecting the high bottom current activity and erosion of the fine sediment fraction (e.g. Hald & Vorren 1984; Mackensen et al. 1985; Jennings & Helgadottir 1994; Wollenburg 1995). This environment provides the optimal living conditions for *C. lobatulus*, as it feeds through the filtering out of the organic matter within the suspended sediment (e.g. Nyholm 1961; Lipps 1983).

At depths of 500-600 m on the East Greenland continental shelf, heavy scouring or ploughing by iceberg keels has been recorded (Dowdeswell et al. 1991, 1993; Mienert et al. 1992; Niessen & Whittington 1995). This implies that surface Holocene sediments deposited on shallow regions of the shelf can be eroded or resuspended by scouring or ploughing action of iceberg keels and in combination with the prevailing bottom current lead to the depletion of the fine grained sediment fraction (Dowdeswell et al. 1994a). This process has also been documented within Holocene sediments deposited in Scoresby Sund (Marienfeld 1991, 1992a). Therefore, it is probable that the mean Holocene sedimentation rates estimated from all of the cores can be significantly higher (cf. Section 5). Furthermore, iceberg scouring or ploughing may affect both the stratigraphy (e.g. Elverhøi 1984; Marienfeld 1991) and the textural and associated properties of glaciomarine sediments (e.g. Vorren et al. 1983).

7.4.2 Influence of iceberg discharge and meltwater on sedimentation, and sediment sources

The fjords and continental shelf of East Greenland are strongly affected by the Greenland Ice Sheet (e.g. Dowdeswell et al. 1994a). Large numbers of icebergs are produced by several fast-flowing outlet glaciers draining part of the Greenland Ice Sheet (Reeh 1985, 1989). Tidewater glaciers draining local ice caps produce smaller icebergs of irregular shapes (Dowdeswell et al. 1994a-b). The icebergs drift through the large fjord complexes and reach the adjacent shelf (Marienfeld 1991; Dowdeswell et al. 1992, 1994a-b; Stein et al. 1993). During melting the icebergs release varying amounts of lithic detritus onto the adjacent continental margin sea floor.

During the interval from Termination Ia to the Younger Dryas cooling event, an increase in the carbonate content is recorded in three cores (PS1923-2, PS1924-1, and PS1925-2) from the inner shelf to the upper slope adjacent to Carlsberg Fjord. High amounts of IRD are similar to those recorded within the last glacial interval and reflect continuous iceberg drift from Carlsberg and/or Kong Oscar fjords between the LGM and the Holocene. The carbonate is thought to be mainly of a terrigenous origin as there is a very low abundance of biogenic carbonate. The detrital carbonate may originate from the glacial erosion of dolomite bedrock distributed locally on Canning Land and Scoresby Land (Henriksen & Higgins 1976). This carbonate has been continuously deposited on the shelf and the upper slope by icebergs and meltwater plumes during the retreat of the shelf ice sheet into Carlsberg Fjord and/or Kong Oscar Fjord. There is evidence of a high amount of discharge

from both icebergs and meltwater during this interval suggested by the increased flux of coarse terrigenous IRD, and by the relatively light $\delta^{18}O$ and $\delta^{13}C$ records on the adjacent continental margin. After the Younger Dryas, the input of terrestrial carbonate decreased drastically probably resulting from a reduction in iceberg rafting of debris and an associated decrease in the IRD supply to the continental margin. During the same interval, there is an increase in the organic carbon content, HI values (≥ 100 mgHC/gC), and heavy $\delta^{13}C$ values, suggesting a slight increase in surface-water productivity.

With the end of the Younger Dryas, glaciers began to rapidly retreat westward (Fig. 31; Funder 1989) contributing to an increase in iceberg calving rates and iceberg drift through the fjord systems (Marienfeld 1991, 1992b). A significant amount of IRD has been deposited within the fjord systems such as Scoresby Sund (e.g. Marienfeld 1991, 1992a-b). Throughout the late Holocene, the majority of the icebergs discharged into Scoresby Sund are derived from the Daugaard-Jensen and Vestfjord glaciers (cf. Marienfeld 1991, 1992a-b; Dowdeswell et al. 1994b). During the same interval, a large number of small- to intermediate-sized glaciers have drained the Geikie Plateau ice cap bordering the southern region of Scoresby Sund. Tertiary basaltic rocks are widely exposed, and is by far the most dominant lithology within the Geikie Plateau region (Funder 1989). The glaciers draining the ice cap transported a large amount of coarse basaltic detritus into the southern region of Scoresby Sund (Marienfeld 1991, 1992a-b). This is documented by the high abundance of basaltic rock fragments that correlate with an enhanced magnetic susceptibility (MS) record within sediment cores recovered from southern Scoresby Sund (e.g. Marienfeld 1991, 1992a). Cores PS1946-2 and PS1947-1 recovered from the shelf south of Scoresby Sund, contain distinctly higher amounts of IRD which correlate very well with high MS values of 1000-2400 (10^{-5} SI) (Fig. 34). Therefore, the higher MS values clearly reflect the higher basaltic rock fragment content within sediments. This is further supported by the sediment component distribution, and the XRD determined bulk sediment mineralogical composition (Evans in prep.). However, in slope cores PS1948-2, PS1949-1, and PS1950-2, the MS values are distinctly lower than compared to those recorded on the shelf (see Fig. 34). The lower values correspond to the marked decrease in the IRD content (Fig. 35). Based on the XRD measured mineralogy data, Evans (pers. commun. 1996) suggests that the Geikie Plateau is a source of terrigenous material but to a less extent. This indicates that a smaller amount of icebergs and IRD originating from the Geikie Plateau region reaches the slope region south of Scoresby Sund. This probably results from a reduced input of meltwater plume activity and iceberg discharge onto the slope area south of Scoresby Sund due to the influence of the southward flowing EGC.

In contrast to the distinct increase in the IRD supply onto the shelf south of Scoresby Sund, a marked decrease in the IRD supply to the adjacent shelf clearly indicates the southward drift of a large number of icebergs after leaving the Scoresby Sund fjord system. In addition, the two cores from the shelf south of Scoresby Sund also indicate the predominance of a large input of meltwater during the late Holocene. The relatively low IRD supply to the shelf region adjacent to Scoresby Sund reveals that only a minority of icebergs reached this region of the shelf. This is further supported by the relatively heavier $\delta^{18}O$ and $\delta^{13}C$ values than compared to those of the two shelf cores

south of Scoresby Sund. The high IRD content containing a high proportion of basaltic rock fragments, and a large volume of meltwater discharge indicate that a large amount of icebergs, and meltwater plume activity were derived from Scoresby Sund and transported southward in the EGC system (cf. Wadhams 1981; Dowdeswell et al. 1992). As clearly indicated by the difference in the investigated parameters, Holocene glaciomarine sediments on the continental margin reveal that local glacial processes play a critical role in the sedimentary environment.
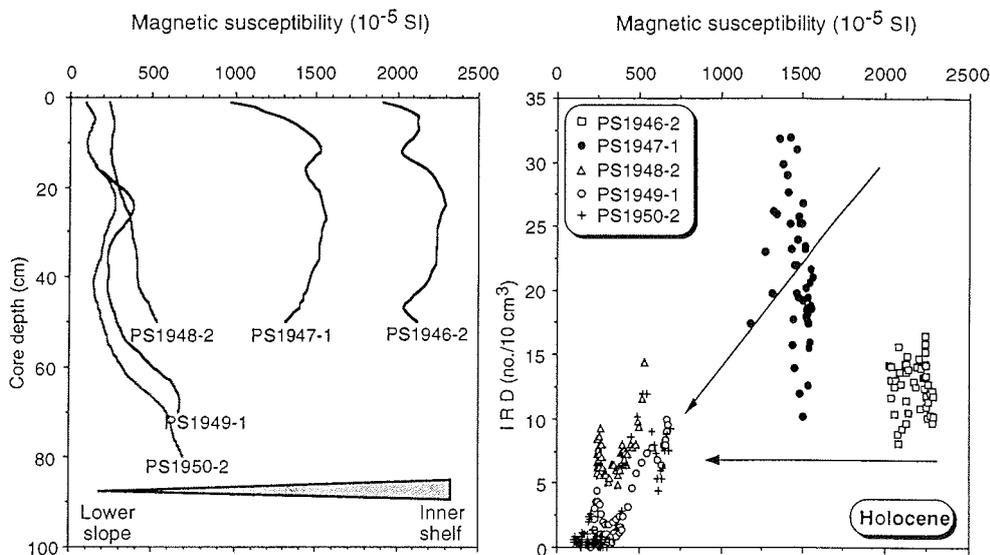
Fig. 34. Holocene magnetic susceptibility (10^{-5} SI) values from Transect C south of Scoresby Sund. MS values are shown against core depth (cm). MS values dramatically decrease from the shelf toward the slope.

Fig. 35. Magnetic susceptibility (10^{-5} SI) values are plotted versus the IRD content (no./10 cm^3) from five sediment cores recoverd from Transect C south of Scoresby Sund.

7.4.3 Productivity and dilution of biogenic carbonate in Holocene sediments

The production of biogenic carbonate within the GIN Sea is closely related to the properties of surface water masses, oceanographic front systems, and the sea-ice cover (Kellogg 1976, 1977; Johannessen et al. 1994) (see Section 7.1). Few nannofossils are observed along the western margin of the Greenland Sea and are absent within surface sediments deposited under the East Greenland Current (e.g. Eide 1990; Samtleben & Schröder 1992; Samtleben et al. 1995). The distribution of the polar planktonic foraminifer N. pachyderma sin. within the Greenland Sea is dependent on the surface water properties associated with summer temperatures below 4°C, sea-ice coverage, and water depths (Bé & Tolderlund 1971; Carstens 1988; Hebbeln & Wefer 1991; Johannessen et al. 1994). The low abundance of nannofossils

and foraminifers within Holocene sediments along the East Greenland continental margin indicates that surface-water productivity is generally very low. This has resulted from enhanced meltwater discharge, a strong influence of cold and low-saline polar waters from the Arctic Ocean, and heavy sea-ice coverage. All these factors induce a lower influx of biogenic carbonate to the glaciomarine sediments. The major factor influencing a benthic biomass is the nutrient distribution where the benthic foraminifers are generally dependent on the planktonic organisms within various food chains (e.g. Struck 1992; Schmiedl 1995; Wollenburg 1995). Therefore, the low abundance of calcareous benthic foraminifers and the absence of agglutinated benthic foraminifers within shelf sediments reflect lower surface-water productivity (e.g. Marienfeld 1992b) and/or unfavourable bottom water conditions. The absence of agglutinated benthic foraminifers may be attributed to decomposition related to strong and corrosive bottom water activity on the shelf.

Based on the oxygen and carbon isotope records, carbonate and organic carbon contents, and grain-size distribution patterns along the East Greenland continental margin, the sedimentary processes and environments reflect a distinct local pattern. The large difference in local glaciomarine environments may significantly influence the surface-water productivity. In particular, a strong meltwater discharge has prevailed along the continental margin south of Scoresby Sund throughout the Holocene. This vast meltwater outflow along the shelf indicated by the extremely light $\delta^{13}C$ values has been contributing to the thick stratification of surface waters prohibiting the exchange of CO_2 between the atmosphere and the ocean. Therefore, the environmental conditions have been unfavourable for surface-water productivity along the shelf south of Scoresby Sund. This is substantiated by the low carbonate content of <1.5 %, and the absence of biogenic components. In addition, the distinct increase in IRD supply is also thought to contribute to the strong dilution of biogenic carbonate. The increased C/N ratios (>10) and low HI values (<50 mgHC/gC) indicate that the organic matter of Holocene sediments is mainly terrigenous in origin and supports a reduction in surface-water productivity. However, the slightly increased amount of organic matter within uppermost sediments reflect, to a certain extent, an increase in surface-water productivity which has resulted from a seasonal reduction in sea-ice cover and a decrease in icebergs discharged from the adjacent fjord systems (cf. Marienfeld 1991a; Stein et al. 1993). This is further supported by the marked decrease in IRD content, reduced C/N ratios (<10), and an increase in HI values (100 mgHC/gC).

8. PALEOCEANOGRAPHIC RECONSTRUCTION ALONG THE WESTERN MARGIN OF THE GREENLAND SEA: SEA-ICE COVER AND MELTWATER DISCHARGE

8.1 Introduction

8.1.1 *N. pachyderma* sin. as a proxy for the paleoceanography in the GIN Sea

The distribution of planktonic foraminifers in the Greenland-Iceland-Norwegian (GIN) Sea is generally related to the surface water oceanography and sea ice conditions (Kellogg 1976, 1977, 1980; Johannessen et al. 1994). During Quaternary glacial-interglacial fluctuations, the polar species *N. pachyderma* sin. is the most dominant planktonic foraminifer in the GIN Sea (Kellogg 1976, 1977; Kellogg et al. 1978). This species is tolerant to water temperatures down as low as -1.4°C (Bé & Tolderlund 1971). In the Greenland Sea and Fram Strait, it preferentially lives in water depths between 50 and 200 m (e.g. Kellogg et al. 1978; Streeter et al. 1982; Carstens 1988; Carstens & Wefer 1992), and is strongly dependent on the variations in the sea-ice cover (Hebbeln & Wefer 1991). In general, the maximum relative abundances of *N. pachyderma* sin. are found within surface sediments deposited under polar water masses covered by a perennial sea-ice cover, and under the Arctic water masses with only a seasonal sea-ice cover (Johannessen et al. 1994). Kellogg (1976, 1977) also defined that the presence of >95 % *N. pachyderma* sin. is indicative of a polar water mass associated with permanent winter sea-ice cover. Therefore, the tests of *N. pachyderma* sin. together with their stable oxygen and carbon isotope records are preferentially used for the establishment of a Quaternary chronostratigraphy, and also as a proxy for the reconstruction of the paleoceanography and paleoenvironment of the GIN Sea during Quaternary glacial-interglacial climate changes (e.g. Kellogg 1976, 1977, 1980; Kellogg et al. 1978; Vogelsang 1990; Weinelt 1993).

The oxygen isotopic composition of *N. pachyderma* sin. is in equilibrium with the isotopic composition of the surface water (Charles & Fairbanks 1990). A change in $\delta^{18}O$ values reflect changes in the oceanic isotopic composition, mainly resulting from the waxing and waning of the great Quaternary ice sheets (Shackleton 1987). In addition, the $\delta^{18}O$ values of the foraminiferal calcite tests are affected by both the temperature and salinity of the ambient water (Emiliani 1955; Shackleton 1967) from which they are developed. The $\delta^{18}O$ records may be strongly influenced by local or regional isotope anomalies that are associated with evaporation, precipitation, sea-ice cover or meltwater discharge. Meltwaters derived from iceberg melting, and glaciofluvial and river discharge are the main contributors to a large extent to the $\delta^{18}O$ anomalies in the tests of *N. pachyderma* sin. in the GIN Sea and Arctic Ocean (Vogelsang 1990; Köhler 1992; Jünger 1994; Spielhagen & Erlenkeuser 1994; Stein et al. 1994a-b). Additionally in the Greenland Sea, the meltwater discharge may be attributed to the outflow of low-saline polar waters from the Arctic Ocean via the EGC (Köhler 1992; Stein et al. 1994a; Nam et al. 1995a). Therefore, large volumes of meltwater discharge into the oceans may influence the $\delta^{18}O$ values of surface waters further reflected in the light $\delta^{18}O$ values of *N. pachyderma* sin..

The $\delta^{13}C$ composition of surface water ΣCO_2 is strongly related to the extent of gas exchange between the atmosphere and the ocean (Kroopnick 1980). Gas exchange preferentially removes the ^{12}C to the atmosphere, and therefore decoupling the $\delta^{13}C$ and nutrients. In the high-latitude oceans, a widespread stratification of surface waters by meltwater discharge, and an extensive sea-ice cover, can strongly prevent the gas exchange between the atmosphere and the ocean, as reflected in the light $\delta^{13}C$ values of N. pachyderma sin.. Additionally, the ^{13}C content of the oceans is determined by the biological productivity of surface water, nutrient cycles, and mixing between water masses of various isotopic composition (Kroopnick 1985; Curry et al. 1988; Charles & Fairbanks 1990). The photosynthesis in surface water preferentially extracts ^{12}C from sea water, resulting in the enrichment of ^{13}C within surface water ΣCO_2 (Curry et al. 1988). After leaving the surface waters of the ocean, the ^{13}C of the total CO_2 dissolved within deep water masses becomes relatively depleted through the remineralisation of organic carbon (as a source of ^{12}C) and the mixing of water masses with various isotopic compositions (Curry et al. 1988; Duplessy et al. 1988a). Accordingly, $\delta^{13}C$ records from planktonic and benthic foraminifers are widely used as useful proxies for the change in paleoproductivity and deep-water circulation during the late Quaternary (e.g. Zahn et al. 1986; Curry et al. 1988; Duplessy et al. 1988a; Sarnthein et al. 1988; Mackensen et al. 1993; McCorkle & Keigwin 1994). This is related to the fact that the present geographic distribution of $\delta^{13}C$ in the ocean is closely related to the oxygen and nutrient content of different water masses, and furthermore, strongly dependent on the general circulation of the ocean (Kroopnick 1985).

8.1.2 Benthic foraminifer O. umbonatus in the GIN Sea

The deep-sea sediments of the GIN Sea are dominated by the benthic foraminiferal species C. wuellerstorfi and O. umbonatus. In the GIN Sea, C. wuellerstorfi is present during interglacial stages, particularly stage 5 and the Holocene. O. umbonatus is by far the dominant species throughout most glacial and interglacial stages (e.g. Belanger 1982; Streeter et al. 1982; Haake & Pflaumann 1989), but the abundance can be suppressed by ice rafting (Ramm 1988).

The $\delta^{13}C$ records of C. wuellerstorfi may reflect the $\delta^{13}C$ of bottom waters as it is preferentially an epifaunal living, benthic foraminifer (Corliss 1985; Mackensen et al. 1985; McCorkle et al. 1990). Therefore, $\delta^{13}C$ values of C. wuellerstorfi are used to reconstruct changes in the deep water circulation intensity and patterns during Quaternary glacial-interglacial cycles (e.g. Curry et al. 1988; Duplessy et al. 1988a; Mackensen et al. 1993; McCorkle & Keigwin 1994). However, in the GIN Sea, the $\delta^{13}C$ values of C. wuellerstorfi are difficult to use as a proxy for bottom water reconstruction as the appearance of this species is mostly confined to warm stages. On the other hand, O. umbonatus occurs throughout late Quaternary glacial-interglacial sediments and therefore, is likely to be very tolerant to changing climatic conditions within the GIN Sea (Haake & Pflaumann 1989). The isotope records of O. umbonatus can also be used as a proxy for an additional

Quaternary stratigraphy within the Greenland Sea (e.g. Jünger 1994). Moreover, $\delta^{13}C$ values of *O. umbonatus* are used to monitor deep-water formation within the GIN Sea (e.g. Jansen & Erlenkeuser 1985; Jünger 1994). However, it must be remembered that $\delta^{13}C$ records of *O. umbonatus* alone cannot be used as a reliable indicator of deep-water formation as the $\delta^{13}C$ values of endofaunal species are controlled by the $\delta^{13}C$ of pore water within bottom sediments (e.g. McCorkle et al. 1985, 1990; Mackensen & Douglas 1989). However, on the basis of the parallel trends between the $\delta^{13}C$ values of *N. pachyderma* sin., *C. wuellerstorfi*, and *O. umbonatus*, Jünger (1994) assumed that the $\delta^{13}C$ values of *O. umbonatus* may be influenced by small vital and habitat effects (cf. Belanger et al. 1981). Based on this assumption and as suggested by Jünger (1994) from the northern Greenland deep sea (Fig. 36b), the $\delta^{13}C$ values of *O. umbonatus* of core PS1730-2 from the deep-sea are used to interpret the ventilation by deep waters.
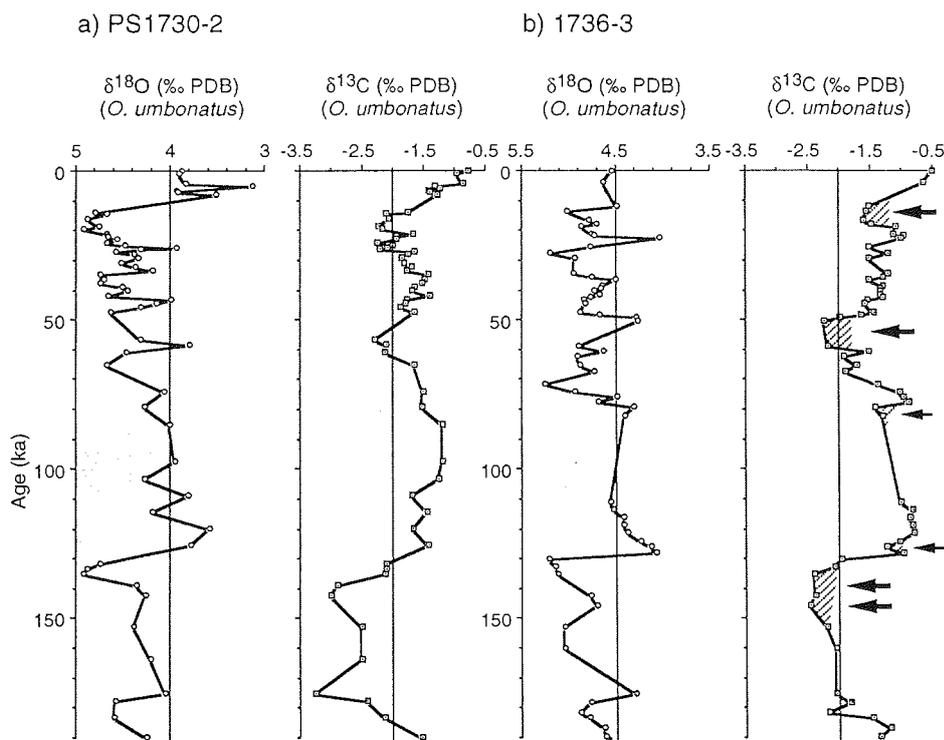
Fig. 36 a-b. $\delta^{18}O$ and $\delta^{13}C$ records of the benthic foraminifer *O. umbonatus* during the last 190 ka. The $\delta^{18}O$ values are corrected by the addition of +0.36‰ to the measured values (Duplessy et al. 1988b) (cf. Fig. 12). (a) deep sea-core PS1730-2, and (b) deep-sea core 1736-1 from the northern Greenland Sea (from Jünger 1994). The hatched areas and arrow mark same time slices with moderate to highly reduced deep water renewal (after Jünger 1994).

8.2 Paleoclimate and paleoceanography of the Greenland Sea in response to glacial-interglacial cycles during the last 245 ka

8.2.1 Interglacial stage 7 (245 - 190 ka)

At the base of stage 7, the appearance of chalk particles in the central Greenland Sea indicates the northward drift of icebergs by northward flowing surface currents (Baumann et al. 1993). The Norwegian Sea during stage 7 is characterised by good ventilation of surface waters due to the influence of the Norwegian Current (e.g. Vogelsang 1990). Furthermore, during substages 7.2 and 7.1 the patterns in surface water convection may be analogous to those of the present Arctic Domain (Vogelsang 1990). However, in the northern Greenland Sea, as reflected by the heavy $\delta^{18}O$ and light $\delta^{13}C$ values of $N.$ $pachyderma$ sin., deep water can only be formed during substages 7.5 and 7.1, whereas the cold periods of 7.4 to 7.2 are marked by the cooling of surface waters (e.g. Jünger 1994; Antonow 1995).

During stage 7, relatively heavy $\delta^{13}C$ values from the adjacent deep sea cores generally reflect the global interglacial patterns (e.g. Ramm 1988; Vogelsang 1990; Baumann et al. 1993; Jünger 1994; Antonow 1995). In contrast, along the East Greenland continental margin, the relatively light $\delta^{18}O$ and $\delta^{13}C$ values of $N.$ $pachyderma$ sin. reveal a distinct meltwater discharge close to the continental margin. The very light $\delta^{18}O$ and $\delta^{13}C$ values coincide well with an increased IRD supply to the slope. A large meltwater influx, and extensive iceberg rafting induced the light $\delta^{18}O$ and $\delta^{13}C$ values and the high IRD content, suggesting the presence of large volumes of icebergs adjacent to the East Greenland continental slope. However, the meltwater discharge close to the East Greenland continental margin seems to be a local signal associated with the Greenland Ice Sheet. During stage 7, the local distribution of meltwater may be attributed to a relatively weak surface water circulation within the GIN Sea (e.g. Baumann et al. 1993).

Based on light oxygen and carbon isotope records, and a very low carbonate content within the three gravity cores adjacent to Scoresby Sund, a cessation in deep-water formation is suggested for substages 7.5 to 7.2 but not substage 7.1 (cf. Jünger 1994; Antonow 1995). The reduced IRD-flux and an increase in the number of foraminiferal specimens (see Fig. 28b-c) during substage 7.1 indicate very little iceberg rafting and increased surface water productivity due to reduced sea-ice coverage. The presence of a specific ash layer within this interval also supports that there was a period of open-water conditions, that permitted ash particles to settle onto the sea floor (e.g. Sejrup et al. 1989; Birgisdórttir 1991; Lackschewitz 1991; Baumann et al. 1993).

During stage 7, the homogeneously overconsolidated diamicton sediments containing a high IRD content indicate an origin from a massive supply of icebergs, that subsequently trigger downslope mass movement via debris flows (Nam et al. in prep.). A similar diamicton sequence within stage 7 is also documented within the northern Greenland Sea (e.g. Antonow 1995). A predominant increase in coarse terrigenous debris (>0.5 mm) at the same interval is also recorded in deep sea sediments from the westernmost Iceland Plateau (e.g. Baumann et al. 1993). A general decrease in the carbonate content is recorded in the GIN Sea (e.g. Henrich et al. 1989; Baumann et al.

1993; Jünger 1994; Antonow 1995), probably indicating a dilution from an increased IRD supply. In general, the climate during interglacial stage 7 was colder than in the Eemian period and the Holocene (e.g. Kellogg 1977; Ramm 1988). According to an absence or drastic decrease in the amount of nannofossils within GIN deep sea sediments, stage 7 seems to be associated with a strongly suppressed productivity within surface waters (Gard 1988; Bleil & Gard 1989), probably the result of an influx of huge quantities of meltwater (e.g. Kellogg et al. 1978), and/or low sea surface temperatures and salinities (e.g. Baumann et al. 1995). The massive meltwater supply onto the East Greenland continental margin induces a widespread stratification of surface waters, and therefore, suppresses the production of planktonic foraminifers. Furthermore, an increase in the supply of coarse-grained terrigenous material and a decrease in surface productivity, resulted in the bottom environments becoming extremely hostile to benthic foraminifers, which is supported by an absence in benthic foraminifers during this interval (Fig. 23a-b).

8.2.2 Glacial stage 6 (190 - 130 ka)

The Greenland Sea was rapidly covered by perennial sea ice with the onset of glacial stage 6. This is indicated by the heavy $\delta^{18}O$ and light $\delta^{13}C$ values (i.e. substage 6.6). The year-round pack ice may have prevented the drift of icebergs resulting in a reduced supply of IRD onto the western margin of the Greenland Sea (Nam et al. 1995a). Based on this assumption, the increased input of terrigenous organic matter indicated by high C/N ratios and low HI indices is thought to be mainly transported by sea-ice. The extensive glacial sea-ice cover strongly suppressed the production of planktonic foraminifers leading to a low flux of biogenic carbonate (Fig. 28a-c). The light $\delta^{13}C$ values of *N. pachyderma* sin. indicate a considerably reduced CO_2 exchange between the atmosphere and the ocean, and a drastic reduction in the ventilation of surface waters due to the perennial sea-ice cover. However, a comparison of the $\delta^{13}C$ values of *N. pachyderma* sin. to those from the lower slope and deep sea (cores PS1726-1 and PS1730-2) reveals that $\delta^{13}C$ values of the upper slope (core PS1725-2) are to some extent much heavier. This may suggest a seasonally fluctuating sea-ice cover associated with minimal iceberg melting close to the continental margin as a result of the influence of a polar water mass with temperatures below freezing point.

After a period of expanded sea-ice cover, indicated by increased meltwater discharge in the GIN Sea, the surface-water condition of substage 6.5 was rapidly converted to more seasonally open-water conditions (e.g. Vogelsang 1990; Jünger 1994). However, in the western part of the GIN Sea, the relatively lower content of calcareous foraminifers probably resulted from the lower salinity and temperature of surface waters due to a cap of meltwater suppressing the production of biogenic carbonate (e.g. Thordardotirr 1977). Although Hebbeln (1991), Henrich (1992), and Henrich et al. (1995) suggested a weak intrusion of Atlantic waters into the GIN Sea, all sediment cores from the western GIN Sea do not reflect any short-term advection of Atlantic waters. The incursion would result in melting of icebergs within the Greenland Sea inducing an increased supply of IRD during this interval, and causing a subsequent dilution of biogenic carbonate. Therefore, in comparison to substage 6.3, the lower carbonate content appears to be

attributed to dilution from increased ice-rafted debris (e.g. slope cores PS1725-2 and PS1726-1). In deep-sea core PS1730-2, this is probably the result of a strong decrease in biogenic production. In addition, the widespread meltwater input may have given rise to a significant stratification of surface waters resulting in the reduction of bottom water production. This is further supported by the light $\delta^{13}C$ values of *N. pachyderma* sin. and *O. umbonatus* (Figs. 36a-b & 37c).

a) PS1725-2   b) PS1726-1

$\delta^{18}O$ (‰ PDB) $\delta^{13}C$ (‰ PDB) $\delta^{18}O$ (‰ PDB) $\delta^{13}C$ (‰ PDB)
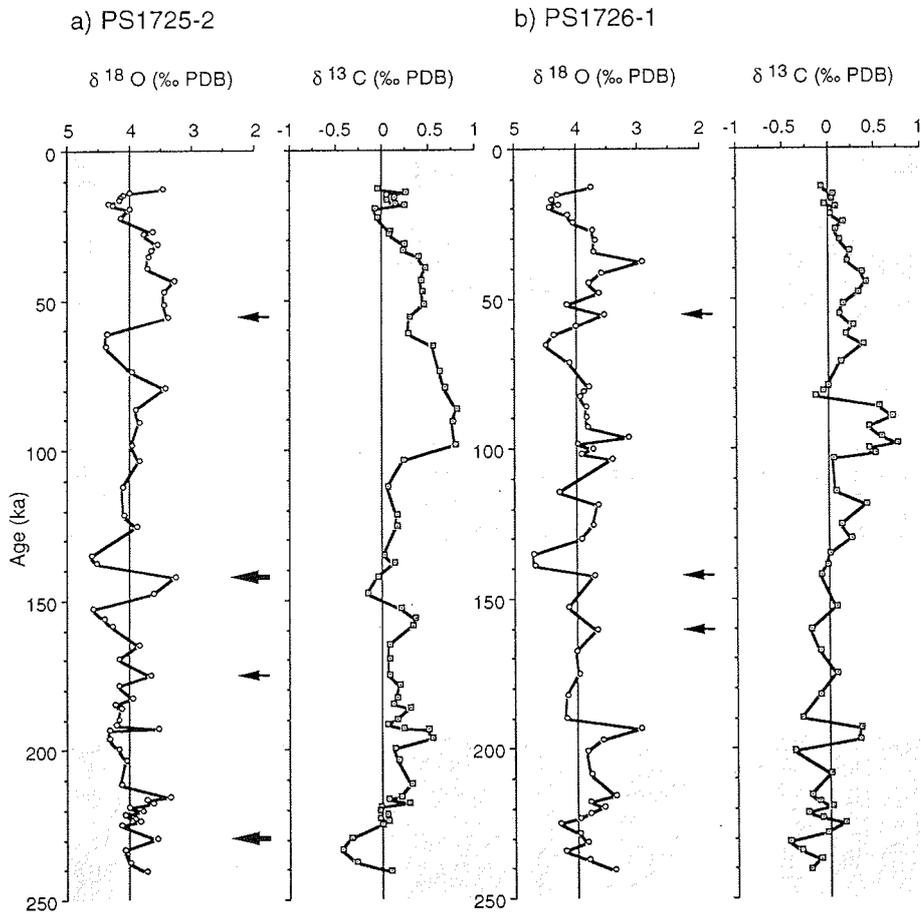
Fig. 37 a-e. $\delta^{18}O$ and $\delta^{13}C$ records of the planktonic foraminifer *N. pachyderma* sin. during the last 245 ka. Three cores (a) PS1725-2, (b) PS1726-1, and (c) PS1730-2 were recovered on the slope and in the deep sea adjacent to Scoresby Sund. Two deep-sea cores (d) PS1927-2 and (e) PS1951-1 were recovered from the deep sea north and south of Scoresby Sund, respectively. Arrows within the oxygen isotope records mark meltwater event within the western part of the Greenland sea.
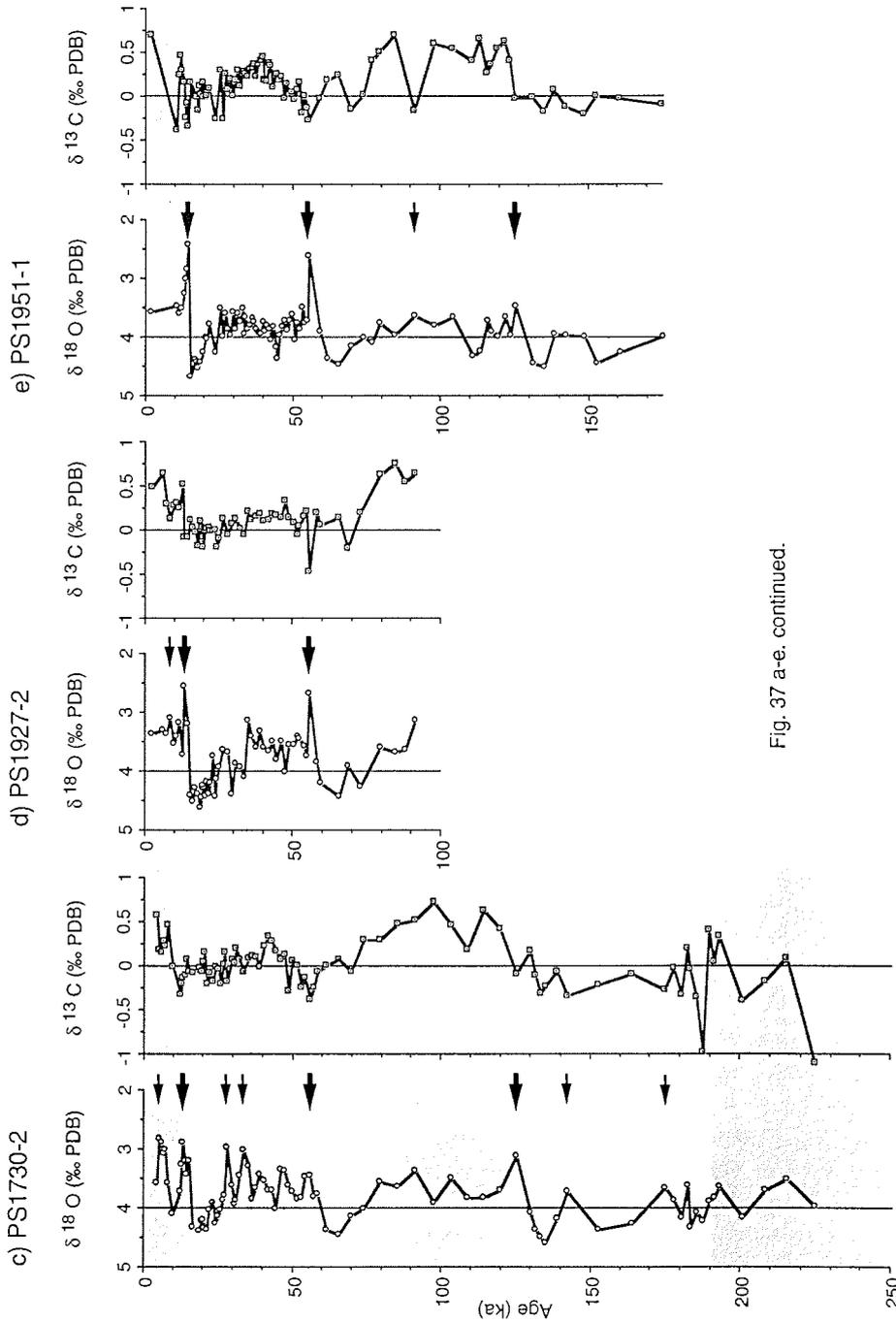
Fig. 37 a-e. continued.

Based on heavy $\delta^{18}O$ and light $\delta^{13}C$ records from substage 6.4, the western Greenland Sea was dominated by very cold surface water conditions and an intense sea-ice coverage (e.g. Jünger 1994; Antonow 1995). A reduced terrigenous accumulation rate is commonly observed within the western Greenland Sea (Jünger 1994; Baumann et al. 1994; Goldschmidt 1995) and is probably the result of an expanded sea-ice cover and reduced ice melting. As previously discussed, the ice margin may have been positioned near the upper slope during this interval. However, relatively heavy $\delta^{13}C$ values on the upper slope (core PS1725-2) may to some extent reflect open-water conditions with reduced sea-ice melting resulting from the strong influence of very cold polar waters of the EGC. A relatively enhanced supply of IRD onto the slope may have resulted from the melting of icebergs near the ice margin. A distinct increase in the carbonate accumulation rate is recorded in the Greenland Sea (Fig. 28a-c; Jünger 1994; Baumann et al. 1994). This indicates seasonally fluctuating open-ocean conditions permitting the production of biogenic carbonate within surface waters. This is further corroborated by relatively heavy $\delta^{13}C$ values and the high occurrence of planktonic foraminifers from both slope cores (PS1725-2 and PS1726-1) which support an increased production within ice-marginal surface waters (Smith et al. 1987; Hebbeln & Wefer 1991; Stein & Stax 1991; Carstens & Wefer 1992; Lloyd et al. 1996a) combined with the ventilation of surface waters and/or a penetration of oxygenated surface waters onto the sea floor. In addition, the penetration of oxygen-enriched surface-water masses onto the slope sea floor may be derived from dense brines released when shelf ice sheets formed close to the continental margin during this interval. In contrast and as suggested by the low occurrence of calcareous foraminifers relative to the continental margin area, light $\delta^{13}C$ values and a low carbonate content within the deep-sea cores PS1730-2 and PS1951-1 may have resulted from an extended sea-ice cover.

The oceanographic pattern within substage 6.3 reflects a major regional melting event in the northern and western GIN Sea (e.g. Jünger 1994; Antonow 1995; Nam et al. 1995a), on the Iceland Plateau (Vogelsang 1990), and on the NE Yermak Plateau (Vogt et al. submitted). However, in the central and eastern sites of the GIN Sea there is no evidence for a meltwater signal (e.g. Vogelsang 1990). Similar to substage 3.31, the meltwater event of substage 6.3 may be associated with the melting of East Greenland glaciers, coupled with an input of isotopically light polar waters via the Transpolar Drift derived from the Arctic Ocean and directed into the western GIN Sea. Furthermore, the meltwater signal recorded on the Iceland Plateau is probably the result of a weak inflow of Atlantic waters, further suggested by the reduced occurrence of the planktonic foraminifer *Globigerina quinqueloba* (Natland) (Bauch 1993), and the widespread occurrence of coccoliths (Baumann 1990). Along the continental margin, the strong influence from marine-based shelf ice sheets on the pronounced meltwater discharge is indicated by an increase in the coarse IRD supply onto the upper slope (PS1725-2). This coarse IRD-supply (>0.5 mm) strongly decreases towards the deep sea implying a major reduction in the drift of icebergs. However, there is a distinct increase in accumulation rates of terrigenous matter, and may be the result of a higher input of relatively fine-grained components through meltwater plume and sea-ice processes (e.g. Pfirman & Solheim 1989; Nürnberg et al. 1994). A relatively high carbonate content and a high abundance of planktonic foraminifers support the strongly reduced sea-ice cover and/or open water

conditions during substage 6.3. During the same time slice, a high amount of coccoliths occurred in the eastern Fram Strait indicating open surface waters resulting from a weak advection of Atlantic waters (Hebbeln 1991). Subsequently and based on litho- and organofacies distribution patterns, Henrich et al. (1995) deduced a similar circulation mode as to the present day situation.

When comparing $\delta^{18}O$ and $\delta^{13}C$ values of N. pachyderma sin. and O. umbonatus from the LGM (approximately 21 to 16 ka) to those of substage 6.2, the relatively heavier $\delta^{18}O$ and lighter $\delta^{13}C$ values of substage 6.2 indicate a period of expanded sea-ice coverage over the Greenland Sea than during the LGM. After a period of widespread meltwater distribution during substage 6.3, huge volumes of fresh meltwater with near-freezing temperatures may have been more rapidly cooled than the ambient with water of normal salinity. The heaviest $\delta^{18}O$ values of substage 6.2 is considered as a typical example of full glacial conditions (e.g. Duplessy & Labeyrie 1994). Therefore, during substage 6.2 the extensive cooling of surface waters resulted in an extensive sea-ice cover throughout the GIN Sea (e.g. Kellogg 1976, 1977, Kellogg et al. 1978; Vogelsang 1990; Köhler 1992; Jünger 1994; Nam et al. 1995a). A dramatic decrease in the carbonate content and planktonic foraminifers is most likely due to the extensive sea-ice cover (e.g. Kellogg 1976). During substage 6.2 and similar to substage 6.6, reduced iceberg drifting occurred resulting in a strong reduction of IRD discharge onto the sea floor. As indicated by the significantly light $\delta^{13}C$ values of N. pachyderma sin., there was also a drastic decrease in the gas exchange between the atmosphere and the ocean.

8.2.3 Interglacial stage 5 (130 - 74 ka)

The transition between stages 6 and 5, i.e. Termination II, is characterised by a rapid deglaciation that reflects the abrupt decay and retreat of the surrounding continental ice sheets. In general and compared to values from the Yermak Plateau and the Fram Strait (e.g. Köhler & Spielhagen 1990; Köhler 1992), $\delta^{18}O$ values along the western margin of the Greenland Sea reveal relatively light values that suggest a continual influence of meltwater discharged from East Greenland glaciers, and/or an inflow of low saline polar waters into the western Greenland Sea. On the other hand, relatively heavy $\delta^{18}O$ values from the Yermak Plateau and the Fram Strait may result from the cooling of Norwegian surface water masses during transportation towards the north (e.g. Köhler 1992). Furthermore, $\delta^{18}O$ values from the Vøring Plateau are very light due to the influence of low-saline and warm North Atlantic water masses (Vogelsang 1990). In addition, $\delta^{18}O$ values from the five gravity cores are relatively heavy during stage 5 in comparison to those of stage 3 and in the Holocene (Fig. 37a-e). As indicated by the relatively heavy $\delta^{18}O$ and $\delta^{13}C$ values during stage 5, this may be attributed not only to the reduced influence of meltwater relative to stage 3 but also to the cooling of surface waters relative to the Holocene. On the other hand, $\delta^{18}O$ values from O. umbonatus within stage 5 are relatively light compared to those of stage 3 and probably reflect changes in deep water conditions (e.g. hydrostatic pressure and bottom

104

water temperature) (Belanger & Streeter 1980; Belanger 1982). This is further substantiated by distinctly heavier $\delta^{13}C$ values from *N. pachyderma* sin. and *C. wuellerstorfi* within stage 5, and reflects the renewal of the Greenland Sea deep water, subsequent well-oxygenated waters, and reduced sea-ice cover probably induced by the inflow of North Atlantic waters into the western Greenland Sea (e.g. Labeyrie & Duplessy 1985; Haake & Pflaumann 1989).

Along the western margin of the Greenland Sea, a small shift in the $\delta^{18}O$ values during Termination II does not exceed the ice volume effect (cf. Vogelsang 1990; Jünger 1994). This may be the result of surface water cooling derived from the strong influence of the cold polar water of the EGC during this period. During substage 5.5 in core PS1725-2 from the upper slope, the relatively heavy $\delta^{18}O$ value is similar to that within glacial stages, and coupled with a light $\delta^{13}C$ value clearly indicates sea-ice covered conditions. The heavy $\delta^{18}O$ values decrease eastward to lighter values, and reach a value of 3.0‰ in all deep-sea cores (Fig. 37c-e). This eastward trend is thought to reflect the decrease in influence of cold waters of the EGC, and/or a weak inflow of warm waters associated with the NAC. However, compared to $\delta^{18}O$ values from the central GIN deep-sea cores during Termination II, $\delta^{18}O$ values of cores PS1730-2 and PS1951-1 define a weak influence from warm North Atlantic surface waters flowing into the western Greenland Sea, that contributes to regional meltwater discharge within the GIN Sea (e.g. Köhler & Spielhagen 1990; Vogelsang 1990; Köhler 1992; Jünger 1994). The meltwater discharge at the stage 6/5 boundary may have contributed to an increase in the IRD supply and a distinct decrease in the biogenic carbonate production. On the contrary, the dominance of *N. pachyderma* sin. in the deep sea, e.g. core PS1730-2, is thought to reflect a strong influence from cold polar water masses with a perennial sea ice cover (cf. Kellogg 1976, 1977; Johannessen et al. 1994) along the western margin of the Greenland Sea.

During the Eemian, a climatic optimum similar to that of the Holocene occurred in the GIN Sea (e.g. Kellogg 1976). The highest planktonic foraminiferal content is recorded during both warm periods and reflects open-water conditions produced from an inflow of warm Atlantic waters into the GIN Sea. This characteristic is generally recorded within sediments from most investigations within the GIN Sea (e.g. Kellogg 1976, 1977, 1980; Ramm 1988; Henrich et al. 1989; Henrich 1992; Baumann et al. 1993, 1994; Jünger 1994). In contrast, a very low carbonate content of <2.5 % in core PS1951-1 from the deep sea north of Iceland, suggests strong biogenic carbonate dissolution during substage 5.5, probably resulting from an increase in pCO_2 within bottom waters. In addition, the lower carbonate content recorded in deep-sea core PS1730-2 may reflect a strong dilution from an increased IRD supply to the sea floor and/or suppressed productivity within surface waters resulting from strong meltwater discharge. On the other hand, a lower carbonate content similar to the record in core PS1951-1 was determined on the two slope cores (PS1725-2 and PS1726-1) adjacent to Scoresby Sund, and is ascribed not only to dilution from increased terrigenous matter, but also to the dissolution caused by an increased CO_2 production from the decomposition of organic carbon. In general, the high inflow of meltwater into the western Greenland Sea was strongly reduced during the later period of the Eemian. After this period, partially or seasonally open-water conditions

may have prevailed in the western part of the Greenland Sea. This is supported by a reduced IRD content and an increase in the carbonate content coupled with abundant planktonic foraminifers. A shift in $\delta^{13}C$ to distinctly heavier values also indicates the transition of surface conditions towards a seasonally reduced sea-ice cover in the Greenland Sea, that permits deep-water formation and strong ventilation of surface waters.

Within the cooling periods of substages 5.4 and 5.2, relatively heavy $\delta^{13}C$ values, a remarkably reduced supply of terrigenous matter, and a distinct increase in the carbonate content reflect seasonally reduced sea-ice cover along the western margin of the Greenland Sea. However, substage 5.4 along the East Greenland continental margin is characterised by relatively heavy $\delta^{18}O$ and light $\delta^{13}C$ values reflecting a cooling of surface water temperatures which contributes to the sea-ice cover. In addition, a markedly increased IRD supply onto the slope area reflects enhanced iceberg drifting probably resulting from the advance of East Greenland glaciers during this period. In contrast, substage 5.2 on the upper slope is characterised by heavy $\delta^{13}C$ values, and an abrupt decrease in the IRD supply onto the continental margin. This indicates a strong, seasonal reduction in the sea-ice cover which permits deep-water formation and an increase in vertical mixing between surface and bottom waters. Furthermore, a distinct increase in the carbonate content corresponding with the enhanced occurrence of calcareous foraminifers during this interval, may be attributed to the penetration of well-oxygenated near surface-water masses towards the sea floor (Zahn et al. 1985). In other words, an abrupt decrease in the IRD supply to the continental margin is thought to be derived from the retreat of East Greenland glaciers during this period.

In general, substage 5.3 seems to be a period of strongly reduced sea-ice cover and increased surface-water productivity. This is also supported by the heavy $\delta^{13}C$ values, high HI values (>100 mgHC/gC), and peaks within the carbonate content corresponding to the abundant occurrence of planktonic foraminifers. Gard & Backman (1990), based on the occurrence of coccoliths, suggested an influence of North Atlantic surface water within the Greenland Sea. However, the abundance of monospecific *N. pachyderma* sin. indicates a dominance of cold polar water masses within the western part of the Greenland Sea. Owing to the heavy $\delta^{13}C$ values from the planktonic and both benthic foraminifers, deep-water formation seems to have taken place within the Greenland deep sea during substage 5.3 (e.g. Vogelsang 1990; Birgisdóttir 1991; Jünger 1994). The high IRD content recorded in cores PS1730-2 and PS1951-1 from the deep sea are not observed in cores PS1725-2 and PS1726-1 from the upper to the lower slope adjacent to Scoresby Sund during this interval (Fig. 29a-c,e). This suggests that icebergs probably derived from the north and transported in the EGC, and melted over the deep sea as probably the result of the weak influence of warm surface waters.

The conditions within substage 5.1 seem to be similar to those of substage 5.3 with respect to the relatively light $\delta^{18}O$ and heavy $\delta^{13}C$ values. In contrast, the pattern within the IRD content of sediments is the reverse of substage 5.3. The IRD-discharge onto the deep sea floor was markedly reduced, whereas it was

enhanced on the slope region. During this interval, most icebergs melted on the continental margin, and very few reached the deep sea. Therefore, a significant decrease in the carbonate content may be the result of an increased dilution from terrigenous matter. In addition, during this interval the local meltwater discharge documented within the Greenland Sea and the Fram Strait (e.g. Köhler & Spielhagen 1990; Köhler 1992; Jünger 1994) is only recorded in core PS1726-1 from the lower slope. However, with the exception of the meltwater signal within core PS1726-1, distinctly heavy $\delta^{13}C$ values of *N. pachyderma* sin., *C. wuellerstorfi*, and *O. umbonatus* suggest strong vertical mixing between surface waters and bottom waters indicating deep-water formation (cf. Jünger 1994). However, a considerable decrease in the carbonate content during this period is most probably the result of dilution from an increased supply of terrigenous sediment.

8.2.4 Glacial stage 4 (74 - 59 ka)

At the stage 5/4 boundary, a drastic change in surface-water conditions is suggested by a rapid shift in $\delta^{18}O$ towards heavy values, and a decrease in carbonate and IRD flux. According to the heavy $\delta^{18}O$ values from *N. pachyderma* sin. and *O. umbonatus*, glacial stage 4 is likely to be characterised by a period of extensive perennial sea-ice cover. Under these conditions, the planktonic foraminifer productivity decreased, reflected by the reduced carbonate content during early stage 4. An extended sea-ice cover may have also prevented iceberg drift into the western region of the Greenland Sea, reflected by a distinct decrease in the supply of coarse-grained terrigenous material. Furthermore, the lower sedimentation rates during stage 4 are mainly attributed to expanded sea-ice covered conditions (Nam et al. 1995a).

Throughout stage 4 there is no evidence for meltwater discharge into the GIN Sea (e.g. Vogelsang 1990; Köhler 1992; Jünger 1994). In contrast, $\delta^{13}C$ values recorded from the continental slope adjacent to Scoresby Sund are relatively heavier than those from the deep sea during early stage 4, and indicate to some extent the ventilation of surface waters close to the continental margin. Furthermore, it is suggested that there were at least seasonally ice-reduced conditions during this interval (Köhler 1992; Jünger 1994). Coccoliths are found in the Fram Strait and the GIN Sea during early stage 4 (Gard 1986, 1987, 1988; Baumann 1990), reflecting periods of seasonally fluctuating ice-free conditions (Gard 1988). Moreover, Gard (1988) suggested an inflow of North Atlantic surface waters into the Fram Strait at the boundary between stages 5 and 4.

During substage 4.2, the relatively heavy $\delta^{18}O$ (4.3-4.5‰) and light $\delta^{13}C$ (<0.25‰) values indicate the strongly reduced ventilation of surface waters resulting from an expanded sea-ice cover which may in turn have led to a weak circulation of surface waters. However, the slight increase in the carbonate content within the three deep-sea cores, probably reflect a seasonally reduced sea-ice cover particularly during the summer. This is further supported by an increased occurrence of planktonic foraminifers. During this period, an increase in the IRD content is recorded in the three deep-sea cores. In contrast, terrigenous IRD supply onto the slope is very low,

107

and may be the result of a more intense sea-ice cover close to the continental margin. Consequently, the increased carbonate content within the slope cores is more likely the result of reduced dilution from terrigenous matter. In addition, it could also be ascribed to the ventilation of the sea floor from well-oxygenated surface waters, as indicated by the relatively increased $\delta^{13}C$ values of the slope adjacent to Scoresby Sund.

8.2.5 Interglacial stage 3 (59 - 25 ka)

At the beginning of stage 3 (the stage 4/3 transition), the $\delta^{18}O$ records of cores PS1927-2 and PS1951-1 show a rapid shift of 1.76‰, reflecting a dramatic change in sea-surface temperatures and/or salinity. Throughout stage 3, $\delta^{18}O$ values of N. pachyderma sin. are characterised by remarkably lighter values of approximately >1‰ in comparison to those from the Norwegian Sea (cf. Vogelsang 1990; Henrich 1992; Köhler 1992). The general depletion in $\delta^{18}O$ values seems to reflect changes in surface-water salinity, derived from an influence of meltwaters from receding East Greenland glaciers. During stage 3, a slightly enhanced surface-water productivity may reflect partially or seasonally reduced sea-ice coverage. In general, relatively heavy $\delta^{18}O$ values of O. umbonatus within stage 3 indicate the cooling of bottom water.

The last glaciation of the Greenland ice core record (e.g. GRIP and GISP2) is characterised by a series of the rapid warm-cold cycles (Dansgaard et al. 1993; Grootes et al. 1993), known as "Dansgaard-Oeschger (D-O) Cycles" (Broecker & Denton 1989) which strongly reflect the unstable climate oscillations around Greenland (e.g. Bond et al. 1993). These millennial-scale climatic variations are bundled into longer cooling D-O cycles, each terminated by an abrupt shift from cold to warm temperatures (Bond et al. 1993), called "Bond Cycles" (Lehman 1993; Broecker 1994). During isotope stage 3, distinct warm-cold D-O cycles are also documented within the $\delta^{18}O$ records of cores PS1730-2, PS1951-1, and PS1927-2 from the deep sea (Fig. 38), suggesting rapid climatic changes around the GIN sea region. In particular, the shift of $\delta^{18}O$ values between the warm and cold intervals vary from 0.4 to 1.07‰, which correspond to a change in ocean temperature of 1.7 to 4.5°C. These shifts are very similar to the temperature changes of 5°C estimated from the North Atlantic (Bond et al. 1993). However, there is no evidence for such large shifts in the SST along the western margin of the Greenland Sea during stage 3. This is further supported by the dominant abundance of N. pachyderma sin. (>95 %) throughout this interval that indicates uniform cold conditions within the surface water. Therefore, shifts in $\delta^{18}O$ record toward light values are thought to reflect changes in the salinity along the western margin of the Greenland Sea, largely induced by the massive discharge of meltwater and icebergs (e.g. Stein et al. 1994a-b; Nam et al. 1995a). Significantly light $\delta^{18}O$ values correlate with relatively light $\delta^{13}C$ values (Fig. 37c), which support an increase in the meltwater discharge. Furthermore, the dramatic decrease in the IRD-flux corresponds to these intervals of increased meltwater input reflecting the repeated retreat of East Greenland glaciers.
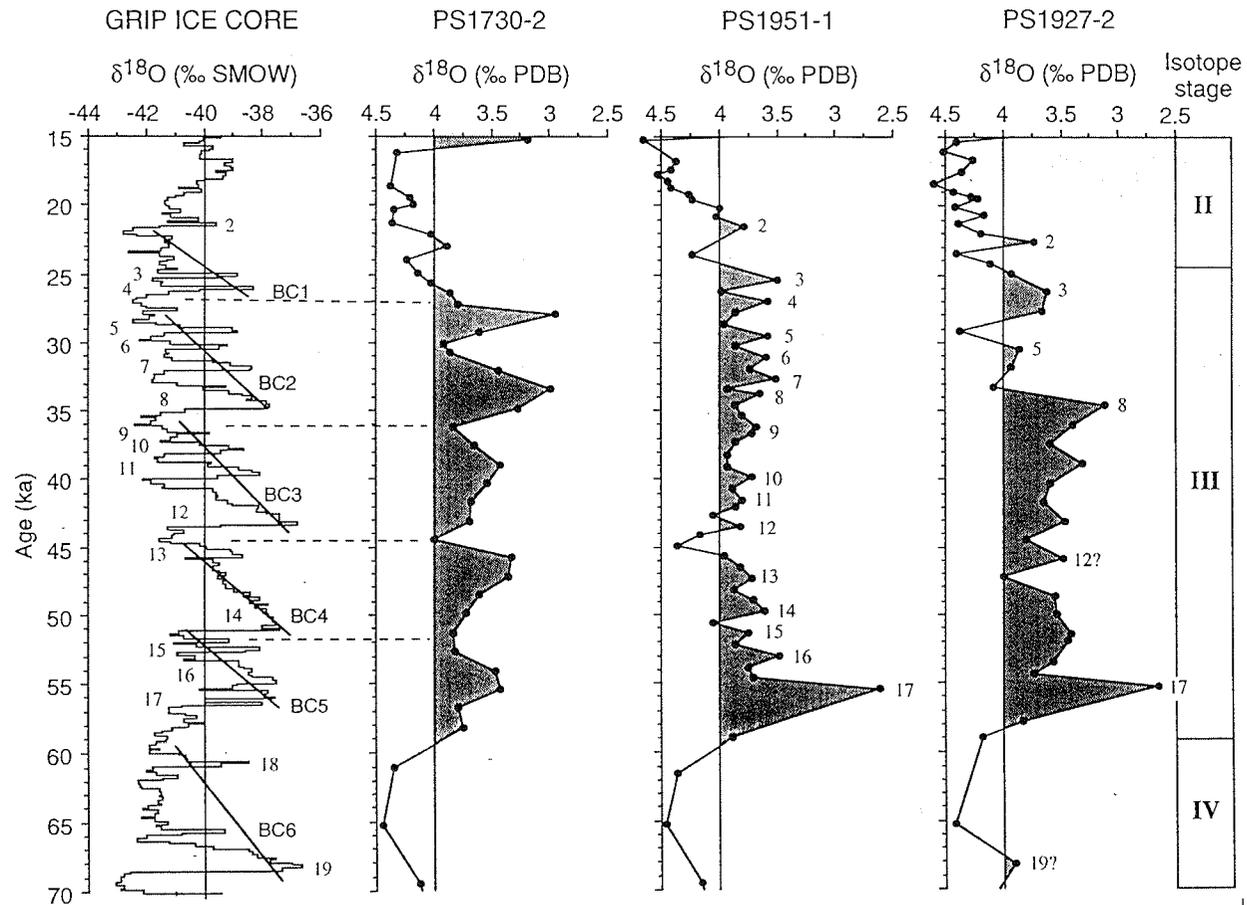
Fig. 38. Comparison of the Dansgaard-Oeschger cycles from the GRIP ice core (Dansgaard et al. 1993) and $\delta^{18}O$ records from the Greenland Sea during the interval between 70 and 15 ka. BC1-6 indicate Bond cycles (Lehman 1993; Broecker 1994). Relatively heavy $\delta^{18}O$ values of core PS1730-2 correlate well with most intense cold phase of a package of several D-O cycles, i.e. Bond cycles. The D-O cycles seem to be correlated with the $\delta^{18}O$ records of core PS1927-2 during stages 3 to 2.

Substage 3.31 is characterised by a distinct shift in $\delta^{18}O$ and $\delta^{13}C$ towards light values. This is further evidence for a major regional meltwater signal that is recorded throughout the GIN Sea (Vogelsang 1990; Lackschewitz 1991; Köhler 1992; Weinelt 1993; Jünger 1994; Baumann et al. 1995; Nam et al. 1995a), the Yermak Plateau (Vogt et al. submitted), the slope northwest of Spitsbergen (Knies 1994), and in the central Arctic Ocean (Köhler 1992; Stein et al. 1994a) within this interval. This major meltwater event may be triggered by the weak inflow of warm North Atlantic water masses during this interval. The light $\delta^{18}O$ and $\delta^{13}C$ values from the central Arctic Ocean are very similar to those from the Iceland Sea (Köhler 1992). Therefore, there seems to be an additional influence from the export of low-saline Arctic waters into the Iceland Sea from the EGC. The occasional presence of some calcareous nannofossils *E. huxleyi* and *Gephyrocapsa* spp. in core V27-60 from the Norwegian Sea (Gard 1988) reflects at least a seasonally reduced sea-ice cover during early stage 3, probably resulted from an advection of Atlantic water masses.

During substage 3.31, on the other hand, the relatively light $\delta^{13}C$ values of *N. pachyderma* sin. reflect a strong reduction in the CO_2 exchange between the surface water and the atmosphere resulting from a meltwater cap. In addition, lower $\delta^{13}C$ values from *O. umbonatus* may indicate the cessation of deep-water formation (e.g. Jünger 1994). If the vertical mixing between surface waters and bottom waters is significantly reduced, bottom waters may have become less oxygenated and nutrient-enriched. This may have resulted in increased dissolution of biogenic carbonate. During this interval, the common occurrence of sponge spicules in core PS1730-2 indicates the cooling of bottom waters (e.g. Williams 1993), which may in turn have caused the increased dissolution of the biogenic carbonate. In particular, the presence of a specific Ash Layer II (Ruddiman & Glover 1972) during early stage 3 indicates a period of open-water conditions but probably with a fluctuating sea-ice cover. A clockwise distribution pattern of ash between the Denmark Strait and the Iceland Plateau suggests a control from the inflow of the warm Irminger Current through the Denmark Strait into the Iceland Sea, which probably contributes to the reduced sea-ice cover during this interval.

As suggested by the light $\delta^{18}O$ and corresponding heavier $\delta^{13}C$ values, the middle stage 3 seems to be a period characterised by reduced sea-ice coverage. In addition to the slightly heavier $\delta^{13}C$ values of *N. pachyderma* sin., the similar patterns of *O. umbonatus* may also indicate a weak or intermittent exchange between surface waters and bottom waters. Therefore, an increase in surface-water productivity, coupled to some extent with well oxygenated bottom waters due to ventilation, may have caused the increased preservation of biogenic carbonate. Furthermore, this period is marked by an increased IRD content and a relatively increased carbonate content on the continental margin, suggesting a decrease in dilution by terrigenous matter. On the other hand, relatively heavier $\delta^{13}C$ values from the continental slope in comparison to those of the deep sea, may reflect a combination of increased carbonate production near the fluctuating sea-ice margin (Hebbeln & Wefer 1991; Carstens & Wefer 1992) and the preservation of biogenic carbonate.

Late stage 3 is generally characterised by regional meltwater discharge into the Greenland-Iceland Sea and the Fram Strait (Köhler 1992; Weinelt 1993;

Jünger 1994; Nam et al. 1995a; Sarnthein 1995). Köhler (1992) suggested that the local appearance of meltwater reflected in isotopic records particularly within the western GIN Sea, is derived from meltwater plumes originating from the Greenland Ice Sheet and/or the Iceland ice cap. Therefore, a distinct increase in the IRD-flux onto the East Greenland continental slope reflects the intensive drift of icebergs from the surrounding land ice sheet during this interval (*see* Section 7.2). A similar increase in the IRD-flux during this period is observed in the three deep-sea cores (Fig 29c-e). On the other hand, an increased carbonate content may indicate a somewhat enhanced production of biogenic carbonate close to the sea-ice margin.

8.2.6 Sea-ice cover and meltwater incursion in the Greenland Sea during the last glacial stage 2

The LGM is generally characterised by the extension of continental ice sheets, greater extent of sea ice, lower sea-surface temperatures, and a sea-level stand of 130 m below present (Hughes et al. 1977; CLIMAP 1981). The majority of continental shelves adjacent to the GIN Sea were covered by large ice sheets (Denton & Hughes 1981), and extended sea ice (Kellogg 1976, 1977, 1980; Kellogg et al. 1978; Streeter et al. 1982).

The heavy $\delta^{18}O$ (4.26-4.30‰) and light $\delta^{13}C$ (<0.25‰) values of the planktonic foraminifer *N. pachyderma* sin., indicate that the majority of the Greenland Sea was covered by sea-ice during the LGM (e.g. Gard & Backman 1990). This is further substantiated by the heavy $\delta^{18}O$ and light $\delta^{13}C$ values of the benthic foraminifer *O. umbonatus* throughout the LGM. The heavy $\delta^{18}O$ and light $\delta^{13}C$ values from *N. pachyderma* sin. and *O. umbonatus* suggest that an extended sea-ice cover during the LGM may have prevented deep-water formation within the Greenland Sea. However, according to increased $\delta^{13}C$ values from the benthic foraminifer *O. umbonatus*, Jünger (1994) suggested the possibility of regional deep-water formation within the northern Greenland Sea prior to substage 2.2. This is similarly indicated in the three deep-sea cores PS1927-2, PS1730-2, and PS1951-1 by an increase in the $\delta^{13}C$ values of *O. umbonatus* and *N. pachyderma* sin., and the increased carbonate content which reflects stronger carbonate preservation related to a slightly enhanced gas exchange.

During the LGM, $\delta^{18}O$ values between 4.26 and 4.30‰ from the western Greenland deep sea are relatively lighter than compared to those of 4.45-4.96‰ from the Norwegian-Greenland Sea (cf. Kellogg et al. 1978; Jones & Keigwin 1988; Sarnthein et al. 1992), and are probably the result of the influence of Arctic water masses with relatively light oxygen isotopes flowing into the western Greenland Sea. This is supported by the light $\delta^{18}O$ values from the Arctic Ocean that are analogous to those from the Iceland Sea (Köhler 1992). At the Yermak Plateau, two meltwater events are recorded between 21 and 18.3 ka (Köhler 1992), but are dated between 23 and 21.5 ka in the western Greenland Sea (Fig. 11). This time lag may be the result of a difference in the local melting of the surrounding land-based glaciers during glacial stage 2. In particular, the Greenland Sea seems to have been influenced by at least seasonally and/or locally fluctuating ice-free or reduced

conditions within the LGM (Nam et al. 1995a; Sarnthein et al. 1995). An increase in both the carbonate content and in the occurrence of calcareous planktonic and benthic foraminifers, and relatively high HI values (>100 mgHC/gC) indicate to some extent increased surface-water productivity near the sea-ice edge (e.g. Smith et al. 1987; Hebbeln & Wefer 1991; Stein & Stax 1991), which strongly supports reduced sea-ice conditions. Hebbeln et al. (1994) also suggested that the Fram Strait was not covered by perennial sea ice but was influenced more by seasonally ice-free conditions during the LGM.

Comparing the $\delta^{18}O$ and $\delta^{13}C$ values of the LGM from the five gravity cores (Fig. 37a-e) with those from the slope areas north and south of Scoresby Sund (Figs. 20c-d & 22c-e) there is a strong indication of major but local meltwater discharge. This is reflected in most of the cores on the adjacent slope during the LGM. In particular, strong meltwater plumes, marked by anomalously light $\delta^{18}O$ and $\delta^{13}C$ values, are documented within the three slope cores south of Scoresby Sund. The significantly light $\delta^{18}O$ (1.92 to 3.0‰) and $\delta^{13}C$ (-1.28 to 0‰) values are extraordinarily similar to values within the Holocene, and result from the massive meltwater discharge from East Greenland during the LGM. The region near the ice margin was characterised by intensive melting during most of the year (Kellogg 1976). Therefore, the distinctly lighter $\delta^{18}O$ and $\delta^{13}C$ values from the upper slope to the lower slope indicate the existence of shelf-based ice sheets that underwent extensive fluctuations close to the East Greenland continental shelf break (see Section 7.3). This is clearly supported by a distinct increase in the supply of IRD onto the slope areas within this interval (Fig. 32). Consequently, a large and widespread input of meltwater estimated from the continental slope cores, suggests that the Greenland Ice Sheet and marine-based ice sheets may have strongly influenced local melting during the LGM. During major melting of the shelf-based ice sheets and icebergs derived from the Greenland Ice Sheet, large volumes of isotopically light meltwater plumes contributed to a local/regional stratification of ocean waters causing a reduction in the ventilation of surface waters, which is reflected in the extremely light $\delta^{13}C$ values from slope cores north and south of Scoresby Sund.

8.2.7 Meltwater events during the last deglaciation (Termination I)

The last glacial-interglacial transition is characterised by large short-lived climatic fluctuations (cf. Berger et al. 1987). These climatic events, referred to as Termination I (Broecker & Van Donk 1970), are indicated by the abrupt shift toward lighter values in the oxygen isotope record documented in widespread deep-sea sediments (Rudimann & McIntyre 1973; Shackleton & Opdyke 1973; Berger 1978; Duplessy et al. 1981, 1986; Zahn et al. 1985; Jones & Keigwin 1988; Koç & Jansen 1994; Stein et al. 1994a), and in the Greenland (Dansgaard et al. 1984, 1993; Dansgaard 1987; Grootes et al. 1993) and Antarctica (Lorius et al. 1979, 1985; Jouzel et al. 1987, 1993) ice cores.

According to many AMS ^{14}C ages from the GIN Sea, the onset of the last deglaciation or Termination Ia, is dated between 16 and 13 ka (cf. Jones & Keigwin 1988; Sarnthein et al. 1992; Weinelt 1993; Koç & Jansen 1994). In the Greenland Sea, the onset of the first Greenland Ice Sheet meltwater signal

is dated between 16.3 ka (^{14}C age) and 15.3 ka (interpolated age) with a midpoint of approximately 15.8 ka (Nam et al. 1995a). The timing of this signal is about 800 years earlier than that of the marine-based Barents shelf ice sheet meltwater signal recorded in the Fram Strait (cf. Jones & Keigwin 1988). In the Amundsen Basin of the central Arctic Ocean, the onset of the first major meltwater event occurred during the same interval and is dated at approximately 15.7 ka (Stein et al. 1994a). The similarity can be explained as either a contemporaneous variation within the Eurasian Arctic and Greenland ice sheets, or an increased export of low-saline waters from the Arctic Ocean via the EGC during the last deglaciation (Stein et al. 1994a-b). Koç & Jansen (1994) also documented an earlier meltwater signal from core PS1842 recovered from the deep sea north of Iceland. The location of core PS1842 is close to that of core PS1730-2. The meltwater signal is AMS ^{14}C dated at approximately 16.1 ka, and interpreted as the initial rise of northern hemisphere insolation after the last insolation minimum. However, a shift in the δ^{18}O value during the transition from the end of the LGM (about 4.5‰) to this first meltwater signal (about 4.0‰) is of less than 0.5‰, which is relatively small compared to that from core PS1730-2 (1.14‰), and the ice-volume effect of 1.3‰. Therefore, the melting signal is thought to be of a local event. Nevertheless, the onset of the first meltwater signal associated with the last deglaciation from evidence in the Greenland deep sea (Koç & Jansen 1994; Nam et al. 1995a), and the central Arctic Ocean (e.g. Stein et al. 1994a) is approximately 0.8 to 1.5 kyr earlier than the major deglaciation event within the GIN Sea (cf. Sarnthein et al. 1992) and the North Atlantic (cf. Bard et al. 1987).

In cores PS1927-2, PS1730-2, and PS1951-1 from the deep sea, the distinct oxygen isotope shifts of 1.14 to 2.24‰ exceed the 1.3‰ values calculated from the global ice-volume effect (Duplessy et al. 1984; Shackleton et al. 1984; Chappell & Shackleton 1986; Labeyrie et al. 1987). Assuming a 0.24‰/°C gradient (Shackleton 1974; Labeyrie et al. 1986), this excess of about 0.76 to 0.94‰ is likely to indicate an increase in temperature of 3.1 to 3.9°C. In general, it is accepted that the ocean surface temperature during the last glaciation maximum (LGM) was several degrees cooler than that at present (cf. Jones & Keigwin 1988). However, in high-latitude polar oceans such as the central Arctic Ocean (e.g. Stein et al. 1994a-b) and the Fram Strait (e.g. Jones & Keigwin 1988), there is no evidence for a 4-5°C increase in temperature during the last deglaciation. The present surface-water temperature of high latitude oceans is mostly near freezing point (<-1°C; Hopkins 1991; Anderson et al. 1994; Hubberten et al. in prep.), and was as low as that during the LGM. Therefore, during the last deglacial transition a temperature change of up to 3.9°C is unrealistic (cf. Stein et al., 1994a-b). In the polar oceans, where surface water is almost at freezing point, the salinity has a greater influence on the δ^{18}O values of *N. pachyderma* sin.. As a result, the δ^{18}O shift of up to 2.24‰ during the last deglaciation is more probably attributed to a significant decrease in surface-water salinity resulting from either an increased supply of freshwater to the ocean following the sequential melting of the great continental ice sheets (Fairbanks et al. 1992) such as the Greenland Ice Sheet, and/or the inflow of low-saline polar waters of the Arctic Ocean along the western margin of the Greenland Sea (Köhler 1992; Stein et al. 1994a-b). The massive discharge of icebergs and meltwater may have led to a large and widespread stratification between surface and deep waters that

strongly prohibited deep-water formation within the GIN Sea (e.g. Vogelsang 1990). Benthic foraminiferal $\delta^{13}C$ records from both North and South Atlantic sediments indicate that the production of NADW was greatly reduced throughout the last deglaciation (Jansen & Veum 1990; Charles & Fairbanks 1992; Keigwin & Lehman 1994).

According to the $\delta^{18}O$ values from the cores along the East Greenland continental slope, Termination Ia is characterised by relatively smaller shifts in the $\delta^{18}O$ records than compared to those of the deep-sea cores. The smaller shifts may be the result of the distinctly lighter $\delta^{18}O$ values during the LGM, where the values are as light or lighter than those within the Holocene (see above). The rapid shift in the $\delta^{18}O$ record of 1.85‰ from 2.75 to 0.9‰ in core PS1948-2 from the upper slope south of Scoresby Sund reflects the more extensive discharge of icebergs from the mouth of Scoresby Sund, and subsequent and significant melting close to the marine-based ice sheet margin during the deglaciation period. During Termination Ia however, the small $\delta^{18}O$ shifts measured in cores PS1725-2 and PS1726-1 from the slope adjacent to Scoresby Sund, may reflect the glacial-interglacial global ice volume signal. The distinctly heavier $\delta^{18}O$ and light $\delta^{13}C$ values suggest that there was no meltwater discharge to this site but rather more extended sea-ice conditions. Therefore, the East Greenland continental margin was probably subjected to very different oceanographic conditions than during the LGM.

On the basis of the different oxygen and carbon isotope records, the surface water conditions along the East Greenland continental margin were strongly different from site to site during the LGM. This is related to a number of forcing factors: 1) the large fjord systems, 2) a strong, local meltwater supply from the seasonally fluctuating shelf-based ice sheets, and 3) the instability of the Greenland Ice Sheet, that combines to control the local depositional environments along the East Greenland continental margin.

8.2.8 Surface oceanographic changes during the Holocene

A major input of meltwater to the western Greenland Sea, as suggested by the lighter $\delta^{18}O$ and $\delta^{13}C$ values of N. pachyderma sin. (Fig. 11), lasted until approximately 13.2 ka. The timing is contemporaneous with the "global meltwater peak" described by Fairbanks (1989). This probably reflects continued meltwater outflow from the Greenland Ice Sheet and an additional influence of meltwater plumes from the Barents Ice Sheet. Light $\delta^{13}C$ values from N. pachyderma sin. and O. umbonatus during this interval may indicate evidence for the cessation of deep water formation, and also a large reduction of North Atlantic Deep Water (NADW) production (Lehman et al. 1991; Weinelt 1993). During the interval from the end of this meltwater event to just prior to the Younger Dryas, the increased $\delta^{13}C$ values recorded in cores PS1927-2 and PS1951-1 probably reflect a change in surface-water masses characterised with seasonally fluctuating ice-free conditions. This period seems to be correlate with the onset of an inflow of Atlantic water into the Norwegian Sea (Lehman & Keigwin 1992).

There is generally little evidence for the Younger Dryas event within the GIN Sea (cf. Vogelsang 1990; Köhler 1992; Baumann et al. 1993; Jünger 1994) and Arctic Ocean (cf. Zahn et al. 1985; Gard 1993; Stein et al. 1994a-b) related to its brief occurrence and low sedimentation rates (e.g. Ruddiman & McIntyre 1981b; Keigwin & Lehman 1994), but is recorded within the ice cores of Greenland (e.g. Dansgaard et al. 1982, 1993; Grootes et al. 1993). In the GIN Sea, this event is closely associated with the Vedde ash layer (10.6 ka). In particular, during the Younger Dryas cooling event the relatively heavy $\delta^{18}O$ and remarkably light $\delta^{13}C$ records from core PS1730-2 suggest a period of expanded sea-ice covered conditions (e.g. Ruddiman & McIntyre 1981b). During this cooling interval, both slope cores adjacent to Scoresby Sund are characterised by a relatively increased influx of IRD compared to that of the late Holocene. The slightly increased IRD supply probably correlates with the Milne Land stade glacial advance in East Greenland (cf. Funder 1989). The sea-ice covered conditions probably prevented deep-water formation, and resulted in a significant reduction of NADW formation during this interval (Boyle & Keigwin 1987). In contrast and based on heavy $\delta^{13}C$ values of the benthic foraminifer *C. wuellerstorfi* from the northeast North Atlantic adjacent to Ireland (core V23-81), Jansen and Veum (1990) suggested a resumption of deep water formation and an increase in deep-water ventilation, resulting from a reduction in meltwater input during this interval. An increased marine organic carbon content indicated by high HI values (>200 mgHC/gC) suggests at least seasonally sea-ice-free conditions, causing an increase in surface-water productivity despite the cold climate conditions of this period. The Younger Dryas cooling event was characterised by large, ice-free surface-water conditions with deep-water convection in the northeast North Atlantic (Jansen & Veum 1990) and in the Norwegian Sea (Jansen & Erlenkeuser 1985; Veum et al. 1992), supported by the heavy $\delta^{18}O$ and $\delta^{13}C$ values of the benthic foraminifer *C. wuellerstorfi*, and the high foraminifer flux (Veum et al. 1992).

Termination Ib (Duplessy et al. 1981) is dated at approximately 7.9 ka within core PS1730-2. This is indicated by distinctly light $\delta^{18}O$ and relatively heavy $\delta^{13}C$ values from *N. pachyderma* sin. and *O. umbonatus*. It has been suggested that the present-day circulation patterns of surface- and deep-water masses within the Greenland Sea may have begun during this period. In particular, the modern surface circulation and the polar front system within the Greenland Sea seems to have been established between 7.4 and 6.1 ka. A distinct increase in the abundance of polar water dinoflagellate cyst species *Operculodinium centrocarpum* occurred in core PS1730-2 at approximately 7 ka (Matthiessen unpub. data), reflecting the dominant influence of cold polar waters (e.g. Harland 1983). The major shift in coccolith and dinoflagellate cyst assemblages (Baumann & Matthiessen 1992), and a maximum in the diatom abundance (Koç et al. 1993), are recorded within the GIN Sea during the same interval. This is most probably associated with the climatic optimum of late Holocene times.

In addition to a significant decrease in the terrigenous input, an increase in $\delta^{13}C$ values and organic carbon content indicates a rapid retreat of the continental ice sheets, enhanced ventilation of surface waters, and at least seasonally reduced sea-ice cover and/or more open ocean conditions,

causing increased surface water productivity (Stein et al. 1993). Therefore, the strong decrease in biogenic carbonate during this interval can be attributed to an increase in the flux of organic carbon to the sea floor, raising the pCO_2 of bottom waters during the decomposition of organic carbon, and thus contributing to carbonate dissolution at the sea floor (de Vernal et al. 1992; Steinsund & Hald 1994). In addition, low carbonate values may be ascribed to increased dilution by terrigenous material and lower production of biogenic carbonate within low-saline and cold polar waters along the continental margin (e.g. Eide 1990; Samtleben & Schröder 1992; Johannessen et al. 1994).

9. CORRELATION OF IRD EVENTS FROM THE GREENLAND SEA WITH CLIMATIC RECORDS FROM THE GRIP ICE CORE AND THE NORTH ATLANTIC HEINRICH EVENTS

9.1 Ice-rafted debris (IRD) as a climatic indicator in the high-latitude oceans

In contrast to the low and temperate latitude oceans, Quaternary sediments of the subpolar and polar oceans are strongly influenced by coarse terrigenous ice-rafted debris (IRD) (e.g. Conolly & Erwing 1965; Kent et al. 1971; Ruddiman 1977; Grobe 1986; Heinrich 1988; Bischof 1994), directly linked to the surrounding large continental ice sheets. The temporal and spatial distribution of IRD in marine sediments reflect changes in the extent, intensity, and fluctuation of the adjacent continental ice sheets (Kent et al. 1971; Ruddiman 1977; Bond et al. 1992b; Andrews et al. 1994; Baumann et al. 1995; Fronval et al. 1995). Therefore, the presence of ice-rafted debris in subpolar and polar marine sediments is a valuable climatic indicator as the fluctuations in the IRD-flux are very sensitive to climate changes around high latitude continents. In general, glacial stages are characterised by a distinct increase in coarse-grained terrigenous material indicating the enhanced discharge of icebergs related to the maximum extension of the continental ice sheets (e.g. Ruddiman 1977; Bond et al. 1992b; Andrews et al. 1993). The sediments of interglacial stages are distinguished by a distinct decrease in the flux of ice-rafted detritus relative to an increase in the biogenic flux (e.g. Heinrich 1988; Bond et al. 1992b; Broecker et al. 1992). The significant decrease in IRD-flux during interglacial periods reflects the rapid retreat of the continental ice sheets resulting in a reduction in the discharge of icebergs into the oceans.

IRD is used as an important climatic indicator for the reconstruction of the paleoclimate and paleoceanography of the GIN Sea during late Quaternary glacial-interglacial oscillations (e.g. Bischof et al. 1990; Spielhagen 1991; Stein et al. 1993; Bischof 1994; Elverhøi et al. 1995; Fronval et al. 1995; Goldschmidt 1995; Nam et al. 1995a-b). Oscillations in the IRD supply to marine sediments are closely related to the distinct climatic changes recorded in the Greenland, Scandinavia, and Barents Sea areas (e.g. Goldschmidt 1994, 1995; Hebbeln et al. 1994; Baumann et al. 1995; Elverhøi et al. 1995; Nam et al. 1995a; Stein et al. 1996). Temporal variations in the composition of IRD within high-latitude marine sediments provide important information on the changes in the loci of major continental glaciations, different source regions of coarse terrigenous sediments, different transport paths of drifting icebergs and sea ice, and in the surface circulation patterns (cf. Smythe et al. 1985; Bischof et al. 1990; Spielhagen 1991; Bischof 1994; Goldschmidt 1994, 1995). In comparison to the Norwegian Sea, the western part of the Greenland Sea is strongly dominated by icebergs and sea-ice, and the cold EGC system. Throughout the Quaternary these factors have contributed to the coarse terrigenous sediment supplied to the heavily ice-covered Greenland Sea. As a result, there is evidence for distinct cyclic increases in the IRD supply along the East Greenland continental margin and in the adjacent deep sea basin during the last two glacial-interglacial periods (Nam et al. 1995a-b; Stein et al. 1996). This is indicative of a periodic discharge of icebergs from glaciers on Greenland during the last 245 ka. In general, the extent and frequency of the IRD-peaks along the East Greenland continental margin is much higher than that recorded from the deep sea. This results from the proximity of glaciers on

117

Greenland that lead to more intensive discharge of icebergs and subsequent melting along the adjacent continental margin (Nam et al. 1995a; Stein et al. 1966). In particular, the deposition of IRD is higher on the lower slope than on the upper slope adjacent to Scoresby Sund (Fig. 39). This is probably attributed to the more intensive influence of cold polar water masses on the upper slope resulting in reduced iceberg melting and therefore, lower deposition of debris in this region.
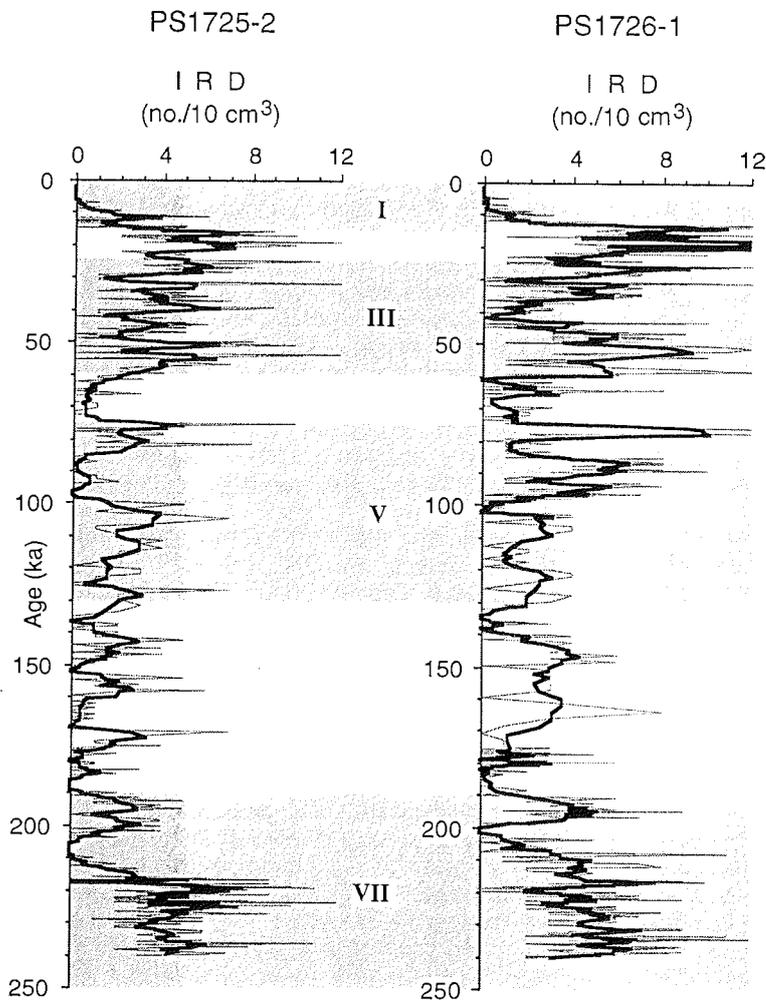

Fig. 39. Variation of ice-rafted debris (IRD, i.e. gravel fraction >2 mm, counted in X-radiographs and expressed as numbers per 10 cm³) within cores PS1725-2 and PS1726-1 recovered on the slope adjacent to Scoresby Sund. The thin-dotted-line in the background indicates the originally counted-IRD content. Amount of IRD is smoothed by the 5-point-moving-average-method (shown as heavy line).

9.2 Correlation of cyclic IRD-Events with the GRIP ice core over the last 225 ka

9.2.1 Greenland ice cores

In the last decade, several ice cores have been drilled in the Greenland and Antarctica ice sheets (Johnsen et al. 1972, 1992; Lorius et al. 1979, 1985; Dansgaard et al. 1982, 1993; Jouzel et al. 1987, 1993; GRIP Members 1993; Grootes et al. 1993). The high-resolution records of $^{18/16}O$, D/H, CO_2, dust, trace element, and methane recorded from the ice cores provide important information on the short-term variability of paleoclimates during the late Quaternary glacial-interglacial cycles (e.g. Dansgaard et al. 1982, 1984, 1985, 1993; Lorius et al. 1985; Dansgaard 1987; Johnsen et al. 1992; Chappellaz et al. 1993). The Greenland ice cores reveal more rapid and abrupt climatic fluctuations than the Antarctic ice cores (e.g. Dansgaard et al. 1982, 1993; Jouzel et al. 1987; 1993; Grootes et al. 1993). In particular, the Greenland ice cores (e.g. Camp Century, Dye 3, Renland, GRIP, and GISP 2) are characterised by a series of extremely rapid fluctuations representing warm-cold cycles during the last glacial period (Dansgaard et al. 1982, 1984, 1985, 1993; Dansgaard 1987; Johnsen et al. 1992; Oeschger 1992; Grootes et al. 1993) that are defined as "Dansgaard-Oeschger Events" (Broecker & Denton 1989). In contrast, $\delta^{18}O$ records from the Vostok ice core show fewer and less abrupt climatic fluctuations than those of the Greenland ice cores during the same intervals (e.g. Oeschger 1992), suggesting less stable climate conditions in Greenland (Bender et al. 1994). In addition, rapid fluctuations representing stadial (cold)-interstadial (mild) episodes are documented in the Greenland ice cores during both glacial-interglacial stages (Johnsen et al. 1992; Dansgaard et al. 1993; Grootes et al. 1993). The repeated abrupt climatic changes within the Greenland ice cores may reflect a complex behaviour of the North Atlantic thermohaline circulation (Bond et al. 1992b; Johnsen et al. 1992). However, similar stadial-interstadial events are also present in the Antarctic Vostok ice core, suggesting a climatic link between Greenland and Antarctica due to partial deglaciation and changes in the ocean circulation (Bender et al. 1994).

In particular, oxygen isotope records measured on the two Greenland ice cores (GRIP and GISP 2) provide new information on the dramatic climate fluctuations in the northern hemisphere over the last 200 ka. According to the records of both ice cores, the climate on Greenland was remarkably stable during the Holocene (except for the Younger Dryas cooling event), while extreme climatic variability characterised the last two glaciations and the last interglacial period (e.g. Dansgaard et al. 1993; GRIP Members 1993; Grootes et al. 1993). In general, the climatic changes recorded in both ice cores correlate well over the last 110 ka (Grootes et al. 1993). On the other hand, there is a striking discrepancy between the two records during the Eemian and into the penultimate glacial period (Grootes et al. 1993; Taylor et al. 1993b). Furthermore, the Eemian interglacial period of the GRIP ice core reveals extremely rapid, short-term (decades to centuries) climatic oscillations (GRIP Members 1993). The apparent instability may reflect an imprint of a more local climate phenomenon above Greenland (Oeschger 1992; McManus et al. 1994), and/or due to an artefact caused by ice-flow deformation (Boulton 1993; Grootes et al. 1993; Taylor et al. 1993b).

9.2.2 Correlation of the GRIP ice core and IRD events from the Greenland Sea
     between 225 and 74 ka

In general, the abrupt climatic fluctuations recorded in the GRIP ice core can
be correlated in sediments of the northern hemisphere subpolar and polar
oceans (e.g. Bond et al 1992b, 1993; Fronval et al 1995). For the Greenland
Sea, the evidence comes from the increase in IRD records within sea-floor
sediments. Nam et al. (1995a-b) and Stein et al. (1996) suggested that the
high frequency of IRD peaks from the East Greenland continental margin
appears to correlate with the cooling cycles of the GRIP ice core during the last
two glacial-interglacial cycles. The same events are well documented in the
Greenland deep sea sediments (Fig. 40). The abrupt increase in IRD content
corresponding to the light $\delta^{18}O$ values of the GRIP ice core occurred not only
during glaciations, but also during interglaciations (Figs. 39-40). It follows that
the light $\delta^{18}O$ values of precipitation generally reflect lowered temperatures
during formation (Grootes et al. 1993). This suggests that the ice-rafting cycles
in the Greenland Sea are directly coupled to the intervals of air temperature
cooling above Greenland. Significant new findings reveal that there are
marked differences in the trends of IRD-cycles in terms of the frequency and
duration of each IRD-event during the interval between 225 and 74 ka
compared to those recorded between 74 and 14.5 ka (Figs. 39-40).

During the interval between 225 and 74 ka, the periodic IRD-events are of a
lower frequency over a relatively long-term period than compared to those
observed during the last glacial period (Fig. 40). A large number of single IRD-
peaks approximating to 10-23 kyr-scale oscillations, have been identified from
the same interval within the slope cores recovered adjacent to Scoresby Sund
(Fig. 39; Nam et al. 1995a). The frequency and duration of these cyclic long-
term IRD-events generally decrease towards the deep sea (e.g. core PS1730-
2). This suggests that most of the icebergs discharged from eastern Greenland
may have, to a large extent, melted along the continental slope close to the
position of the polar front, resulting in a reduction of the IRD deposited on the
deep sea floor. On the other hand, the duration of the IRD events of 5 to 10 kyr
on the continental slope may reflect a more significant local signal that
originates from the repeated advance of East Greenland glaciers. The distinct
IRD-events were usually followed by a period of abruptly decreased IRD
supply reflecting a strong reduction in the iceberg discharge that probably
results from a further landward retreat of continental glaciers during this
interval. A similar pattern was found to occur in the GRIP ice core during the
same interval.

During glacial stage 6, there are three to five distinct IRD-events that
correspond to the cooling periods recorded in the GRIP ice core (Fig. 40).
Similar ice-rafting events have been recorded in the North Atlantic during
glacial stage 6 (Bond 1995a). This implies that during the penultimate glacial
period the northern North Atlantic region may have been subjected to several
abrupt climatic changes but with much slower-paced pulses than during the
last glaciation. The other three to four periodic IRD-events appear to be coeval
with the cooling phases in the GRIP ice core during the last interglacial period
reflecting the instability of the ice sheet along the eastern Greenland margin.
At the onset of the Eemian, a marked increase in the IRD supply to the
Greenland Sea may have been the result of the decay in East Greenland
glaciers.

120

GRIP ICE CORE   PS1730-2

$\delta^{18}O$ (‰ SMOW)   I R D (no./10 cm^3)   Isotope
                                                        stage
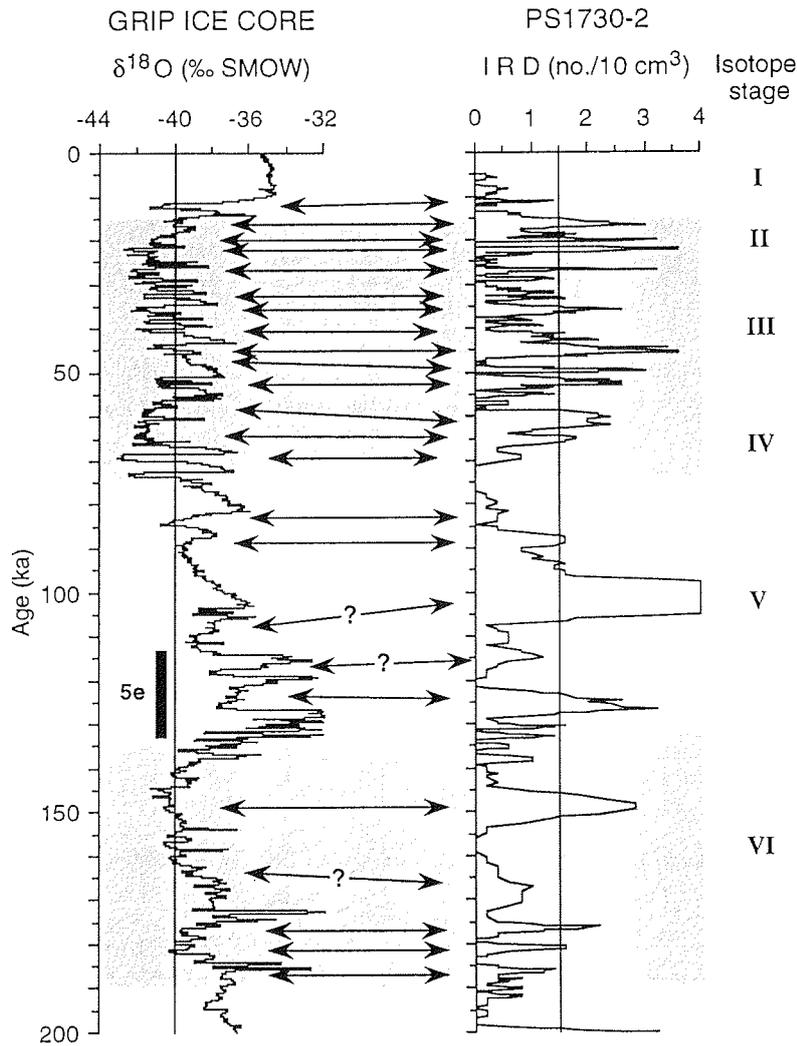

Fig. 40. Comparison of the oxygen isotope records of the GRIP ice core (Dansgaard et al. 1993) and IRD records from the Greenland deep sea (core PS1730-2) during the last two glacial-interglacial cycles. A tentative correlation between IRD peaks and cold intervals of the GRIP record has been made (arrows). 5e is the Eemian interglaciation.

The very rapid warm-cold climatic fluctuations of the Eemian measured from the GRIP ice core (GRIP Members 1993) seem to correlate with the decrease-increase in the IRD flux in the deep-sea core PS1730-2 (Fig. 40). Based on the abrupt decrease in sea surface temperatures (SST) and sea surface salinity (SSS) from the Norwegian Sea, Cortijo et al. (1994) suggested that there was a more moderate cooling and freshening of the North Atlantic during the middle of the Eemian. A similar abrupt fluctuation in temperatures is

121

reflected within pollen records from lakes of NW Europe (e.g. France and NW Germany) during the Eemian interval (Field et al. 1994; Thouveny et al. 1994), supporting the rapid Eemian climate instabilities observed in the North Atlantic region. Furthermore, if the correlation between very rapid warm-cold oscillations and decreased-increased IRD-cycles is accurate, then the abrupt and frequent climatic changes of the Eemian may be explained by several theories: 1) a decrease in the thermohaline circulation resulting from the massive input of icebergs and meltwater flux (Broecker et al. 1990; Bond et al. 1993), 2) an enhanced variability in the hydrological cycle associated with the warmer climate of the Eemian (Weaver & Hughes 1994), 3) an increase in the inflow of less saline North Pacific surface waters through the Bering Strait (Shaffer & Bendtsen 1994), or 4) changes in the balance of precipitation and evaporation over the high-latitude North Atlantic (Cortijo et al. 1994; Keigwin et al. 1994).
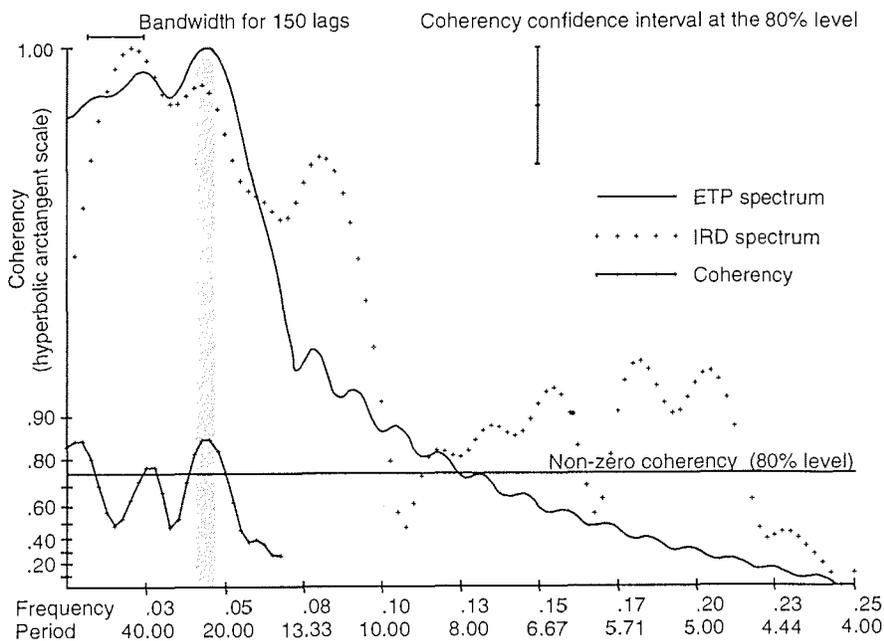
Fig. 41. Cross spectral analysis comparing IRD records of deep-sea core PS1730-2 with the summed variance of Earth's eccentricity, till, and precession (ETP ΔT= 0.5) signal (Imbrie et al. 1984). Solid line with thin crosses represent confidence interval at the 80 % level. The 80 % test statistic for non-zero coherency is indicated by a horizontal straight line. Frequencies are in cycles per thousand years. Result shows that coherence to ETP is demonstrated for the 23-kyr frequency band in IRD records during the time interval 225-60 ka.

During the past 250 ka, a power spectrum of 60°N summer insolation shows a stronger signal associated with the 23 kyr precessional cycle than for the 41 kyr obliquity cycle (Hays et al. 1976). Generally, at latitudes north of 65°N, summer insolation at the top of the atmosphere is dominated by the 23 kyr

precessional cycle (Ruddiman & McIntyre 1981a). The isotope records_of the GRIP ice core reveal a strong obliquity cycle and a considerably weak precession signal (24/18 kyr) (Dansgaard et al. 1993). Cross spectral analysis of core PS1730-2 may suggest that the 23 kyr precessional periodicity, particularly between 225 and 60 ka, is significant for controlling the huge iceberg surges and therefore, the increased IRD-flux into the Greenland deep sea (Fig. 41). In contrast, the 23 kyr precession is insignificant during the last 60 ka, as a result of reduced power. The dominant 23 kyr frequency in the IRD-flux must be coherent with orbital changes in northern hemisphere insolation. Periods of increased IRD supply correlate well with high summer insolation at 70°N (Fig. 42). The mass balance of the ice sheets is very sensitive to summer heating at high latitudes in the northern hemisphere. Thus, ice decay may be favoured by high summer insolation (promoting enhanced ice ablation) controlling the ice volume (Ruddiman & McIntyre 1981a). This suggests that most of the Greenland Ice Sheet may have experienced a predominantly 23 kyr cycle of growth and decay. Therefore, the cyclic IRD-events recorded between 225 and 60 ka can be interpreted as resulting from large 23 kyr scale oscillations in the volume of the adjacent Greenland Ice Sheet. The Scandinavian Ice Sheet is also located in a region of a dominant 23 kyr insolation change, and in turn most probably influencing the Norwegian Sea and northeast Atlantic (Ruddiman & McIntyre 1981a). During periods when air temperatures dropped across a critical threshold, the ice sheets started to shrink and calve icebergs. Iceberg calving may have been largest when the ice sheets attained their maximum extent (Oerlemans 1993). Additionally, the higher solar radiation incident on the surface initiated rapid decay of the continental glaciers (Ruddiman & McIntyre 1981a; Heinrich 1988), contributing to the increase in discharge of meltwater and icebergs into the GIN Sea during the early phase of ice-sheet collapse (cf. Bond et al. 1993).

9.2.3 Correlation of "IRD Events" in the Greenland Sea with "Dansgaard-Oeschger Cycles" in the GRIP ice core

$\delta^{18}O$ records from the Greenland ice cores (e.g. Dansgaard et al. 1982, 1993; Oeschger 1992; Grootes et al. 1993) reveal repeated millennial-scale climate oscillations (Dansgaard-Oeschger Cycles) during the last glaciation. In particular, a package of several D-O cycles seems to be bundled into longer cycles of gradual cooling over millennia (Bond et al. 1993). Each of these cycles, called "Bond Cycles" (Lehman 1993; Broecker 1994), culminates in evidence for brief but massive discharge of icebergs into the North Atlantic (Bond et al. 1993). This evidence is reflected in short-term IRD-cycles in the marine sediments adjacent to East Greenland. A large number of IRD-cycles is best documented in the Greenland deep-sea core PS1730-2, yielding an average frequency of 1 to 3 kyr similar to the time scales recorded in the GRIP ice core (Dansgaard et al. 1993), and in the North Atlantic (e.g. Bond & Lotti 1995). Approximately eleven major IRD-events occurred during this period (Fig. 43), indicating the repeated massive discharge of icebergs calved by glaciers, that result from the instability of the Greenland Ice Sheet. In addition to the major IRD-events, several smaller IRD-cycles occurred between the major IRD-events. In particular, the smaller IRD-cycles are bundled into major IRD-events with asymmetric shapes and sharp boundaries (cf. Bond et al. 1993), which closely correlate to the Bond cycles in the GRIP ice core and in the North Atlantic (Bond et al. 1993).
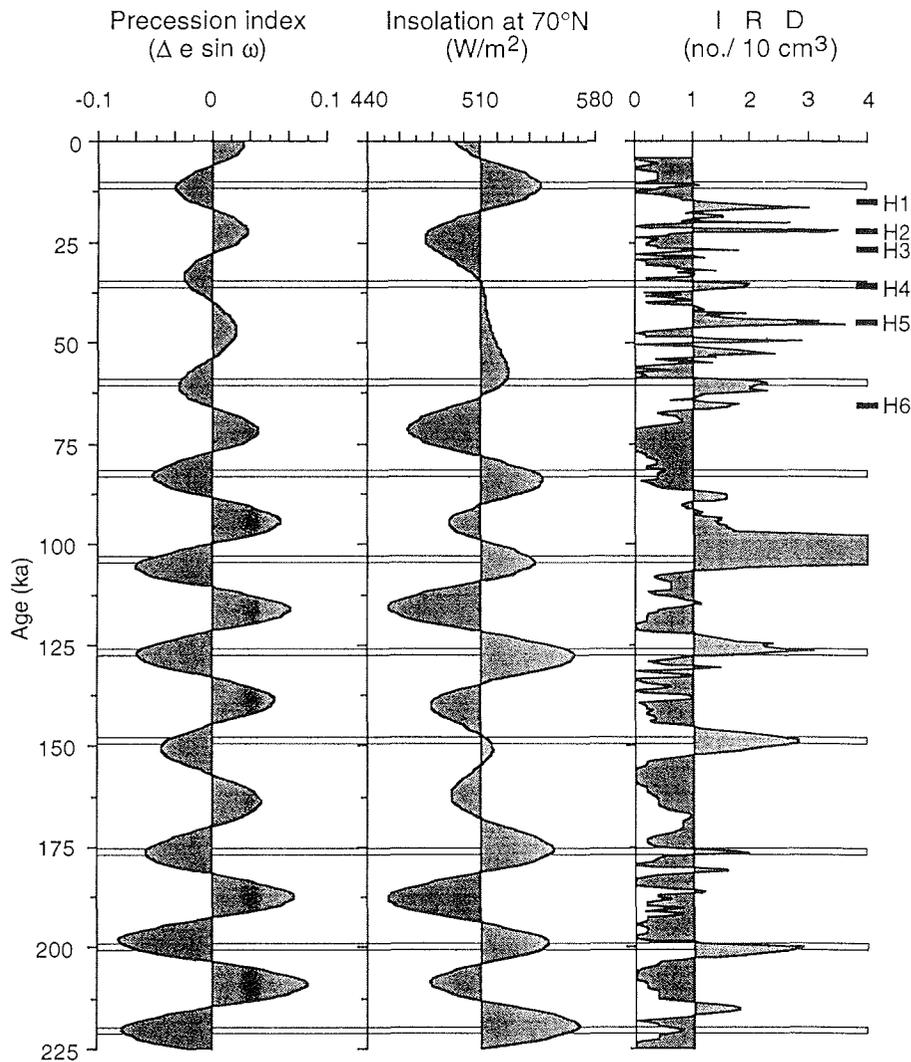
Fig. 42. Comparison of the precession index and northern hemispheric summer half-year insolation at 70°N (Berger 1978) with IRD records from the Greenland deep sea. Results shows a link between the IRD records and precessional (23 kyr) insolation variations between 225 and 60 ka. H6-H1 indicates a temporal correlation with Heinrich Events in the North Atlantic (Bond et al. 1992b, 1993).

There is a good correlation between major IRD-events and GRIP $\delta^{18}O$-cycles over the last 70 ka (Fig. 43). During stage 3, five major IRD-events (H´5c-H´5b-H´5-H´4-H´3) are documented in core PS1730-2, that correlate with the most intense cooling periods of the D-O cycles (i.e. Bond cycles from BC6 to BC2) in the GRIP records. Similarly, the cooling periods over Greenland seem to

correlate with the cold climate records observed in the North Atlantic (Bond et al. 1993), on the Vøring Plateau (Fronval et al. 1995), and in France (Thouveny et al. 1995), although there is a discrepancy concerning the correlation between the GRIP records and paleoclimatic events monitored from the different regions. This discrepancy might have arisen from the different time scales established for each age model (cf. Bond et al. 1993; Dansgaard et al. 1993; Fronval et al. 1995; Thouveny et al. 1995). Nevertheless, it is suggested that the repeated fluctuations of the Greenland Ice Sheet would be more directly reflected in the adjacent Greenland Sea than in the other regions. This is strongly supported by the relatively short-term, ice-rafting cycles of the Greenland Sea that coincide with the millennial-scale cooling periods of the GRIP records. In addition, another four IRD-events during the LGM, and one during the Younger Dryas correspond to the cooling episodes recorded in the GRIP ice core. This correlation indicates a close relationship between the changes in hemispheric temperatures on Greenland and the discharge of icebergs into the Greenland Sea.

During stage 3, significantly light $\delta^{18}O$ values correlate with relatively light $\delta^{13}C$ values reflecting an increase in the meltwater discharge. Furthermore, the dramatic decrease in the IRD-flux corresponds to these intervals of increased meltwater input and reflect the repeated retreat of East Greenland glaciers. In contrast, the cooling periods, as suggested by the heavy $\delta^{18}O$ records of *N. pachyderma* sin., correlate well with the significant increase in the IRD content. The IRD-events are coeval with the cold phases (i.e. Bond cycles) of the D-O cycles recorded in the GRIP ice core during the last 60 ka (Fig. 43), indicating that large volumes of icebergs were discharged during the maximum extension of the glaciers on Greenland. Furthermore, the major IRD events that include several events contemporaneous with North Atlantic Heinrich Events, correlate well with the heavier $\delta^{18}O$ records of *N. pachyderma* sin. (Fig. 43) implying an increase in the discharge of icebergs during the cooling phases of the Greenland Sea. Subsequently, large volumes of icebergs may have contributed to the cooling of the surface water of the ocean by extracting energy both for the latent heat of melting and for that required for warming (Ruddiman & McIntyre 1981a). As a result, the IRD-events that correspond to the cooling intervals of the Greenland Sea and to the cooling phases of the D-O cycles on Greenland, may indicate a close linkage between ice sheet behaviour and ocean-atmosphere temperature changes around Greenland. The synchronous events are also imprinted in the North Atlantic (e.g. Bond et al. 1993; Bond & Lotti 1995) and Norwegian sea regions (e.g. Fronval et al. 1995), reflecting the coherent fluctuation in the large continental ice sheets due to the oceanic-hemispheric heat transport in the northern hemisphere (Bond et al. 1993; Lehman 1993).

125

9.3 Correlation of Heinrich Events with Heinrich-type IRD-Events

9.3.1 North Atlantic Heinrich Event

A series of distinct layers rich in terrigenous ice-rafted detritus were recorded in northern North Atlantic deep-sea sediments (Heinrich 1988). These layers are characterised by an increase in terrigenous coarse ice-rafted debris (IRD), a low abundance of foraminifers, and a prominent presence of detrital limestone and dolomite (about 20-25 %) (Heinrich 1988; Andrews & Tedesco 1992; Bond et al. 1992b; Broecker et al. 1992; Andrews et al. 1993). The lower abundance of planktonic foraminifers probably resulted from either a distinct decrease in the surface-water productivity or from the dilution from the significantly increased supply of terrigenous coarse IRD (Broecker et al. 1992). However, within these distinct layers *N. pachyderma* sin. is the dominant planktonic foraminiferal species (e.g. Heinrich 1998; Bond et al. 1992b; Broecker et al. 1992), indicating an increase in the penetration of polar water into the northeast Atlantic around 50°N (Bond et al. 1992b; Maslin et al. 1992). This reflects a decrease in both sea-surface temperature and salinity during this interval (e.g. Bond et al. 1992b; Broecker et al. 1992; Rahman 1995). The layers, were deposited with a frequency of approximately every 7 to 10 kyr during the last glacial period across the northern North Atlantic (40 to 65°N), and are defined as "Heinrich Layers" or "Heinrich Events" (Andrews & Tedesco 1992; Bond et al. 1992b; Broecker et al. 1992; Andrews et al. 1993, 1994; Grousset et al. 1993; Bond & Lotti 1995; Dowdeswell et al. 1995). The North Atlantic Heinrich Events occurred at approximately 67-66 (H6), 52-50 (H5), 37-35.5 (H4), 27 (H3), 21-22 (H2) and 14.5 (H1) ka (Broecker et al. 1992; Bond et al. 1992b, 1993; Grousset et al. 1993; Manighetti et al. 1995).

The Heinrich Layers are characterised by the high concentration of detrital carbonate (H5, H4, H2, H1) in the southwest margin of the northern North Atlantic (e.g. Bond et al. 1992b; Andrews et al. 1994). There is a distinct eastward decrease in the carbonate content within the Heinrich Layers, indicating that the carbonate-bearing icebergs originated in the Hudson Strait and adjacent shelf regions (Andrews & Tedesco 1992; Bond et al. 1992b; Broecker et al. 1992; Andrews et al. 1993). The absence of the carbonate-rich layers south of the IRD belt (Ruddiman 1977) suggests that rapid melting of icebergs occurred before they reached the warmer water south of the glacial polar front (Ruddiman 1977; Bond et al. 1992b). Further to the north and east of the IRD belt, H3 and H6 contain no detrital carbonate, which suggests a different source for the detrital material brought to this region by icebergs (Broecker et al. 1992; Grousset et al. 1993; Gwiazda et al. 1995). Grousset et al. (1992, 1993) suggested that H6 and H3 may have originated from the Eastern Greenland or Scandinavian ice sheets. This is further supported by the Nd-Sr isotope records (Grousset et al. 1992). In contrast, Bond and Lotti (1995) demonstrated that there is a narrow layer of detrital carbonate grains during Heinrich Event 3, and suggested that icebergs originated partly from the Labrador Sea during this interval. In general, it is known that the Heinrich Layers were caused by several periods of massive iceberg discharge from the Laurentide Ice Sheet that covered North America during the last glacial period (Bond et al. 1992b; Andrews et al. 1993, 1994; Dowdeswell et al. 1995). Compared to North Atlantic Heinrich layers, the XRD determined carbonate mineral contents from Greenland marine sediments are generally very low (Evans unpubl. data).
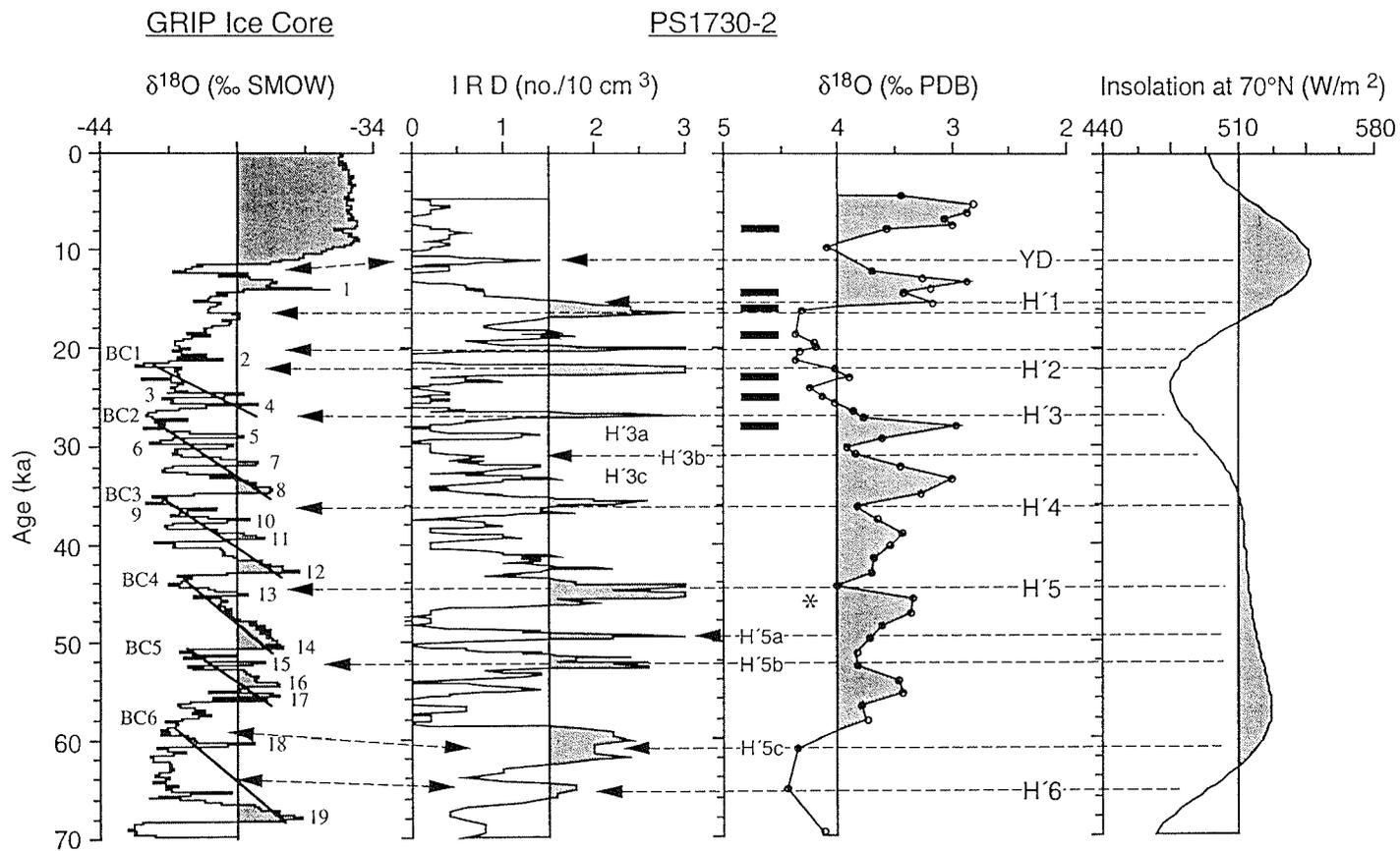
Fig. 43. Correlation of the $\delta^{18}O$ records from the GRIP ice core with the major IRD-events and $\delta^{18}O$ records from the Greenland Sea. Arrows indicate correlation between parameters. Numbers in the GRIP ice core are interstadial numbers (Dansgaard et al. 1993). Black bars in the oxygen records mark AMS ^{14}C datings measured from the planktonic foraminifer *N. pachyderma* sin. (*see* Fig. 11). Note that asterisk is the position of a volcanic ash layer recorded in the deep-sea core PS1951-1. IRD events H´6-H´1 coincide with Heinrich Events H6-H1 in the North Atlantic (e.g. Bond et al. 1992b, 1993). BC1-6 indicate Bond cycles (Lehman 1993; Broecker 1994). Insolation at 70°N is also illustrated after Berger (1978).

9.3.2 Correlation between IRD-events and North Atlantic Heinrich events and the implications for paleoceanography and paleoclimate

Distinct IRD-events in the Greenland Sea display the same frequency and high-amplitude pattern as several of the North Atlantic IRD-cycles (e.g. Bond et al. 1993; Bond & Lotti 1995). Among them, six (Heinrich-type) IRD-events correspond to the North Atlantic Heinrich Events H6 to H1 (Fig. 43). In addition, there are several small layers of enhanced IRD between the Heinrich-type events (H´). These layers also seem to be synchronous with small ice-rafting cycles that occur between the Heinrich Events in the North Atlantic during the last 40 ka (cf. Bond & Lotti 1995). This would imply that coherent fluctuations on the millennial time scale took place between the Greenland and Laurentide ice sheets during the last glaciation. As previously discussed, the North Atlantic Heinrich events and Heinrich-type IRD-events correlate to the periods of ocean and atmosphere cooling around Greenland. These IRD-events are coincident with the Dansgaard-Oeschger cooling cycles over Greenland, and are probably the response to the same climate forcing that caused the above mentioned cooling cycles (Bond & Lotti 1995). In the Greenland Sea, the duration of Heinrich-type events ranges between 0.5 and 2 kyr, which is relatively longer than compared to the record in the North Atlantic (cf. Bond et al. 1993; Dowdeswell et al. 1995). This duration is very similar to the cold events recorded in the Greenland ice cores (Johnsen et al. 1992; Dansgaard et al. 1993; Grootes et al. 1993), and suggests that IRD-events in the Greenland Sea are closely related to the fluctuations in the Greenland Ice Sheet.

The origin of H6 is suggested to be from the eastern Greenland or Scandinavia ice sheets (Grousset et al. 1992). However, Goldschmidt (1994) threw doubt on the Fennoscandian or Arctic origin for H6 because of a low IRD supply into the central Greenland and Norwegian seas. Along the western margin of the Greenland Sea, high amounts of IRD (H´6) indicate that large volumes of icebergs were discharged from glaciers draining the eastern margin of the Greenland Ice Sheet during this interval. During this period a major hiatus exists in the terrestrial records of East Greenland, and probably relates to extensive glacial erosion (Funder et al. 1994). In addition, the existence of extended glaciers on Greenland is further suggested by lighter $\delta^{18}O$ values recorded from the GRIP ice core. During the same period, heavier $\delta^{18}O$ values of N. pachyderma sin. indicate that ocean waters of the Greenland Sea were probably colder than those of the LGM (Fig. 43). Within this interval, there is evidence of a relatively low IRD-flux onto the upper slope reflecting a major decrease in the melting of icebergs due to colder conditions in the western Greenland Sea (Nam et al. 1995a). Under increasingly cooling oceanic conditions, icebergs discharged from the eastern margin of the Greenland Ice Sheet would have survived much longer and drifted much further southward. A number of icebergs may have reached the central and eastern regions of the North Atlantic due to the anticlockwise polar gyre common in glacial periods (e.g. Robinson et al. 1995), where they encountered warmer waters and subsequently melted contributing to the deposition of H6. However, a detailed mineralogical and/or petrographic investigation of the IRD is necessary in order to better identify the origin of H6. Following H´6, a high amplitude IRD-flux (H´5c) occurred between 63 and 58 ka, which probably correlates to the maximum glaciation in Scandinavia (e.g. Baumann et al. 1995). The high IRD-flux (H´5c) reflects the collapse of

extended ice sheets as the summer insolation initially increased (Fig.-43). A dramatic reduction in the IRD-flux occurred when summer insolation reached its maximum between 58 and 54 ka, which corresponds to the early stage 3 meltwater event within the GIN Sea.

In North Atlantic deep-sea sediments, a specific ash layer is recorded between H6 and H5 (e.g. Heinrich 1988), which is used as a proxy for stratigraphic correlation with H5 (e.g. Bond et al. 1992b, 1993; Broecker et al. 1992; Fronval et al. 1995; Robinson et al. 1995). The ash-layer event occurred between 65 and 59 ka (Ruddiman & Glover 1972; Heinrich 1988; Broecker et al. 1992; Bond et al. 1993). Similarly, a distinct ash zone was present on the northwest Iceland Plateau (core PS1951-1) during early stage 3. The age of this ash is dated by linear interpolation at approximately 48-49 ka (Fig. 43), and appears to be correlative to sediments from the GIN Sea (Lackschewitz 1991; Fronval et al. 1995) and the Denmark Strait (Kellogg et al. 1978).

Despite the large age discrepancy of up to 10 ka, it is suggested that both ash layers may be identical. Presumably the large age difference between both ash layers could be attributed to an inaccuracy in the stratigraphy resulting from the estimated date of the ash layer. According to $\delta^{18}O$ records of planktonic foraminifers *G. bulloides* and *N. pachyderma* sin. in core Me69-17 (*see* Heinrich 1988; Broecker et al. 1992) and DSDP Site 609 (*see* Bond et al. 1993), the ash layer in the North Atlantic is identified within the interval following substage 3.3 (defined by Martinson et al. (1987)). This means that the age of the North Atlantic ash was most likely overestimated, i.e. too old (cf. Heinrich 1988; Broecker et al. 1992; Bond et al. 1993). Therefore, the timing of the North Atlantic ash is thought to be approximately <50 ka, which is similar to that determined from the GIN Sea. It is suggested that the age of the North Atlantic H5 may be younger than 50 ka (cf. Bond 1995b). Subsequently, and owing to the correlation between both ash layers, H′5 appears to be coeval to the North Atlantic H5. Similarly, Fronval et al. (1995) also correlated a distinct IRD-peak (44-43 ka) from the Vøring Plateau with H5 (~50 ka) based on the occurrence of an ash layer. In addition, two distinct IRD-peaks (H′5b-H′5a) between H′5c and H′4 may correlate to the glaciations of Scandinavia (e.g. Baumann et al. 1995) and NW Europe (e.g. Thouveny et al. 1994) as well as with the cooling periods over Greenland.

Heinrich layer H4 is coincident with H′4 at approximately 36-34 ka. In addition, the three small IRD-peaks (H′3c-H′3b-H′3a) are probably related to those between H4 and H3 (Bond & Lotti 1995) as well as the cold period *Pinus* events of Florida, USA (Grimm et al. 1993), reflecting synchronous climate change in the northern hemisphere during the last 40 ka. The abrupt climate oscillations are also substantiated by the transition toward high dust and sea salt concentrations in the GISP2 ice core during glacial stadials (Mayewski et al. 1994), that indicate rapid change in atmospheric circulation and sea-ice cover during the same interval (Mayewski et al. 1993; Taylor et al. 1993b). In the Greenland Sea, the three youngest Heinrich-type events are AMS ^{14}C dated at approximately 28 to 26.5 (H′3), 22 to 20 (H′2), and 15 to 14 (H′1) ka, which correspond to the Heinrich events H3 to H1 respectively.

During the interval 17 to 15.3 ka, i.e. the transition from the LGM to the onset of Termination Ia, a high amount of icebergs with the associated IRD were discharged into the Greenland Sea as the summer insolation initially rose.

Following this interval, a large volume of meltwater were discharged between 15.3 and 13.2 ka (Termination Ia), which correlates to North Atlantic H1. This timing indicates the last rapid retreat of the Greenland Ice Sheet synchronous with the Fennoscandian, Barents, and Laurentide ice sheets (Jones & Keigwin 1988; Lehman & Keigwin 1992; Stein et al. 1994a-b; Nam et al. 1995a). The Younger Dryas cooling event (~10.6 ka) also displays a slightly increased IRD-flux which correlates to that recorded in the GRIP ice core, and the H0 Event in the North Atlantic (e.g. Bond et al. 1993).

A high number of IRD-events analogous to Heinrich Events are recorded in the Norwegian Sea and reflect the repeated advance of the Fennoscandian Ice Sheet (Baumann et al. 1995; Fronval et al. 1995). In addition, the temporal correlation between the Heinrich-type events in the Greenland Sea with North Atlantic Heinrich Events suggests that the collapse of the Laurentide and Greenland ice sheets occurred on the same time scale. The apparent evidence of millennial-scale IRD-events in the North Atlantic (e.g. Bond et al. 1993; Bond & Lotti 1995), Norwegian Sea (e.g. Fronval et al. 1995), and Greenland Sea indicates the coherent fluctuation of the large northern hemisphere ice sheets (Laurentide/Greenland and Fennoscandian/Barents ice sheets) probably caused by the change in the ocean-atmosphere thermohaline circulation (Broecker et al. 1990; Bond et al. 1993). Furthermore, the abrupt climate changes during the last glaciation are synchronously recorded not only in the northern hemisphere (e.g. Grimm et al. 1993; Thouveny et al. 1994; Clark & Bartlein 1995; Porter & Zhisheng 1995; Thunell & Mortyn 1995), but also in the southern hemisphere (e.g. Lowell et al. 1995). Accordingly, the glacial climate variability seems not to be a regional record restricted to the North Atlantic region (cf. Dansgaard et al. 1993), but rather to a global or hemispheric phenomenon (e.g. Clark & Bartlein 1995; Lowell et al. 1995; Porter & Zhisheng 1995; Rahman 1995). Therefore, Kennett and Ingram (1995) and Behl and Kennett (1996) hypothesised that the inter-ocean paleoceanographic changes were linked directly through global climate change transmitted through the atmosphere.

In general, the cause of high-frequency ice-rafting events is still under discussion. It remains to be answered whether the cyclic discharge of icebergs on a millennial-scale were triggered by external climate forcing or internal ice sheet dynamics. Heinrich (1988) suggested that cyclic IRD-events were probably triggered by an enhanced surging of the ice sheet responding to changes in insolation. However, as shown in Figure 43, there appears to be no apparent match between major IRD-events and insolation changes (e.g. Bond et al. 1992b; Maslin et al. 1995), indicating that insolation alone does not control climate instability. In fact, IRD-cycles on time-scales of a few millennial recorded in the Greenland Sea and the North Atlantic (Bond & Lotti 1995) are much too frequent to yield any direct relationship to Milankovitch orbital forcing. However, H'1 and H'6 coincide with large scale deglaciation in which the summer insolation initially rose, which implies that the initial melting phase might be partly trigged by climate or a climate-driven mechanism (Bond & Lotti 1995; Maslin 1995). In contrast, MacAyeal (1993) suggested that Heinrich Events may have resulted from internal ice sheet dynamics (binge/purge model), inducing a periodic and abrupt surge of icebergs into the ocean.

It is generally thought that during an ice age the existence of extensive continental ice sheets may have wielded an important influence upon climatic

oscillations. Therefore, the elevation of the huge continental ice sheets may have played a critical role in the large-scale features within the atmospheric circulation (Manabe & Broccoli 1985). The high elevation of the Laurentide Ice Sheet is probably responsible for extensive northerly winds over the western part of the North Atlantic exerting a strong influence on the cooling of surface waters during glacial periods (Manabe & Broccoli 1985). Therefore, the cooling associated with a northerly wind anomaly may reduce sea-surface evaporation by either the thermodynamic effect or by the maintenance of the sea-ice cover (MacAyeal 1993). During periods when the northern hemispheric ice sheets collapsed, large volumes of icebergs were discharged into the North Atlantic and may have resulted in stronger salinity stratification causing the turn-off or reduction of NADW production (Broecker et al. 1990). Accordingly, a large input of icebergs and meltwater into the GIN Sea derived from the adjacent continental ice sheets may have led to the cessation of deep-water formation, which subsequently contributed to the reduction of NADW. Reduced NADW formation led to substantial changes in the global pattern of oceanic thermohaline circulation in the world's ocean (Broecker & Denton 1989). During glacial periods, on the other hand, following the collapse of the ice sheets and the subsequent retreat of the ice margin, the flux of icebergs into the ocean was significantly reduced, resulting in increased surface salinity which in turn strongly influenced the thermohaline circulation of the North Atlantic (e.g. Bond et al. 1993). The melting of the continental glaciers in the northern hemisphere also induced a complete reorganisation of global atmospheric circulation. The abrupt climatic changes documented in $\delta^{18}O$ records in the GRIP ice core and IRD-cycles from the Greenland Sea may have been the result of a turn-on and -off effect of the North Atlantic conveyor circulation during that interval (e.g. Broecker et al. 1990).

10. CONCLUSIONS

Stable oxygen and carbon isotope records and sedimentological and geochemical investigations of glaciomarine sediments recovered from the East Greenland continental margin provide important information about sedimentary processes and environments, and the changes in the paleoclimate and paleoceanography of the western part of the Greenland Sea during late Quaternary glacial-interglacial cycles. In particular, the glaciomarine sediments recovered from three W-E transects running from the heavily ice-covered shelf to the deep sea provide an opportunity of understanding the East Greenland glacial history associated with fluctuations in the stability of the Greenland Ice Sheet during glacial-interglacial cycles.

The results obtained from the glaciomarine sediments investigated along the East Greenland continental margin and adjacent deep sea can be summarised as follows:

- Sediment composition and glacial history along the western margin of the Greenland Sea

1) The glaciomarine sediments recovered along the East Greenland continental margin are generally characterised by a high amount of terrigenous components and a low amount of biogenic carbonate throughout the last 245 ka. The carbonate content of <10 % reflects low surface water productivity resulting from the persistent and strong influence of cold and low-saline polar waters of the EGC and an extensive sea-ice cover.

2) The dominant occurrence of *N. pachyderma* sin. (>95 %) throughout the sediment sequences of glacial and interglacial periods reflects very low SST and a permanent winter sea-ice cover along the East Greenland continental margin. It is also suggested that there has been little incursion of North Atlantic water into the western margin of the Greenland Sea throughout the last 245 ka. Hence, an input of Atlantic water during the Eemian may not have propagated fully into the western part of the Greenland Sea in order to change the surface water oceanography, but instead contributed to the reduced sea-ice cover.

3) The predominance of terrigenous ice-rafted debris (IRD) within glaciomarine sediments reflects the almost permanent presence of large volumes of debris-laden icebergs mostly discharged from East Greenland glaciers. A higher supply of coarse terrigenous matter may also have caused lower carbonate content of sediments due to the increased dilution.

4) A high number of major IRD pulses along the western margin of the Greenland Sea indicate fluctuations of the glaciers of the eastern margin of the Greenland Ice Sheet during the last two glacial-interglacial cycles. Major pulses of IRD occur close to the oxygen isotope stage boundaries reflecting the repeated advance and/or collapse of East Greenland glaciers. Similar pulses also occur at certain intervals within glacial and interglacial periods, implying that glaciers advanced and retreated along the East Greenland continental margin during glacial as well as interglacial stages.

5) Compared to glacial stage 2, a lower flux of IRD during glacial stages 6 and 4 is ascribed to an expanded sea-ice cover preventing the drift of icebergs across the Greenland Sea. In contrast, there are periods of increased carbonate content coinciding with a high number of planktonic foraminifers during the Saalian (stage 6) glaciation and the LGM. The surface-water productivity indicates that during the last two glacial periods the western region of the Greenland Sea has not been covered by year-round sea-ice, but has been at least seasonally ice-free along the fluctuating ice margin induced by summer melting. During the same interval, a large volume of icebergs were discharged into the Greenland Sea. These not only caused an increased IRD supply to the sea floor, but also contributed to the surface-water productivity through an increased influx of nutrients from iceberg melting in summer months.

6) In general, the major IRD peaks recorded in glaciomarine sediments can be correlated with the East Greenland glacial history derived from terrestrial records. The interval of ca. 50 ka between the Mønselv interstade and the Flakkerhuk stade, however, is indicated as a hiatus on eastern Greenlan, whereas at least five repeated advance and retreat of glaciers beyond the coastline are proposed during 65-61, 59-51, 48-42, 35-31, and 28-25 ka. Furthermore, the repeated advance and retreat of the Greenland Ice Sheet seems to be comparable with that of the Scandinavian and the Barents Sea Shelf ice sheets over the last 200 ka.

7) According to the massive IRD supply, the distinct increase in the accumulation rate of terrigenous material and the massive diamictons deposited on the slope areas north and south of Scoresby Sund, the maximum seaward extent of the grounding line of the ice sheet may have been at the continental shelf break during the LGM (about 21-16 ka). This time span coincides in its age and duration with the culmination of the "Flakkerhuk stade" described in the Jameson Land/Scoresby Sund area.

- Paleoceanography of the western margin of the Greenland Sea

1) $\delta^{18}O$ records of *N. pachyderma* sin. from the western part of the Greenland Sea reflect a similar pattern as the global isotope record, with some excursions towards lighter values representing local and/or regional meltwater events. These resulted from the retreat of East Greenland glaciers coupled with the import of isotopically light polar waters of the EGC transported from the Arctic Ocean into the Greenland Sea. Distinct meltwater events are recorded at the stage boundaries from glacial to interglacial stages (i.e. 6/5, 4/3, and 2/1) reflecting the collapse and retreat of the Greenland Ice Sheet. However, the $\delta^{18}O$ values from the western part of the Greenland Sea are generally heavier than compared to those from the Norwegian Sea indicating prevailing cold conditions in the surface water along the East Greenland continental margin due to a strong influence of the cold and low-saline Arctic polar waters.

2) According to distinct shifts towards heavy $\delta^{18}O$ and light $\delta^{13}C$ values during the transition from interglacial to glacial stages (7/6, 5/4, and 3/2), the Greenland Sea has been subjected to the abrupt and rapid changes in the

extension of the sea-ice cover. The surface water environment strongly restricted the biological productivity, and prevented the exchange of CO_2 with the atmosphere and the ventilation of surface waters resulting in a lower flux of carbonate and the subsequent dissolution of biogenic carbonate.

3) The onset of the first meltwater signal during the last deglaciation is dated at 15.8 ka, i.e. similar to that recorded from the Fram Strait and the Amundsen Basin of the central Arctic Ocean. Thus, the onset of the first meltwater signal associated with the last deglaciation based on evidence from the Greenland Sea and the central Arctic Ocean is approximately 0.8 to 1.5 kyr earlier than the major deglacial event within the GIN Sea and the North Atlantic. In particular, the shifts of $\delta^{18}O$ values during Termination Ia are up to 2.24‰ which exceed the global ice-volume effect (ca. 1.3‰). The difference (up to 0.94‰) is thought to reflect changes in surface-water salinity resulting from the increase in freshwater supply to the Greenland Sea from the melting of the Greenland Ice Sheet and/or an inflow of low-saline Arctic polar waters. During the last deglaciation, the massive discharge of icebergs and meltwater led to a large and widespread stratification of surface waters that strongly prevented deep-water formation of the GIN Sea resulting in great reduction in the production of NADW.

- Correlation between the IRD-events and the D-O cycles and Heinrich-events

1) A comparison of IRD records from the Greenland Sea and the oxygen isotope records from the GRIP Summit Ice Core reveal that the distinct IRD-peaks correlate to intervals of cold air temperatures over Greenland. In particular, the interval between 225 and 74 ka exhibit IRD-events characterised by a lower frequency and relatively long-term duration compared to those of the last glacial period. During the interval between 225 and 60 ka, the amplitude of the IRD-peaks reached maximum values during northern hemisphere summer insolation maxima, and minimum values during insolation minima. The fluctuations in the IRD-flux supplied to the Greenland Sea seem to be linked to variations in the northern hemisphere summer insolation caused by the Earth's orbital precession cycle (23-kyr). Based on the co-variation between periods of increased IRD-input and summer insolation maxima at 70°N, it is suggested that climate variations on orbital time scales were linked to the growth and decay of the Greenland Ice Sheet which periodically triggered massive iceberg discharge to the Greenland Sea during that time interval.

2) The Heinrich-type IRD-events recorded in the Greenland Sea correlate well with the North Atlantic "Heinrich Events". The synchronous events can be correlated with those recorded from the Norwegian Sea reflecting and supporting the coherent fluctuations in the large northern hemisphere ice sheets (i.e. the Greenland/ Laurentide and the Fennoscandian/Barents Sea Shelf ice sheets). Despite the still controversial hypotheses of a forcing mechanism (whether the millennial scales collapses of the continental ice sheets were triggered by external climate forcing or internal ice sheet dynamics), the rapid climatic oscillations on time scales shorter than those of Milankovitch orbital cycles seem to reflect rather a global or interhemispheric climate change than a regional phenomenon restricted to the North Atlantic region.

134

3) During the last glacial period, the IRD-events along the East Greenland continental margin occurred frequently at very short-term intervals of 1 to 3 kyr. This suggests that rapid collapses of the Greenland Ice Sheet occurred on millennial scales. The IRD-events on millennial scales correlate well to cooling phases of the "Dansgaard-Oeschger Cycles" in the GRIP ice cores, reflecting a close link between the oscillations in air temperatures on Greenland and the discharge of icebergs into the Greenland Sea. Furthermore, the heavy $\delta^{18}O$ records of *N. pachyderma* sin. correlate well with the significant increase in the IRD content corresponding to the most intense, longer cooling periods of the D-O cycles (i.e. the "Bond Cycles"), indicating a close linkage between ice-sheet behaviour and ocean-atmosphere temperature changes around Greenland.

11. ACKNOWLEDGEMENTS

136

of Bremen) is also thanked for reading some of the manuscript and improving English.

I would like to thank my parents, sisters, and brother for their love and devotion and their continued financial support for my studying and living in Germany. Last but not least, I thank my wife, In-Ock Koh and my son, Dong-Kun for all their support, love, and devotion. This thesis is dedicated to the memory of my grandfather.

12. REFERENCES

Aagaard, K. 1968. Circulation of the Greenland Sea. In: United States Navy, Proc. 5th Symp. Military Oceanography, Panama City, Fla., v. 1. Alexandria, Va., Oceanographer of the Navy, Part 1: 335-363.

Aagaard, K. & Coachman, L.K., 1968a. The East Greenland Current North of Denmark Strait: Part I. Arctic, 21: 181-200.

Aagaard, K. & Coachman, L.K., 1968b. The East Greenland Current North of Denmark Strait: Part II. Arctic, 21: 267-290.

Aagaard, K., Swift, J.H. & Carmack, E.C., 1985. Thermohaline circulation in the Arctic Mediterranean seas. Jour. Geophy. Res., 90 (C3): 4833-4846.

Anderson, J.B., 1975. Factors controlling $CaCO_3$ dissolution in the Weddell Sea from foraminiferal distribution patterns. Marine Geology, 19: 315-332.

Anderson, J.B. & Molina, B.F., 1989. Glacial-marine sedimentstion. Short course in Geology, V. 9. American Geophysical Union, Washington, D.C.: 127 pp.

Anderson, L.G., Björk, G., Holby, O., Jones, E.P., Kattner, G., Koltermann, K.P., Liljeblad, B., Lindegren, R., Rudels, B. & Swift, J., 1994. Water masses and circulation in the Eurasian Basin: Results from the Oden 91 North pole Expedition. J. Geophys. Res., 99 (C2): 3273-3283.

Andrews, J.T. & Tedesco, K., 1992. Detrital carbonate-rich sediments, northwestern Labrador Sea: Implications for ice-sheet dynamics and iceberg rafting (Heinrich) events in the North Atlantic. Geology, 20: 1087-1090.

Andrews, J.T., Tedesco, K. & Jennings, A.E., 1993. Heinrich Events: Chronology and Processes, East-Central Laurentide Ice Sheet and NW Labrador Sea. In: W. Peltier (ed.), Ice in the climate system. Springer-Verlag, New York, NATO ASI Ser. I 12: 167-186.

Andrews, J.T., Erlenkeuser, H., Tedesco, K., Aksu, A.E. & Jull, A.J.T., 1994. Late Quaternary (Stage 2 and 3) Meltwater and Heinrich Events, Northwest Labrador Sea. Quat. Res., 41: 26-34.

Antonow, M., 1995. Sedimentationsmuster um den Vesteris Seamount (zentrale Grönlandsee) in den letzten 250.000 Jahre. PhD Dissertation (unpublished), Universität Kiel, 115 pp.

Bard, E., Arnold, M., Maurice, P., Duprat, J., Moyes, J. & Duplessy, J.-C., 1987. Retreat velocity of the north Atlantic polar front during the last deglaciation determined by ^{14}C accelerator mass spectrometry. Nature, 328: 791-794.

Bard, E., 1988. Correction of AMS-^{14}C ages measured in planktonic foraminifera: Paleoceanographic implications. Paleoceanography, 3: 635-645.

Barry, R.G., 1989. The present climate of the Arctic Ocean and possible past and future states. In: Y. Herman (ed.), The Arctic Seas: Climatology, oceanography, geology, and biology. New York (Van Nostrand Reinhold), 1-46.

Bauch, H., 1993. Planktische Foraminiferen im Europäischen Nordmeer - ihre Bedeutung für die paläo-ozeanographische Interpretation während der letzten 600.000 Jahre. Berichte SFB 313, Universität Kiel, 40; 108 pp.

Baumann, K.-H., 1990. Veränderlichkeit der Coccolithenphoridenflora des Europäischen Nordmeeres im Jungquartär. SFB Berichte, Universität Kiel, 22: 146 pp.

Baumann, K.-H. & Matthiessen, J., 1992. Variations in surface water mass conditions in the Norwegian Sea: Evidence from Holocene coccolith and dinoflagellate cyst assemblages. Marine Micropaleontology, 20: 129-146.

Baumann, K.-H., Lackschewitz, K.S., Erlenkeuser, H., Henrich, R. & Jünger, B., 1993. Late Quaternary calcium carbonate sedimentation and terrigenous input along the east Greenland continental margin. Marine Geology, 114: 13-36.

Baumann, K.-H., Lackschewitz, K.S., Spielhagen R.F. & Henrich, R., 1994. Reflection of continental ice sheets in late Quaternary sediments from the Nordic Seas. Zbl. Geol. Paläont. Teil I, H. 7/8: 897-912.

Baumann, K.-H., Lackschewitz, K.S., Mangerud, J., Spielhagen R.F., Wolf-Welling, T.C.W., Henrich, R. & Kassens, H., 1995. Reflection of Scandinavian Ice Sheet fluctuations in Norwegian Sea sediments during the past 150,000 years. Quat. Res., 43: 185-197.

Baumann, M., 1990. Coccoliths in sediments of the eastern Arctic Basin. In: U. Bleil & J. Thiede (eds.), Geological history of the polar oceans: Arctic versus Antarctic. Dordrecht: Kluwer Academic Publishers, NATO ASI Series, C 308: 437-445.

Bé, A.W. & Tolderlund, D.S., 1971. Distribution and ecology of living planktonic foraminifera in surface waters of the Atlantic and Indian Oceans. In: B.M. Funnel & W.R. Riedel (eds.), The micropaleontology of the oceans: 105-144.

Behl, R.J. & Kennett, J.P., 1996. Brief interstadial events in the santa Barbara basin, NE Pacific, during the past 60 kyr. Nature, 379: 243-246.

Belanger, P.E. & Streeter, S.S., 1980. Distribution and ecology of benthic foraminifera in the Norwegian-Greenland Sea. Marine Micropaleontology, 5: 401-428.

Belanger, P.E., Curry, W.B. & Matthews, R.K., 1981. Core top evaluation of benthic foraminiferal isotopic ratios for paleoceanographic interpretations. Paleogeogr., Paleoclimatol., Palaeoecol., 33: 205-220.

Belanger, P.E., 1982. Paleo-oceanography of the Norwegian Sea during the past 130,000 years: coccolithophorid and foraminifera data. Boreas, 11: 29-36.

Bender, M., Sowers, T., Dickson, M.-L., Orchardo, J., Grootes, P., Mayewski, P.A. & Messe, D.A., 1995. Climate correlations between Greenland and Antarctica during the past 100,000 years. Nature, 372: 663-666.

Berger, A.L., 1978. Long-term variations of Caloric insolation resulting from the Earth's orbital elements. Quaternary geology, 9: 139-167.

Berger, W.H., 1978. Oxygen-18 stratigraphy in deep-sea sediments: additional evidence for the deglacial meltwater effect. Deep-Sea Res., 25: 473-480.

Berger, W.H., Burke, S. & Vincent, E., 1987. Glacial-Holocene transition: Climate pulsations and sporadic shutdown of NADW production. In: W.H. Berger & L.D. Labeyrie (eds.), Abrupt climatic changes - Evidence and implications. Dordrecht: Kluwer Academic Publishers, NATO ASI Series, Vol. C 216: 279-287.

Birgisdóttir L, 1991. Die paläo-ozeanographische Entwicklung der Islandsee in der letzten 550 000 Jahre. Berichte SFB 313, Universität Kiel, 34: 112 pp.

Biscaye, P.E., Kolla, V. & Turekian, K.K., 1976. Distribution of calcium carbonate in surface sediments of the Atlantic Ocean. Jour. geophys. Res., 81: 2595-2603.

Bischof, J., Koch, J., Kubisch, M., Spielhagen, R.F. & Thiede, J., 1990. Nordic Seas surface ice drift reconstructions: evidence from ice rafted coal fragments during oxygen isotope stage 6. In: J.A. Dowdeswell & J.D. Scourse (eds.), Glaciomarine Environments: Processes and sediments. Geological Society Special Publication No. 53: 235-251.

Bischof, J.F., 1991. Dropstones im Europäischen Nordmeer - Indikatoren für Meeresströmungen in den letzten 30.000 Jahren. SFB Berichte, Universität Kiel, 30: 200 pp.

Bischof, J.F., 1994. The decay of the Barents ice sheet as documented in nordic seas ice-rafted debris. Marine Geology, 117: 35-55.

Bleil, U. & Gard, G., 1989. Chronology and correlation of Quaternary magnetostratigraphy and nannofossil biostratigraphy in Norwegian-Greenland Sea sediments. Geol. Rundsch., 78/3: 1173-1187.

Bohrmann, G., Henrich, R. & Thiede, J., 1990. Miocene to Quaternary paleoceanography in the northern North Atlantic : Variability in carbonate and biogenic opal accumulation. In: U. Bleil & J. Thiede (eds.), Geological history of the polar oceans: Arctic versus Antarctic. Dordrecht: Kluwer Academic Publishers, Nato ASI Series, C 308: 647-675.

Bond, G., Broecker, W., Lotti, R. & McManus, J., 1992a. Abrupt color changes in isotope stage 5 in North Atlantic deep sea cores: Implications for rapid change of climate-driven events. In: G.J. Kukla & E. Went (eds.), Start of a Glacial. Springer-Verlag Berlin Heidelberg, NATO ASI Series I, Vol. 3: 185-205.

Bond, G., Heinrich, H., Broecker, W., Labeyrie, L., McManus, J., Andrews, J., Huon, S., Jantschik, R., Clasen, S., Simet, C., Tedesco, K., Klas, M., Bonani, G. & Ivy, S., 1992b. Evidence for massive discharges of icebergs into the North Atlantic ocean during the last glacial period. Nature, 360: 245-249.

Bond, G., Broecker, W., Johnsen, S., McManus, J., Labeyrie, L., Jouzel, J. & Bonani, G., 1993. Correlations between climate records from North Atlantic sediments and Greenland ice. Nature, 365: 143-147.

Bond, G., 1995a. Millennial-scale climate shifts during marine isotope stage 3 in the North Atlantic Ocean. EOS Trans. AGU, Spring Meeting Suppl., 76: 169.

Bond, G. 1995b. Climate and the conveyor. Nature, 377: 383-384.

Bond, G.C. & Lotti, R., 1995. Iceberg discharges into the North Atlantic on millennial time scales during the last glaciation. Science, 267: 1005-1010.

Bordowskiy, O.k., 1965. Sources of organic matter in marine basins. Marine Geology, 3: 5-31.

Boulton, G.S., 1975. Processes and patterns of subglacial sedimentation: a theoretical approach. In: A.E. Wright & F. Moseley (eds.), Ice ages: Ancient and Modern. Liverpool, Seel House Press: 7-42.

Bourke, R.H., Newton, J.L., Paquette, R.G. & Tunnicliffe, M.D., 1987. Circulation and water masses of the East Greenland Shelf. Jour. Geophy. Res., 92: 6729-6740.

Boyle, E.A. & Keigwin, L.D., 1987. North Atlantic thermohaline circulation during the past 20,000 years linked to high-latitude surface temperature. Nature, 330: 35-40.

Broecker, W.S. & van Donk, J., 1970. Insolation changes, ice volumes, and the ^{18}O record in deep-sea cores. Rev. Geophys. and Space Phys., 8: 169-197.

Broecker, W.S. & Peng, T.-H., 1982. Tracers in the Sea. Columbia University, 690 pp.

Broecker, W.S., Andree, M., Bonani, G., Wolfli, W., Oeschger, H. & Klas, M., 1988a. Can the Greenland climatic jumps be identified in records from ocean and land ?. Quat. Res., 30: 1-6.

Broecker, W.S., Andree, M., Wolfli, W., Oeschger, H., Bonani, G., Kennett, J. & Peteet, D., 1988b. The chronolgy of the last deglaciation: Implications to the cause of the Younger Dryas Event. Paleoceanography, 3: 1-19.

Broecker, W.S. & Denton, G.H., 1989. The role of ocean-atmosphere reorganisations in glacial cycles. Geochim. Cosmochim. Acta, 53: 2465-2501.

Broecker, W.S. Bond, G. & Klas, M., 1990. A salt oscillator in the glacial Atlantic ?, 1. The concept. Paleoceanography, 5: 469-477.

Broecker, W.S., Bond, G., Klass, M., Clark, E. & McManus, J., 1992. Origin of the northern Atlantic's Heinrich events. Climate Dynamics, 6: 265-273.

Broecker, W.S., 1994. Massive iceberg discharges as triggers for global climate change. Nature, 372: 421-424.

Carstens, J. 1988. Verteilung planktischer Foraminiferen in Oberflachen-wässern der Framstrasse, Nordatlantik. Diplomarbeit (Teil B) (Unpublished), im FB Geowiss., Universität Bremen, 55pp.

Carstens, J. & Wefer, G., 1992. Recent distribution of planktonic foraminifera in the Nansen Basin, Arctic Ocean. Deep-Sea Res., 39: S507-S524.

Chappell, J. & Shackleton, N.J., 1986. Oxygen isotopes and sea level. Nature, 324: 137-140.

Chappellaz, J., Blunier, T., Raynaud, D., Barnola, J.M., Schwander, J. & Stauffer, B., 1993. Synchronous changes in atmospheric CH_4 and Greenland climate between 40 and 8 kyr BP. Nature, 366: 443-445.

Charles, C.D. & Fairbanks, R.G., 1990. Glacial to interglacial changes in the isotopic gradients of southern ocean surface water. In: U. Bleil & J. Thiede (eds.), Geological history of the polar oceans: Arctic versus Antarctic. Dordrecht: Kluwer Academic Publishers, NATO ASI Series, C 308: 519-538.

Charles, C.D. & Fairbanks, R.G., 1992. Evidence from Southern Ocean sediments for the effect of the North Atlantic deep-water flux on climate. Nature, 355: 416-419.

CIA (Central Intelligence Agency), 1978. Polar Regions Atlas: Washington (CIA).

Clark, P.U. & Bartlein, P.J. 1995. Correlation of late Pleistocene glaciation in the western United States with North Atlantic Heinrich events. Geology, 23: 483-486.

CLIMAP, 1981. Seasonal reconstruction of the earth's surface at the last glacial maximum. Geological Society American Map and Chart Series MC-36.

Coachman, L.K. & Aagaard, K., 1974. Physical oceanography of Arctic and Subarctic Seas. In: Y. Herman (ed.), Marine Geology and oceanography of the Arctic Seas. Springer, New York, Inc., 1-72.

Conolly, J.R. & Erwing, M., 1965. Ice-rafted detritus as a climatic indicators in Antarctic deep-sea cores. Science, 150: 1822-1824.

Cordes, D., 1990. Sedimentologie und Paläomagnetik an Sedimenten der Maudkuppe (Nordöstliches Weddelmeer). Berichte zur Polarforschung Alfred-Wegener-Institut, Bremerhaven, 71: 158 pp.

Corliss, B.H., 1985. Microhabitats of benthic foraminifera within deep-sea sediments. Nature, 314: 435-438.

Cortijo, E., Duplessy, J.C., Labeyrie, L., Leclaire, H., Duprat, J. & van Weering, T.C.E., 1994. Eemian cooling in the Norwegian Sea and North Atlantic ocean preceding continental ice-sheet growth. Nature, 372: 446-449.

Cronin, T.M., Holtz Jr., T.R., Stein, R., Spielhagen, R., Fütterer, D. & Wollenburg, J., 1995. Late Quaternary paleoceanography of the Eurasian Basin, Arctic Ocean. Paleoceanography, 10: 259-281.

Curry, W.B., Duplessy, J.C., Labeyrie, L.D., Oppo, D. & Kallel, N., 1988. Quaternary deep-water circulation changes in the distribution of $\delta^{13}C$ of

deep water ΣCO_2 between the last glaciation and the Holocene. Paleoceanography, 3: 317-342.

Damuth J.E., 1978. Echo character of the Norwegian-Greenland Sea: Relationship to Quaternary sedimentation. Marine Geology, 28: 1-36.

Dansgaard, W., Clausen, H.B., Grundestrup, N., Hammer, C.U., Johnsen, S.J., Kristinsdorttir, P.M. & Reeh, N., 1982. A new Greenland deep ice core. Science, 218: 1273-1277.

Dansgaard, W., Johnsen, S.J., Clausen, H.B., Dahl-Jensen, D., Grundestrup, N. & Hammer, C.U., 1984. North Atlantic climatic oscillations revealed by deep Greenland ice cores. In: J.E. Hansen & T. Takahashi (eds.), Climate processes and climate sensitivity. AGU, Washington, DC, Geophysical Monograph 29: 288-298.

Dansgaard, W., Clausen, H.B., Grundestrup, N., Johnsen, S.J. & Rygner, C., 1985. Dating and climatic interpretation of two deep Greenland ice cores. In: C.C. Langway Jr., H. Oeschger & W. Dansgaard (eds.), Greenland ice core: Geophysics, geochemistry, and the environment. AGU Washington, DC, Geophysical Monograph 33: 71-76.

Dansgaard, W., 1987. Ice core evidence of abrupt climatic changes. In: W.H. Berger & L.D. Labeyrie (eds.), Abrupt climatic change - Evidence and implications, NATO ASI Series, C 216: 223-233.

Dansgaard, W., Johnsen, S.J., Clausen, H.B., Dahl-Jensen, D., Grundestrup, N.S., Hammer, C.U., Hvidberg, C.S., Steffensen, J.P., Sveinbjörnsdottir, A.E., Jouzel, J. & Bond, G., 1993. Evidence for general instability of past climate from a 250-kyr ice-core record. Nature, 364: 218-220.

Dean, W.E., Gardner, J.V. & Anderson, R.Y., 1994. Geochemical evidence for enhanced preservation of organic matter in the oxygen minimum zone of the continental margin of northern California during the late Pleistocene. Paleoceanography, 9: 47-61.

Denton, G.H. & Hughes. T.J., 1981. The last great ice sheets. New York, John Wiley and Sons: 484 pp.

de Vernal, A., Bilodeau, G., Hillaire-Marcel, C. & Kassou, N., 1992. Quantitative assessment of carbonate dissolution in marine sediments from foraminifer living vs. shell ratios, Davis Strait, northwest North Atlantic. Geology, 20: 527-530.

Dowdeswell, J.A., Villinger, H., Whittington, R.J. & Marienfeld, P., 1991. The Quaternary marine record in the Scoresby Sund fjord system, East Greenland: Preliminary results and interpretation. In: P. Möller, C. Hjort & Ó. Ingólfsson (eds.), The Last Interglacial-Glacial Cycle: Jameson Land and Scoresby Sund, East Greenland. LundQua Rep. Ser., 33: 149-155.

Dowdeswell, J.A., Whittington, R.J. and Hodgkins, R., 1992. The sizes, frequencies and freeboards of East Greenland icebergs observed using ship radar and sextant. Jour. Geophys. Res., 97: 3515-3528.

Dowdeswell, J.A., Villinger, H., Whittington, R.J. & Marienfeld, P., 1993. Iceberg scouring in Scoresby Sund and on the East Greenland continental shelf. Marine Geology, 111: 37-53.

Dowdeswell, J.A, Whittington, R.J. & Marienfeld, P., 1994a. The origin of massive diamicton facies by iceberg rafting and scouring, Scoresby Sund, East Greenland. Sedimentology, 41: 21-35.

Dowdeswell, J.A., Uenzelmann-Neben, G., Whittington, R.J. & Marienfeld, P., 1994b. The Late Quaternary sedimentary record in Scoresby Sund, East Greenland. Boreas, 23: 294-310.

Dowdeswell, J.A., Maslin, M.A., Andrews, J.T. & McCave, I.N., 1995. Iceberg production, debris rafting, and the extent and thickness of Heinrich layers (H-1, H-2) in North Atlantic sediments. Geology, 23: 301-304.

Drewry, D.J., 1986. Glacial geologic processs. Edward Arnold, London: 276 pp.

Duplessy, J.-C., Bé, A.W.H. & Blanc, P.L., 1981. Oxygen and carbon isotopic composition and biogeographic distribution of planktonic foraminifera in the Indian Ocean. Palaeogeogr., Palaeoclimatol., Palaeoecol., 33: 9-16.

Duplessy, J.C., Shackleton, N.J., Matthews, R.K., Prell, W., Ruddiman, W.F., Caralp, M. & Hendy, C.H., 1984. ^{13}C record of benthic foraminifera in the last interglacial ocean: Implications for the carbon cycle and the global deepwater circulation. Quat. Res., 21: 225-243.

Duplessy, J.C., Arnold, M., Maurice, P., Bard, E., Duprat, J. & Moyes, J., 1986. Direct dating of the oxygen-isotope record of the last deglaciation by ^{14}C accelerator mass spectrometry. Nature, 320: 350-352.

Duplessy, J.C., Shackleton, N.J., Fairbanks, R.G., Labeyrie, L., Oppo, D. & Kallel, N., 1988a. Deep water source variations during the last climatic cycle and their impact on the global deepwater circulation. Paleoceanography, 3: 343-360.

Duplessy, J.-C., Labeyrie, L. & Blanc, P.L., 1988b. Norwegian sea deep water variations over the last climatic cycle: Paleo-oceanographical implications. In: H. Wanner & U. Siegenthaler (eds.), Long and short term variability of climate. Spriger Verlag, Heidelberg, v. 16: 83-116.

Duplessy, J.-C., Labeyrie, L., Juillet-Leclerc, A., Maitre, F., Duprat, J. & Sarnthein, M., 1991. Surface salinity reconstruction of the North Atlantic Ocean during the last glacial maximum. Oceanol. Acta, 14: 311-324.

Duplessy, J.-C., Bard, E., Labeyrie, L., Duprat, J. & Moyes, J., 1993. Oxygen isotope records and salinity changes in the northeastern Atlantic Ocean during the last 18,000 years. Paleoceanography, 8: 341-350.

Duplessy, J.C., Labeyrie, L.D., 1994. Surface and deep water circulation changes during the last climatic cycle. In: J.-C. Duplessy & M.-T. Spyridakis (eds.). Long-term climatic variations: Data and modelling. Springer-Verlag, Berlin Heidelberg, NATO ASI Series, Vol. I 22; 277-298.

Eide, L.K., 1990. Distribution of coccoliths in surface sediments in the Norwegian-Greenland Sea. Marine Micropaleontology, 16: 65-75.

Elverhøi, A., 1984. Glacigenic and associated marine sediments in the Weddel Sea, fjords of Spitsbergen and the Barents Sea: a review. Marine Geology, 57: 53-88.

Elverhøi, A. & Dowdeswell, J.A., 1991. Polar North Atlantic Margins (PONAM). ESF - Communications, 25: 16-17.

Elverhøi, A., Andersen, E.S., Dokken, T., Hebbeln, D., Spielhagen, R., Svendsen, J.I., Sørftlaten, M., Rørnes, A., Hald, M. & Forsberg, C.F., 1995. The growth and decay of the Late Weichselian Ice Sheet in western Svalvard and adjacent areas based on provenance studies of marine sediments. Quat. Res, 44: 303-316.

Emerson, S. & Hedges, J.I., 1988. Processes controlling the organic carbon content of open ocean sediments. Paleoceanography, 3: 621-634.

Emiliani, C., 1955. Pleistocene temperatures. Journal of Geology, 63: 538-578.

Espiltalié, J., Laporte, J.L., Madec, M, Marquis, F., Leplat, P., Paulet, P. & Boutefeu, A., 1977. Methode rapide de chatacterisation des roches mértes de leur potential petrolier en de leur degré d'evolution. Rev. Inst. Fr. Pet., 32: 23-42.

Fairbanks, R.G., 1989. A 17,000-year glacio-eustatic sea level record: influence of glacial melting rates on the Younger Dryas event and deep-ocean circulation. Nature, 342: 637-642.

Fairbanks, R.G., Charles, C.D. & Wright, J.D., 1992. Origin of global meltwater pulses. In: R.E. Taylor (ed.), Radocarbon after Four Decades. Springer, Berlin, 473-500.

Field, M.H., Huntley, B. & Müller, H., 1994. Eemian climate fluctuations observed in a European pollen record. Nature, 371: 779-783.

Fronval, T., Jansen, E., Bloemendal, J. & Johnsen, S., 1995. Oceanic evidence for coherent fluctuations in Fennoscandian and Laurentide ice sheets on millennium timescales. Nature, 374: 443-446.

Funder, S. & Hjort, C., 1978. Weichsel interstadial(er) i Østgrønland. Aldersbestemmelse og geologi. And Isens udbredelse i Østgrønland i sen Weichsel og tidlig Flandern - morfologisk afgraensning og absolut datering; 13. Nordiske Vintermøde (abstarct); Geologisk Centralinstitut, Copenhagen, 85 pp.

Funder, S., 1984. Chronology of the last interglacial/glacial cycle in Greenland: first approximation. In: W.C. Mahaney (ed.), Correlation of Quaternary chronologies. Norwich, Geo Books, 261-279.

Funder, S., 1989. Quaternary Geology of the ice-free areas and adjacent shelves of Greenland. In: R.J. Fulton (ed.), Quaternary Geology of Canada and Greenland. Geological Survey of Canada, Geology of Canada, no. 1 (Geol. Soc. Amer., The Geology of the North America, v. K-1), 743-792.

Funder, S., Hjort, C. & Landvik, J.Y., 1994. The last glacial cycles in East Greenland, an overview. Boreas, 23: 283-293.

Gard, G., 1986. Calcareous nannofossil biostratigraphy of late Quaternary Arctic sediments. Boreas, 15: 217-229.

Gard, G., 1987. Late Quaternary calcareous nannofossil biostratigraphy and sedimentation patterns: Fram Strait, Arctica. Paleoceanography, 2: 519-529.

Gard, G., 1988. Late Quaternary calcareous nannofossil biozonation, chronology and paleoceanography in areas north of the Faeroe-Island Ridge. Quat.-Sci. Rev., 7: 65-78.

Gard, G. & Backman, J., 1990. Synthesis of Arctic and subarctic coccolith biochronology and history of North Atlantic Drift Water influx during the last 500,000 years. In: U. Bleil & J. Thiede (eds.), Geological history of the polar oceans: Arctic versus Antarctic. Dordrecht: Kluwer Academic Publishers, NATO ASI Series, C 308: 417-436.

Gard, G., 1993. Late Quaternary coccoliths at the North Pole: Evidence of ice free conditions and rapid sedimentation in the central Arctic Ocean. Geology, 21: 227-230.

Gealy, E.L., 1971. Saturated bulk density, grain density, and porosity of sediment cores from the western Equatorial Pacific: Leg 7, Glomar Challenger. In: E.L., Winterer et al. (eds.). Initial Reports DSDP, 7, Washington (U.S. Govt. Printing Office): 1081-1104.

Goldschmidt, P.M., 1994. The ice-rafting history in the Norwegian-Greenland Sea for the last two glacial/interglacial cycles. Berichte SFB 313, Universität Kiel, 50: 103 pp.

Goldschmidt, P.M., 1995. Accumulation rates of coarse-grained terrigenous sediment in the Norwegian-Greenland Sea: signals of continental glaciation. Marine Geology, 128: 137-151.

Gordienko, P.A. & Laktionov, A.F., 1969. Circulation and physics of the Arctic Basin waters. In: A.L. Gordon & F.W.G. Baker (eds.), Annals of the International Geophysical Year, Oceanography, 46: 94-112.

Gordon, A.L., 1986. Interocean exchange of thermohaline water. Jour. Geophys. Res., 91: 5037-5046.

Grimm, E.C., Jacobson, Jr., G.L., Watts, W.A., Hansen, B.C.S. & Maasch, K.A., 1993. A 50,000-year record of climate oscillations from Florida and its temporal correlation with the Heinrich events. Science, 261: 198-200.

GRIP (Greenland Ice-core Project) Members, 1993. Climate instability during the last interglacial period recorded in the GRIP ice core. Nature, 364: 203-207.

Grobe, H., 1986. Spätpleistozäne Sedimentationsprozesse am antarktischen Kontinentalhang vor Kapp Norvegia, östliche Weddell See. Berichte zur Polarforschung Alfred-Wegener-Institut, Bremerhaven, 27: 120 pp.

Grobe, H., 1987. A simple method for the determination of ice-rafted debris in sediment cores. Polarforschung, 57: 123-126.

Grootes, P.M., Stuiver, M., White, J.W.C., Johnsen, S. & Jouzel, J., 1993. Comparison of oxygen isotope records from the GISP2 and GRIP Greenland ice cores. Nature, 366: 552-554.

Grosswald, M.G., 1980. Late Weichselian ice sheet of northern Eurasia. Quat. Res., 13: 1-32.

Grousset, F., Laberyie, L., Sinko, J., Bond, G., Duprat, J., Cremer, M. & Huon, S., 1992. Patterns of ice-rafted detritus in the glacial North Atlantic (40-55°). GEOMAR Report, 15: 129.

Grousset, F.E., Laberyie, L., Sinko, J.A., Cremer, M., Bond, G., Duprat, J., Cortijo, E. & Huon, S., 1993. Patterns of ice-rafted detritus in the glacial North Atlantic (40-55°N). Paleoceanography, 8: 175-192.

Gwiazda, R.H., Hemming, S.R. & Broecker, W.S., 1995. Multiple continental sources of Heinrich layer 3 grains as determined by Pb isotopic analysis of ice-rafted feldspars. EOS Trans. AGU, Spring Meeting suppl., 76: 169.

Haake, F.-W. & Pflaumann, U., 1989. Late Pleistocene foraminiferal stratigraphy on the Vøring Plateau, Norwegian Sea. Boreas, 18: 343-356.

Hald, M. & Vorren, T., 1984. Modern and Holocene foraminifera and sediments on the continental shelf off Troms, North Norway. Boreas, 13: 133-154.

Hambrey, M., 1994. Glacial environments. UCL (University College London) Press, London: 296 pp.

Hamilton, E.L., 1971. Prediction of in situ acoustic and elastic properties of marine sediments. Geophysics, 36: 266-284.

Hansen, B. & Meincke, J., 1979. Eddies and meanders in the Iceland-Færœ Ridge area. Deep-Sea Res., 26: 1067-1082.

Hansen, A.L., Jørgensen, M.E., Houmark-Nielsen, M. & Kronborg, C. 1994. Late Pleistocene stratigraphy and depositional environments of the Fynselv area, Jameson Land, East Greenland. Boreas, 23: 385-397.

Harland, R., 1983. Distribution maps of recent dinoflagellate cysts in bottom sediments from the North Atlantic Ocean and adjacent seas. Palaeontology, 26: 321-387.

Hastings, A.D., 1960. Environment of Southeast Greenland. Headquarters Quartermaster Research and Engineering Command, U.S. Army, EP-149.

Hays, J.D., Imbrie, J. & Shackleton, N.J., 1976. Variations in the Earth's Orbit: Pacemaker of the Ice Ages. Science, 194: 1121-1132.

Hebbeln, D., 1991. Spätquartäre Stratigraphie und Paläozeanographie in der Fram-Straße. Berichte FB Geowiss., Universität Bremen, 22: 174 pp.

Hebbeln, D. & Wefer, G., 1991. Effects of ice coverage and ice-rafted material on sedimentation in the Fram Strait. Nature, 350: 409-411.

Hebbeln, D., 1992. Weichselian glacial history of the Svalbard area: correlating the marine and terrestrial records. Boreas, 21: 295-304.

Hebbeln, D., Dokken, T., Andersen, E.S., Hald, M. & Elverhøi, A., 1994. Moisture supply for northern ice-sheet growth during the Last Glacial Maximum. Nature, 370: 357-360.

Heinrich, H., 1988. Origin and consequences of cyclic ice rafting in the Northeast Atlantic Ocean during the past 130,000 years. Quat. Res., 29: 142-152.

Henrich, R., 1986. A calcite dissolution pulse in the Norwegian-Greenland Sea during the last deglaciation. Geol. Rundsch., 75: 805-827.

Henrich, R., Kassens, H., Vogelsang, E. & Thiede, J., 1989. Sedimentary facies of glacial-interglacial cycles in the Norwegian Sea during the last 350 ka. Marine Geology, 86: 283-319.

Henrich, R., 1992. Beckenanalyse des Eropäischen Nordmeeres: Pelagische und glaziomarine Sedimentflüsse im Zeitraum 2,6 Ma bis rezent. Habilitation (unpublished), Universität Kiel, 345 pp.

Henrich, R., Wagner, T., Goldschmidt, P. & Michels, K., 1995. Depositional regimes in the Norwegian-Greenland Sea: the last two glacial to interglacial transitions. Geol. Rundsch., 84: 28-48.

Henriksen; N. & Higgins, A.K., 1976. East Greenland Caledonian fold belt. In: A. Escher & W.S. Watt (eds.), Geology of Greenland. The Geological Survey of Greenland, 183-246.

Hjort, C., 1979. Glaciation in northern East Greenland during the Late Weichselian and Early Flandrian. Boreas, 8: 281-296.

Hjort, C., 1981. A glacial chronology for the northern East Greenland. Boreas, 10: 259-274.

Hopkins, T.S., 1991. The GIN Sea - A synthesis of its physical oceanography and literature review 1972-1985. Earth-Sci. Rev., 30: 175-318.

Hubberten, H.W. & Meyer, G., 1989. Stable isotope measurements on foraminifera tests: experiences with an automatic commercial carbonate preparation device. Terra Abstracts, 1: 80-81.

Hubberten, H.W., Grobe, H., Jokat, W., Melles, M., Niessen, F. & Stein, R., 1995. Glacial history of East Greenland explored. EOS, Transactions, Amer. Geophys. Union, 76 (36): 353, 356.

Hughes, T., Denton, G.H. & Grosswald, M.G., 1977. Was there a late-Würm Arctic Ice Sheet. Nature, 266: 596-602.

Hurdle, B.G. (ed.), 1986. The Nordic Seas. Springer, New York, 776 pp.

Imbrie, J., Hays, J.D., Martinson, G.D., McIntyre, A., Mix, A.C., Morley, J.J., Pisias, N.G., Prell, W.L. & Schackleton, N.J., 1984. The orbital theory of Pleistocene climate: support from a revised chronology of the marine $\delta^{18}O$ record. In: A. Berger; J. Imbrie, J. Hays, G. Kukla & B. Saltzman (eds.), Milankovitch and climate, Part I. D. Reidel Publishing Company, NATO ASI Series, C 126: 269-305.

Imbrie, J., Boyle, E.A., Clemens, S.C., Duffy, A., Howard, W.R., Kukla, G., Kutzbach, J., Martinson, D.G., McIntyre, A., Mix, A.C., Molfino, B., Morley, J.J., Peterson, L.C., Pisias, N.G., Prell, W.L., Raymo, M.E., Schackleton, N.J. & Toggweiler, J.R., 1992. On the structure and origin of major glaciation cycles, 1. Linear responses to Milankovitch foring. Paleoceanography, 7: 701-738.

Imbrie, J., Berger, A., Boyle, E.A., Clemens, S.C., Duffy, A., Howard, W.R., Kukla, G., Kutzbach, J., Martinson, D.G., McIntyre, A., Mix, A.C., Molfino, B.,

Morley, J.J., Peterson, L.C., Pisias, N.G., Prell, W.L., Raymo,–M.E., Schackleton, N.J. & Toggweiler, J.R., 1993. On the structure and origin of major glaciation cycles, 2. The 100,000-year cycle. Paleoceanography, 8: 699-735.

Israelson, C., Funder, S. & Kelly, M., 1994. The Aucellaelv stade at Aucellaelv, the first Weichselian glacier advance in Scoresby Sund, East Greenland. Boreas, 23: 424-431.

Jacobs, S.S., Gordon, A.L. & Amos, A.F., 1979. Effects of glacial ice melting on the Antarctic surface water. Nature, 277: 469-471.

Jansen, E. & Erlenkeuser, H., 1985. Ocean circulation in the Norwegian Sea during the last deglaciation: Isotopic evidence. Paleogeogr., Paleoclimatol., Paleoecol., 49: 189-206.

Jansen, E., Sjøholm, J., Bleil, U. & Erichsen, J., 1990. Neogene and Pleistocene glaciations in the northen hemisphere and late Miocene-Pleiocene global ice volume fluctuations: Evidence from the Norwegian Sea. In: U. Bleil & J. Thiede (eds.), Geological history of the polar oceans: Arctic versus Antarctic. Dordrecht: Kluwer Academic Publishers, NATO ASI Series, C 308: 677-705.

Jansen, E. & Veum, T., 1990. Evidence for two-step deglaciation and its impact on North Atlantic deep-water circulation. Nature, 343: 612-616.

Jennings, A.E. & Helgadottir, G., 1994. Foraminiferal assenblages from the fjords and shelf of eastern Greenland. Jour. Foraminiferal Res., 24: 123-144.

Johannessen, O.M., 1986. Brief overview of the physical oceanography. In B.G. Hurdle (ed.), The Nordic Seas. Springer, New York Inc.: 103-127.

Johannessen, T., Jansen, E., Flatøy, A. & Ravelo, A.C., 1994. The relationship between surface water masses, oceanographic fronts and paleoclimatic proxies in surface sediments of the Greenland, Iceland, Norwegian Seas. In: R. Zahn, T.F. Pedersen, M.A. Kamins & L. Labeyrie (eds.), Carbon cycling in the glacial ocean: Constraints on the ocean's role in global change. NATO ASI Series, I 17: 61-85.

Johnsen, S.J., Dansgaard, W., Clausen, H.B. & Langway Jr., C.C., 1972. Oxygen isotope profiles through the Antarctic and Greenland ice sheets. Nature, 235: 429-434.

Johnsen, S.J., Clausen, H.B., Dansgaard, W., Fuhrer, K., Gundestrup, N.S., Hammer, C.U., Iversen, P., Jouzel, J., Stauffer, B. & Steffensen, J.P., 1992. Irregular glacial interstadials recorded in a new Greenland ice core. Nature, 359: 311-313.

Johnson, G.L. & Eckhoff, O.B., 1966. Bathymetry of the north Greenland Sea. Deep-Sea Res., 1161-1173.

Jones, G.A. & Keigwin, L.D., 1988. Evidence from Fram Strait (78° N) for early deglaciation. Nature, 336: 56-59.

Jouzel, J., Lorius, C., Merlivat, L. & Petit, J.-R., 1987. Abrupt climatic changes: The Antarctic ice record during the late Pleistocene. In: W.H. Berger & L.D. Labeyrie (eds.), Abrupt climatic change - Evidence and implications, NATO ASI Series, C 216: 235-245.

Jouzel, J. Barkov, N.I., Barnola, J.M., Bender, M., Chappellaz, J., Genthon, C., Kotlyakov, V.M., Lipenkov, V., Lorius, C., Petit, J.R., Raynaud, D., Raisbeck, Ritz, C., Sowers, T., Stievenard, M., Yiou, F. & Yiou, P., 1993. Extending the Vostok ice-core record of palaeoclimate to the penultimate glacial period. Nature, 364: 407-412.

Jünger, B., 1994. Tiefenwassererneuerung in der Grönlandsee während der letzten 340 000 Jahre. GEOMAR Report, 35: 6+109 pp.

Keigwin, I.D., Curry, W.B., Lehman, S.J. & Johnsen, S., 1994. The role of the deep ocean in North Atlantic climate change between 70 and 130 kyr ago. Nature, 371: 323- 326.

Keigwin, I.D. & Lehman, S.J., 1994. Deep circulation change linked to Heinrich event 1 and Younger Dryas in a middepth North Atlantic core. Paleoceanography, 9: 185-194.

Kellogg, T.B., 1976. Late Quaternary climatic changes: Evidence from deep-sea cores of Norwegian and Greenland Seas. In: R.M. Cline & J.D. Hays (eds.): Investigation of Late Quaternary Paleoceanography and Paleo-climatology. Geol. Soc. Amer. Mem., 145: 77-110.

Kellogg, T.B., 1977. Paleoclimatology and paleoceanography of the Norwegian and Greenland seas: The last 450,000 yr. Marine Micropaleontology, 2: 235-249.

Kellogg, T.B., Duplessy, J.C. & Shackleton, N.J., 1978. Planktonic foraminiferal and oxygen isotopic stratigraphy and paleoclimatology of Norwegian Sea deep-sea cores. Boreas, 7: 61-73.

Kellogg, T.B., 1980. Paleoclimatology and paleo-oceanography of the Norwegian and Greenland seas: glacial-interglacial contrasts. Boreas, 9: 115-137.

Kennet, J.P. & Ingram, B.L., 1995. A 20,000-year record of ocean circulation and climate change from the Santa Barbara basin. Nature, 377: 510-514.

Kent, D., Opdyke, N.D. & Erwing, M., 1971. Climate change in the North Pacific using ice-rafted detritus as a climate indicator. Geol. Soc. Amer. Bull., 82: 2741-2754, 8 figs.

Knies, J., 1994. Spätquartäre Sedimentation am Kontinentalhang nordwestlich Spitzbergens. - Der letzte Glazial/Interglazial-Zyklus. Diplomarbeit (unpublished), im FB Geowiss. und Geogr. der J.L. Universität Giessen, 95 pp.

Koç Karpuz, N. & Schrader, H., 1990. Surface sediment diatom distribution and Holocene paleotemperature variations in the Greenland, Iceland and Norwegian Sea. Paleoceanography, 5: 557-580.

Koç Karpuz, N. & Jansen, E., 1992. A high-resolution diatom record of the last deglaciation from the SE Norwegian Sea: Documentation of rapid climatic changes. Paleoceanography, 7: 499-520.

Koç, N., Jansen, E. & Haflidason, H., 1993. Paleoceanographic reconstructions of surface ocean conditions in the Greenland, Iceland and Norwegian Sea through the last 14 ka based on diatoms. Quat.-Sci. Rev., 12: 115-140.

Koç, N. & Jansen, E., 1994. Response of the high-latitude Northern Hemisphere to orbital climate forcing: Evidence from the Nordic Seas. Geology, 22: 523-526.

Köhler, S.E.I. & Spielhagen, R.F., 1990. The enigma of oxygen isotope stage 5 in the central Fram Strait. In: U. Bleil & J. Thiede (eds.), Geological history of the polar oceans: Arctic versus Antarctic. Dordrecht: Kluwer Academic Publishers, NATO ASI Series, C 308: 489-497.

Köhler, S.E.I., 1992. Spätquartäre paläo-ozeanographische Entwicklung des Nordpolarmeeres und europäischen Nordmeeres anhand von Sauerstoff- und Kohlenstoffisotopenverhältnissen der planktischen Foraminifere Neogloboquadrina pachyderma (sin.). GEOMAR Report, 13: 104 pp.

Kroopnick, P.M., 1980. The distribution of ^{13}C in the Atlantic Ocean. Earth Planet. Sci. Lett., 49: 469-484.

Kroopnick, P.M., 1985. The distribution of ^{13}C of ΣCO_2 in the world oceans. Deep-Sea Res., 32: 57-84.

Kvambekk, Å. S. & Vinje, T. 1993. The ice transport through the Fram Strait. Nansen Centennial Symposium, Bergen, Norway. Abstract (unpaginated).

Labeyrie, L.D. & Duplessy, J.-C., 1985. Changes in the oceanic $^{13}C/^{12}C$ ratio during the last 140,000 years: high latitude surface water records. Palaeogeogr., Palaeoclimatol., Palaeoecol., 50: 217-240.

Labeyrie, L.D., Pichon, J.J., Labracherie, M., Ippolito, P., Duprat, J. & Duplessy, J.-C., 1986. Melting history of Antarctica during the past 60,000 years. Nature, 322: 701-706.

Labeyrie, L.D., Duplessy, J.C. & Blanc, P.L., 1987. Variations in mode of formation and temperature of oceanic deep water over the past 125,000 years. Nature, 327: 477-482.

Lackschewitz, K.S., 1991. Sedimentationsprozesse am aktiven mittelozeanischen Kolbeinsey Rücken, nördlich von Island. Geomar Report, 9: 133 pp.

Lackschewitz, K.S. & Wallrabe-Adams, H.-J., 1991. Composition and origin of sediments on the mid-oceanic Kolbeinsey Ridge, north of Iceland. Marine Geology, 101: 71-82.

Landvik, J.Y., Lyså, A., Funder, S. & Kelly, M., 1994. The Eemian and Weischelian stratigraphy for the Langelandselv area, Jameson Land, East Greenland. Boreas, 23: 412-423.

Lehman, S.J., Jones, G.A., Keigwin, L.D., Andersen, E.S., Butenko, G. & Østmo, S.-R., 1991. Initiation of Fennoscandian ice-sheet retreat during the last deglaciation. Nature, 349: 513-516.

Lehman, S.J. & Keigwin, L.D., 1992. Sudden changes in North Atlantic circulation during the last deglaciation. Nature, 356: 757-762.

Lehman, S.J., 1993. Ice sheets, wayward winds and sea change. Nature, 365: 108-110.

Lipps, J.H., 1983. Biotic interactions in benthic foraminifera. - In: M.J.S. Trevesz & P.L. McCall (eds.), Biotic interaction in recent and fossil benthic communities. Plenum Press, New York: 331-376.

Lloyd, J.M., Kroon, D., Boulton, G.S., Laban, C. & Fallick, A., 1996a. Ice rafting history from the Spitsbergen ice cap over the last 200 kyr. Marine Geology, 131: 103-121.

Lloyd, J.M., Kroon, D., Laban, C. & Boulton, G.S., 1996b. Deglaciation history and paleoceanography of the western Spitsbergen margin since the last glacial maximum. In: J. Andrews, W.E.N. Austin, H. Bergsten & A.E. Jennings (eds.), Late Quaternary Paleoceanography of the North Atlantic Margins, Geol. Soc. Spec. Publ. No. 111, London: 289-301.

Lorius, C., Merlivat, L., Jouzel, J. & Pourchet, M., 1979. A 30,000 yr isotope record from Antarctic ice. Nature, 280: 644-648.

Lorius, C., Jouzel, J., Ritz, C., Merlivat, L., Barkov, N.I., Korotkevich, Y.S. & Kotlyakov, V.M., 1985. A 150,000 year climatic record from Antarctic ice. Nature, 316: 591-596.

Lowell, T.V., Heusser, C.J., Andersen, B.G., Moreno, P.I., Hauser, A., Heusser, L.E., Schlüchter, C., Marchant, D.M. & Denton, G.M., 1995. Interhemispheric Correlation of Late Pleistocene Glacial Events. Science, 269: 1541-1549.

Lyså, A. & Landvik, J.Y., 1994. Cyclic changes in the sedimentary environment during the last interglacial-glacial cycle; coastal Jameson Land, East Greenland. Palaeogeogr., Palaeoclimatol., Palaeoecol., 112: 143-156.

Mackensen, A., 1985. The distribution of living benthic foraminifera on the continental slope and rise off Southwest Norway. Marine Micropaleontology, 9: 275-306.

Mackensen, A. & Douglas, R.G., 1989. Down-core distribution of live and dead deep-water benthic foraminifera in box cores from the Weddell Sea and the California continental borderland. Deep-Sea Res., 36: 879-900.

Mackensen, A., Hubberten, H.-W., Bickert, T., Fischer, G. & Fütterer, D.K., 1993. The $\delta^{13}C$ in benthic foraminiferal tests of *Fontbotia wuellerstorfi* (Schwager) relative to $\delta^{13}C$ of dissolved inorganic carbon in southern ocean deepwater: Implications for glacial ocean circulation models. Paleoceanography, 8: 587-610.

Mackensen, A., Grobe, H., Hubberten, H.-W. & Kuhn, G., 1994. Benthic foraminiferal assemblages and the $\delta^{13}C$-signal in the Atlantic sector of the southern ocean: Glacial-to-interglacial contrasts. In: R. Zahn et al. (eds.), Carbon cycling in the glacial ocean: Constraints on the ocean´s role in global change. NATO ASI Series, I 17: 105-144.

MacAyeal, D.R., 1993. Binge/purge oscillations of the Laurentide ice Sheet as a cause of the North Atlantic´s Heinrich events. Paleoceanography, 8: 775-784.

Manabe, S. & Broccoli, A.J., 1985. The influence of continental ice sheets on the climate of an ice age. Jour. Geophys. Res., 90: 2167-2190.

Mangerud, J., Lie, S.E., Furnes, H., & Kristiansen, I.L., 1984. A Younger Dryas ash bed in Western Norway, and its possible correlations with tephra in cores from the Norwegian Sea and the North Atlantic. Quat. Res., 21: 85-104.

Mangerud, J., 1991. The Scandinavian ice sheet through the last interglacial/glacial cycle: In B. Frenzel (ed.), Klimageschichtliche Probleme der letzten 130.000 Jahre. G. Fischer, Stuttgart: 307-330.

Mangerud, J. & Svendsen, J.I., 1992. The last interglacial-glacial period on Spitsbergen, Svalbard. Quat. Sci. Rew., 11: 633-664.

Mangerud, J. & Funder, S., 1994. The interglacial-glacial record at the mouth of Scoresby Sund, East Greenland. Boreas, 23: 349-358.

Manighetti, B., McCave, I.N., Maslin, M. & Shackleton, N.J., 1995. Chronology for climate change: Developing age models for the Biogeochemical ocean flux study cores. Paleoceanography, 10: 513-525.

Marienfeld, P., 1991. Holozäne Sedimentationsentwicklung im Scoresby Sund, Ost-Grönland. Berichte zur Polarforschung Alfred-Wegener-Institut, Bremerhaven, 96: 166 pp.

Marienfeld, P., 1992a. Postglacial sedimentary history of Scoresby Sund, East Greenland. Polarforschung: 60 (3), 181-195.

Marienfeld, P., 1992b. Recent sedimentary processes in Scoresby Sund, East Greenland. Boreas, 21: 169-186.

Martinson, D.G., Pisias, N.G., Hays, J.D., Imbrie, J., Moore, T.C. & Shackleton, N.J., 1987. Age dating and the orbital theory of ice ages: Development of high-resolution 0 to 300,000-year chronostratigraphy. Quat. Res., 27: 1-29.

Maslin, M.A., Shackleton, N.J., Duplessy, J.-C. & Arnold, M., 1992. Temperature and salinity history of the last deglaciation and Heinrich ice-rafting events I to IV in the NE Atlantic. GEOMAR Report, 15: 190 (Abstract).

Maslin, M.A., Shackleton, N.J. & Pflaumann, U., 1995. Surface water temperature, salinity, and density changes in the northeast Atlantic during the last 45,000 years: Heinrich events, deep water formation, and climate rebounds. Paleoceanography, 10: 527-544.

Matthiessen, J., 1995. Distribution patterns of dinoflagellate cysts and other organic-walled microfossils in recent Norwegian-Greenland Sea sediments. Marine Micropaleontology, 24: 307-334.

Mayewski, P.A., Meeker, L.D., Whitlow, S., Twickler, M.S., Morrison, M.C., Alley, R.B., Bloomfield, K. & Taylor, K., 1993. The armosphere during the Younger Dryas. Science, 261: 195-197.

Mayewski, P.A., Meeker, L.D., Whitlow, S., Twickler, M.S., Morrison, M.C., Bloomfield, P., Bond, G.C., Alley, R.B., Gow, A.J., Grootes, P.M., Messe, D.A., Ram, M., Taylor, K.C. & Wumkes, W., 1994. Changes in atmospheric circulation and ocean ice cover over the North atlantic during the last 41,000 years. Science, 263: 1747-1751.

McCorkle, D.C., Ermerson, S.R. & Quay, P.D., 1985. Stable carbon isotopes in marine porewaters. Earth and Planet. Sci. Lett., 74: 13-26.

McCorkle, D.C., Keigwin, L.D., Corliss, B.H. & Ermerson, S.R., 1990. The influence of microhabitats on the carbon isotopic composition of seep sea benthic foraminifera. Paleoceanography, 5: 161-185.

McCorkle, D.C. & Keigwin, L.D., 1994. Depth profiles of $\delta^{13}C$ in bottom water and core top *C. wuellerstorfi* on the Ontong Java Plateau and Emperor Seamounts. Paleoceanography, 9: 197-208.

McManus, J.F., Bond, G.C., Broecker, W.S., Johnsen, S., Labeyrie, L. & Higgins, S., 1994. High-resolution climate records from the North Atlantic during the last interglacial. Nature, 371: 326-329.

Mejdahl, V. & Funder, S., 1994. Luminescence dating of Late Quaternary sediments from East Greenland. Boreas, 23: 525-535.

Mienert, J., Andrews, J.T. & Milliman, J.D., 1992. The East Greenland continental margin (65° N) since the last deglaciation: Changes in seafloor properties and ocean circulation. Marine Geology, 106: 217-238.

Miller, G.H., Sejrup, H.P., Lehman, S.J. & Forman, S.L., 1987. The last glacial-interglacial cycle, western Spitsbergen, Svalbard Archipelago. Polar Res., 5: 279-280.

Miller, G.H., Sejrup, H.P., Lehman, S.J. & Forman, S.L., 1989. Glacial history and marine environmental change during the last interglacial-glacial cycle, western Spitsbergen, Svalbard. Boreas, 18: 273-296.

Molina, B.F., 1972. Pleistocene ice rafting in the North Atlantic Ocean. PhD Thesis, Columbia, University of South Carolina: 103 pp.

Möller, P., Hjort, C. & Ingòlfsson, Ó., 1991. The last interglacial/glacial cycle: Preliminary report on the PONAM fieldwork in Jameson Land and Scoresby Sund, East Greenland. Lundqua Report, 33: 181 pp.

Möller, P., Hjort, C., Adrielsson, L. & Salvigsen, O. 1994. Glacial history of interior Jameson Land, East Greenland. Boreas, 23: 320-348.

Müller, P., 1977. C/N ratios in Pacific deep-sea sediments: Effect of inorganic ammonium and organic nitrogen compounds sorbed by clays. Geochim. Cosmochim. Acta, 41: 765-776.

Munsell Soil Colour Charts, 1954. Munsell Colour Co., Inc., Baltimore: 23 pp.

Myhre, A.M., Thiede, J. & Firth, J.V.et al., 1995. Proc. ODP, Init. Reports 151. College Station, TX (Ocean Drilling Program). 926 pp.

Nam, S.-I., Fütterer, D.K., Grobe, H., Hubberten, H. & Stein, R., 1994. Late Quaternary glacial/interglacial variations in sedimentary processes along the East Greenland continental margin. Terra Antarctica, 1: 431-432.

Nam, S.-I., Stein, R., Grobe, H. & Hubberten, H., 1995a. Late Quaternary glacial-interglacial changes in sediment composition at the East Greenland continental margin and their paleoceanographic implications. Marine Geology, 122: 243-262.

Nam, S.-I., Stein, R., Grobe, H. & Hubberten, H., 1995b. Short-term variations of Ice-rafted debris (IRD) at the East Greenland continental margin: Implications for the Greenland Ice Sheet evolution during the past 60,000 years. Terra Nostra (Schriften der Alfred-Wegener-Stiftung 1/95): 74 (Abstract).

Niessen, F. & Whittington, R., 1995. Marine sediment echosounding using PARASOUND. In: H.-W. Hubberten (ed.), Die Expedition ARKTIS-X/2 mit FS "Polarstern" 1994, Berichte zur Polarforschung Alfred-Wegener-Institut, Bremerhaven, 174: 62-68.

Norddahl, H., 1981. A prediction of minimum age for the Weichselian maximum glaciation in North Iceland. Boreas, 10, 471-476.

Norddahl, H., 1983. Late Quaternary stratigraphy of Fnjoskadalur Central North Iceland. LUNDQUA Thesis 12, Lund University.

Nowaczyk, N.R., 1991. Hochauflösende Magnetostratigraphie spätquartärer Sedimente arktischer Meeresgebiete. Berichte zur Polarforschung Alfred-Wegener-Institut, Bremerhaven, 78: 187 pp.

Nürnberg, D., Wollenburg, I., Dethleff, D., Eicken, H., Kassens, H., Letzig, T., Reimnitz, E. & Thiede, J., 1994. Sediments in Arctic sea ice: Implications for entrainment, transport and release. Marine Geology, 119: 185-214.

Nyholm, K.-G., 1961. Morphogenesis and biology of the foraminifer Cibicides lobatulus. Zoologiska Bidrag från Uppsala, 33: 157-196.

Oerlemans, J., 1993. Evaluating the role of climate cooling in iceberg production and the Heinrich events. Nature, 364: 783-786.

Oeschger, H., 1992. Working hypotheses for glaciation/deglaciation mechanisms. In: G.J. Kulka & E. Went (eds.), Start of a Glacial, NATO ASI Series, I 3: 273-289.

Paetsch, H., Botz, R., Scholten, J.C. & Stoffers, P., 1992. Accumulation rates of surface sediments in the Norwegian-Greenland Sea. Marine Geology, 104: 19-30.

Paquette, R.G., Bourke, R.H., Newton, J.L. & Perdue, W.F., 1985. The East Greenland Polar Front in autumn. Jour. Geophys. Res., 90: 4866-4882.

Perry, P.K., Fleming, H.S., Cherkis, N.Z., Feden, R.H. & Massengill, J.V., 1980. Bathymetry of the Norwegian-Greenland and western Barents Seas (map). Naval Research Laboratory, Acoustic Division, Environmental Sciences Branch, Washington, D.C..

Perry, P.K., 1986. Bathymetry. In B.G. Hurdle (ed.), The Nordic Seas. Springer, New York, Inc., 211-234.

Peters, K.E., 1986. Guidelines for evaluating petroleum source rock using programmed pyrolysis. Am. Assoc. Pet. Geol. Bull., 70: 318-329.

Pfirman, S. & Solheim, A., 1989. Subglacial meltwater discharge in the open-marine tidewater glacier environment: Observations from Nordaustland, Svalbard Archipelago. Marine Geology, 86: 265-281.

Pfirman, S., Gascard, J.-C., Wollenburg, I., Mudi, P. & Abelmann, A., 1989. Particle-laden Eurasian Arctic sea ice: Observations from July and August 1987. Polar Res., 7: 59-66.

PONAM Final Report - Polar North Atlantic Margins: Late Cenozoic Evolution. An ESF Research Programme, Strasbourg Cedex, France: 36 pp.

Porter, S.C. & Zhisheng, A., 1995. Correlation between climate events in the North Atlantic and China during the last glaciation. Nature, 375: 305-308.

Quadfasel, D. & Meincke, J., 1987. Note on the thermal structure of the Greenland Sea gyres. Deep-Sea Res., 34: 1883-1888.

Rahman, A., 1995. Reworked nannofossils in the North Atlantic Ocean and subpolar basins: Implications for the Heinrich events and ocean circulation. Geology, 23: 487-490.

Ramm, M., 1988. A stratigraphic study of late Quaternary sediments on the Vøring-Plateau, Eastern Norwegian Sea. Marine Geology, 83: 159-191.

Redfield, A.C., Ketchum, B.H. & Richard, F.A., 1963. The influence of organisms on the composition of seawater. In: M.N. Hill (ed.), The Sea, Wiley-Interscience, New York, v. 2: 26-77.

Reeh, N., 1985. Greenland ice-sheet mass balance and sea level change. In: M.F. Meier, D.G. Aubrey, C.R. Bentley, W.S. Broecker, J.E. Hansen, W.R. Peltier & R.C.J. Somerville (eds.), Glaciers, ice sheets and sea level: Effects of a CO_2-induced climate change. Nat. Acad. Press, Washington D.C.: 155-171.

Reeh, N., 1989. Dynamic and climatic history of the Greenland Ice Sheet. In: R.J. Fulton (ed.), Quaternary Geology of Canada and Greenland. Geological Survey of Canada, Geology of Canada, no. 1: 795-822.

Robe, R.Q., 1980. Iceberg drift and deterioration. In: S. Colbeck (ed.), Dynamics of Snow and Ice Masses. Academic Press, New York, 211-259.

Robinson, S.G., Maslin, M.A. & McCave, I.N., 1995. Magnetic susceptibility variations in Upper Pleistocene deep-sea sediments of the NE Atlantic: Implications for ice rafting and paleocirculation at last glacial maximum. Paleoceanography, 10: 221-250.

Ruddiman, W.F. & Glover, L.K., 1972. Vertical mixing of ice-rafted volcanic ash in North Atlantic sediments. Geol. Soc. Amer. Bull., 83: 2817-2836.

Ruddiman, W.F. & McIntyre, A., 1973. Time-transgressive deglacial retreat of polar waters from the North Atlantic. Quat. Res., 3: 117-130.

Ruddiman, W.F. & McIntyre, A., 1976. Northeast Atlantic paleoclimatic changes over the past 600,000 years. Geol. Soc. Amer. Memoir, 145; 111-146.

Ruddiman, W.F., 1977. North Atlantic Ice-Rafting: a major change at 75,000 years before the present. Science, 196: 1208-1211.

Ruddiman, W.F. & McIntyre, A., 1981a. Oceanic mechanisms for amplification of the 23,000-year ice-volume cycle. Science, 212: 617-627.

Ruddiman, W.F. & McIntyre, A., 1981b. The North Atlantic ocean during the last deglaciation. Palaeogeogr., Palaeoclimatol., Palaeoecol., 35: 145-214.

Samtleben, C. & Schröder, A., 1992. Living coccolithophore communities in the Norwegian-Greenland Sea and their record in sediments. Marine Micropaleontology, 19: 333-354.

Samtleben, C., Schäfer, P., Andruleit, H., Baumann, A., Baumann, K.-H., Kohly, A., Matthiessen, J., Schröder-Ritzrau, A. & 'Synpal' Working Group., 1995. Plankton in the Norwegian-Greenland Sea: from living communities to sediment assemblages - an actualistic approach. Geol. Rundsch., 84: 108-136.

Sarnthein, M., Winn, K., Duplessy, J.-C. & Fontugne, M.R., 1988. Global variations of surface ocean productivity in low and mid latitudes: Influence on CO_2 reservoirs of the deep ocean and atmosphere during the last 21,000 years. Paleoceanography, 3: 361-399.

Sarnthein, M., Jansen, E., Arnold, M., Duplessy, J.C., Erlenkeuser, H., Flatoy, A., Veum, T., Vogelsang, E. & Weinelt, M.S, 1992. δ^{18}-O time-slice reconstruction of meltwater anomalies at Termination I in the North Atlantic between 50° and 80°N. In: E. Bard & W.S. Broecker (eds.), The Last Deglaciation: Absolute and Radiocarbon Chronologies. NATO ASI Series, I 2: 183-200.

Sarnthein, M., Jansen, E., Weinelt, M., Arnold, M., Duplessy, J.C., Erlenkeuser, H., Flatøy, A., Johannessen, G., Johannessen, T., Jung, S., Koc, N., Labeyrie, L., Maslin, M., Pflaumann, U. & Schulz, H., 1995. Variations in Atlantic surface ocean paleoceanography, 50°-80°N: A time-slice record of the last 30,000 years. Paleoceanography, 10: 1063-1094.

Schmiedl, G., 1995. Rekonstruktion der spätquartären Tiefenwasserzirkulation und Produktivität im östlichen Südatlantik anhand von benthischen Foraminiferenvergesellschaftungen. Berichte zur Polarforschung Alfred-Wegener-Institut, Bremerhaven, 160: 207 pp.

Schrader, H. & Koç Karpuz, N., 1990. Norwegian-Iceland Seas: Transfer functions between marine planktonic diatoms and surface water temperature. In: U. Bleil & J. Thiede (eds.), Geological history of the polar oceans: Arctic versus Antarctic. Dordrecht: Kluwer Academic Publishers, NATO ASI Series, C 308: 337-361.

Sejrup, H.P., Sjøholm, J., Furnes, H., Beyer, I., Eide, L., Jansen, E. & Mangerud, J., 1989. Quaternary tephrachronology on the Iceland Plateau, north of Iceland. Jour. Quat. Sci., 4: 109-114.

Shackleton, N.J., 1967. Oxygen isotope analyses and Pleistocene temperatures re-assessed. Nature, 215: 15-17.

Shackleton, N.J. & Opdyke, N.D., 1973. Oxygen isotope and paleomagnetic stratigarphy of equatorial Pacific Core V28-238: oxygen isotope temperatures and ice volume on a 10^5 year and 10^6 year scale. Quat. Res., 3: 39-55.

Shackleton, N.J., 1974. Attainment of isotopic equilibrium between ocean water and benthic foraminifera genus *Uvigerina*: isotopic changes in the ocean during the last glacial. C.N.R.S. Coll., 219: 203-209.

Shackleton, N.J., Backman, J., Zimmerman, H., Kent, D.V., Hall, M.A., Roberts, D.G., Schnitker, D., Baldauf, J.G., Desprairies, A., Homrighausen, R., Huddlestun, P., Keene, J.B., Kaltenback, A.J., Krumsiek, K.A.O., Morton, A.C., Murray, J.W. & Westberg-Smith, J., 1984. Oxygen isotope calibration of the onset of ice-rafting and history of glaciation in North Atlantic region. Nature, 307: 620-623.

Shackleton, N.J., 1987. Oxygen isotopes, ice volume and sea level. Quat. Sci. Rev., 6: 183-190.

Shaffer, G. & Bendtsen, J., 1994. Role of the Bering Strait in controlling North Atlantic ocean circulation and climate. Nature, 367: 354-357.

Shepard, F.P., 1954. Nomenclature based on sand-silt-clay ratios. J. Sed. Pet., 24: 151-158.

Smith, Jr., W.O., Baumann, M.E.M., Wilson, D.L. & Aletsee, L., 1987. Phytoplankton biomass and productivity in the marginal ice zone of the Fram Strait during summer 1984. Jour. Geophys. Res., 92: 6777-6786.

Smythe, Jr., F.W., Ruddiman, W.F. & Lumsden, D.N., 1985. Ice-rafted evidence of long-term North Atlantic circulation. Marine Geology, 64: 131-141.

Spielhagen, R.F. 1991. Die Eisdrift in der Framstrasse whärend der letzten 200.000 Jahre. GEOMAR Report, 4: 133 pp.

Spielhagen, R.F. & Erlenkeuser, H., 1994. Stable oxygen and carbon isotopes in planktonic foraminifers from Arctic Ocean surface sediments: Reflection of the low salinity surface water layer. Marine Geology, 119: 227-250.

Stein, R., ten Haven, H.L., Littke, R., Rullkötter, J. & Welte, D.H., 1989. Accumulation of marine and terrigenous organic carbon at Upwelling Site 658 and Nonupwelling Sites 657 and 659: Implications for the reconstruction of paleoenvironments in the eastern subtropical Atlantic

through Late cenozoic times. In: W. Ruddiman et al. (eds.), Proc. ODP, Sci. Results, 108: 361-385.

Stein, R., 1991. Accumulation of organic carbon in marine sediments. Lecture Notes in Earth Sciences 34, Springer, Heidelberg, 217 pp.

Stein, R. & Stax, R., 1991. Late Quaternary organic carbon cycles and paleoproductivity in the Labrador Sea. Geo-Marine Letters, 11: 90-95.

Stein, R., Grobe, H., Hubberten, H., Marienfeld, P. & Nam, S., 1993. Latest Pleistocene to Holocene changes in glaciomarine sedimentation in Scoresby Sund and along the adjacent East Greenland Continental Margin: Preliminary results. Geo-Marine Letters, 13: 9-16.

Stein, R., Nam, S.-I., Schubert, C., Vogt, C., Fütterer, D. & Heinemeier, J., 1994a. The Last Deglaciation Event in the Eastern Central Arctic Ocean. Science, 264: 692-696.

Stein, R., Schubert, C., Vogt, C. & Fütterer, D., 1994b. Stable isotope stratigraphy, sedimentation rates, and salinity changes in the Latest Pleistocene to the Holocene eastern central Arctic Ocean. Marine Geology, 119: 333-355.

Stein, R., Grobe, H. & Wahsner, M., 1994c. Organic carbon, carbonate, and clay mineral distributions in eastern central Arctic Ocean surface sediments. Marine Geology, 119: 269-285.

Stein, R., Schubert, C., Grobe, H. & Fütterer, D., 1994d, Late Quaternary changes in sediment composition in the central Arctic Ocean: Preliminary results of the Arctic'91 expedition. In: D.K. Thurston & K. Fujita (eds.), 1992 Proceedings International Conference on Arctic Margins. - OCS Study MMS 94-0040. Anchorage, Alaska. 363-368.

Stein, R., Nam, S.-I., Grobe, H. & Hubberten, H., 1996. Late Quaternary glacial history and short-term ice-rafted debris fluctuations along the East Greenland continental margin. In: J. Andrews, W.E.N. Austin, H. Bergsten & A.E. Jennings (eds.), Late Quaternary Paleoceanography of the North Atlantic Margins, Geol. Soc. Spec. Publ. No. 111, London: 135-151.

Steinsund, P.I. & Hald, M., 1994. Recent calcium carbonate dissolution in the Barents Sea: Paleoceanographic applications. Marine Geology, 117: 303-316.

Streeter, S.S., Belanger, P.E., Kellogg, T.B. & Duplessy, J.C., 1982. Late Pleistocene paleo-oceanography of the Norwegian-Greenland Sea: benthic foraminiferal evidence. Quat. Res., 18: 72-90.

Struck, U., 1992. Zur Paläo-Ökologie benthischer Foraminiferen im Europäischen Nordmeer während der letzten 600 000 Jahre. Berichte SFB 313, Universität Kiel, 38: 129 pp.

Stuiver, M., Kromer, B., Becker, B. & Ferguson, C.W., 1986. Radiocarbon age calibration back to 13,300 years BP and the ^{14}C age matching of the German oak and US bristlecone pine chronologies. In: M. Stuiver & R.S. Kra (eds.), Proceedings of 12th International ^{14}C Conference. Radiocarbon, 28 (2B): 969-979.

Svendsen, J.I. & Mangerud, J., 1992. Paleoclimatic inferences from glacial fluctuations on Svalbard during the last 20,000 years. Climate Dynamics, 6: 213-220.

Svendsen, J.I. & Mangerud, J., Elverhøi, A., Solheim, A. & Schüttenhelm, R.T.E., 1992. The late Weichselian glacial maximum on western Spitsbergen inferred from offshore sediment cores. Marine Geology, 104: 1-17.

155

Swift, J.H. & Aagaard, K., 1981. Seasonal transitions and water mass formation in the Iceland and Greenland Seas. Deep-Sea Res., 28: 1107-1129.

Swift, J.H., 1986. The Arctic Waters. In: B.G. Hurdle (ed.), The Nordic Seas. Springer, New York, Inc.: 129-153.

Swift, J.H. & Koltermann, K.P., 1988. The origin of Norwegian Sea Deep Water. Jour. Geophy. Res., 93: 3563-3569.

Talwani, M. & Eldholm, O., 1977. Evolution of the Norwegian-Greenland Sea. Geol. Soc. Amer. Bull. 88: 969-999.

Taylor, K.C., Lamorey, G.W., Doyle, G.A., Alley, R.B., Grootes, P.M., Mayewski, P.A., White, J.W.C. & Barlow, L.K., 1993a. The 'flickering switch' of late Pleistocene climate change. Nature, 361: 432-436.

Taylor, K.C., Hammer, C.U., Alley, R.B., Clausen, H.B., Dahl-Jensen, D., Gow, A.J., Grundestrup, N.S., Kipfstuhl, J., Moore, J.C. & Waddington, E.D., 1993b. Electrical conductivity measurements from the GISP2 and GRIP Greenland ice cores. Nature, 366: 549- 552.

Thiede, J. & Hempel, G., 1991. Die Expedition ARKTIS-VII/1 mit FS „Polarstern" 1990. Berichte zur Polarforschung Alfred-Wegener-Institut, Bremerhaven, 80: 137 pp.

Thordardotirr, T., 1977. Primary production in North Icelandic waters in relation to recent climatic changes. In: M.J. Dunbar (ed.), Polar Oceans. Arctic Inst. of North America, Calgary. 655-665.

Thouveny, N., de Beaulieu, J.-L., Bonify, E., Creer, K.M., Guiot, J., Icole, M., Johnsen, S., Jouzel, J., Reille, M., Williams, T. & Williamson, D., 1994. Climate variations in Europe over the past 140 kyr deduced from rock magnetism. Nature, 371: 503-506.

Tissot, B.P. & Welte, D. H., 1984. Petroleum Formation and Occurrence. Springer, Heidelberg, 699 pp.

Thunell, R.C. & Mortyn, G., 1995. Glacial climate instability in the Northeast Pacific Ocean. Nature, 376: 504-506.

Tveranger, J., Houmark-Nielsen, M., Løvberg, K. & Mangerud, J., 1994. Eemian-Weichselian startigraphy of the Flakkerhuk ridge, southern Jameson Land, East Greenland. Boreas, 23: 359-384.

Tzedakis, P.C., Bennett, K.D. & Magri, D., 1994. Climate and the pollen record. Nature, 370: 513.

Uenzelmann-Neben, G., Jokat, W. & Vanneste, K., 1991. Quaternary sediments in Scoresby Sund, East Greenland: their distribution as revealed by reflection seismic data. Lundqua Report, 33: 139-148.

van Andel, T.H., Heath, G.R. & Moore, T.C., 1975. Cenozoic history and paleoceanography of the central equatorial Pacific. Mem. Geol. Soc. Amer., 143: 134 pp.

Vanneste, K., Uenzelmann-Neben, G. & Miller, H., 1995. Seismic evidence for long-term history of glaciation on central East Greenland shelf south of Scoresby Sund. Geo-Marine Lett., 15: 63-70.

Veum, T., Jansen, E., Arnold, M., Beyer, I. & Duplessy, J.-C., 1992. Water mass exchange between the North Atlantic and the Norwegian Sea during the past 28,000 years. Nature, 356: 783-785.

Vinje, T.E., 1977. Sea ice conditions in the European sector of the marginal seas of the Arctic, 1966-75. Arbok, Nor. Polarinst.: 163-174.

Vogelsang, E., 1990. Paläo-Ozeanographie des Europäischen Nordmeeres an Hand stabiler Kohlenstoff- und Sauerstoffisotope. Berichte SFB 313, Universität Kiel, 23: 136 pp.

Vogt, C., Knies, J., Grobe, H., Stein, R. & Spielhagen, R.F. Late Quaternary paleoceanography near the NW-Spitsbergen coast and on the Yermak Plateau. Submitted to Paleoceanography.

Vogt, P.R., 1986. Seafloor topography, sediments, and paleoenvironments. In:B.G. Hurdle (ed.), The Nordic Seas. Springer, New York, Inc.: 287-386.

Vorren, T.O., Hald, M., Edvardsen, M. & Lind-Hansen, O.-W., 1983. Glacigenic sediments and sedimentary environments on continental shelves: General principles with a case study from the Norwegian shelf. In: J. Ehlers (ed.), Glacial Deposits in northern Europe. Balkema, Rotterdam, 61-73.

Vorren, T.O., Lebesbye, E., Andreassen, K. & Larsen, K.-B., 1989. Glacigenic sediments on a passive continental margin as exemplified by the Barents Sea. Marine Geology, 85: 251-272.

Vosgerau, H., Funder, S., Kelly, M., Knudsen, K.L., Kronborg, C., Madsen, H.B. & Sejrup, H.P., 1994. Paleoenvironments and changes in relative sea level during the last interglaciation at Langelandselv, Jameson Land, East Greenland. Boreas, 23: 398-411.

Wadhams, P., 1981. The ice cover in the Greenland and Norwegian Seas. Rev. Geophys. Space Physics, 19: 345-393.

Wadhams, P., 1986. The sea ice cover. In: B.G. Hurdle (ed.), The Nordic Seas. Springer, New York, Inc.: 21-84.

Wagner, T., 1993. Organisches Material in pelagischen Sedimenten: Glaziale/Interglaziale Variationen im Europäischen Nordmeer. Berichte SFB 313, Universität Kiel, 42: 138 pp.

Wagner, T. & Henrich, R., 1994. Organo- and lithofacies of glacial/interglacial deposits of the Norwegian-Greenland Sea: responses to paleoceanographic and paleoclimatic changes. Marine Geology, 120: 335-364.

Weaver, A.J. & Hughes, T.M.C., 1994. Rapid interglacial climate fluctuations driven by North Atlantic ocean circulation. Nature, 367: 447-450.

Weeks, W., 1986. Physical properties of the ice cover of the Greenland Sea. CRREL-SR-82-28, U.S. Army Cold Regions Research and Engineering Laboratory, Hannover, N.H.

Weinelt, M., 1993. Veränderungen der Oberflächenzirkulation im Europäischen Nordmeer whärend der letzten 60.000 Jahre - Hinweise aus stabilen Isotopen. Berichte SFB 313, Universität Kiel, 41: 106 pp.

Williams, K.M., 1993. Ice sheet and ocean interactions, margin of the east Greenland ice sheet (14 ka to Present): Diatom evidence. Paleoceanography, 8: 69-83.

Wollenburg, I., 1993. Sedimenttransport durch das arktische Meereis: Die rezente lithogene und biogene Materialfracht. Berichte zur Polarforschung Alfred-Wegener-Institut, Bremerhaven, 127: 159 pp.

Wollenburg, J., 1995. Benthische Foraminiferenfaunen als Wassermassen-, Produktions- und Eisdriftanzeiger im Arktischen Ozean. Berichte zur Polarforschung Alfred-Wegener-Institut, Bremerhaven, 179: 227 pp.

Zahn, R., Markussen, B. & Thiede, J., 1985. Stable isotope data and depositional environments in the late Quaternary Arctic Ocean. Nature, 314: 433-435.

Zahn, R., Winn, K. & Sarnthein, M., 1986. Benthic foraminiferal $\delta^{13}C$ and accumulation rates of organic carbon: Uvigerina peregrina and Cibicidoides wuellerstorfi. Paleoceanography, 1: 27-42.